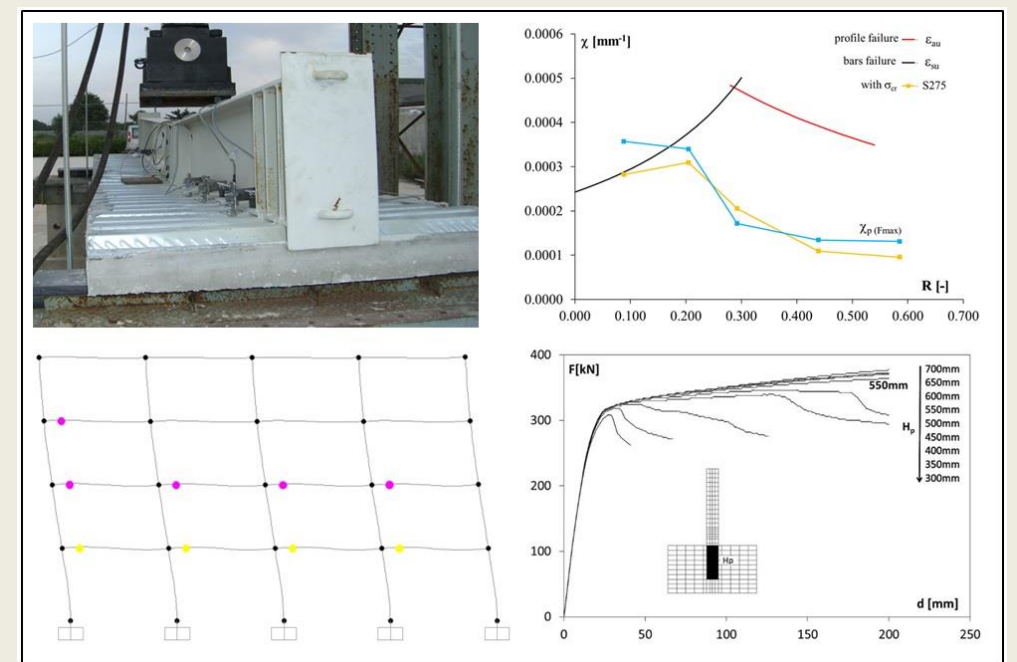




UNIVERSITY OF NAPLES FEDERICO II
PH.D. PROGRAMME IN SEISMIC RISK
XXV CYCLE

Fernando Rossi

THE ROTATIONAL CAPACITY OF THE STEEL-CONCRETE
COMPOSITE BEAMS UNDER HOGGING MOMENT AND
THE SEISMIC PERFORMANCE OF THE COMPOSITE FRAMES



The Rotational Capacity of the Steel-Concrete Composite Beams Under
Hogging Moment and the Seismic Performance of the Composite Frames

Fernando Rossi

2013

2013

UNIVERSITY OF NAPLES FEDERICO II

PH.D. PROGRAMME IN SEISMIC RISK

COORDINATOR PROF. ALDO ZOLLO

XXV CYCLE



FERNANDO ROSSI

PH.D. THESIS

THE ROTATIONAL CAPACITY OF THE STEEL- CONCRETE COMPOSITE BEAMS UNDER HOGGING MOMENT AND THE SEISMIC PERFORMANCE OF THE COMPOSITE FRAMES

TUTOR: PROF. MARIA ROSARIA PECCE

2013

Abstract

The use of steel-concrete composite framed buildings is particularly efficient for their high lateral stiffness, strength and ductility; therefore the structural performance achievable with these systems makes them particularly suitable for applications in seismic zone. However the current state of technical knowledge concerning the characterization of the structural behavior of steel-concrete composite systems subjected to seismic actions is not exhaustive and requires additional theoretical and experimental studies in order to better understand their behavior and improve the design procedures. Often these shortcomings mean that the choice of the framed structure as seismic resistant systems falls in reinforced concrete or steel buildings. In fact, in the case of the steel-concrete composite framed structures the complexity of the problem is increased by the identification of the role of the connection between the reinforced concrete component and the steel one.

In light of this assumption, the research project undertaken in the three-years of PhD study has been addressed to the analysis of the seismic performance of the steel-concrete composite frames and the development of advanced computational models for the seismic design of this type of structure.

In particular two aspects were selected and developed in this research field: the rotational capacity of steel-concrete composite beams under hogging moments and the rotational capacity of the connection between the composite columns and the foundation.

All the decisions regarding the materials/connection models had the aim of characterizing as better as possible the three-dimensional FE models of the composite beams and the base column connection. The effectiveness of the models were investigated by the comparison between numerical and

experimental results; the experimental tests on the composite beams subjected to hogging moments, had carried out by myself previously.

After the calibration of the models, parametric analyses were performed. In the case of the beams an innovative approach for defining the moment-curvature relationships, considering the effect of the local buckling, was assessed together with an equivalent plastic hinge length, obtaining the procedure to calculate the rotational capacity. Also for the base column connection a plastic hinge length was defined, taking into account the effect of the fixed end rotation, in the case of a socket connection.

Both the results, for beams and columns, represent the instruments for a reliable non linear analysis of the composite frames in which the dissipation of the seismic energy is addressed at the end of the beams and at the base connection, as typically aimed to the framed structures.

The last step of this research was the implementation of the relationships assessed for the rotational capacity for the beams and the base of the columns, in the nonlinear model of a composite frame designed according to the requirements of the standards, both national and European.

The results of the analyses, in terms of behavior factors and over-strength ratio, point out the good performances of the composite frames and their promising use to reduce the seismic risk of new buildings.

ACKNOWLEDGEMENTS

Desidero ringraziare la mia famiglia per il continuo sostegno morale che mi ha garantito, soprattutto nel primo anno di questa esperienza straordinaria del dottorato: un pensiero va a chi non c'è più e che forse sarebbe contento per questo risultato. Grazie a Laura che ormai mi sopporta, è proprio il caso, e mi sostiene da un bel po' di tempo. Grazie anche alla parte di famiglia che risiede "da quella via": Cosimo mi ha sempre consigliato come un padre e insieme a Tina, zia e i ragazzi sono la mia seconda casa.

Grazie agli amici...tutti! Quelli con cui sono cresciuto e quelli che ho incontrato strada facendo. Il valore dell'amicizia, anche tra non poche difficoltà e incomprensioni, è qualcosa che arricchisce ognuno di noi.

Grazie ai "miei" tesisti. Spero di aver dato loro almeno quanto loro hanno dato a me. Seguirli è sempre una bella soddisfazione, soprattutto quando l'entusiasmo per quello che si fa prende il sopravvento sulle difficoltà.

Il dottorato mi ha anche regalato l'amicizia di Angelo (AG, come lui stesso sigla qualche volta). Persona straordinaria con cui mi diverte sempre confrontarmi su qualsiasi cosa: il calcio (purtroppo è juventino!), cose riguardanti l'ingegneria o cose di vita quotidiana. Le sue riflessioni non sono mai banali.

Come non banale è l'amicizia di Fabio, per cui nutro stima e affetto e che considero un esempio di virtù morali e di dedizione al lavoro come alle cose care. Ormai abbiamo fatto parecchia strada assieme dal quel primo giorno che ci incontrammo in un'aula a seguire il corso di Fisica 1. Da appassionati di ciclismo, direi che con il dottorato si chiude il nostro "trittico del Nord". Il nostro dottorato come una Roubaix: il pavè arso dal sole alza polvere che si impasta al sudore e taglia il fiato; poi magari piove e quel pavè diventa tuo amico solo se l'agilità delle gambe fa sì che le ruote lo accarezzino, piuttosto che picchiarlo. L'ennesimo tratto di pavè "nell'inferno del Nord" che infine può regalare la vittoria semplicemente di un pezzo di pavè.

Infine, e qui vorrei che la mia penna fosse più forbita, desidero ringraziare la prof. Pecce. Le parole non possono esprimere quello che vorrei ma....Questi dieci anni di percorso hanno cambiato la mia vita, non solo scientifica. La prof

possiede qualità umane e morali che oggi è sempre più difficile trovare nelle persone. La capacità di trasmettere l'entusiasmo per il cercare e per la conoscenza spesso non si trova neanche nei giovani, a volte spenti o mai accesi da quella curiosità che dovrebbe distinguerli. Alla prof va la mia gratitudine per quello che mi insegna giorno per giorno, per il coinvolgimento in tutte le attività accademiche, per la fiducia che ripone in me e che forse a volte non merito. Tutto ciò che so è quello che mi ha insegnato; tutto ciò che non so è quello che non ho saputo imparare o che distrattamente ho ignorato. Sicuramente lei non si è mai risparmiata, anche in questo lavoro di tesi: le correzioni, i suggerimenti, i confronti sono stati innumerevoli. Spero che il cammino al suo fianco sia appena all'inizio.

Infine, mi scuso con tutti per le mie mancanze come figlio, fratello, amante, amico, tutor, allievo... perché a volte distratto e preso sempre da altro.

Table of content

1. CHAPTER 1. INTRODUCTION	pag. 1
1.1 Why the use of steel-concrete composite construction	” 1
1.2 Problem statement and aim of the thesis	” 2
1.3 Outline of the thesis	” 5
2. CHAPTER 2. THE NON LINEAR BEHAVIOUR OF COMPOSITE BEAMS	pag. 8
2.1 Introduction	” 8
2.2 Behavior of composite beams under sagging flexural moment	” 14
2.3 Behavior of composite beams under hogging flexural moment	” 19
2.4 The role of the shear connection between concrete and steel	” 38
2.5 Experimental data on the rotational capacity	” 47
2.6 The available formulations for the estimation of the rotational capacity	” 54
3. CHAPTER 3. THE FE MODELLING OF COMPOSITE BEAMS SUBJECT TO HOGGING MOMENT	pag. 70
3.1 Models available for composite beams	” 70
3.2 The FE model developed for the composite beams	” 78
3.3 The tension stiffening effect in DIANA	” 93
3.4 The residual stresses	” 103
3.5 Local and global buckling	” 105
3.6 Features and behaviour of the tested beams	” 106
3.6.1 <i>Experimental characterization of the materials</i>	” 109
3.6.2 <i>Evaluation of the actual characteristics of the beams</i>	” 111
3.6.3 <i>Instrumentation</i>	” 114

3.6.4 <i>Results</i>	” 115
3.7 The FE model of the composite beams tested	” 121
3.8 Calibration of the FE model by means of a numeric-experimental comparison	” 126
 4. CHAPTER 4. THEORETICAL AND NUMERICAL ANALYSES OF COMPOSITE BEAMS UNDER HOGGING MOMENTS	pag. 143
4.1 The behavior of the composite cross-section subjected to hogging moment	” 143
4.1.1 <i>Theoretical analysis</i>	” 143
4.1.1.1 <i>The role of the hardening and the critical stress</i>	“ 150
4.1.2 <i>The numerical analysis</i>	“ 152
4.1.3 <i>The role of the steel hardening</i>	“ 155
4.2 The numerical analysis of the composite beams subjected to hogging moment	” 159
4.2.1 <i>The effect of the hardening</i>	” 164
4.2.2 <i>The effect of the connection deformability</i>	” 169
4.3 The equivalent plastic hinge length	” 172
4.4 Conclusions	” 176
 5. CHAPTER 5. THE BASE CONNECTION OF COMPOSITE COLUMNS	pag. 191
5.1 The base column connection of steel and composite columns	” 192
5.2 Experimental tests	” 216
5.2.1 <i>Specimen description</i>	” 216
5.2.2 <i>Test results and specimens performance</i>	“ 221
5.3 The analyses from the 3D finite element model	” 225

5.3.1. <i>The 3D numerical model</i>	”	225
5.3.2. <i>Material models</i>	”	227
5.3.3. <i>Discussion</i>	”	229
5.3.4. <i>Parametric analysis</i>	”	232
5.3.4.1. <i>Effect of the embedded height</i>	”	232
5.3.4.2 <i>Evaluation of the elastic rigidity of the base connection</i>	”	239
5.4 Mono-dimensional modelling of the column with a socket type connection	”	243
5.4.1 <i>The moment curvature relationship</i>	“	243
5.4.2 <i>Definition of the plastic hinge length</i>	”	245
5.4.3 <i>The non-linear mono-dimensional model with a semi-rigid connection at the base</i>	”	247
5.5 Conclusions	”	249
6. CHAPTER 6. THE STEEL-CONCRETE COMPOSITE FRAMES		pag. 256
6.1 Introduction	”	256
6.2 The response of steel-concrete composite frames under seismic action	“	257
6.3 The design of a composite frame	”	274
6.4 The non-linear analysis of the steel-concrete composite MRF	“	283
6.4.1 <i>The moment-curvature relationships of beams and columns</i>	”	284
6.4.2 <i>The plastic hinge length</i>	”	290
6.4.3 <i>The non-linear response</i>	“	293
6.5 Conclusions	”	299

CHAPTER 1. INTRODUCTION

1.1 Why the use of steel-concrete composite construction

The use of steel-concrete composite framed buildings is particularly efficient for their high lateral stiffness, the strength and the ductility (Cosenza et al., 1997). Structural performance achievable with these systems makes them particularly suitable for applications in seismic zone (Hajjar, 2002; Plumier, 2004; Thermou et al., 2004).

The current state of technical knowledge concerning the characterization of the structural behavior of steel-concrete composite systems subject to gravitational loads and especially to seismic actions is not exhaustive and requires additional theoretical and experimental studies in order to better understand their behavior and to improve the design. There are many aspects of the national standard code (NTC, 2008) and its guideline (Circolare, 2009) which are not of immediate application, or require precise quantitative references for their verification. Likewise, in international standards or guidelines (CEN, 2008-a; CEN 2008-b; AISC, 2010), there are several aspects that require further theoretical and experimental developments.

Often these shortcomings mean that the choice of the framed structure as seismic resistant system falls on reinforced concrete structures or steel. In fact, in the case of reinforced concrete structures and steel the experimental results and theoretical models developed, although still require further studies, have now identified the main aspects of the mechanisms that govern the nonlinear behavior of them under monotonic and cyclic actions and have led to the simplified modeling also suitable for design applications. Conversely, in the case of the steel-concrete composite framed structures the complexity of the problem is increased by the identification of the role of the connection between

the reinforced concrete component and steel one; also the experimental data and theoretical studies on the modeling is still limited and in Italy the development of technologies and standards, especially for use in seismic areas, is relatively recent.

Regarding to the wide problem of the influence of the non-linear behavior on the performance of the framed structures and the concept of plastic hinge to analyze their ductility capacity, it should be noted that even today there are no established formulas that allow to evaluate the ultimate rotational capacity of the composite beams, such as to allow the use of the lumped plasticity approach, particularly suitable for practical applications, conversely to what happens for the reinforced concrete and the steel (Circolare 617/09).

In many cases, because of the shortcomings of standards for the evaluation of the plastic rotational capacity of composite elements, reference is erroneously made to the relationship valid for steel members, neglecting, therefore, the mechanical interaction between steel and concrete components that characterizes a composite element and, then, some important mechanisms and parameters. Since for the “capacity design” approach a correct design for seismic actions allow the development of the dissipative zones, identified as plastic hinges, at the beam ends, near the nodal zone, and at the column bases, the plastic rotational capacity of the composite elements assumes a fundamental importance for assessing the global non-linear behavior of the structure.

1.2 Problem statement and aim of the thesis

In a seismic design based on the limit state concept and on structural performance criteria (also called "performance-based design"), the calculation of the external forces at the ultimate limit state requires procedures that allow to take into account for the actual capacity of the structural materials in terms

of strength and ductility and lead to the global redistribution of themselves. For framed structures (MRFs) the nonlinear behavior, taking into account for the actual constitutive relationships of the materials and their interaction, can be evaluated numerically and essentially with two alternative approaches: the distributed plasticity and the lumped plasticity. This latter approach allows to concentrate the damage along a portion of the element, the so-called critical zone or plastic hinge, in a single cross-section in which the moment-plastic rotation, or the moment-curvature relationship followed by the length of plastic hinge, is placed. Therefore the user of this approach defines a priori the deformation capacity and the length of the critical zone (equivalent plastic hinge) through simple theoretical relationships or closed formulas that are provided by numerical or experimental studies.

It seems obvious that the model with lumped plasticity is simple, but its effectiveness is due almost exclusively to the definition of the moment-rotation relationships included in the plastic hinges.

Certainly the definition of reliable moment-rotation relationships for the plastic hinges is an essential element for analyzing the performance of the composite frames and to improve the design rules able to ensure the safety of the composite structures above all in presence of the seismic actions and to encourage its use.

Since this research topic has not yet reached significant results because of the limited experimental data available, if compared to more traditional types such as R. C. and steel structures, this thesis aims to analyze the topic mainly through numerical modeling to identify some simple relationship useful to the development of reliable non-linear analysis with the lumped plasticity in the beams and in the column base connection.

The logical path to the characterization of the seismic response of a composite MRF is developed in a such way which is also common to other typologies of constructions above mentioned, reinforced concrete and steel structures. In a hierarchical scheme, as in the figure 1.1, it could be noted as the starting point is the material and as from it, through the cross-sections and the entire element, it is possible to arrive at the definition of the whole system.

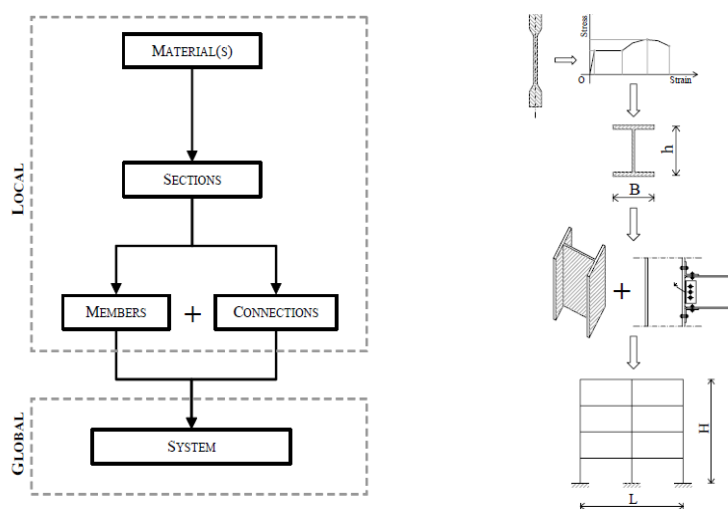


Figure 1.1

All the decisions regarding the material models have had the aim of characterizing in the best way the three-dimensional FE model of the composite elements, beams and base columns. Since the seismic-resistant scheme adopted in this study (MRF) implies, as already mentioned, the concentration of the damage in the cross-sections of the beam ends and at the base of the columns, the FEM modeling has focused on beams, in particular subject to negative moment, and on the base connections, in particular of innovative type. The FE models developed, both for the composite beams that for the columns, were calibrated on the experimental results in order to understand which aspects are relevant in the same modeling. Each choice is

made taking into account also for the computational cost which is almost always in conflict with that of precision.

The complete models of the composite beam and the base columns have been implemented and compared with experimental results showing a good agreement. The particular models of the various elements, as mentioned above, have had the aim to deepen any local aspects which otherwise would not be able to take in light. The FE models of the base connection and the composite beam were useful to carry out a parametric analysis for estimating the deformation capacity in the plastic field of these elements and, therefore, for studying which are the influence exerted by various parameters on their local and global response. The parametric analyses and experimental data available were aimed to formulate simple relationships on local plastic capacities, the so-called plastic hinges, to be used in the analysis of the performance of an entire frame made in order to characterize the non-linear response of a such system.

The relationships on the available rotational capacity suggested in this thesis were therefore used in the nonlinear analyses performed with the lumped plasticity approach on a composite frame designed according to the requirements of the standards, both national and European.

Finally, the response of the composite frame was calculated with the relationships proposed in this work in order to better understand what could be the real deformation capacity of a composite system.

1.3 Outline of the thesis

The present work, as already mentioned, has the aim to characterize the seismic response of steel-concrete composite frames. To this order, Chapter 2 identifies the main scientific research on the rotational capacity of composite beams and summarizes in tabular form the main experimental data and the parameters

considered in them. Chapter 3 sets out the criteria used and the choices made in the finite element modeling (FEM) of a composite beam subjected to hogging moment. This model is calibrated on the experimental results reported in (Pecce et al., 2010) on the composite beams subjected to negative moment. In the same chapter is a summary of these experimental data and, finally, their comparison with the numerical model that showed a good agreement. Chapter 4 shows the parametric analysis performed on the beam model developed in the previous chapter. At the end of the parametric analysis, an innovative approach for moment-curvature relationships is proposed to use with an equivalent plastic hinge length derived from numerical analyzes. Chapter 5 shows the main scientific contributions on the rotational capacity of the partially-encased composite columns and on the non-linear behavior of the innovative base connections. In the same chapter the experimental data on the behavior of the traditional base connections, bolted plate, and innovative connection, embedded type, are summarized. These results were useful to calibrate the FE models developed on the innovative base connection (embedded) used for the subsequent parametric analysis. The parametric analysis on the FE model and the study with simple analytical model has been allowed to arrive at a formula for the deformation capacity of the base innovative connection. Chapter 6 sets out the criteria used in the design of a composite frame following the national and international standards and summarizes the results of a series of non-linear analyses performed on the designed MRF in order to better understand which parameters influence the deformation capacity of such systems. This last chapter is also devoted to the analysis of nonlinear composite frame in which the plastic capacities were marked with the formulations proposed in the previous chapters. Then, the capacity of the frame so characterized was compared with those calculated with a less innovative approach.

REFERENCES

- American Institute of Steel Construction, “Seismic Provisions for Structural Steel Buildings”, Chicago, IL, USA, 2010.
- CEN Eurocode 4, “Design of composite steel and composite structures. Part 1.1: General rules and rules for buildings”, Eur. Comm. for Stand., Brussels, Belgium, (2008a).
- CEN Eurocode 8. Design provisions for earthquake resistance of structures. Part 1.1: General rules. Specific rules for various materials and elements. Eur. Comm. for Stand., Brussels, Belgium, (2008-b).
- Circolare 2 febbraio n.617, 2009. Istruzioni per l’applicazione delle “Nuove norme tecniche per le costruzioni” di cui al D.M. 14 gennaio 2008.
- Cosenza E., Zandonini R., “Composite Construction, in Handbook of Structural Engineering – W.F. Chen Ed. CRC, 1997.
- Hajjar, J.F., “Composite Steel and Concrete Structural Systems for Seismic Engineering”, Journal of Constructional Steel Research, vol. 58(5-8), 2002, pp. 702-723.
- Min. LL.PP, DM 14 gennaio 2008. Norme Tecniche per le Costruzioni (NTC), Gazzetta Ufficiale della Repubblica Italiana, n.29.
- Pecce, M., Rossi, F., Bibbò, F. A., Ceroni, F., “Experimental behaviour of composite beams subjected to hogging moment”, Steel & Composite Structures An International Journal, Vol. 12, No. 5, 2012.
- Plumier, A., “General report on local ductility. Journal of Constructional Steel Research. 55(1-3), 2004, pp. 91-107.
- Thermou, G. E., Elnashai, A. S., Plumier, A., Doneux, C., “Seismic design and performance of composite frames”, Journal of Constructional Steel Research, vol. 60(1), 2004, pp. 31-57.

CHAPTER 2. THE NON LINEAR BEHAVIOUR OF COMPOSITE BEAMS

2.1 Introduction

The composite beams are generally made by coupling steel profile at the bottom with a slab of reinforced concrete in the upper part, connected through shear stud connectors, which introduce an additional element of variability in the structural behavior of the element.

Depending on the mode of coupling of the two materials, concrete and steel, different types of composite beams (fig. 2.1, 2.2 and 2.3) can be realized. In fact, further the traditional one with a steel profile and a RC slab, other types have the steel profile partially or totally embedded in concrete, allowing for a better cooperation between the two materials due to the increased amount of adherent surface. Despite this solution certainly represents an improvement in performance of the beams with respect to the problems of fire resistance, durability and local and global buckling of the profile, these types are not much used as they clash with the fact that their construction is quite laborious. Thus, from the point of view of construction, the solution with the uncoated beam is the most advantageous, especially when the profiled sheets are used for the slab providing a fast execution and feasibility that are typical of steel structures.

Composite structures, especially composite beams, were born from the idea of optimizing the performance of the two materials, especially when notable spans length is required in buildings or in bridges. Indeed, in a simple pinned beam, under positive bending, it is optimal to address the compression to the concrete and the tension to the steel profile, obtaining a system that is much more rigid than the steel one and also avoiding either the problem of concrete

cracking, typical of RC beams, that the problem of deformability and buckling typical of the steel beams.

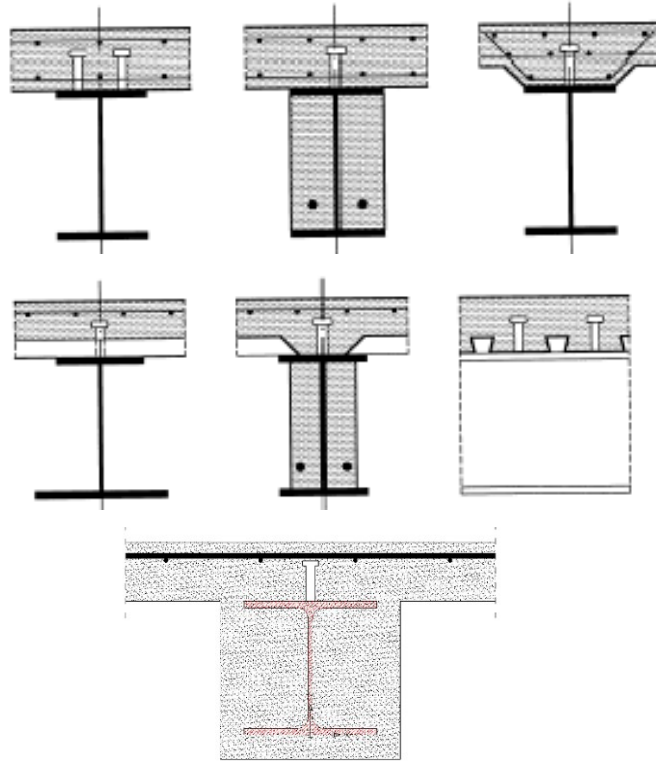


Figure 2.1: Different types of composite beams.

If the first applications of composite structures for bridges and some buildings date back to the late '800 (Cosenza and Zandonini, 1997, Moore, 1988), composite beams experienced a period of strong interest from the world of science and technology from the beginning of the second half of the twentieth century. These issues and the access to the technology of welded studs gave rise to a series of studies (Siess et al., 1951, Siess et al., 1952, Viest et al., 1952, Viest et al 1954) addressed to understand the real capacities in strength and ductility of the composite system.

In the middle of the twentieth century a number of studies were focused on the continuous composite beams of the bridges, most in the United States and

England where many steel bridges had been erected. The adoption of the continuous patterns, clearly, meant to increase the overall performance of the beams especially in terms of deformation, allowing also to develop span lengths even more relevant with respect to the use of a simple pinned scheme. However in the continuous beams the section is stressed by both the sagging and hogging flexural moment, but in the case of composite beams the hogging moment requires tensile stresses in the concrete slab and compressive stresses in the steel profile; these conditions correspond to the worst use of the two materials since concrete has a low tensile strength and the steel profile in compression is sensible to local buckling.

The impetus to the study of this system (Baldwin et al. 1965) occurred in the light of the fact that several bridges with continuous beams exhibited considerable problems of cracking, more than relevant, at the supports with a consequent loss of the continuous scheme and increment of deflections. The excessive cracking compromised the effectiveness of the connection that almost never was made with welded studs but with spirals or steel angles; in addition, at the positive moment region the beams did not show a large ductility and assumed a softening behavior rather than an hardening one as might be expected when the steel is tension because no attention was given to the control of the plastic neutral axis depth to exploit in the best way the low ductility of the concrete and to activate the hardening branch of the steel profile.

From these studies over the years other researchers (Barnard et al., 1965; Johnson et al., 1967) have discussed the possibility of applying the plastic method for the calculation of continuous beams and which type of precautions could prevent secondary phenomena that prevent the full exploitation of the capacities of composite sections.

Other studies such as (Adekola, 1968) were interested in the variability of the effective width in composite beams; these studies have regarded the collaboration of the concrete slab width that is larger than the flange of the steel profile. In Fig. 2.4 the typical distribution of the stresses along the width of the concrete slab, due to the shear lag effect, is represented, underlining the meaning of the effective width that is necessary to introduce in evaluating the resistance and rigidity of the composite beam.

The problem of the effective width still arouses much attention by the research, in fact, some researchers rather recently (Amadio et al., 2002 and 2004, Castro et al., 2007, Nie et al., 2008) have shown, through the development of FEM models based on the few experimental works available, as the effective width in the elastic field is very different from that in the plastic field which is typically greater. The determination of this geometric/mechanical property depends not only on the beam length but also on other parameters: the degree of connection, the thickness of the slab, the type of load, but the codes approaches is usually simple; for example in Fig. 2.4 it is reported the provision of the Eurocode 4 to establish the effective width in a continuous beam, and its value depends on the distribution of the bending moment along the beam.

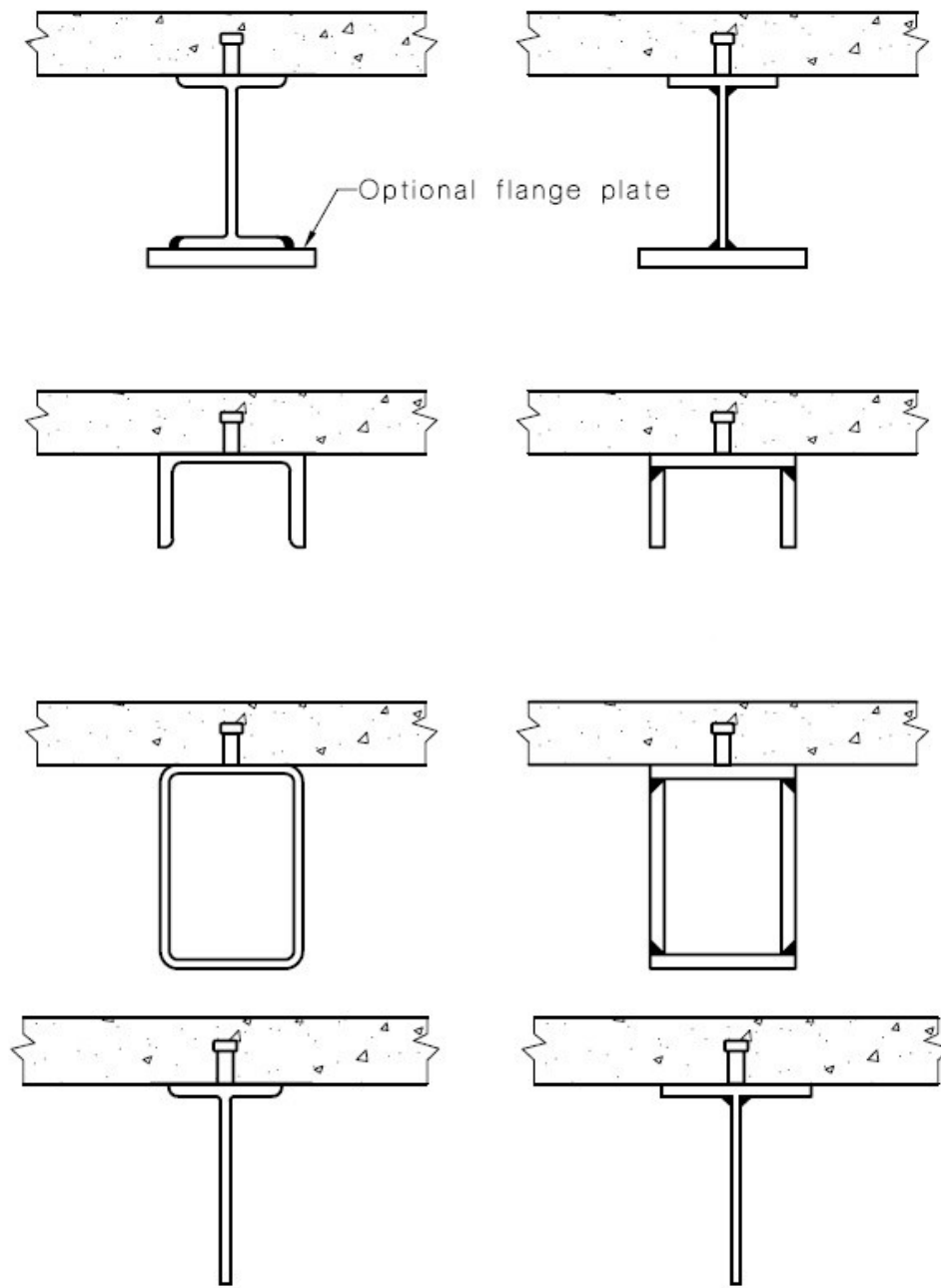


Figure 2.2: Composite beam sections (Australian Standard. AS 2327.1-2003).

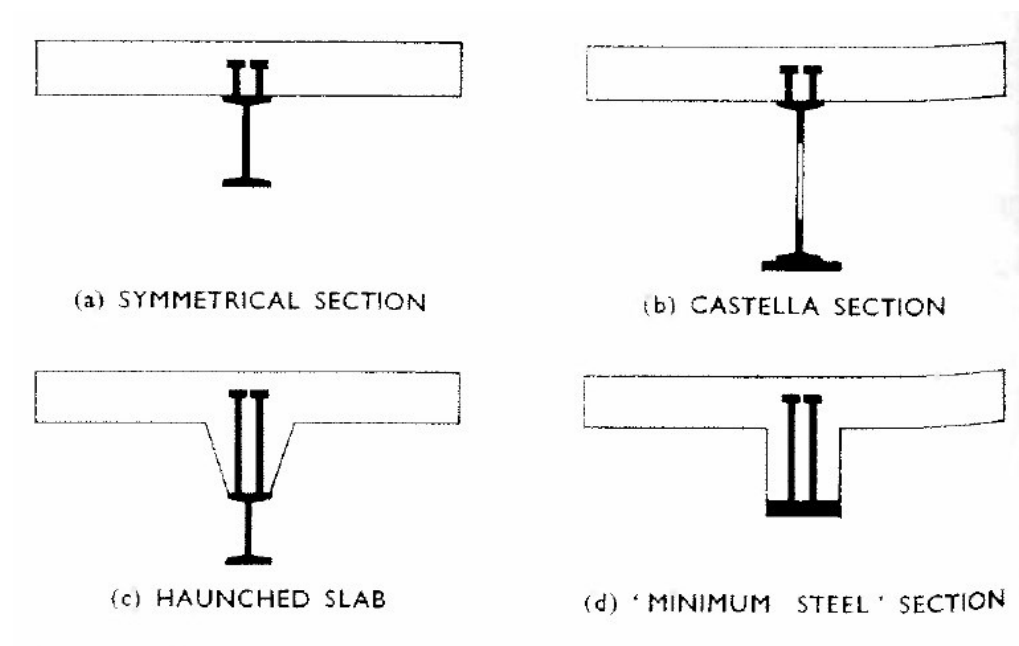


Figure 2.3: Other composite beam types (Chapman, 1964).

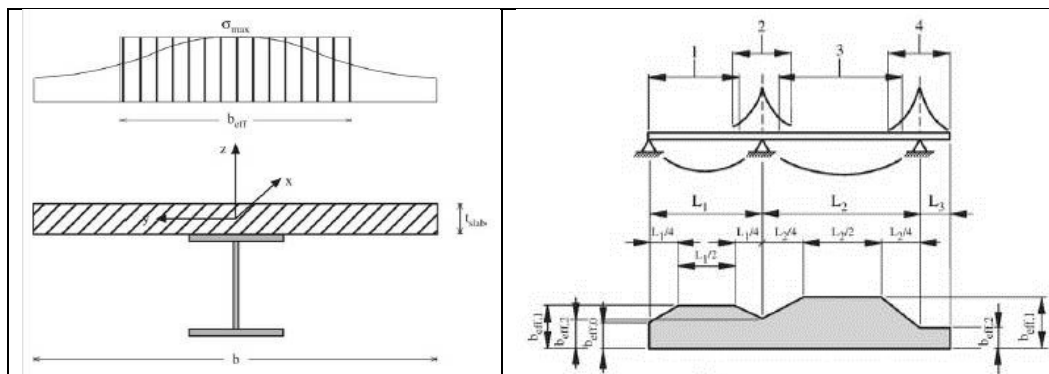


Figure 2.4: Distribution of stresses due to shear lag phenomenon and the determination of the effective width in a continuous composite beam according Eurocode4.

In the following paragraphs the behavior of the composite beams is introduced separating the case of the elements subjected to sagging and hogging flexural moments.

2.2 Behavior of composite beams under sagging flexural moments

Composite beams subjected to sagging moment take the best features of the two components: the concrete structural slab is in compression and the steel profile is in tension.

Typically a composite beam subjected to sagging moment in elastic conditions is characterized by a linear stress distribution as in figure 2.5, where σ_c is the concrete stress, σ_s is the stress in the reinforcing steel bar, and σ_a is the stress in the steel profile; the approach assumes the perfect bond at the slab-profile interface.

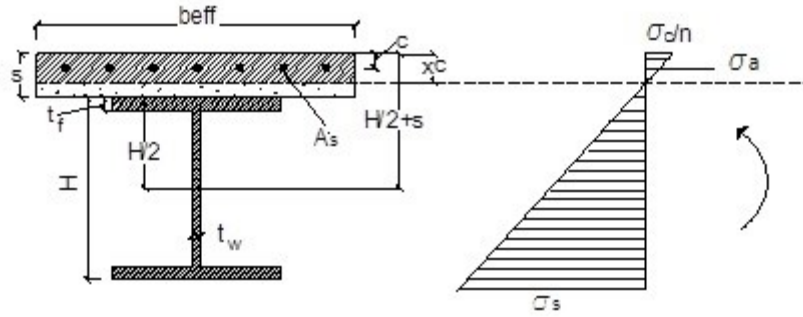


Figure 2.5: Stress distribution under sagging moment (elastic field) when the neutral axis is in the concrete slab.

It is well-known that the position of the elastic neutral axis, x_c , can be evaluated by the translation equilibrium along the beam axis; then the calculation of the inertia of the cracked section, I_2 , is given by the following expression:

$$I_2 = n \cdot b_{eff} \cdot x_c^3 / 3 + A'_s (x_c - c)^2 + I_a + A [H/2 + s - x_c]^2$$

where I_a is the inertia of the steel profile. It is worth to notice that, usually, the neutral axis is located in the slab so that the compression is entirely supported

by the concrete. Using the Navier rule, the following expression can be adopted for evaluating the stresses in the steel or concrete :

$$\sigma = \frac{M}{I_2} y$$

the moment at the yielding can be estimated by fixing the maximum value of σ_s in tension equal to the yielding stress, f_{yd} :

$$M_{Rd} = \frac{f_{yd} \cdot I_c}{(H + s - x_c)}$$

Analogously the stress in the reinforcing bars and in the concrete are evaluated by the following expressions:

$$\sigma'_s = \frac{M_{Rd}}{I_2} (x_c - c) \qquad \sigma_c = n \frac{M_{Rd}}{I_2} \cdot x_c$$

Instead, in the plastic field, the stress distribution of (fig. 2.6), that is a block stress distribution, can be assumed to evaluate the plastic moment, neglecting the steel hardening.

Some studies (Chapman, 1964; Yam et al., 1968; Rotter et al., 1979; Ansourian, 1982) focused on the rotational capacity of a composite beam subjected to positive moment, have shown that this is limited by the low ductility of concrete. Therefore this capacity could be enhanced controlling the depth of the neutral axis; reducing the depth of the neutral axis the strain of the steel profile at the ultimate conditions increases and so the ultimate curvature increases. In (Rotter et al., 1979), after a comparison of numerical and experimental results reported in (Chapman et al., 1964), it was leading a large parametric study with different sets of features such as the strength of concrete and its ultimate strain, up to more than 0,5%, or the yield strength (f_y) of the constructional steel, the size of the concrete slab, the height of the steel joist, the percentage of the reinforcing steel and its arrangement in the slab, the length of the plateau yield strength and hardening modulus.

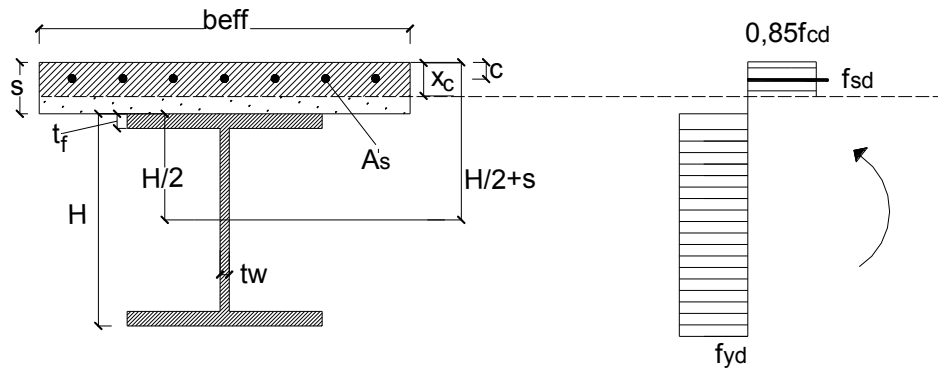


Figure 2.6: Distribution of stresses for plastic bending moment when the neutral axis is in the concrete slab.

The results show that the composite sections subjected to sagging moment can be classified as:

- *strain softening*, when they fail not completely drawing the branch of hardening of the steel joist in tension and their low ductility is governed by the softening branch of concrete in compression;
- *strain hardening*, when they fail drawing the branch of hardening of the steel joist.

It is clear how it is important for the redistribution of moments in continuous beams that the sections assume this second "classification". After these studies, the paper (Ansourian, 1982) reports the study and test results of four composite beams in which it was changed the parameter χ , that is a function of the section geometry and the mechanical properties of the concrete and steel joist; it can be assumed $\chi = 1$ when the depth of the neutral axis at the collapse (Fig. 2.7) is such that the maximum deformation in concrete (ε_{cu}) and the bottom flange of the steel profile reaches the beginning of the hardening branch (ε_{sh}). When this parameter is less than 1 the beams are considered brittle, while become ductile when the value 1 is overcome. For the four beams tested this parameter varies

from 0.65 to 3.0, and the results, (Fig. 2.8), confirm the criterion above mentioned.

It was recommended to adopt a value of χ at least equal to 1.4, which ensures a sufficient ductility for the moment redistribution in continuous beams. However, it should be highlighted that the values of χ have been obtained with a constructional steel characterized by an average deformation ε_{sh} equal to 1.3%.

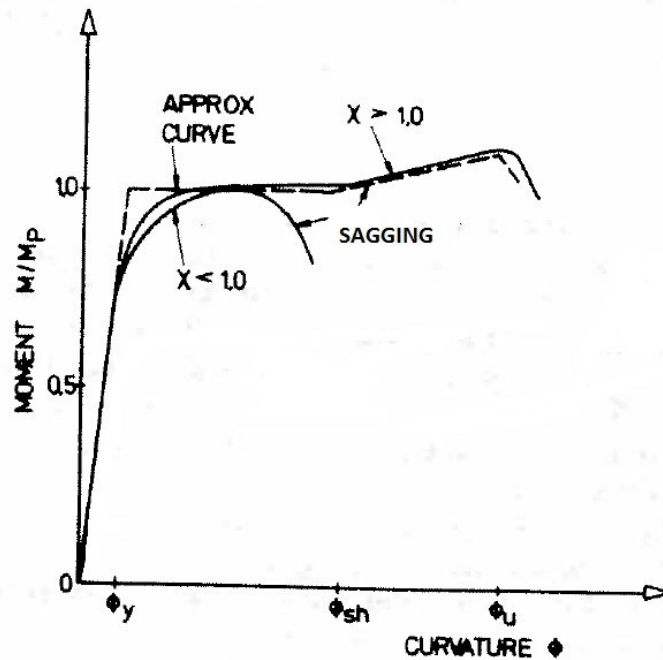


Figure 2.7: Moment-curvature relationships for softening sections ($\chi < 1$) and hardening sections ($\chi > 1$) (Ansourian, 1982).

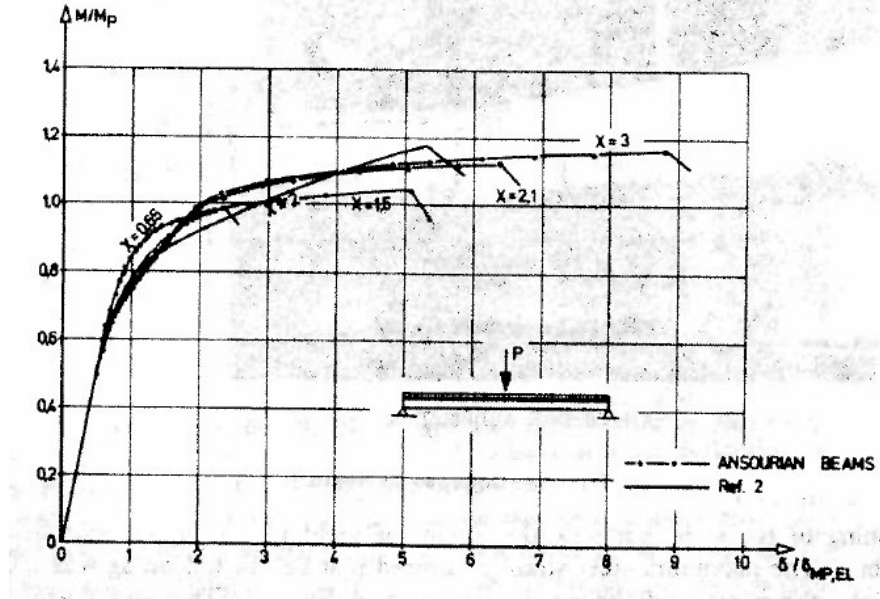


Figure 2.8: The four beams tested where the parameter χ varies from 0.65 to 3.0. The results show how the ductility increases.

Finally, on the basis of numerical results and experimental evidence, a possible expression for the plastic rotational capacity of composite beams subjected to sagging moment was indicated by the author:

$$\theta_{pr} = 2.3\chi - 1.85$$

In (Chapman et al., 1964), it is confirmed again as the ductility of a composite section can be increased by the control of the neutral axis and an adequate percentage of reinforcement in compression. However this reinforcement must be ignored, even in the calculation of the resistance, if it is not well constrained to the buckling by stirrups. In fact, as it happens in a concrete section, even for a composite section the flexural ductility could be enhanced by the reinforcing bars in compression, if well bracketed in order to avoid buckling.

Alternatively, some studies, both in the past (Chapman, 1964) and more recently (Vasdravellis et al., 2012), have been focused on the effect of an axial

force on the capacity of a composite beam under sagging bending moment. In (Vasdravellis et al., 2012) it is highlighted, both experimentally and numerically, such as the collapse mechanism of the composite beam moves from the concrete to the connectors as the tensile axial force increases. Even in (Nie et al., 2004) there are reported numerous tests performed on composite beams subjected to sagging moment but the tests are focused on the contribution of the concrete slab to the shear strength, highlighting how it might increase the resistance of 30-35% respect to that of the steel profile alone.

2.3 Behavior of composite beams under hogging flexural moment

The composite beams subjected to hogging moment do not optimize the exploitation of the mechanical properties of the component materials, on the contrary evidence the typical problems of RC and steel sections.

Firstly in the elastic field the stiffness of the section is much lower than the one of the section under sagging moment due to the cracking of concrete (fig. 2.9).

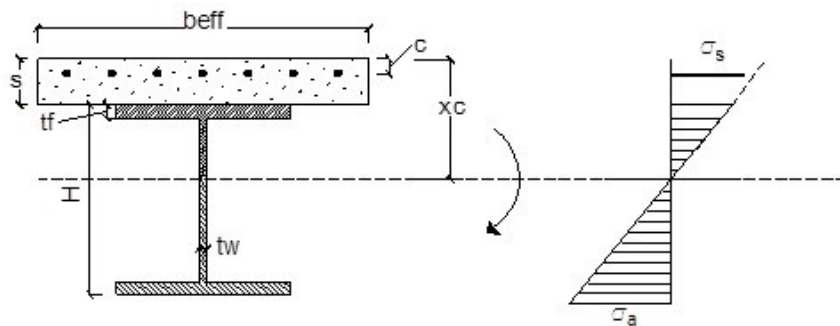


Figure 2.9: Distribution of stresses due to the hogging in the elastic field.

The neutral axis and the inertia, after concrete cracking, can be evaluated as follows:

$$x_c = \frac{(A_s \cdot c) + (b \cdot t_f \cdot s) - [t_w / 2 \cdot (t_f + s)^2] + [t_w / 2 \cdot (H + s - t_f)^2] + [b \cdot t_f \cdot (H + s)]}{A_s + (b \cdot t_f) - [t_w \cdot (t_f + s)] + [t_w \cdot (H + s - t_f)] + (b \cdot t_f)}$$

$$I_2 = A_s (x_c - c)^2 + I_a + A [(H/2 + s) - x_c]^2$$

where I_a represents the inertia of the steel profile.

Therefore the yielding moment can be determined with the same formulation used for the case of sagging moment:

$$M_{Rd} = \frac{f_{yd} \cdot I_2}{x_c}$$

In the plastic field (Fig. 2.10) the rotational capacity in the regions subjected to hogging moment depends on more factors, discussed in the following, than in the case of sagging moment that are degree of connection, percentage of steel reinforcement in tension, mechanical ratio between the reinforcement in tension and the steel profile, the ratio between the span length of the beam and the height of the steel profile.

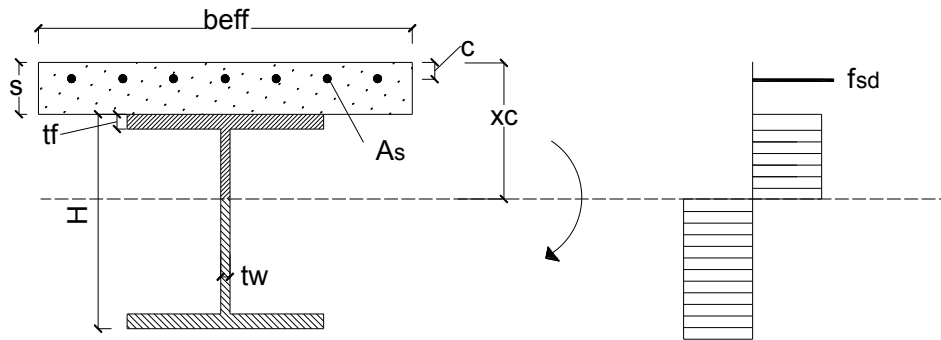


Figure 2.10: Distribution of stresses due to hogging plastic moment.

Conversely to the behaviour under sagging moment, in the case of hogging moment the ductility of the reinforcing bars influences the rotational capacity

of the composite beams as evidenced in some experimental tests when the collapse occurred just after the collapse of the reinforcing bars in tension. In fact, the Eurocode 4 (also NTC2008) prescribes the use of steel reinforcement with high ductility for the design of continuous beams designed by plastic analysis. On the other hand, the recent development of industrial production have led to an improvement of the mechanical properties of the steel for reinforced concrete structures which are also characterized by a high degree of weldability. However, thanks to the new manufacturing technologies implemented, the steel reinforcement currently available on the European market is generally characterized by excellent resistance but, at the same time, by a reduced ductility. The key role of the reinforcement in the development of the rotational capacity of composite beams was pointed out by (Fabbrocino et al., 2001), by a non-linear monodimensional model, calibrated on experimental tests, and used for a numerical analysis; in particular the authors emphasize the following aspects:

- in presence of full shear connections, the main mechanical parameter that influences the plastic rotation is the ultimate strain ε_u of the reinforcing bars as the slip at the interface between slab and steel profile assumes negligible values ;
- in presence of partial shear connections the most important contribution to the rotational capacity is due to the slip at the interface and depends on the sliding capacity of the shear connectors and then the influence of the steel reinforcement is negligible;
- the percentage of reinforcement must meet a minimum value in order to ensure the achievement of the yield strength in the profile flange in compression, at the same time, promoting a wide distribution of plasticization;

-
- the percentage of reinforcement must meet a maximum value in order to limit the depth of the neutral axis; by this way the part of the steel profile in compression is limited and , the local buckling phenomena are controlled;
 - the use of reinforcing bars with small diameters can lightly contributes to increase the ductility trough the distribution of the cracks and the yielding penetration of the reinforcing bars as happens in RC elements;
 - an high ratio f_t / f_y (ratio between the ultimate and the yield strength) of the reinforcing steel allows a high penetration of the yielding between two adjacent cracks.

In other papers (Climenhaga et al., 1972; Hamada et al., 1976; Chen et al., 2007), the parameter that governs the position of the neutral axis was established by the ratio $R = A_s f_{sk} / A_p f_{yk}$,(ie the ratio between the mechanical resistance of the longitudinal reinforcing bars and that of the steel profile). Also in (Loh et al., 2004) the direct influence of this parameter on the local buckling was underlined; increasing its value the collapse occurred with local buckling (Fig 2.11).

The local buckling phenomenon is clearly influenced also by the shape of the profile; the influence of the mechanical and geometrical characteristics of the joist on the local buckling such as on the rotational capacity of composite beams subjected to hogging moment was confirmed by the tests of various researchers (Climenhaga et al., 1972, Johnson et al., 1966; Kemp, 1987; Hamada et al., 1976; Ansourian, 1977).

As well known, the local buckling can be controlled by the values of the local slenderness (width/thickness) of the sub-components of the section (flange and web). In particular the European code (Eurocode 3) (figs. 2.12 and 2.13) identifies 4 classes of profiles corresponding to various performances in terms

of plastic behaviour: profiles of class 1 can develop a high plastic rotation before local buckling occurs, profiles of class 2 can reach the plastic moment and develop a limited plastic rotation, profiles of class 3 do not reach the plastic moment but only the yielding one, profiles of class 4 can have local buckling in the elastic range. The behavior of the profiles of the 4 classes is represented in the graph of figure 2.14, where the typical moment-curvature relationship is drawn.

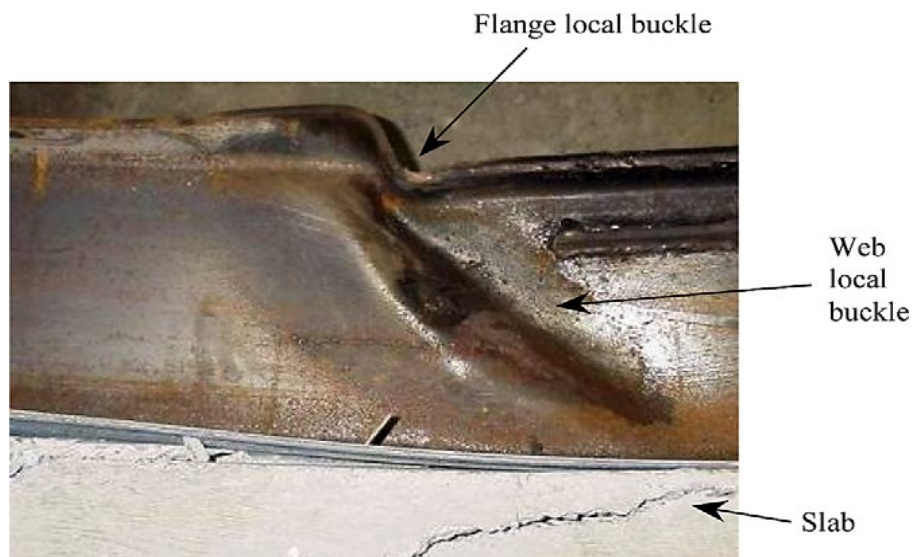


Figure 2.11: Local buckling of the joist in a steel-concrete composite beam (Loh et al., 2004).

Internal compression parts					
Class	Part subject to bending	Part subject to compression	Part subject to bending and compression		
Stress distribution in parts (compression positive)					
1	$c/t \leq 72\epsilon$	$c/t \leq 33\epsilon$	when $\alpha > 0,5$: $c/t \leq \frac{396\epsilon}{13\alpha - 1}$ when $\alpha \leq 0,5$: $c/t \leq \frac{36\epsilon}{\alpha}$		
2	$c/t \leq 83\epsilon$	$c/t \leq 38\epsilon$	when $\alpha > 0,5$: $c/t \leq \frac{456\epsilon}{13\alpha - 1}$ when $\alpha \leq 0,5$: $c/t \leq \frac{41,5\epsilon}{\alpha}$		
Stress distribution in parts (compression positive)					
3	$c/t \leq 124\epsilon$	$c/t \leq 42\epsilon$	when $\psi > -1$: $c/t \leq \frac{42\epsilon}{0,67 + 0,33\psi}$ when $\psi \leq -1^{*)}$: $c/t \leq 62\epsilon(1 - \psi)\sqrt{(-\psi)}$		
$\epsilon = \sqrt{235/f_y}$	f_y	235	275	355	420
	ϵ	1,00	0,92	0,81	0,75

*) $\psi \leq -1$ applies where either the compression stress $\sigma < f_y$ or the tensile strain $\epsilon_y > f_y/E$

Figure 2.12: Table 5.2 from EC3 – Maximum ratio width to thickness for compressed parts in the 4 classes.

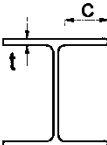
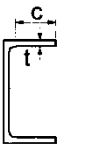
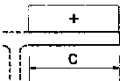
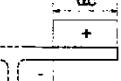
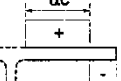

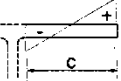
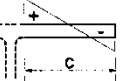
Outstand flanges					
					
Rolled sections			Welded sections		
Class	Part subject to compression	Part subject to bending and compression			
		Tip in compression		Tip in tension	
Stress distribution in parts (compression positive)					
1	$c/t \leq 9\epsilon$	$c/t \leq \frac{9\epsilon}{\alpha}$		$c/t \leq \frac{9\epsilon}{\alpha\sqrt{\alpha}}$	
2	$c/t \leq 10\epsilon$	$c/t \leq \frac{10\epsilon}{\alpha}$		$c/t \leq \frac{10\epsilon}{\alpha\sqrt{\alpha}}$	
Stress distribution in parts (compression positive)					
3	$c/t \leq 14\epsilon$	$c/t \leq 21\epsilon\sqrt{k_\sigma}$ For k_σ see EN 1993-1-5			
$\epsilon = \sqrt{235/f_y}$	f_y	235	275	355	420
	ϵ	1,00	0,92	0,81	0,75

Figure 2.13: Table 5.2 from EC3 – Maximum ratio width to thickness for compressed parts

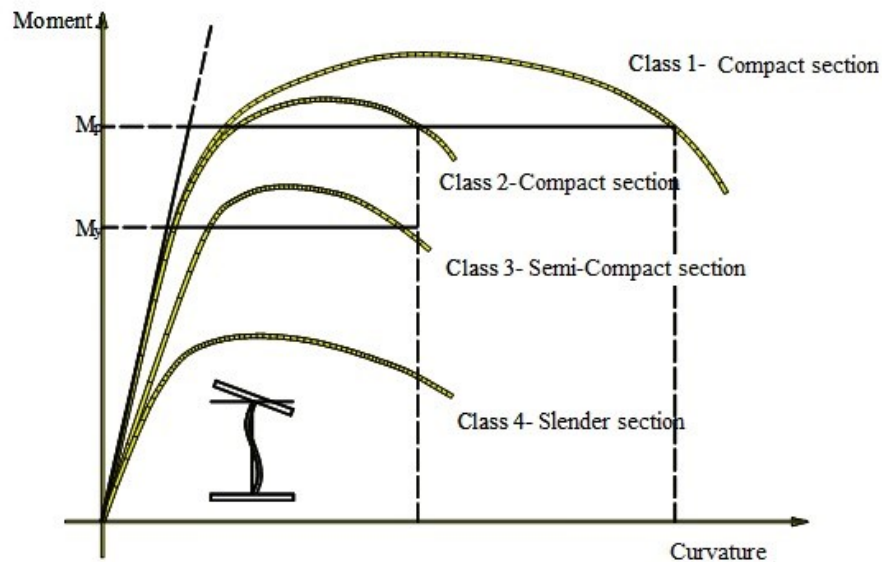


Figure 2.14: Behavior of the steel sections for the 4 classes.

In two papers (Climenhaga et al. 1972 (a) and (b)), an extensive study, experimental and numerical, about the effect of the slenderness of the web and the mechanical R ratio on the plastic capacity is reported. For this purpose, an experimental program on 17 simple supported beams subjected to hogging moment was carried out. Only two beams were realized with the concrete slab while the others were constructed with the steel profile and a steel plate welded at the flange in tension to realize the effect of the reinforcement. Four basic groups (fig. 2.15) were identified depending on the behavior and the rotational capacity recorded. From the figure it can be seen how the buckling phenomenon has an increasing effect on the rotational capacity rising from squat profiles to slender profiles; in fact the beams in group D did not even reach the plastic resistance. The authors, as other authors (Kemp, 1985), explain how the buckling of the flange appears when the yield strength spreads to a length approximately equal to the wavelength, but the rotational capacity is much influenced by the boundary provided by the web; consequently its slenderness and the depth of the neutral axis (i.e. the height of the profile in compression), governed by R ratio, become the factors governing the plastic rotational capacity. Furthermore, the slender sections are more sensible to the lateral buckling that combining with the local one do not allow to reach the plastic resistance. The same authors in the second paper (Climenhaga et al. 1972 (b)), confirm that, depending on the geometrical and mechanical characteristics of the composite beams, one of the two mechanisms of buckling (fig 2.16) can govern but sometimes there is an interaction range.

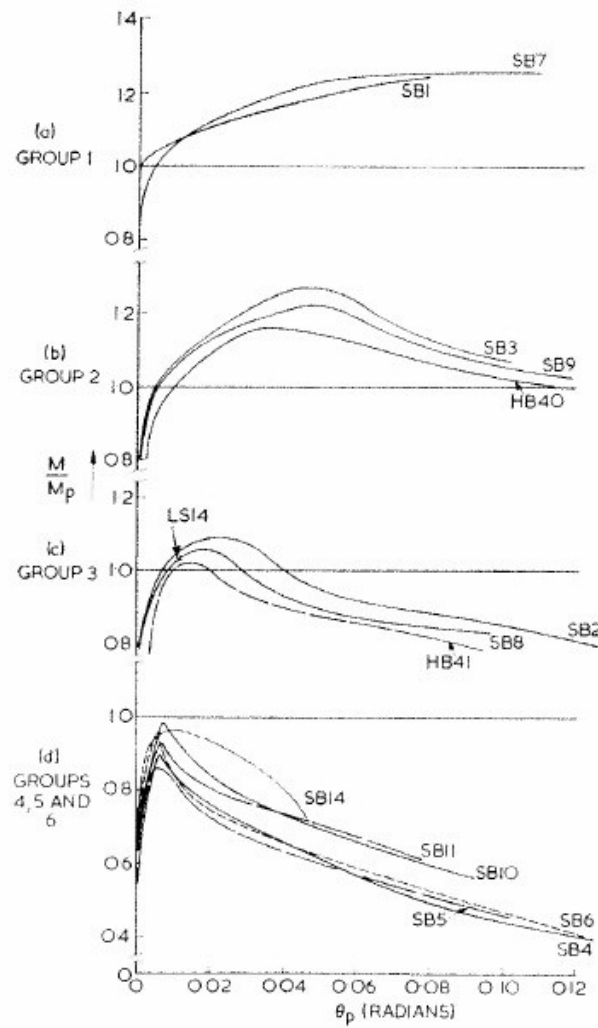


Figure 2.15. Behavior of the composite beams in (Climenhaga et al., 1972).

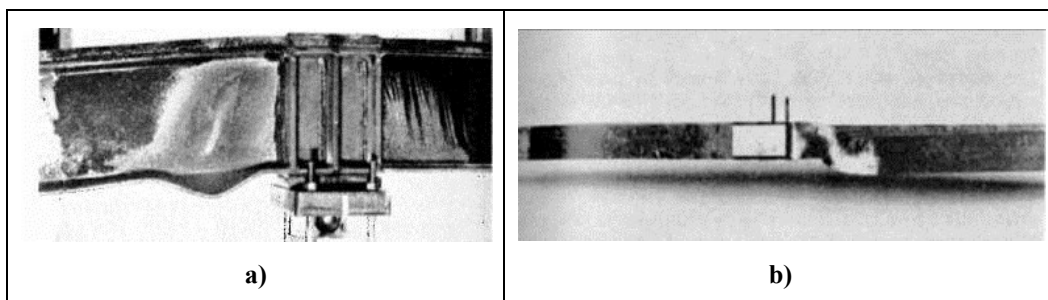


Figure 2.16: Experimental tests of (Climenhaga et al., 1972). a) Local buckling of the flange and web; b) Lateral buckling.

Finally the web buckling can be reduced placing suitable stiffeners (fig. 2.17) at the center of the web, as the comparison of results on beams with and without stiffeners confirm. This technique of "reinforcement" is shown and recommended also in (Kemp, 1987).

Another geometrical parameter is the ratio H_p/L , between the height of the steel beam and the beam span, that is a measure of shear-bending interaction; in fact, experimental researches (Johnson et al. , 1972) have shown that this ratio plays an important role because it directly affects the buckling of the web. In the case of the experimental program cited the ratio was varied from 0.07 to 0.28 but had no effect or influence on the response of the web.

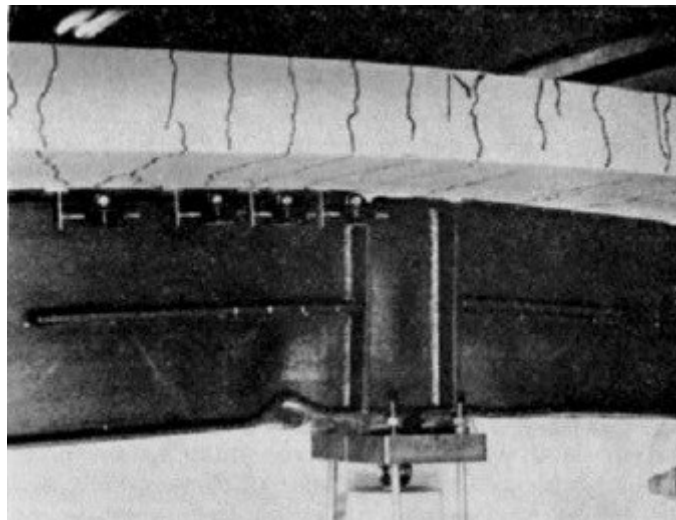


Figure 2.17: Local buckling of the flange and web in the case of stiffened web (Climenhaga et al., 1972).

In (Nie et al., 2008), for three composite beams tested under hogging moment the R ratio was varied in order to assess its influence and show how the beam with the highest R is the less ductile.

Similarly in (Chen et al., 2007) a simple formulas is proposed for calculating the rotational capacity of composite beams subjected to hogging bending

moment as a function of the ultimate strain of the steel profile in compression. For the evaluation of this ultimate strain, it was focused the attention again on the factor R . So the ultimate strain becomes a function of R ratio and the rule is:

$$\varepsilon_{su} = \frac{3000 \cdot 10^{-6}}{R + 0.05}$$

Another expression for the ultimate strain of steel in compression is given in (Kemp, 1985); the author summarizes the work of other authors (Stowell, 1950, Lay et al., 1965 and 1967; Southward, 1969) and returns the following formulation:

$$\varepsilon_c = 1.33 \left(\frac{t_f}{b_f} \right)^2 + 6.6 \left(\frac{t_f}{l_p} \right)^2$$

The above equation enables the theoretical prediction of the critical stress, σ_{cr} , leading to the local buckling of the compressed flange plate that has a direct influence on the rotational capacity. The main difficulties in the theoretical approach to the evaluation of the critical stress of the flange plate is that its value depends on the stress state, elastic or plastic, of the web. As an alternative, the use of empirical relationships based upon experimental evidence is justified. By using data from a great number of stub column tests, the following expression is reported in (Kato, 1989 and 1990):

- for H-section members:

$$\frac{1}{s} = 0.6003 + \frac{1.600}{\alpha_f} + \frac{0.1535}{\alpha_w}$$

where:

- $\alpha_f = \frac{E}{\sigma_y} \left(\frac{t_f}{b_f/2} \right)^2$ is the slenderness parameter of the flange;

- $\alpha_w = \frac{E}{\sigma_y} \left(\frac{t_w}{d_w} \right)^2$ is the slenderness parameter of the web;
- $s = \frac{\sigma_{cr}}{\sigma_y}$

Therefore, the theoretical analyses of the local buckling do not take into account the effects due to the stress gradient in the buckled zone, which derive from the longitudinal variation of the bending moment. Also in the formulation of Kato (1989 and 1990) this effect is not taken into account for.

On the basis of the experimental evidence it can be stated that the average length of the zone, where local buckling of the compressed flange occurs, is approximately $1.2b_f$ (Kuhlmann, 1989). Therefore, the influence of the stress gradient on the critical stress depends on the b_f/L ratio. The analysis of the experimental data collected has led, by means of a multiple regression analysis, to the following empirical relationship (Mazzolani et al., 1992):

$$\frac{1}{s} = 0.546321 + 1.632533\lambda_f^2 + 0.062124\lambda_w^2 - 0.602125\frac{b_f}{L} + 0.001471\frac{E}{E_h} + 0.007766\frac{\varepsilon_h}{\varepsilon_y}$$

where:

$$\lambda_f = \frac{b_f}{2t_f} \sqrt{\varepsilon_y}$$

$$\lambda_w = \frac{d_{we}}{t_w} \sqrt{\varepsilon_y}$$

d_{we} is part of the web in compression.

The interaction of the local buckling with global phenomenon of lateral buckling is represented in a model of continuous inverted U frame (U-frame model, Fig. 2.18), inspired mainly to the problems of buckling at the supports of the bridge girders (Bradford et al., 1987). This method is present in some

foreign standard code as AS4100 and also in the (EC4, 2004; Circolare 617/2009) but no rule is reported in the last version of Eurocode 4 for the evaluation of the critical moment. Generally, it was referred to Annex B of the UNI ENV 1994-1-1 (1994); to this regard the formulation of critical moment is the following one:

$$M_{cr} = \frac{k_c C_4}{L} \left[\left(GI_{at} + k_s L^2 / \pi^2 \right) \cdot E_a I_{atz} \right]^{1/2}$$

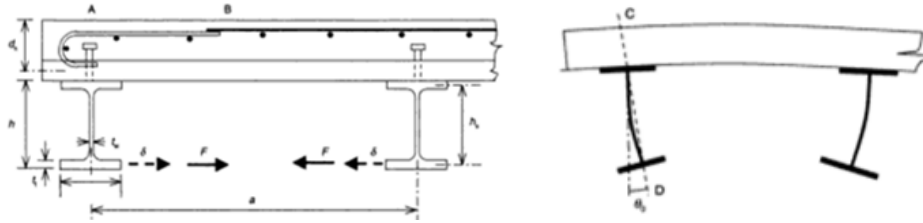


Figure 2.18: Deformed shape for the distortional buckling of the composite beams subjected to hogging moment.

The method of U-frame model is based on the schematization of the flange in compression as a beam loaded with an axial force and bounded at the edge with a bed of translational springs of stiffness K_f , which introduces the constraint due to the web; in fact, as reported also in (Belluzzi, 1982), the stiffness of the springs is given by the out of plane flexural stiffness of the web. So the method is based on an expression of the modified critical load of the flange:

$$N_{cr} = \frac{\pi^2 EI_F}{L^2} + \frac{\alpha L^2}{\pi^2}$$

Noting that the sum of these two terms is constant and equal to αEI_F , and that their sum is minimum when they are equal, it follows that:

$$(N_{cr})_{min} = 2\sqrt{\alpha \cdot EI_F}$$

where α represents the stiffness of the springs and EI_F is the bending stiffness of the flange in its plane.

In (Bradford, 1998), an analytical model is developed to calculate the distortional buckling, extending the U-frame model. In particular, it was emphasized that it is important not only taking into account an elastic constraint continuous to the translation but also introducing a rotational constraint (fig. 2.19), whose role is evidenced by the graphs (fig. 2.20). In the graphs the trend of the critical moment is shown, dimensionless respect to the resistance, two separate beams with the slenderness ratio L/h (10 and 20) versus the stiffness of the rotational constraint (α_z) (fig. 2.20a), and the trend (fig. 2.20b) of the same critical moment versus the slenderness L/h (length/height section) for different values of α_z , according to the U-frame model and according to the solution proposed by the author.

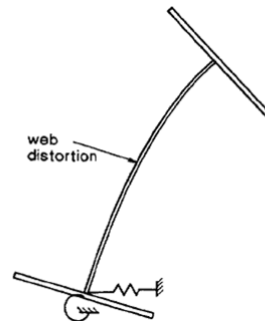


Figure 2.19: Deformed shape due to distortional buckling of an I-section with an elastic constraint.

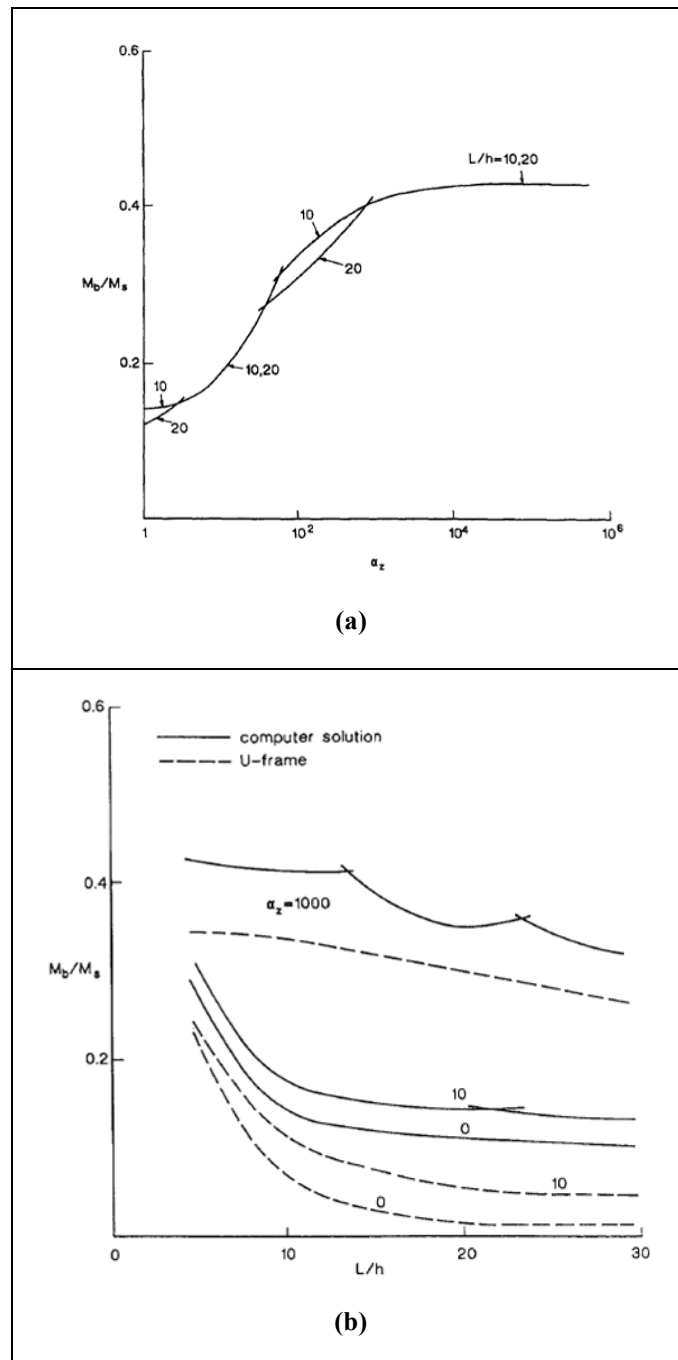


Figure 2.20: Trend of the critical moment versus α_z (a) and L/h ratio, for different values of α_z (b).

The same author (Bradford et al., 2006), regarding the factors that could influence the critical load for distortional buckling evaluate the buckling load varying the main features of the steel joist, K , using an analytical model:

$$K = \sqrt{\frac{\pi^2 EI_{\omega}}{GJL^2}}$$

where E is the Young's modulus, I_{ω} is the warping constant, GJ is the torsional stiffness and L is the free length of the beam. Considering some typical configurations of load and constraint, it was also considered the influence of the other two parameters, α and γ :

$$\alpha = \frac{k_z}{(\pi^2 GJ/L^2)}$$

$$\gamma = \frac{t_w^3 L^2}{6(1-\nu)Jh_w}$$

Where, apart from the symbols already explained, k_z expresses the degree of constraint of the concrete slab on the flange in tension, ν is the Poisson's ratio, h_w and t_w are the height and thickness of the web of the steel profile.

The parameter α , then summarizes the degree of restraint offered by the ensemble stud-flange and concrete slab (fig. 2.21), while γ takes into account the stiffness to the distortional buckling offered by the -flange in compression restrained by the web.

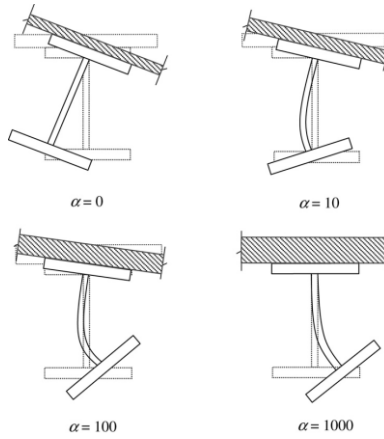


Figure 2.21: Deformed shape varying the α parameter.

The graphs obtained by the parametric analysis evidence how α , apart from the case of distributed load, has a negligible effect on the critical load; in Figs. 2.22, 2.23 and 2.24 the results of the analysis are reported with the critical moment and load non-dimensional with respect to the design nominal strength.

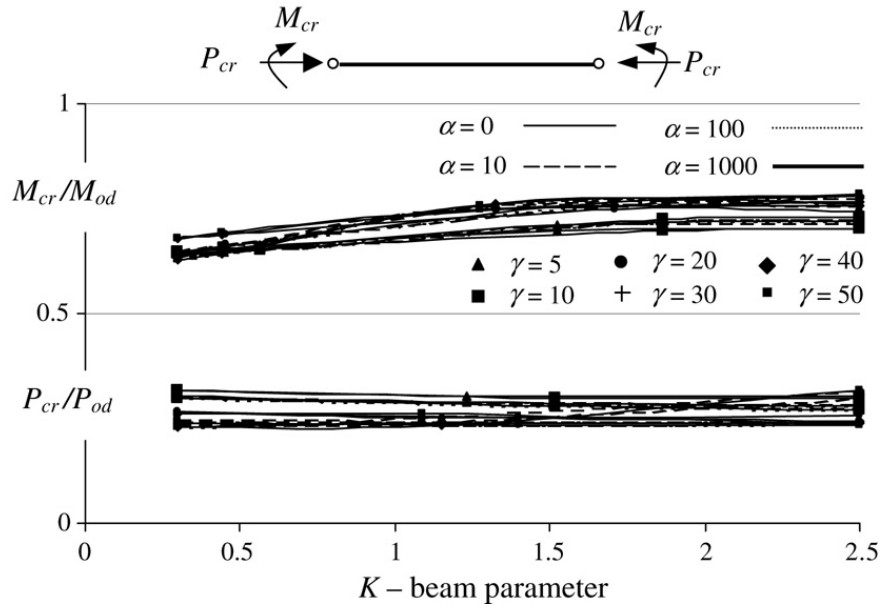


Figure 2.22: Variability of the critical load versus k , α and γ for a constant bending moment.

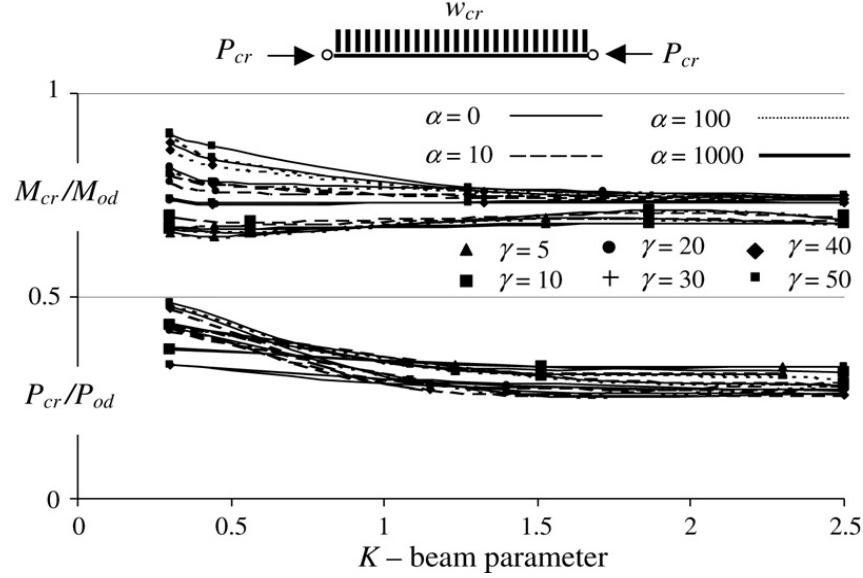


Figure 2.23: Variability of the critical load to vary of k , α and γ for a uniform load

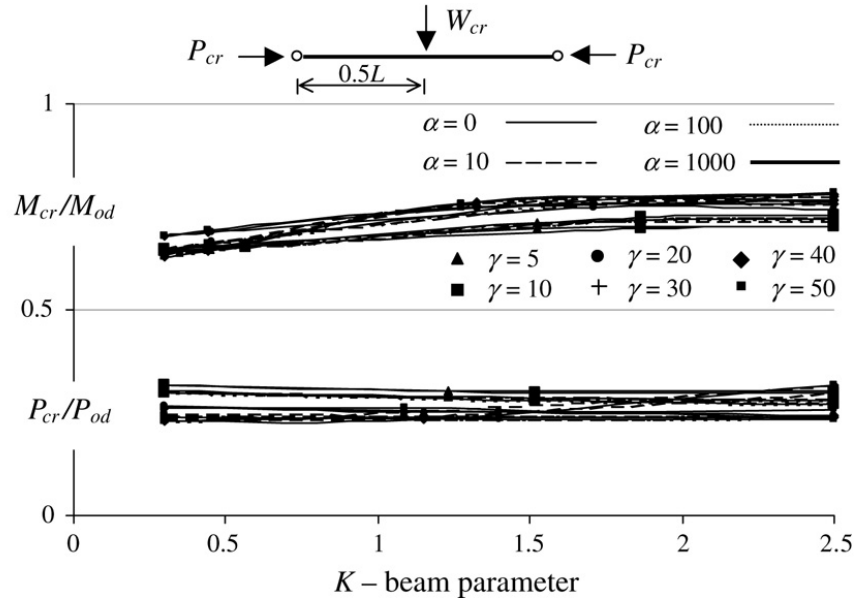


Figure 2.24: Variability of the critical load to vary of k , α and γ for a concentrated load

Apart from this influence of the whole stud-flange in tension and slab, in both papers (Bradford, 1998; Bradford et al., 2006), and also in the U-frame model, the author takes into account the out of the plane flexural stiffness of the web and the flexural stiffness of the flange in compression, perpendicular to the plane of the web (fig. 2.25).

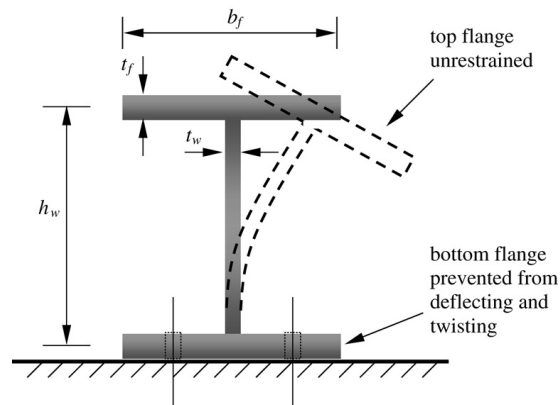


Figure 2.25: Deformed shape for distortional buckling.

Clearly increasing the height of the web (h_w) and considering flanges not very wide (b_f), this stiffness decreases, enhancing the probability of distortional buckling.

To overcome this type of buckling the European standard (EC4) recommends to use oblique steel profiles that inhibit the lateral-distorsional buckling of the flange in compression. This solution was also used in the tests carried out by (Vasdravellis et al., 2012) (fig. 2.26) and the study was focused on the role of the axial force due to the interaction of the steel profile and reinforcement steel on the response of the composite beams subjected to hogging moment. It could be noted that avoiding the buckling of the profile the normal stresses can increase giving the brittle fracture of the bars or the studs.



Figure 2.26: Diagonal bracing for lateral-distortional buckling.

2.4 The role of the shear connection between concrete and steel

One of the factors that influence much the rotational capacity of composite beams under both sagging and hogging bending moment is the connection between the steel profile and the concrete slab. It influences the overall deformability of the composite system and the failure mechanism. Until the early 50's when the stud connectors were introduced, the connections were generally made with spirals, with pieces shaped steel or with elements in C shape. Just in (Viest et al., 1952 and 1954) it is shown a remarkable experimental campaign on various types of connectors (figs. 2.27, 2.28 and 2.29).

The mechanism of failure of the studs (fig. 2.30) could be characterized by the rupture of the weld used for connecting the devices to the steel beam, the crushing of the concrete or the failure of the connectors.

Bul. 405. CHANNEL SHEAR CONNECTORS AND COMPOSITE T-BEAMS

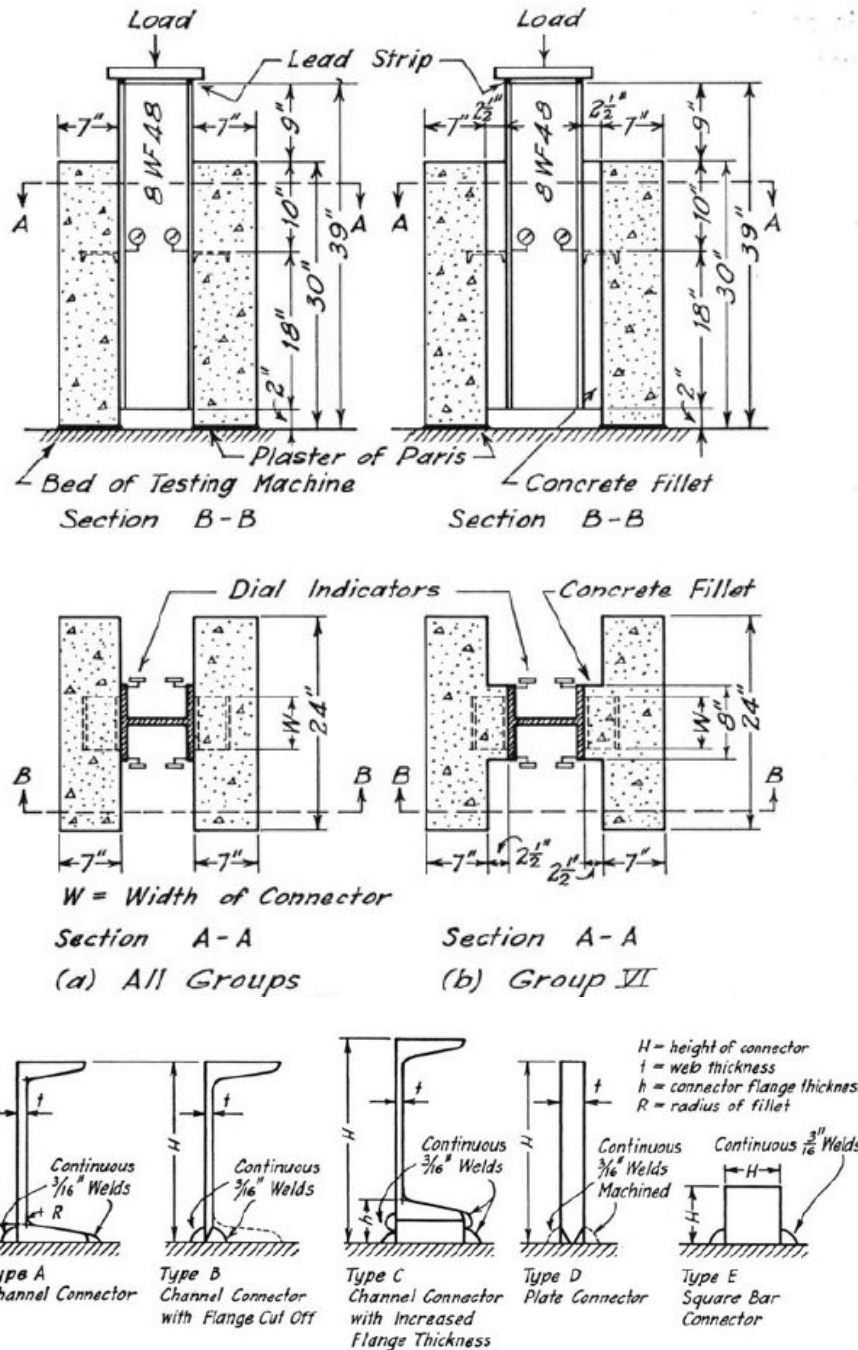


Figure 2.27: Test scheme and connectors type (Viest et al., 1952).

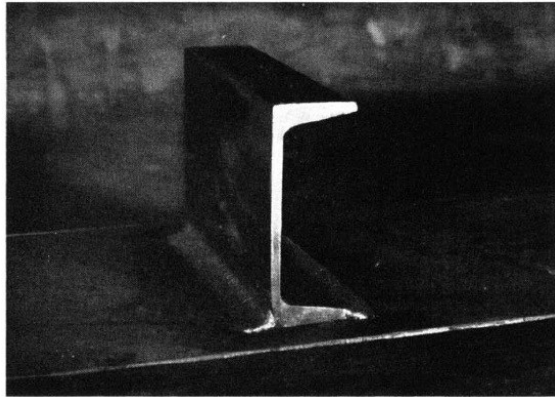


Figure 2.28: Channel type connector.

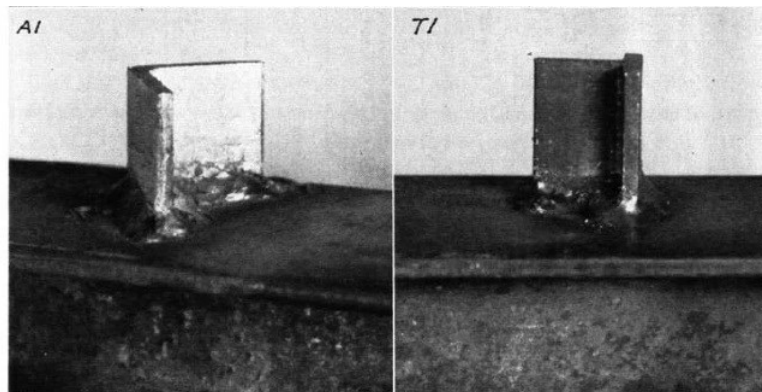


Figure 2.29: Shear connectors type (Viest et al., 1954).

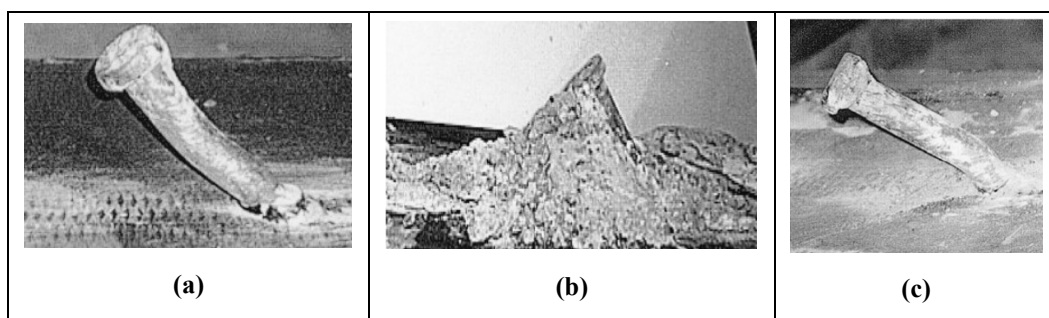


Figure 2.30: Different failure mechanism of the shear studs, (a) weld failure, (b) concrete failure, (c) ductile failure.



Figure 2.31: Interface sliding between joist-slab of a concrete-steel composite beam.

The two former mechanisms are characterized by the sudden drops of the resistance, a brittle failure, while the latter, due to the ductility of the steel of the connectors, is more ductile. The behaviour of the studs is also influenced by the different stress conditions that the concrete slab could experience. The possibility of a stiffness reduction for shear connectors in cracked regions is suggested in (Johnson et al., 1969) and may be modeled generalizing the P– s relationships as follows:

$$P = \psi_1 \cdot P_{max} \cdot (1 - e^{-\psi_2 \cdot \beta_2 \cdot s})^{\alpha_c} \Rightarrow k(s) = \frac{\psi_1 \cdot P_{max}}{i_c} \cdot \frac{(1 - e^{-\psi_2 \cdot \beta_2 \cdot s})^{\alpha_c}}{s}$$

where ψ_1 and ψ_2 are two coefficients not greater than 1 (fig. 2.32). Coefficient ψ_2 only results in a decrease of secant stiffness without reducing the asymptotical value P_{max} ; on the contrary, coefficient ψ_1 mainly affects the maximum load. Both coefficients could be assumed on the basis of the experimental tests reported in (Johnson et al., 1969).

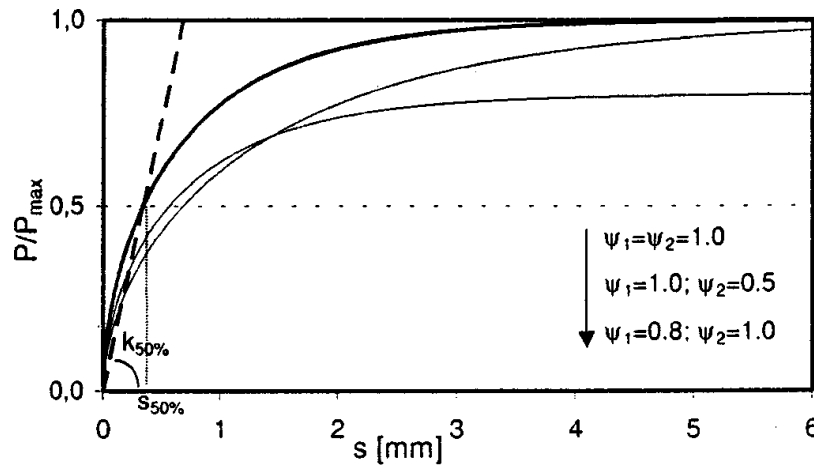


Figure 2.32: P-s relationships for connectors.

Other studies gave attention to the use of connections with studs (Chapman et al. 1964; Johnson et al. 1967), their strength and ductility and the most suitable distribution to be taken, according an elastic or plastic behaviour (fig. 2.33 and 2.34). In (Yam et al. 1968) it is reported a numerical-experimental comparison on the effect of the distribution of the studs along the beam; it is evident that in the beams with connectors distribution according to the shear trend (elastic behaviour of the connection), the slips are more relevant near the median line and lower at the supports when the loading levels are low. While in the case of constant spacing according to the plastic theory, the slips are almost constant along the span length of the beam. Consequently, in the case of distribution of the shear studs according to the elastic theory the connection can suddenly collapse in the central part of the beam reducing the rotational capacity of the beam.

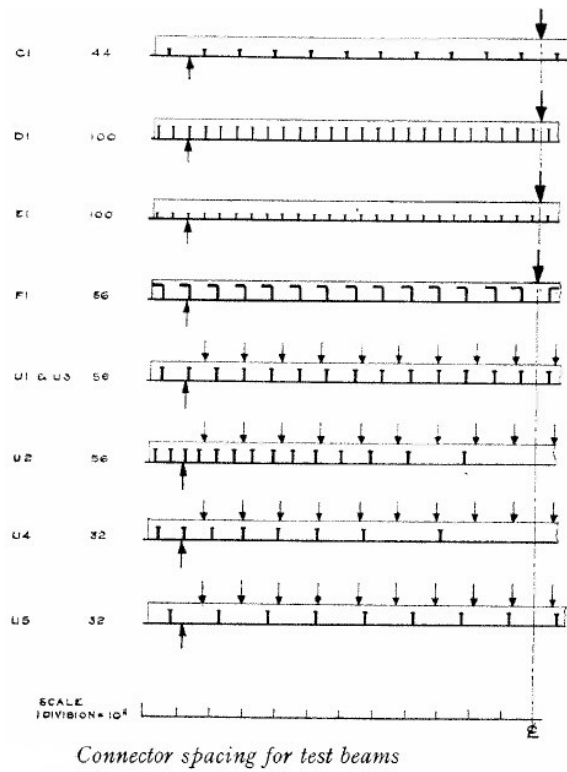


Figure 2.33: Different distribution of the connectors studs (Chapman et al., 1964).

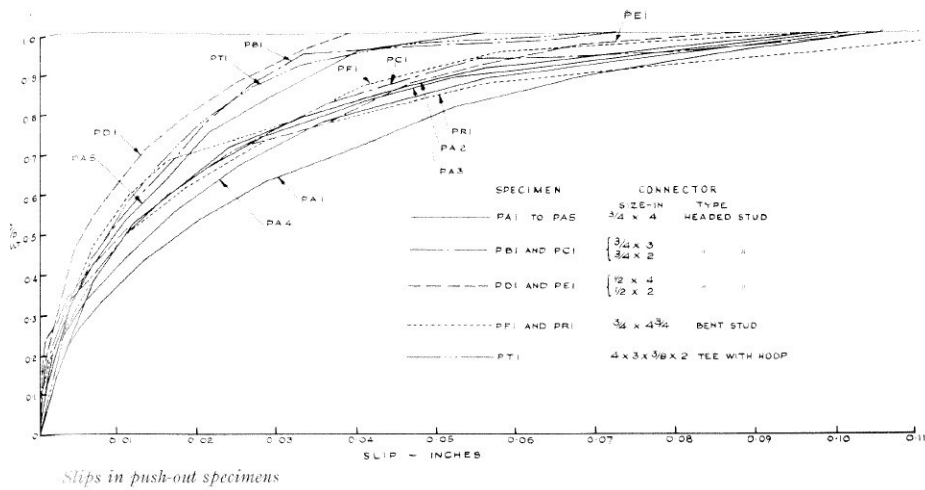


Figure 2.34: Results of the push-out tests on connectors studs (Chapman et al., 1964).

In conclusion if the beam can reach the plastic resistance it is necessary that also the connection has a plastic behaviour and distribution.

Another concept has to be introduced for the beams that reaches the plastic moment, that is the one of the partial and full connection. The number of connectors that realizes the full connection, N_f , is the one necessary to the transfer of the maximum plastic force between the steel profile and the concrete slab, more connectors cannot enhance the resistance of the section; the partial connection is realized with a number of connectors, N , lower than that required one for the full connection, therefore the plastic moment cannot be attained and the strength of the beam is related to the failure of the connection.

In particular, the mechanical characteristics of the connection between the steel profile and the slab are synthetically expressed by the parameter N/N_f , which represents the ratio between the number N of connectors present along the composite beam and the number N_f of connectors strictly necessary to ensure the full recovery of the bending resistance. The dependence of the plastic rotation of the beam on the level of interaction and geometry of the connection can be summarized as follows:

- in the case of shear connection for full recovery of resistance ($N/N_f \geq 1$) (FCS, ie Full Connection Strength) the collapse of the beam occurs as a result of different phenomena (such as the buckling of the steel profile, the fracture of the reinforcement of the slab, etc..) excluding the failure of the connectors. Consequently, in such cases the dependence of the rotational capacity of the plastic hinges can be attributed to the characteristics of the remaining components of the composite beam section;

- in the case of connection for partial recovery of strength ($N/N_f < 1$) (PCS, ie Partial Connection Strength) the collapse of the beam can also occur for the crisis of the connectors as a result of their collapse (brittle or ductile as shown in fig. 2.30) or excessive slips (as shown in fig. 2.31).

In the field of the partial shear connection the influence of the arrangement of connectors on the rotational capacity of plastic hinges is negligible but the calculation of the deformation becomes more complicated; in fact the slips at the interface between the slab and the steel profile needs to be considered by the introduction of equations of equilibrium and congruence. The scientific contributions to the correct evaluation of the role, both in the elastic and plastic field, of the partial interaction both on the resistance and deformability are numerous, and approach the subject by both numerical and experimental studies (Newmark et al., 1951; Dai, 1963; Cosenza et al. 1997, Gattesco, 1999; Amadio et al., 2012); other papers evidence the efficiency of the shear connection under different conditions depending on the details of construction and position (fig. 2.35) of the stud connectors (Barnard et al., 1965; Ranzi et al., 2009); others researchers (Johnson et al., 1967; Ollgaard et al. 1971) (fig. 2.36) focused on the characterization of the shear force-slip relationship of the connectors to be used in any numerical analysis. Some researchers studied the effect of the resistance of the studs on the ductility of the composite beams (Oehlers et al. 1995) (fig. 2.37).

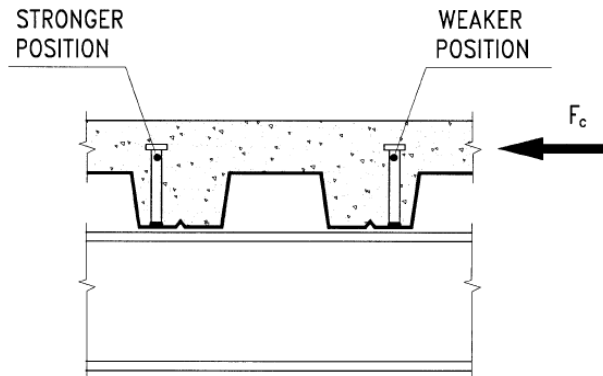


Figure 2.35: The influence of different position of the stud on the response of connection.

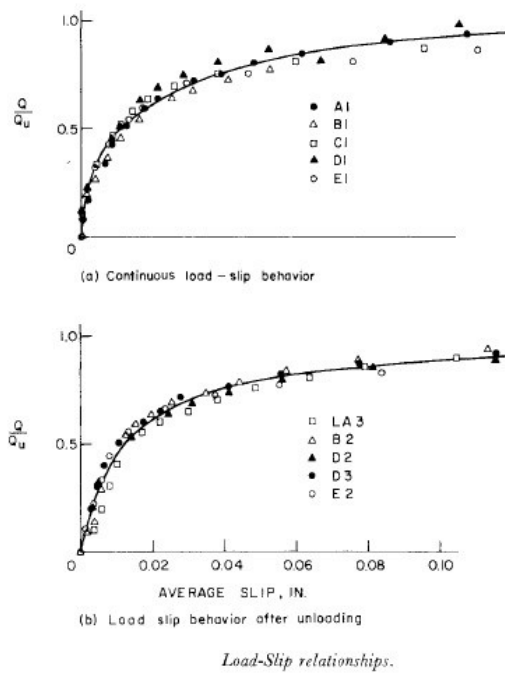


Figure 2.36: Force-slip relationship of shear connectors (Ollgaard et al., 1971).

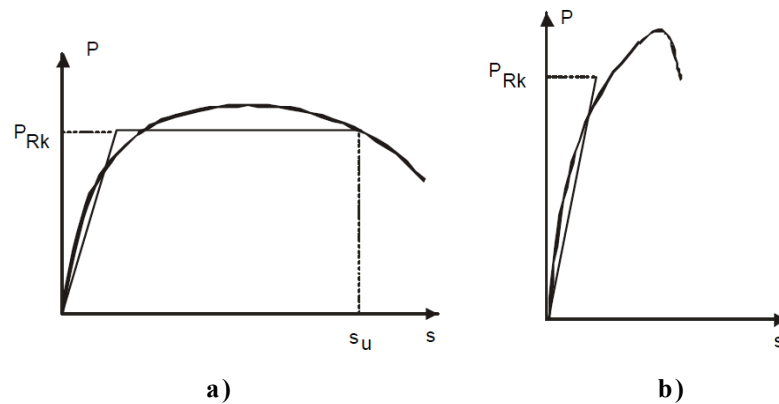


Figure 2.37: Different behavior of shear connectors: a) ductile; b) brittle.

2.5 Experimental data on the rotational capacity

In this paragraph it is synthesized the state of the art of experimental tests on composite beams subjected to sagging and hogging moment in order to have information about the plastic rotational capacity. The steel profiles used are double-T and have an height ranging between 180mm and 360mm with concrete slabs, either with full slab and profiled sheets, with width between 515mm and 1600mm and average height about 120mm . The reinforcement percentage of the slabs is below 2% for most cases; all the specimens have been arranged with adequate transverse reinforcement against the local problems due to the action of concentrated studs. The degree of connection is equal to a minimum of 0.33 to a maximum of 1.85 with a variation that emphasizes the great influence of the connection on the performance of the beams. In all cases stiffener plates at the points of application of the loads were welded to the web to reduce the local buckling. The lengths range of the beams is between about 2.0m and 5.5m. The most part of these various experimental programs (Climenhaga et al., 1972; Hamada et al., 1973; Kemp et al., 1995; Dekker et al., 1995; Amadio et al., 2004; Fabbrocino et al., 2001; Loh et al., 2004; Nie et al., 2008; Pecce et al., 2010) regards the behavior of composite

beams subjected to hogging moment while other experimental tests (Chapman et al., 1964; Mallick et al., 1975; Barnard, 1975) regards the effect of sagging moment. The tests were carried out on simply supported beams loaded to obtain hogging and sagging moment, therefore the plastic rotation was measured when the rotation at the supports after the plasticity was reached in middle of the element; in other cases the tests were developed on continuous beams evaluating the plastic rotation at the central support. According to the topics illustrated in the previous paragraphs it was identified a set of parameters representative of the strength and ductility of steel-concrete composite beams with respect to which the list of the experimental results is performed:

- the ratio $M_{pl} / M_{pl,a}$, which represents the over-strength, in terms of ultimate moment, of the steel-concrete composite beam with respect to the steel profile alone;
- the ratio $R = (A \cdot f_y)_r / (A \cdot f_y)_a$, which compares the resistance of the reinforcement (subscript r) with that of the steel profile (subscript a). This parameter is useful to identify the position of the neutral axis of the section and, therefore, the portion of the joist subjected to compression in order to estimate the possible buckling of the steel profile that could affect the rotational capacity;
- the ratio L / H_{tot} , which is a global parameter of slenderness of the member being L the distance between the supports and H_{tot} the height of the composite beam;
- the ratio $(f_t / f_y)_r$, which represents the over-strength of the reinforcement bars;

-
- the ratio $(\varepsilon_u / \varepsilon_y)_r$ between the ultimate strain and the yield strength of the reinforcing bars, significant for the ductility of steel;
 - the ratio N / N_f , which represents the degree of the shear connection, as mentioned above;
 - the parameter ρ , which represents the geometric percentage of the reinforcement in the slab;
 - the ratio H_p / B , which represents the degree of slenderness of the steel section for the lateral buckling;
 - the ratios b_f / t_f and h_w / t_w , which represent the slenderness of the sub-components of the steel section that control the local buckling phenomena;
 - the parameter L_v is the shear span length, equal to the ratio of the bending moment to the shear force, M/V , or, geometrically, the distance between the point of maximum moment and the point where the moment is zero; it could take into account the influence of the moment gradient;
 - H_p is the height of the steel profile;
 - The ratio L_v/H_p , is a parameter that takes into account the ratio between the shear and moment, since the shear force could influence the buckling of web.

In the Table 2.1 the experimental results on the rotational capacity in hogging moment region obtained by various authors are summarized. The plastic rotation is calculated as the difference between the ultimate rotation, in correspondence of a load equal to 85% of the maximum detected on the descending branch of the load-displacement curve, and the rotation at yielding. According to the study reported in (Kemp, 1986) the Table 2.1 takes into account for the parameters directly linked to the local buckling phenomena and

the global slenderness of the composite element. The importance of these parameters are also discussed in (Bradford et al., 2000) that reviewed the research regarding the local and lateral-distortional buckling, and its interaction, in the hogging moment region of continuous composite beams, and provided design proposals.

Experimental tests		PARAMETERS													
		θ_{pl} [mrad]	P1	P2	P3	P4	P5	P6	P7	P8	P9	P10	P11	P12	P13
			$M_{pl}/M_{pl,a}$	$A_r \cdot f_{y,r}/A_p \cdot f_{y,p}$	L/H	$(f_t/f_y)_r$	N/N_f	ρ [%]	$(\varepsilon_u/\varepsilon_y)_r$	H_p/B	b_f/t_f	h_w/t_w	L_v mm	H_p mm	L_v/H_p
Climenhaga and Johnson (1972)	SB1	80		0.38	0.07		>1			1.67	4.22	23	1880	127	14.80
	SB7	112		0.42	0.1		>1			1.67	4.22	23	1270	127	10.00
	SB3	102		0.45	0.11		>1			1.52	6.69	31	1880	203.2	9.25
	SB9	119		0.45	0.16		>1			1.52	6.69	31	1270	203.2	6.25
	HB40	120		0.42	0.16		>1			1.52	6.69	31	1270	203.2	6.25
	SB2	68		0.42	0.11		>1			1.52	7.90	33	1880	203.2	9.25
	SB8	52		0.42	0.16		>1			1.52	7.90	33	1270	203.2	6.25
	HB41	52		0.27	0.2		>1			2.50	7.10	40	1270	254	5.00
	SB14	40		0.27	0.24		>1			3.00	4.70	46	1270	304.8	4.17
	SB4	24		0.37	0.16		>1			3.00	6.65	50	1880	304.8	6.17
	SB10	20		0.29	0.24		>1			3.00	6.65	50	1270	304.8	4.17
	SB5	20		0.44	0.19		>1			2.80	7.10	56	1880	355.6	5.29
	SB11	27		0.23	0.28		>1			2.80	7.10	56	1270	355.6	3.57
	SB6	18		0.38	0.22		>1			3.05	7.96	62	1880	406.4	4.63
Hamada (1973)	CB2	8		0.42			>1	1.6		1.88	8.2	58	1630	306	5.33
	CB3	25		0.42			>1	1		1.86	10.7	50	1630	310	5.26
Fabbrocino et al. (2001)	A1	164	1.27	0.14	12	1.16	1	0.6	52	1	10.1	14.35	1805	180	10.03
	B1	145	1.27	0.14	12	1.16	1	0.6	52	1	10.1	14.35	1805	180	10.03
Kemp et al.	MR2	3	1.3	0.17	8.98	-	1	0.3	10	3	6.7	49.5	1830	300	6.10

(1995)	LR2	25	1.28	0.15	13.4	-	1	0.3	10	3	6.7	49.5	2745	300	9.15
	SR	21	1.16	0.08	4.5	-	1	0.3	13	3	6.7	49.5	915	300	3.05
	LSR	49	1.37	0.26	13.6	-	1	0.5	4	3	6.7	49.5	2645	300	8.82
	SSR	60	1.38	0.26	4.5	-	1	0.5	4	3	6.7	49.5	915	300	3.05
Loh et al. (2004)	CB1	31	1.99	0.35	6.79	1.27	0.83	2	85	2	7.4	46.4	1250	248	5.04
	CB2	158	1.99	0.35	6.79	1.27	0.5	2	85	2	7.4	46.4	1250	248	5.04
	CB3	152	1.99	0.35	6.79	1.27	0.33	2	85	2	7.4	46.4	1250	248	5.04
	CB4	11	1.99	0.35	6.79	1.27	0.83	2	85	2	7.4	46.4	1250	248	5.04
	CB5	64	1.99	0.35	6.79	1.27	0.5	2	85	2	7.4	46.4	1250	248	5.04
	CB6	92	1.99	0.35	6.79	1.27	0.33	2	85	2	7.4	46.4	1250	248	5.04
	CB7	166	1.48	0.17	6.79	1.27	1	1	85	2	7.4	46.4	1250	248	5.04
	CB8	28	2.32	0.52	6.79	1.27	0.88	2.9	85	2	7.4	46.4	1250	248	5.04
Amadio et al. (2004)	B1	87	1.45	0.18	12.7	1.29	1	1	10	1	10.1	14.35	1600	180	8.89
	B2	110	1.45	0.18	12.7	1.29	1	1	10	1	10.1	14.35	1600	180	8.89
Nie et al. (2008)	SB6	72	1.47	0.23	11.6	1.47	1.85	0.6	154	2	4.08	25.31	1800	200	9.00
	SB7	67	1.66	0.36	11.6	1.47	1.16	1	154	2	4.08	25.31	1800	200	9.00
	SB8	58	1.78	0.5	11.6	1.47	0.84	1.4	154	2	4.08	25.31	1800	200	9.00
Pecce et al. (2010)	Beam 1	35	1.29	0.12	8.16	1.26	0.9	0.6	57	2.1	4.96	37.3	2000	360	5.56
	Beam 2	41	1.29	0.12	8.16	1.26	1.3	0.6	57	2.1	4.96	37.3	2000	360	5.56
	Beam 3	40	1.29	0.12	8.16	1.26	1.6	0.6	57	2.1	4.96	37.3	2000	360	5.56
	Beam 4	45	1.42	0.19	8.16	1.26	1.1	0.8	57	2.1	4.96	37.3	2000	360	5.56

Table 2.1: Main experimental results by various authors on rotational capacity in hogging moment region

From the Table 2.1 it is possible to obtain any consideration on the rotational capacity in hogging regions. The experimental tests provided by Climenhaga et al. (1972) are focused on the role of the local buckling of the web (parameter P10) and its relation with the mechanical ratio between the reinforcement bars and the steel profile (parameter P2). From these data it is possible to observe how increasing the slenderness of the web there is the decreasing of the rotation. In the figure 2.38 this trend is reported.

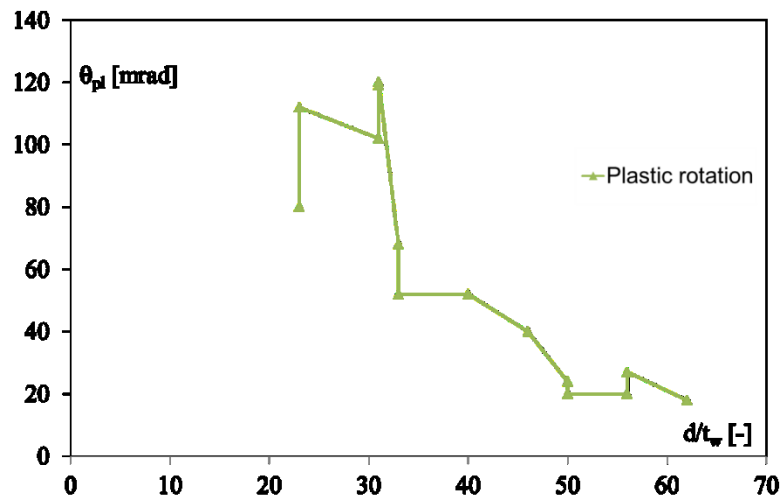


Figure 2.38: The variation of the plastic rotation versus d/t_w ratio for the composite beams experimented in Climenhaga et al. (1972).

Also in Hamada et al. (1973), the experimental program was focused on the role of local buckling and an high slenderness of web was adopted for the specimens. The consequence was a low value of the rotational capacity.

Basing on the experimental tests the plastic rotation, θ_{pl} , assumes lower values for both low slenderness of the beam (due to the reduced rotation permitted by a stocky beam) and high slenderness (due to the onset of buckling). It seems that the parameter ρ reduces the plastic rotation when it assumes excessively low or high values; this result is typical of RC elements in which great amounts of reinforcement reduce the yielding propagation in the steel reinforcement, and small amounts can produce brittle failures during cracking. On the

contrary, the over-strength $(f_u/f_y)_r$ does not seem to be a significant parameter for the examined composite beams because high values of this ratio have always been used. Regarding the effect of the partial shear connection, θ_{pl} decreases when the degree of the connection increases. Finally, an increase in the ratio $(\varepsilon_u/\varepsilon_y)_r$ implies, in general, an increment in the plastic deformation of the composite beams; however, it is no more influential when a certain value is exceeded.

2.6 The available formulations for the estimation of the rotational capacity

The implementation of the non-linear analysis of frame structures by the approach with lumped plasticity requires the evaluation of the moment-rotation law i.e. the knowledge of the plastic rotational capacity. This knowledge is quite advanced for the reinforced concrete structures and steel ones, which can rely on a significant amount of experimental data and analytical studies. On the other hand for the composite beams the situation is quite different, and the lack of data, in the case of a problem affected by many variables, makes very hard to carry out a statistical and systematic study adequate to reach a formulation for the calculation of the plastic rotations, even if some proposals are available in the literature.

In (Kemp et al., 2001), as well as providing simplified expressions for the calculation of the required rotation at the nodes, it was provided an expression of the ultimate rotational capacity θ_u (available rotation) of the composite beam subjected to hogging moment. The rotational capacity of the beam is divided into two parts, one due to the reinforcing bars in tension (θ_{ay}) and the other one which takes into account the effect of tension stiffening of concrete between the cracks (θ_{acr}). The formula was derived on the basis of experimental observations on the composite joint with dual cantilever beams (Kemp et al., 1995), and is as follows:

$$\theta_u = \theta_{ay} + \theta_{acr} = 0,5 \cdot \left[\varphi_{mp} + \left(\frac{M_t}{EI_{cr}} \right) - \frac{M_{mp} + M_t}{EI_{ucr}} \right] \cdot L_t$$

It takes into account the whole flexural stiffness of the beam, without cracking, (EI_{ucr}) and that one with the cracking of the concrete slab (EI_{cr}), the maximum moment (M_{mp}) at the connection between the beam and the column, the ultimate curvature of the last section at the connection with the column (ϕ_{mp}) and the transition moment (M_t). In fact, as shown in figure 2.39, it was identified a transition zone in which there is the transition from an effective section which is that of the joint, wherein only the part of the profile in compression which is connected with the bolts and the reinforcing bars in tension are considered (fig. 2.40), to a section in which there is the full reaction of the whole composite section subjected to hogging moment. For simplicity of calculation, it can be assumed that in this zone there are also the cracks in the concrete and its length is assumed fixed and equal to 1.7 times the height of the steel profile, according to experimental observations.

In Figure 2.39 it is highlighted the variation of the plastic curvature, dimensionless with respect to the elastic one, in the transition zone, assuming a linear trend.

In the papers of other authors (Fabbrocino, 1997; Fabbrocino et al., 2001) an analytical model was introduced for executing a parametric study on the influence of the over-strength ratio (f_t/f_y) of the reinforcement in tension on the plastic rotational capacity under hogging moment versus the variation of the slenderness L/h . The results of these analyses were statistically elaborated and presented in the graph of fig. 2.41.

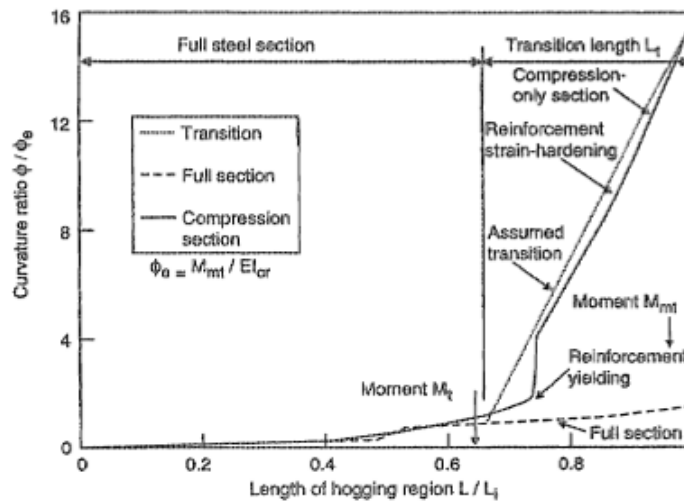


Figure 2.39: Trend of the curvatures in the transaction zone.

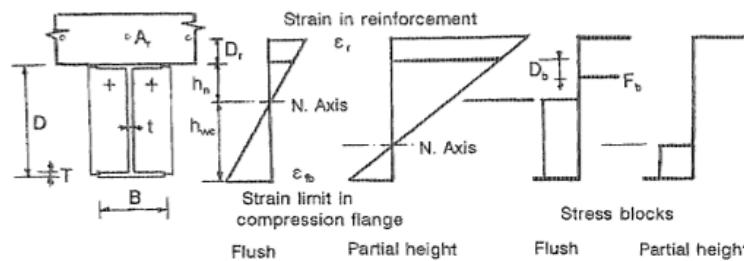


Figure 2.40: Effective section at the connection between the beam and column.

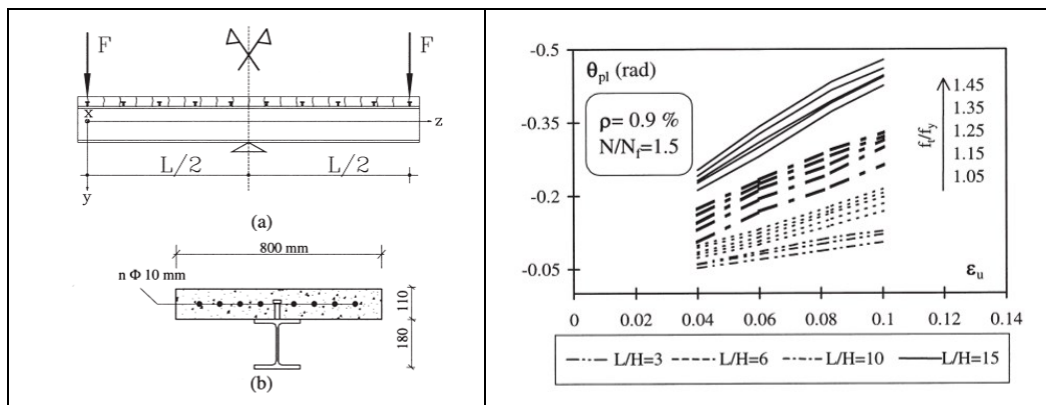


Figure 2.41: The model and the rotational capacity versus the slenderness and the over-strength ratio of the reinforcing steel (Fabbrocino et al. 2001).

Basing on the trend of the results, the authors suggested the following formula:

$$\theta_{pl} = A \cdot (\varepsilon_u - \varepsilon_y)^\alpha \cdot \left(\frac{f_t}{f_y} - 1 \right)^\beta$$

where A is the area of the reinforcement, ε_y , ε_u and (f_t/f_y) are the yielding and ultimate strain and the over-strength ratio of the reinforcement; the coefficients α and β depend on the slenderness L/h . Clearly, as also stated by the authors, the other parameters are not taken into account in the approach.

Another formulation very simple for the calculation of the plastic rotation is shown in (Chen et al., 2008) and it is reported in the following:

$$\theta_u = \varphi_u \cdot l_p = \left(\frac{\varepsilon_{su}}{y_s} - \varphi_e \right) \cdot l_p$$

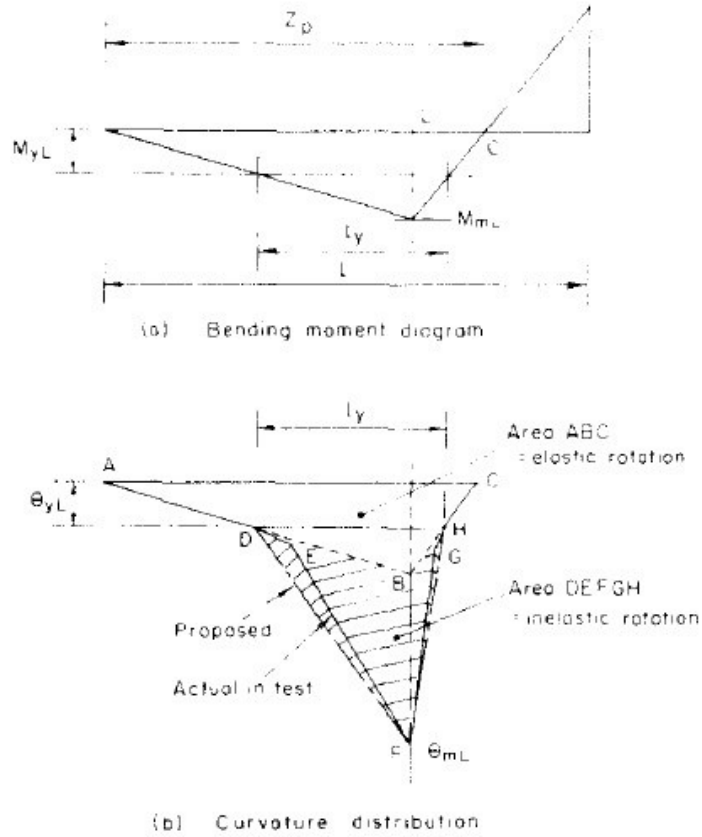
The formula is simple in that it expresses the product between an ultimate curvature (ϕ_u), clean of the elastic part (ϕ_e), and a length of plastic hinge (l_p). Even in this case the length of the plastic hinge is established on experimental basis and equal to 1.75 times the total height of the composite beam. Particular attention is paid to the index R , i.e. the ratio of the strength of the reinforcing bars in tension and the strength of the steel profile, previously introduced as a significant parameter.

In particular, the following expression of the ultimate strain is suggested:

$$\varepsilon_{su} = \frac{3000 \times 10^{-6}}{R + 0,05}$$

This index governs the position of the neutral axis and consequently the rate of steel profile subjected to compressive stresses and therefore potentially more or less exposed to local buckling phenomena.

It can be find another tentative of formulation of the plastic rotation of composite beams in (Mallick et al., 1975) but it was fitted on the tested beams, that were quite compact.



Modified curvature distribution at failure in positive moment zone of beams in Group 2.

Figure 2.42: Bending diagram and curvature distribution (Mallick et al., 1975).

According to the figure 2.42, it was found that the plastic rotation for composite beams subjected to sagging moment can be expressed as:

$$\phi'_{PL} = 0.46 \cdot (\theta_{PL} \cdot l_y + \theta_{yL} \cdot z_p)$$

Where 0,46 is a correction factor, l_y is the yield length of beam, z_p is the distance between the two points where the bending moment is zero, θ_y is the yielding curvature and θ_{PL} is the maximum plastic curvature, computed as follows:

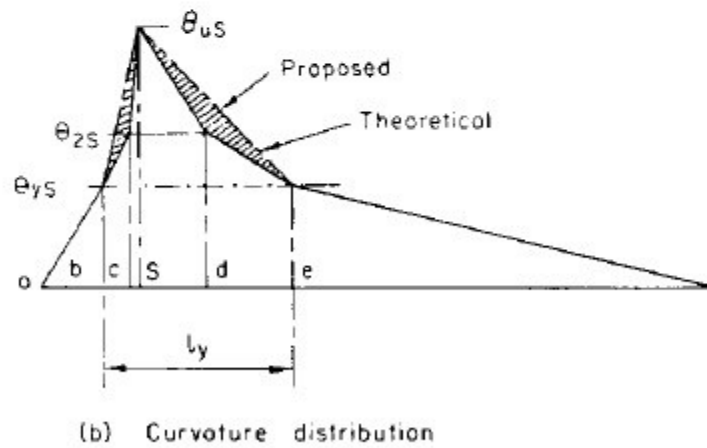
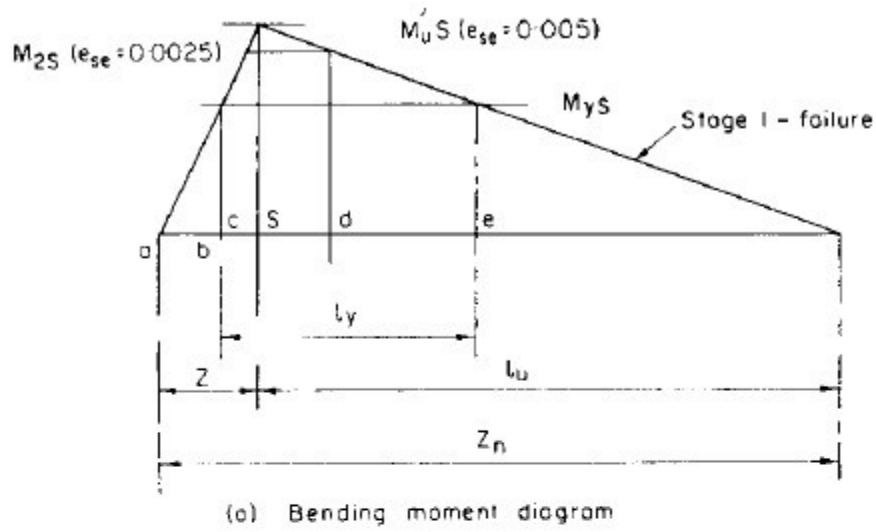
$$\theta_{PL} = \left[\frac{M_{uL}}{M_{yL}} \cdot \frac{z_p}{l_y} \right]^2 \cdot \theta_{yL}$$

where M_{yL} is the yielding moment and M_{uL} is the ultimate moment.

Based on figure 2.43, for the length of composite beam subjected to hogging moment it was given a similar expression:

$$\phi_{2S} = 0.50 \cdot (\theta_{2S} \cdot l_y + \theta_{yS} \cdot z_n)$$

where 0,5 is a correction factor, l_y is the yield length of beam, z_n is the distance between the two points where the bending moment is zero, θ_{yS} is the yielding curvature and θ_{2S} is the maximum plastic curvature, computed as in the previous case of sagging moment and with a maximum value of the compressive strain in the steel joist equal to 0,005. In fact, in the figure 2.43 three stages are highlighted that correspond to three different values of the compressive strain in the joist: stage 1 corresponds to the maximum compressive strain of 0.005 and maximum moment M_{uS} ; stage 2 corresponds to the compressive strain of 0.0025 and moment M_{2S} ; stage 3 corresponds to the yielding strain ε_y in compression and yielding moment M_{yS} .



Modified curvature distribution at failure in negative moment zone of beams in Group 2.

Figure 2.43: Bending diagram and curvature distribution (Mallick et al., 1975).

REFERENCES

- Adekola, A. O., “Effective width of composite beams of steel and concrete”, *The Structural Engineer*, vol. 46 (9), 1968, pp. 285–289.
- Amadio, C., Fragiaco, M., "Effective width evaluation for steel–concrete composite beams", *Journal of Constructional Steel Research*, vol. 58, 2002, pp. 373–388.
- Amadio, C., Fragiaco, M., Macorini, L., "Evaluation of the deflection of steel-concrete composite beams at serviceability limit state", *J. of Constructional Steel Research*, vol. 73, 2012, pp. 95–104.
- Amadio, C., Fedrigo, C., Fragiaco, M., Macorini, L., "Experimental evaluation of effective width in steel–concrete composite beams", *Journal of Constructional Steel Research*, vol. 60, 2004, pp. 199–220.
- Ansourian, P., “Plastic rotation of composite beams”, *Journal of Structural Division*, vol. 108, N. ST3, ASCE, March 1982.
- Ansourian, P., "The stability of composite beams in negative bending", *The stability of steel structures*, Liegi, April 1977, pp. 145-154.
- Ansourian, P., "The behaviour and the design of composite beams", *ACMSM 9*, The ninth Australasian conference on the Mechanics of Structures and Materials, University of Sydney, August 1984.
- AS4100, Australian standards, “Steel structures”, 1998.
- Australian Standard, Composite structures Part 1: Simply supported beams, AS 2327.1—2003.
- Baldassino, N., Seema, Zandonini, R., "La componente soletta nei giunti composti acciaio-calcestruzzo”, *VII Workshop italiano sulle strutture composte*, Benevento, Ottobre 2008.
- Baldwin, J. W., Henry, J. R., Sweeney, G. M., “Study of composite bridges stringers. Phase 2: Development of rational analysis of composite beams which was programmed for use on computer. Experimental testing of eight

- composite beams to study behavior and verify analysis”, University of Missouri, Engineering Experiment Station, 1965, pp. 226.
- Ballio, G., Mazzolani, F. M., “Strutture in acciaio” HOEPLI, 1979.
- Barnard, P. R., "A Series of Tests on Simply Supported Composite Beams", Journal Proceedings of the American Concrete Institute, issue 4, vol. 62, April 1965, pp. 443-456.
- Barnard, P. R., Johnson, R. P., “Ultimate strength of composite beams”, Proceedings in Institution of Civil Engineers, vol. 32, 1965, pp. 161-179.
- Barnard, P. R., Johnson, R. P., “Plastic behaviour of continuous composite beams”, Proceedings in Institution of Civil Engineers, vol. 32, 1965, pp. 180-197.
- Belluzzi, O., “Scienza delle costruzioni”, volume quarto, Zanichelli Bologna, Giugno 1982.
- Bibbò, F. A., Rossi, F., “Travi composte acciaio-calcestruzzo: prove sperimentali”, Premio di Laurea “Sergio Rotili”, Hevelius Edizioni, marzo 2010, pp.118. (Tesi di Laurea Specialistica).
- Braconi, A., Bursi, O. S., Fabbrocino, G., Salvatore W., Tremblay, R., “Seismic performance of a 3D full-scale high-ductility steel–concrete composite moment-resisting structure—Part I: Design and testing procedure”, Earthquake Engng Struct. Dyn., vol. 37, 2008, pp. 1609–1634.
- Braconi, A., Bursi, O. S., Fabbrocino, G., Salvatore W., Taucer, F., Tremblay, R., “Seismic performance of a 3D full-scale high-ductility steel–concrete composite moment-resisting structure— Part II: Test results and analytical validation”, Earthquake Engng Struct. Dyn., vol. 37, 2008, pp. 1635–1655.
- Bradford, M. A., “Inelastic buckling of I-beams with continuous elastic tension flange restraint”, Journal of Constructional Steel Research, vol. 48, 1998, pp. 63-77.

- Bradford, M. A., Johnson, R. P., "Inelastic buckling of composite bridge girders near internal supports", *Proc. Instn. Civ. Engrs, Part 2*, vol. 83, 1987, pp. 143-159.
- Bradford, M. A., Kemp, A. R., "Buckling in continuous composite beams", *Prog. Struct. Engng Mater.*, vol. 2, 2000, pp. 169-178.
- Bradford, M. A., Vrcelj, Z., "Elastic distortional buckling of continuously restrained I-section beam-columns", *Journal of Constructional Steel Research*, vol. 62, 2006, pp. 223-230.
- Bursi, O. S., Gramola, G., "Behaviour of composite substructures with full and partial shear connection under quasi-static cyclic and pseudo-dynamic displacements", *Materials and Structures/Materiaux et Constructions*, Vol. 33, April 2000, pp. 154-163.
- Bursi, O. S., Sun, F., Postal, S., "Non-linear analysis of steel-concrete composite frames with full and partial shear connection subjected to seismic loads", *Journal of Constructional Steel Research*, vol. 61, 2005, pp. 67-92.
- Castro, J. M., Elghazouli, A. Y., Izzuddin, B. A., "Assessment of effective slab widths in composite beams", *Journal of Constructional Steel Research*, vol. 63, 2007, pp. 1317-1327.
- Ceroni, F., "Experimental tests and modeling of tension stiffening in RC Ties strengthened with FRP laminates", *Tesi di dottorato in Ingegneria delle Strutture*, XV Ciclo, 2002.
- Chapman, J. C., "Composite construction in steel and concrete – The behavior of composite beams", *The Structural Engineer*, vol. 42 (4), April 1964, pp. 115-125.
- Chen, S., Jia, Y., "Required and available moment redistribution of continuous steel-concrete composite beams", *Journal of Constructional Steel Research*, vol. 64, 2008, pp. 167-175.
- Climenhaga, J. J., Johnson, R. P., "Local Buckling in continuous composite beams", *The structural engineer*, vol. 9, , September 1972, pp. 367-374.

- Climenhaga, J. J., Johnson, R. P., "Moment-Rotation Curves for locally buckling Beams", Journal of Structural Division, vol. 98, N. ST6, ASCE, June 1972, pp.1239-1254.
- CNR 10011, "Costruzioni in acciaio – Istruzioni per il calcolo, l'esecuzione, il collaudo e la manutenzione" CNR Bollettino Ufficiale – Norme tecniche, 1985
- CNR 10016, "Strutture composte di acciaio e calcestruzzo – Istruzioni per l'impiego nelle costruzioni", CNR Bollettino Ufficiale – Norme tecniche, parte IV, 1999.
- Cosenza, E., Pecce, M., "Analisi matriciale di travi continue composte con connessione deformabile a comportamento lineare", C.T.A., Giornate italiane della costruzione in acciaio, Ancona, Ottobre 1997, pp. 208-219.
- Cosenza, E., Zandonini, R., "Composite Construction", in Structural Engineering Handbook, Ed. Chen Wai-Fah, Boca Raton: CRC Press LLC, 1999.
- Dai, P. K-H, "Analitical study of composite beams with inelastic shear connection", PhD thesis, University of Illinois, 1963, pp. 160.
- Dekker, N. W., Kemp, A. R., Trinchero, P., "Factors influencing the strength of continuous composite beams in negative bending", Journal of Constructional Steel Research, vol. 34, 1995, pp. 161-185.
- Dubina, D., Ungureanu, V., "Effect of imperfections on numerical simulation of instability behaviour of cold-formed steel members", Thin-Walled Structures, vol. 40, 2002, pp. 239 – 262.
- Eurocode 2, "Design of concrete structures – Part 1.1: General rules and rules for buildings" ENV 1992-1-1, 1992.
- Eurocode 3, "Design of steel structures – Part 1.1: General rules and rules for buildings" ENV 1993-1-1, 1992.
- Eurocode 4, "Design of composite steel and concrete structures – Part 1.1: General rules and rules for buildings" ENV 1994-1, 2004

- Eurocode 8, “Design of structures for earthquake resistance – Part 1: General rules, seismic actions and rules for buildings” ENV 1998-1, 1998.
- Fabbrocino, G., “Modellazione e comportamento sperimentale di travi continue composte acciaio-calcestruzzo”, Tesi di dottorato in Ingegneria delle Strutture, X ciclo, Università degli Studi di Napoli “Federico II”, 1997.
- Fabbrocino, G., Manfredi, G., Cosenza, E., “Ductility of composite beams under negative bending: an equivalence index for reinforcing steel classification”, *Journal of Constructional Steel Research*, vol. 57, 2001, pp. 185-202.
- Fu, F., Lam, D., Ye, J., "Parametric study of semi-rigid composite connections with 3-D finite element approach", *Engineering Structures*, vol. 29, 2007, pp. 888–898.
- Gattesco, N., "Analytical modeling of nonlinear behavior of composite beams with deformable connection", *J. of Constructional Steel Research*, vol. 52, 1999, pp. 195–218.
- Green, T.P., Leon, R.T., Rassati, G.A., “Bidirectional Tests on Partially Restrained, Composite Beam-to-Column Connections”, *Journal of Structural Engineering*, Vol. 130, No. 2, 2004, pp. 320-327.
- Hamada, S., Longworth, J., “Ultimate strength of continuous composite beams”, *Journal of Structural Division*, Vol. 102, No. ST7, ASCE, July 1976, pp. 1463-1478.
- Yam, L. C. P., Chapman, J. C., "The inelastic behaviour of simply supported composite beams of steel and concrete", *ICE Proceedings*, Vol. 41, Issue 4, 01 December 1968, pp. 651–683
- Johnson, R. P., “Composite structures of steel and concrete”, Blackwell Publishing, Second Edition, 1994.
- Johnson, R. P., Finlinson, J. C. H., Heyman, J., "A plastic composite design", *Proceedings in Institution of Civil Engineers*, vol. 32, October 1965, pp. 198-209.

- Johnson, R. P., Greenwood, R. D., Van Dalen, K., “Stud shear-connectors in hogging moment regions of composite beams”, *Struct. Eng.*, vol. 47, 1969, pp. 345–350.
- Johnson, R. P., Van Dalen, K., Kemp, A. R., “Ultimate strength of continuous composite beams”, *Proceedings of the conference on Structural Steelwork*, British Constructional Steelwork Association, November 1967, pp. 27-35.
- Johnson, R. P., Willmington, R. T., "Vertical shear strength of compact composite beams", *Proc. Inst. Civ. Engrs., Suppl. 1*, 1972, pp. 1-16.
- Johnson, R. P., Willmington, R. T., "Vertical shear strength of compact composite beams", *Proc. Inst. Civ. Engrs., Part 2*, 1972, pp. 1-16.
- Kato, B., “Rotation capacity of H-section members as determined by local buckling”, *Journal of Constructional Steel Research*, vol. 17, 1990, pp. 33-94.
- Kato, B., “Deformation capacity of steel structures”, *Journal of Constructional Steel Research*, vol. 13, 1989, pp. 95-109.
- Kemp, A. R., “Interaction of Plastic local and Lateral Buckling”, *Journal of Structural Engineering*, ASCE, vol. 111, n. 10, 1985, pp. 2181-2196.
- Kemp, A. R., "Quantifying ductility in continuous composite beams", *Composite Construction in Steel and Concrete*, *Proceedings of an Engineering Foundation conference*, ASCE, 1987, pp. 107-121.
- Kemp, A. R., "Factors affecting the rotation capacity of plastically designed members”, *The structural engineer. Part B*, vol. 64B, issue 2, 1986, pp. 28-35.
- Kemp, A. R., Dekker, N. W., Trinchero, P., “Differences in inelastic properties of steel and composite beams”, *Journal of Constructional Steel Research*, vol. 32, 1995, pp. 303-332.
- Kemp, A. R., Nethercot, D. A., “Required and available rotations in continuous composite beams with semi-rigid connections”, *Journal of Constructional Steel Research*, vol. 57, 2001, pp. 375-400.

- Kuhlmann, U., “Definition of the flange slenderness limits on the basis of the rotation capacity values”, *Journal of Constructional Steel Research*, 1989, pp. 21-40.
- Lay, M. G., Galambos, T. V., “Inelastic steel beams under uniform moment”, *Journal of Structural Division, ASCE*, vol. 91, December 1965, pp. 67-93.
- Lay M. G., Galambos T. V. “Inelastic steel beams under moment gradient” *Journal of Structural Division, ASCE*, vol. 93, February (1967) p. 381-399.
- Loh, H. Y., Uy, B., Bradford, M. A., “The effects of partial shear connection in the hogging moment regions of composite beams, Part I – Experimental study”, *Journal of Constructional Steel Research*, vol. 60, 2004, pp. 897-919.
- Mallick, S. K., Chattopadhyay, S. K., "Ultimate Strength of Continuous Composite Beams" *Building Science*, Vol. 10, issue 3, October 1975, pp. 189-198.
- Mazzolani, F. M., Piluso, V., “Evaluation of the rotation capacity of the steel beams and beam-columns”, 1st Cost C1 Workshop, Strasbourg, October 1992.
- Mazzolani, F. M., Piluso, V., “Theory and Design of seismic resistant Steel Frames”, Spon Press, 1996.
- Moore, W. P., “An Overview of Composite Construction in the United States - Composite Construction in Steel and Concrete”, C.D. Buckner and I.M. Viest Ed. ASCE, 1998, pp. 1-17.
- Nakashima, M., Matsumiya, T., Suita, K., Zhou, “Full-Scale Test of Composite Frame under Large Cyclic Loading”, *Journal of Structural Engineering*, Vol. 133, No. 2, 2004, pp. 297-304.
- Newmark, N. M., Siess, C. P., Viest, "Tests and Analysis of Composite Beams with Incomplete Interaction", *Proc. of Society for Experimental Stress Analysis*, Vol. 9, N. 19, 1951, pp. 75-92.

- Nie, J., Fan, J., Cai, C. S., “Experimental study of partially shear-connected composite beams with profiled sheeting”, *Engineering Structures*, vol. 30, 2008, pp. 1–12.
- Nie, J., Tian, C-Y., Cai, C. S., "Effective width of steel–concrete composite beam at ultimate strength state", *Engineering Structures*, vol. 30, 2008, pp. 1396–1407.
- Oehlers, D. J., Sved, G., “Composite beams with limited slip capacity shear connector”, *Journal of Structural Engineering*, Vol. 121, No.6, ASCE, June 1995, pp. 932-938.
- Ollgaard, J. G., Slutter, R. G., Fisher, J. W., “Shear strength of stud connectors in lightweight and normal weight concrete”, *AISC, Engineering Journal*, 1971.
- Pecce, M., Bibbò, F. A., Rossi, F., Ceroni, F., “Experimental results of steel-concrete composite beams under hogging moment”, 4th International Conference on Steel & Composite Structures, Sydney, Australia, July 2010.
- Pecce, M., Ceroni, F., Bibbò, F. A., Rossi, F., “Comportamento sperimentale di travi composte soggette a momento negativo”, *Atti del VII Workshop italiano sulle strutture composte*, Ottobre 2008, pp. 9-22.
- Pecce, M., Rossi, F., Bibbò, F. A., Ceroni, F., “Experimental behaviour of composite beams subjected to hogging moment”, *Steel & Composite Structures An International Journal*, Vol. 12, No. 5, 2012.
- Ranzi, G., Bradford, M. A., Ansourian, P., Filonov, A., Rasmussen, K. J. R., Hogand, T. J., Uy, B., "Full-scale tests on composite steel-concrete beams with steel trapezoidal decking", *J. of Constructional Steel Research*, vol. 65, 2009, pp. 1490-1506.
- Rotter, J. M., Ansourian, P., "Cross-section behaviour and ductility in composite beams", *Proceedings, Institution of Civil Engineers, Part 2*, 1979, 67, June, pp. 453-474.

- Siess, C. P., Viest, I. M., Newmark, N. M., “Small-Scale Tests of Shear Connectors and Composite Beams”, Bulletin N. 396, University of Illinois, Engineering Experiment Station, 1952.
- Southward, R. E., “Local buckling in universal sections”, Internal Report, University of Cambridge Engineering Department, 1969.
- Stowell, E. Z., “Compressive Strength of Flanges”, Technical Note N. 2020, National Committee for Aeronautics, 1950.
- Vasdravellis, G., Uy, B., Tan, E. L., Kirkland, B., “The effects of axial tension on the sagging-moment regions of composite beams”, Journal of Constructional Steel Research, vol. 72, 2012, pp. 240–253.
- Vasdravellis, G., Uy, B., Tan, E. L., Kirkland, B., “The effects of axial tension on the hogging-moment regions of composite beams”, Journal of Constructional Steel Research, vol. 68, 2012, pp. 20–33.
- Viest, I. M., Siess, C. P., Appleton, J. H., Newmark, N. M., “Full-Scale Test of Channel Shear Connectors and Composite T-Beams”, Bulletin N. 405, University of Illinois, Engineering Experiment Station, 1952.
- Viest, I. M., Siess, C. P., “Design of Channel Shear Connectors for Composite T-Beam Bridges”, Public Road, Vol. 281, N. 1, 1954, pp. 9-169.

CHAPTER 3. THE FE MODELLING OF COMPOSITE BEAMS SUBJECT TO HOGGING MOMENT

3.1 Models available for composite beams

The development of a finite element model of any structural system implies to face several problems: the models of the materials, the type of finite element more suitable for the problem, the reproduction of the constraints and load conditions, the type of analysis to perform on the model, the methods of convergence, the type of numerical control, and so on.

The attention and the detail to spend for these parameters are of great importance for the good reproduction of reality and in order to carry out a reliable result. So every choice, made in setting up the numerical model, is contextualized to the result that you want to arise.

The modeling of steel-concrete composite beams is particularly onerous and difficult because the coupling of two elements, one for the reinforced concrete part and the other for the steel profile. This coupling adds an additional element of variability in the models that takes the form of additional boundary conditions and congruence. In general, in the literature the modeling of composite beams identifies two solutions: the mono-dimensional models, mostly theoretical, and the numerical models by finite elements (FEM).

In (Cosenza et al., 1993 and 1997) it is shown the analytical study of composite beams with linear deformable connection for reaching some closed-form solutions in the calculation of the deformation and the sliding between two components. A kinematic model (fig. 3.1) is taken as reference to discuss the differential equations that govern the problem in the hypothesis of linear behaviour of all the components and to develop the matrix form of the force method.

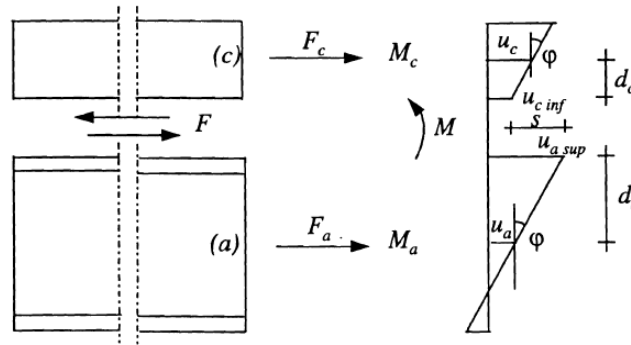


Figure 3.1: Kinematic model of the composite element.

Also in (Faella et al., 2003), a finite-element procedure considering nonlinear load–slip relationship for shear connectors is presented. Such a procedure accounts for the concrete slab cracking and the resulting tension stiffening effect; it also assumed different load–slip relationships for shear connectors in cracked slab (fig. 3.2). Some experimental comparisons showed the accuracy of the proposed procedure. A wide parametric analysis is performed with reference to the evaluation of deflections for simply supported composite beams. Finally, a simplified method which is able to evaluate deflections for beams with nonlinear behaving shear connection is presented.

Likewise, other authors (Gattesco, 1999; Oven et al., 1997) have focused their attention to the study and research of an analytical model that takes into account for the deformability of the connection between the two elements in both the linear and non-linear field. Both papers compare the analytical models with experimental results finding a good agreement. In particular in (Gattesco, 1999) a numerical procedure based on the arc-length procedure is developed to better identify the softening behavior of the composite beam system. The numerical model is based on a mono-dimensional approach but the beam element is developed considering the composite system (steel profile, slab and connection) according the schematization reported in (fig. 3.3).

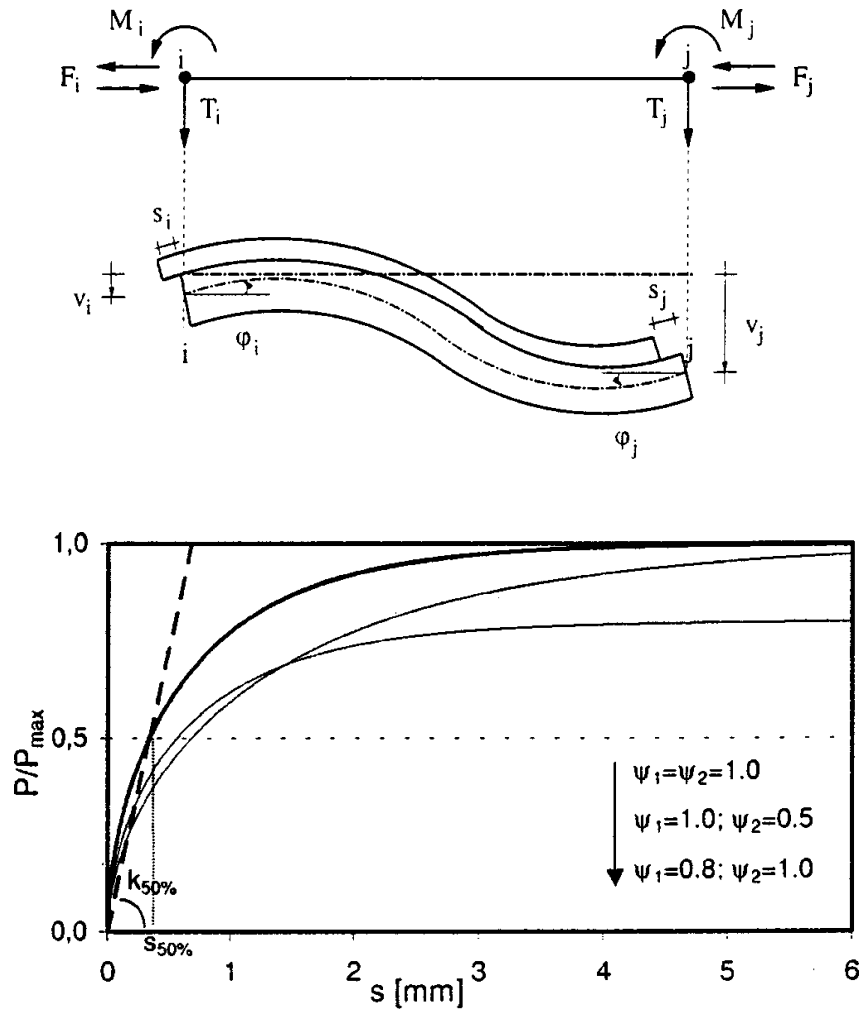


Figure 3.2: Nodal forces and displacements of composite beam with flexible connection and different load-slip relationship (Faella et al., 2003).

In (Ranzi et al., 2007) an analytical model for the analysis of steel–concrete composite beams with partial shear interaction including the shear deformability of the steel component is reported (fig. 3.4). This model is obtained by coupling an Euler–Bernoulli beam for the reinforced concrete slab to a Timoshenko beam for the steel beam. The steel of the beam and the steel of the slab reinforcement are modeled by using linear elastic laws, while the time-dependent behavior of the slab concrete is included by using a general

linear viscous–elastic integral-type constitutive law. The numerical solution is obtained by means of the finite element method and numerical simulations are carried out to compare the response of the composite beams with and without the shear deformability.

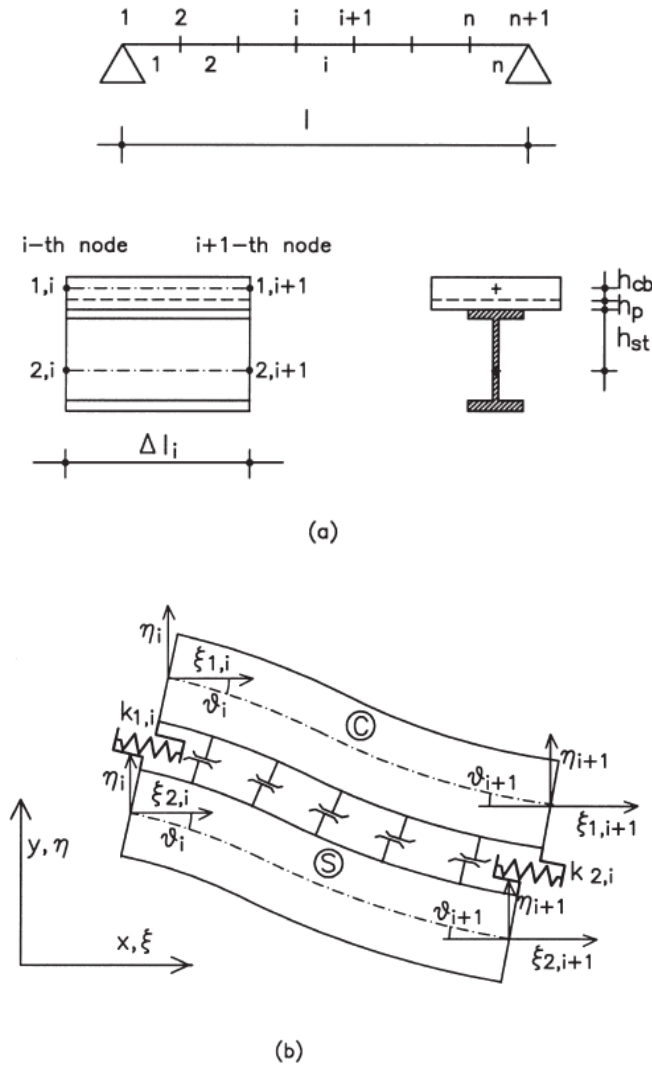


Figure 3.3: a) Beam sub-division; b) 8 nodes FEM element.

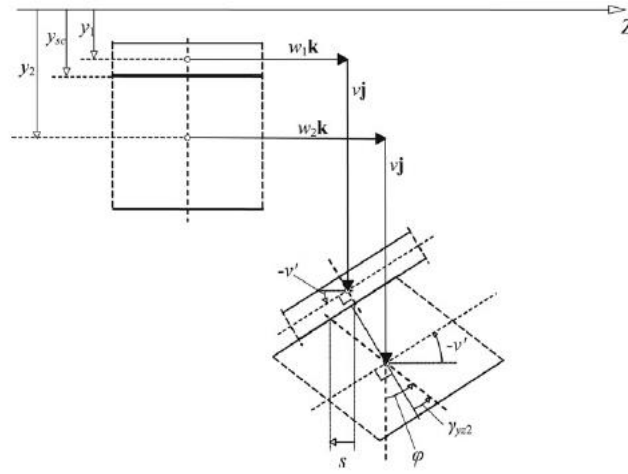


Figure 3.4: Euler-Bernoulli Timoshenko element (Ranzi et al., 2007).

In (Fabbrocino et al., 2000) a method of analysis for continuous composite beams (fig. 3.5) considering post-elastic behaviour of the element and the connection is proposed, that is based on a mono-dimensional approach with a specific kinematic model of the cross section. The model takes into account the slip at the slab-profile interface and the slip at the concrete-reinforcement interface; the numerical solution is attained through an iterative procedure by the shooting method applied to the slips at sections where there are known. This approach allows the introduction of a constitutive relationship for bond between reinforcing bars and concrete in the theoretical analysis; thus, the tension stiffening effect in the negative bending moment regions can be computed, and the actual mechanical behavior of the reinforcing bars of the slab can be analyzed. The same authors in (Fabbrocino et al., 1999) report the adapted approach for the composite beam subjected to sagging moment and compare the local and global measures with experimental results of other authors with a good agreement (fig. 3.6)

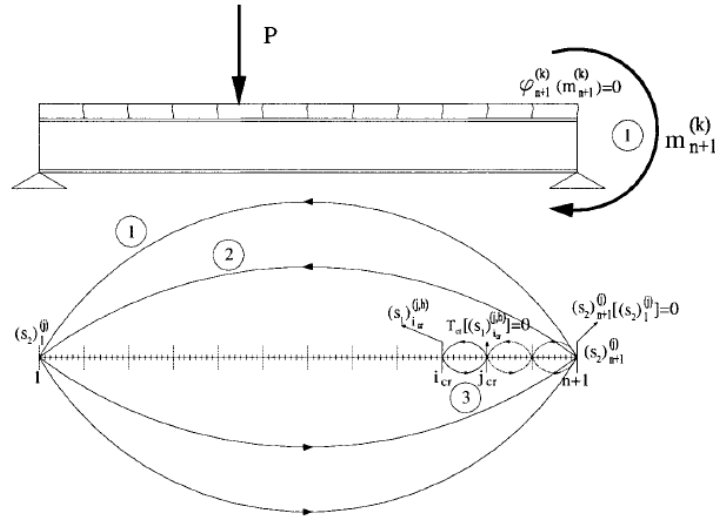


Figure 3.5: Beam discretization and strategy of iterative solution in (Fabbrocino et al., 2000).

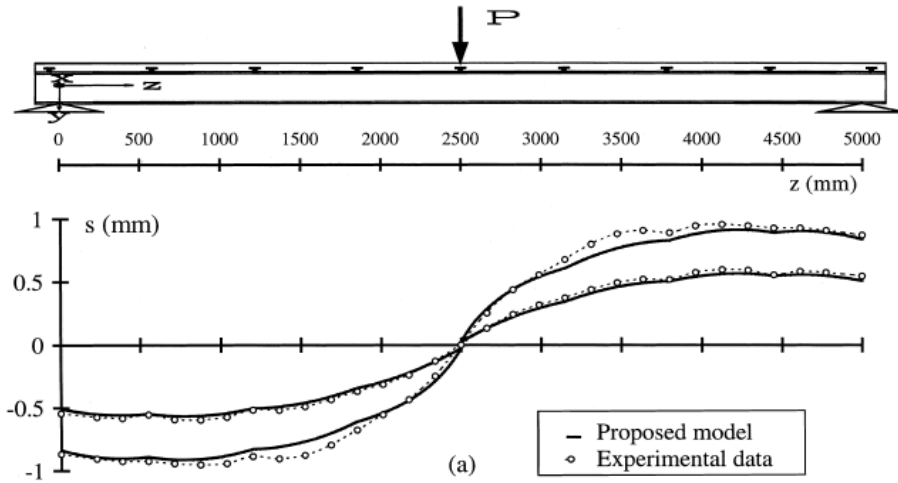


Figure 3.6: Numeric-experimental comparison of local measures for a composite beam subjected to sagging moment (Fabbrocino et al., 1999).

The layered element approach (fig. 3.7) is reported in (Sebastian et al., 2000) where attention is drawn to the usefulness of the layering technique in determining local stress redistributions associated with progressive through-

depth cracking and yielding in the slab and steel beam elements. Concrete is represented as a nonlinear elastic isotropic material before cracking and nonlinear orthotropic thereafter, while steel is taken to be initially elastic with strain-hardening capabilities after yielding.

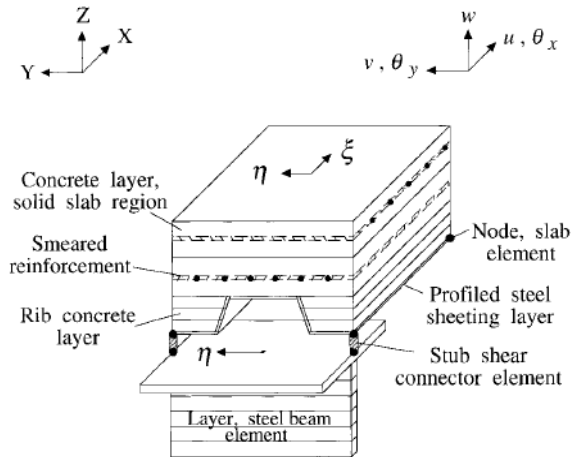


Figure 3.7: Layered element (Sebastian et al., 2000).

In (Fu et al., 2006) it is described a tri-dimensional finite element model of a composite connection (fig. 3.8) of steel beams and precast hollow core slabs. A finite element model to simulate the structural behaviour of the composite beam is described and is used to study the behaviour of a wide range of composite connections to gain a better understanding of the structural behaviour especially the moment–rotation characteristic of the connections. Parametric studies are carried out to investigate the structural behaviour with variations (fig. 3.9) of: the size of the beam, the thickness of the endplate, the thickness of the column web, the depth of the precast hollow cored slab and the stud spacing.

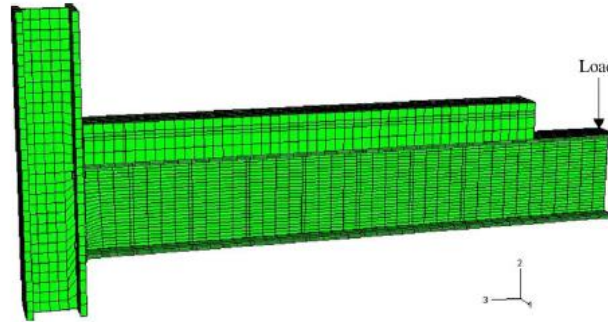


Figure 3.8: FE model of composite joint (Fu et al., 2006)

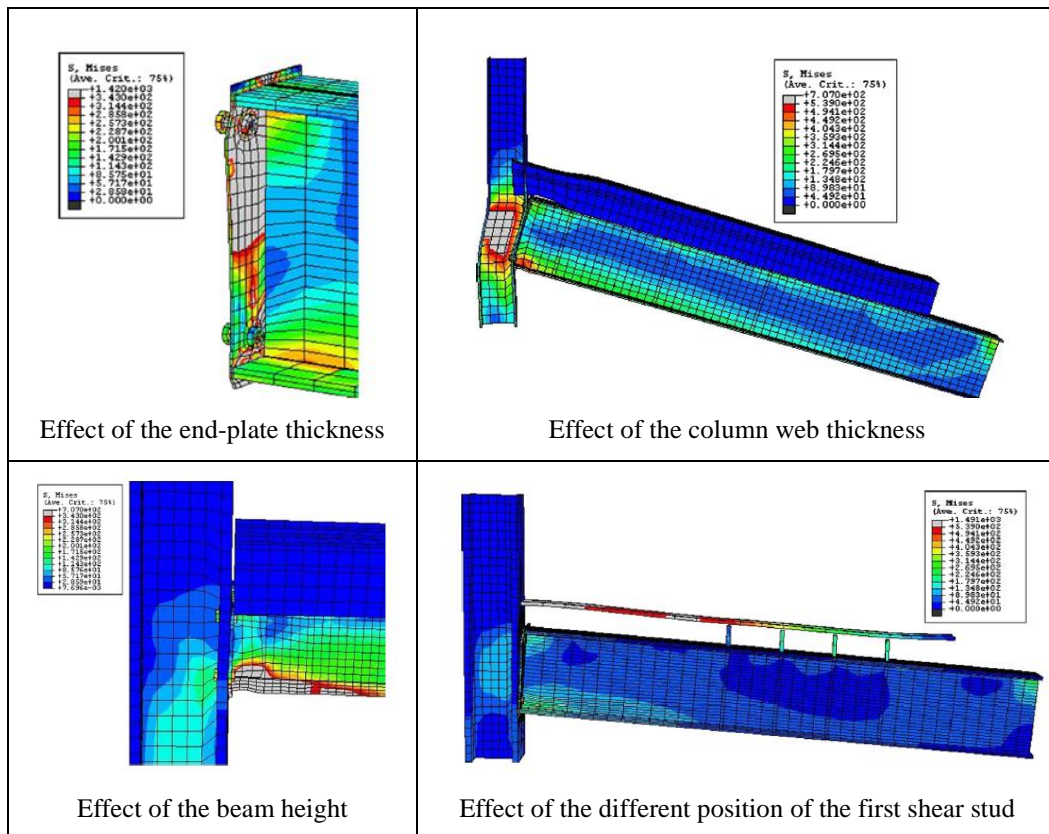


Figure 3.9: Different effects on the response of the composite joint (Fu et al., 2006)

In (Wang et al., 2008), two-dimensional finite element models, developed in Abaqus, employing plane stress elements are established to examine the structural behaviour of perforated composite beams, and shear connectors with non-linear deformation characteristics that are incorporated into the models

through the use of both vertical and horizontal springs. The same approach is extended in (Wang et al., 2007) where also the initial imperfection is introduced to take into account the effect of the local buckling on the plastic capacity of continuous composite beams.

Also in (Zhou et al., 2007) a FEM model is adopted for the study of composite beams, previously tested. In this case the steel joist is modeled by a monodimensional element (beam element) linked to the slab modeled with shell elements by means of spring elements that have a nonlinear relationship.

3.2 The FE model developed for the composite beams

The finite element method (Finite Element Method - FEM), proposed for the first time by Clough in 1960, is one of the most used and studied numerical methods in engineering. The FE model is widely used in the engineering problems as it is capable of treating the heterogeneity and the non-linear behavior of the materials. Therefore, it is able to take into account for the different problems related to the boundary conditions. The FE method is based on the process of discretization of the macro-model in a number of sub-domains, defined elements, rather simple and with a regular shape, which may vary from triangles to squares or tetrahedra, characterized by a fixed number of nodes. It should be emphasized that the accuracy of the model depends, mainly, by the size of the elements used in the meshing process.

This is evidenced by the reduction of some mistakes in a proportional manner with the reciprocal distance between the nodes: in general as they are more closely spaced as it is expected the better result. However, it has to be borne in mind that, within certain intervals, the mesh is able to optimize the analysis but it must take into account for the computational effort because the close mesh can cause problems of numerical convergence. There are different types, free

or commercial, Finite Element Analysis software. In this work the software Diana 9.4.4. was used.

This software bases its analysis on the development of three phases:

- PRE - PROCESSING: the physical and the geometrical construction of the model. The software allows to go on in a specific environment defined iDiana.
- PROCESSING: the step in which the resolution of the finite element model is attained;

POST - PROCESSING: the step that presents the results.

In this section it is discussed the development of a finite element model of the steel-concrete composite beams, consisting of a steel I-beam and a reinforced concrete slab connected by shear stud devices. The first model was calibrated on the results of the experimental tests conducted on the composite beams subject to hogging moment. Afterward the same model was used to conduct a parametric analysis reported in the section 4.

In the FE modeling of some structural elements it is necessary to consider various aspects:

- the choice of the approach that can be one-dimensional, two-dimensional and three-dimensional;
- the choice of the finite element type more akin to the behavior of the system;
- the choice of the analysis type consistent with the issues addressed by which to get reliable results;
- the definition of the geometry of the system;
- the adoption of the constitutive laws to reproduce in a suitable way the mechanical properties of the materials composing the element;

- the adoption of the adequate constrain conditions compatible with the possible degrees of freedom of the system as a whole, and for each element itself;
- the application of adequate load conditions with their relative distribution.

All these aspects have to be treated with a level of detailing which depends on the final target of the study

Model: COMPOD
Analysis: DIANA
Model Type: Structural 3D

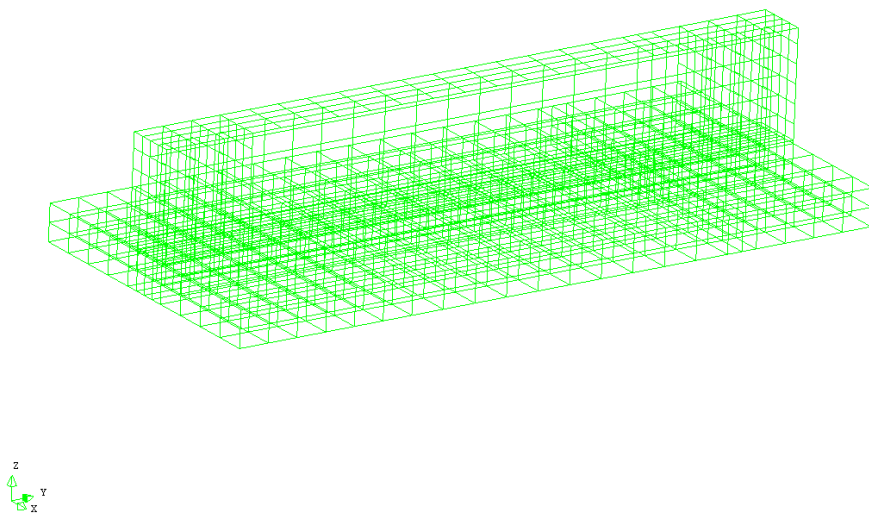


Figure 3.10: The model of the composite beam implemented in DIANA.

As mentioned, the three-dimensional FE model was implemented (fig. 3.10) using the finite element software DIANA 9.4.4 TNO. The steel profile beam was modeled using two-dimensional elements of the type curved shell elements or curved shell quadrilateral with 8 nodes (CQ40S) that provide a higher sensitivity to the buckling problems, both locally and globally.

Curved Shell elements (Fig. 3.11) in Diana are obtained by degeneration of the solid iso-parametric ones introducing two assumptions on shell:

- the axis orthogonal to the average surface of the shell remains linear, but not necessarily orthogonal to the average area of the deformed configuration: theory of Mindlin-Reissner;
- the stress in the direction orthogonal to the shell, σ_{zz} , are neglected;

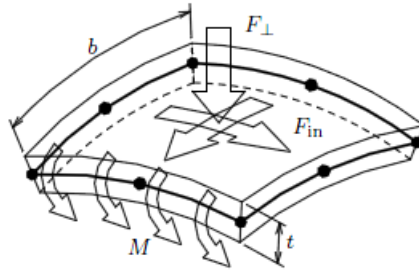


Figure 3.11: Curved shell element.

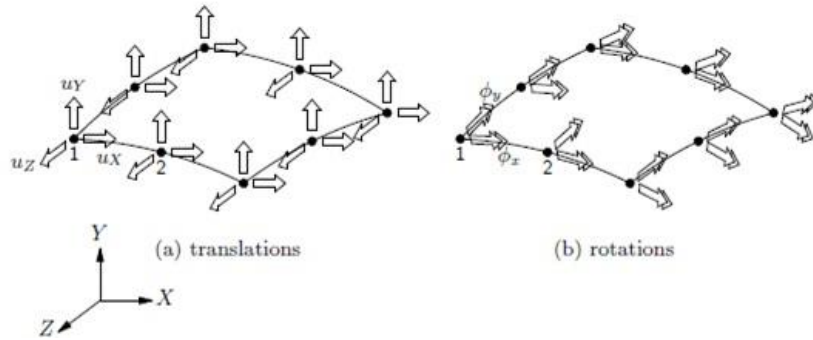


Figure 3.12: Displacements for the curved shell element.

The CQ40S element is an eight-node quadrilateral iso-parametric curved shell element. It is based on quadratic interpolation and Gauss integration over the $\xi\eta$ element area. The integration in ζ direction (thickness) may be Gauss or Simpson type. The polynomials for the translations u and the rotations ϕ can be expressed as:

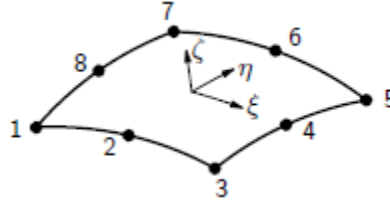


Figure 3.13: The curved shell element CQ40S.

$$u_i(\xi, \eta) = a_0 + a_1\xi + a_2\eta + a_3\xi\eta + a_4\xi^2 + a_5\eta^2 + a_6\xi^2\eta + a_7\xi\eta^2$$

$$\varphi_i(\xi, \eta) = b_0 + b_1\xi + b_2\eta + b_3\xi\eta + b_4\xi^2 + b_5\eta^2 + b_6\xi^2\eta + b_7\xi\eta^2$$

Typically, for a rectangular element, these polynomials yield approximately the following strain and stress distribution along the element area in a ζ lamina. The strain ε_{xx} , the curvature κ_{xx} , the moment m_{xx} , the membrane force n_{xx} and the shear force q_{xz} are linear in x direction and quadratic in y direction. The strain ε_{yy} , the curvature κ_{yy} , the moment m_{yy} , the membrane force n_{yy} and the shear force q_{yz} are linear in y direction and quadratic in x direction.

For the concrete slab the solid brick-type elements (fig. 3.14) with 20 nodes (CHX60) and six rectangular surfaces were chosen. The brick elements are capable of modeling three-dimensional structural elements.

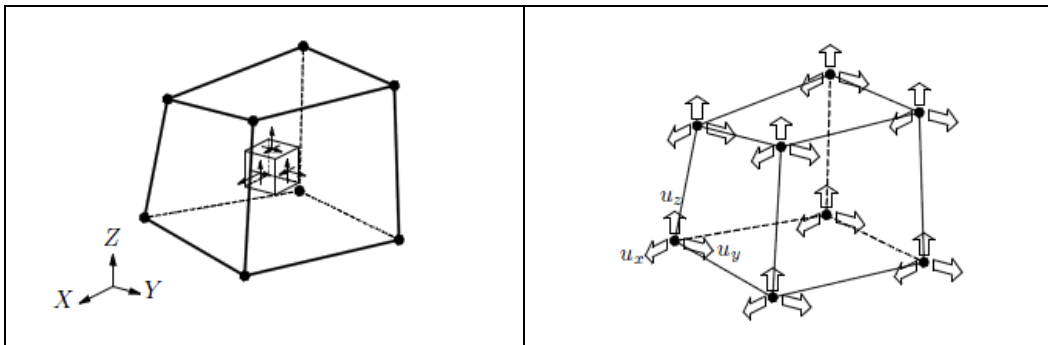


Figure 3.14: Generic solid element.

The CHX60 element (fig. 3.15) is a twenty-node isoparametric solid brick element. It is based on quadratic interpolation and Gauss integration.

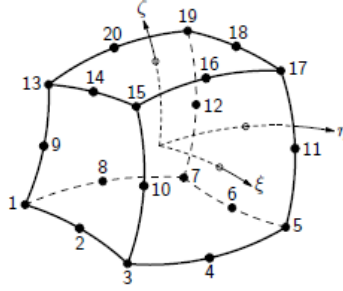


Figure 3.15: Brick - Type CHX60.

The polynomial for the translations u_x, y, z can be expressed as:

$$\begin{aligned}
 u_i(\xi, \eta, \zeta) = & a_0 + a_1\xi + a_2\eta + a_3\zeta + a_4\xi\zeta + a_5\eta\zeta + a_6\xi\eta + a_7\xi^2 + a_8\eta^2 \\
 & + a_9\zeta^2 + a_{10}\xi\eta\zeta + a_{11}\xi^2\eta + a_{12}\xi^2\zeta + a_{13}\xi\eta^2 + a_{14}\xi\zeta^2 \\
 & + a_{15}\eta^2\zeta + a_{16}\eta\zeta^2 + a_{17}\xi^2\eta\zeta + a_{18}\xi\eta^2\zeta + a_{19}\xi\eta\zeta^2
 \end{aligned}$$

Typically, a rectangular brick element approximates the following strain and stress distribution over the element volume. The strain ε_{xx} and stress σ_{xx} are linear in x direction and quadratic in y and z direction. The strain ε_{yy} and stress σ_{yy} are linear in y direction and quadratic in x and z direction. The strain ε_{zz} and stress σ_{zz} are linear in z direction and quadratic in x and y direction. By default Diana applies a $3 \times 3 \times 3$ integration scheme.

The reinforcement in the slab can be modeled in two ways: embedded elements or beam elements.

Embedded reinforcements add stiffness to the finite element model. The main characteristics of embedded reinforcements are:

- Reinforcements are embedded in structural elements, the so-called “mother elements”;

- Diana neglects the space occupied by an embedded reinforcement;
- The mother element neither diminishes in stiffness, nor in weight;
- The reinforcement does not contribute to the weight (mass) of the element.

Standard reinforcements do not have degrees of freedom of their own. In standard reinforcements the strains in the reinforcements are computed from the displacement field of the mother elements. This implies perfect bond between the reinforcement and the surrounding material.

One of the most advantage of this approach is that preparing a finite element mesh the technique of embedding allows the lines of the reinforcement to deviate from the lines of the mesh. This permits the user to generate the finite element mesh without having to anticipate on the location of reinforcements.

For the embedded approach the total length of the bar is considered to be divided in several particles (fig. 3.16).

By definition, a particle must be completely inside a structural element. The so-called location points define the position of the particles in the finite element model. Some location points are the intersections of the bar with the element boundaries. Other location points are in-between these intersections, these points define the curvature of the bar. Usually, the location points are determined automatically by DIANA from input of larger sections; this process is called preprocessing of reinforcement location.

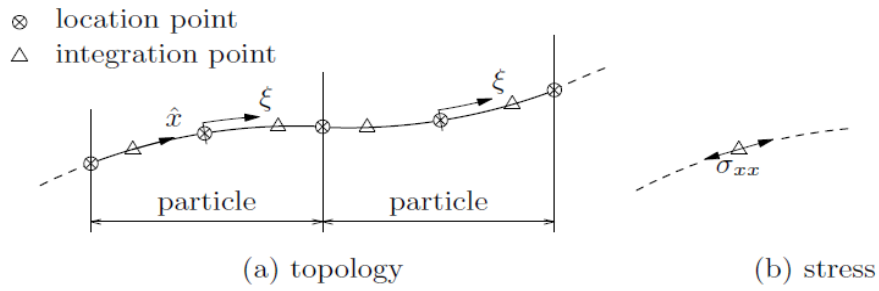


Figure 3.16: Reinforcement bar; a) topology; b) stress.

To embed a bar reinforcement in solid elements, DIANA needs to know the location points of the particle for each solid element that is embedded (fig. 3.17).

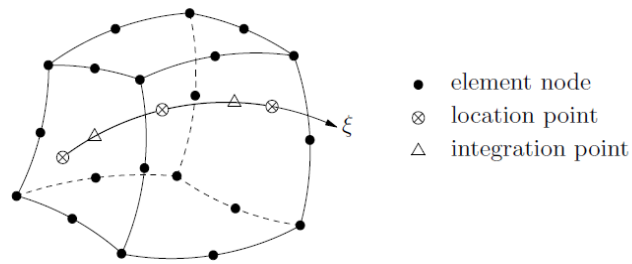


Figure 3.17: BAR particle in solid element.

Alternatively, for steel reinforcement a modeling based on the beam elements can be chosen, such as the type L13BE.



Figure 3.18: L13BE element.

The element L13BE (Fig. 3.18) has two nodes and belongs to the category of the three-dimensional elements, BEAM of class II. The basic variables of the L13BE element are u_x , u_y and u_z , and rotations ϕ_x , ϕ_y and ϕ_z of the nodes and the additional variable Δ_{ux} representing the elongation in the x direction (the axis) of the element.

The polynomials of the displacements can be expressed as:

$$\begin{aligned}u_x(\xi) &= a_0 + a_1\xi + a_2\xi^2 \\u_y(\xi) &= b_0 + b_1\xi + b_2\xi^2 + b_3\xi^3 \\u_z(\xi) &= c_0 + c_1\xi + c_2\xi^2 + c_3\xi^3\end{aligned}$$

To model the connection between the steel profile and the concrete slab it was added an interface element that takes into account the behavior of the connection.

The interface element has a negligible height (equal to about half the thickness of the flange) and is considered uniformly distributed along the beam with a width equal to the dimension of the flange plate that is in contact with the concrete slab. After the geometry of the interface is assigned, its mechanical characteristics have to be established. The stiffness of the interface was implemented as different along the three directions:

- Along the y axis, that is the one of the beam axis, the interface behavior is non-linear and it has to reply the bond-slip law of the connectors;
- In the z direction, orthogonal to the axis of the beam, it is assumed a high axial stiffness to avoid the problem of up-lift;
- Along the x axis, in the plane of the section, it was considered a shear stiffness equal to that of the generic stud.

The interface proceeds was modeled inserting a solid element between the upper face of the concrete slab and lower surface of the steel flange. The choice of the mesh sizing for the interface was established to ensure the correspondence between the nodes of the slab elements and those of the flange

of the profile. Given that the elements used are CHX60 (slab) and CQ40S (steel profile), respectively, solid elements and shell elements, the CQ48I shell element was used for the interface elements.

These elements describe the behavior of the shear connection (the interface) in terms of a relationship between the normal and tangential stresses and the relative displacements, both normal and tangential.

The CQ48I (fig. 3.19) is an interface element of the plane type, placed between two faces of three-dimensional type. The local axes xyz are evaluated in the first node with x between the first and the second node and z perpendicular to the plane. The variables are oriented according to the local system xyz . The element is based on quadratic interpolation.

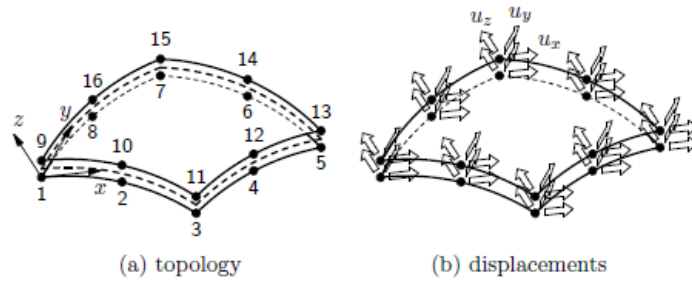


Figure 3.19: CQ48I Element.

The mesh of the model (fig. 3.20) can be more or less close depending on the necessity of describing geometric details or special physical problems.

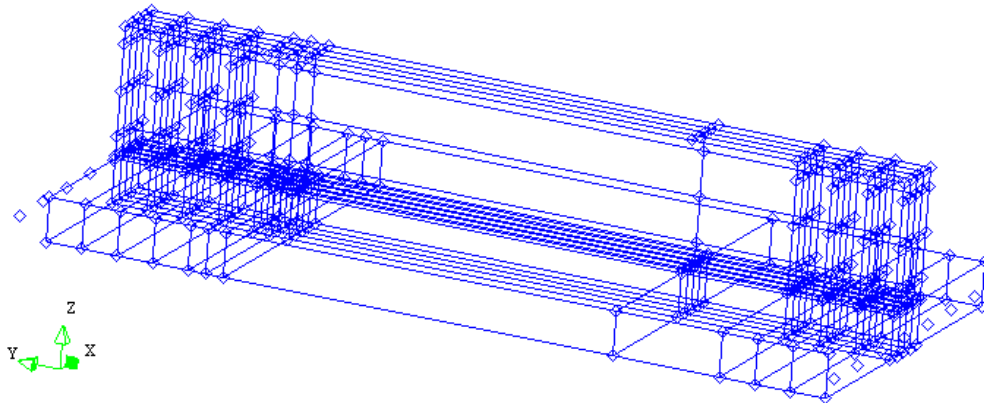


Figure 3.20: Geometry of the composite beam in DIANA.

Another key issue in the development of a model is the definition of the mechanical properties of the materials and their constitutive relationship through suitable models. The materials considered for the composite beam model are the following ones:

- Structural Steel (steel profile of the composite beam);
- Concrete (the slab of the composite beam);
- Steel reinforcement in the slab;
- Nelson Studs connecting the two components.

All the materials were assumed as isotropic and homogeneous. The constitutive laws used for the reinforcement and the structural steel (fig. 3.21) are elastic-perfectly plastic (EPP) until the attaining of the ultimate strain (ε_{us}) or elastic-plastic with hardening (EPH) (fig. 3.22). In particular, the former relationship was used in the calibration of the model by the experimental results, while the latter was used in the parametric analysis to evaluate the influence of the hardening on the response of the composite beams.

Regarding the EPH relationship, the elastic part was defined simply with the Young's modulus (E_s) and the yield stress (f_{yk}), while for the plastic part the value of f_{yk} was assigned up to a value of deformation (ε_h) when the hardening

branch starts, i.e. a tri-linear law according to the approximation of the experimental one was considered.

The figure 3.22 shows the constitutive law adopted for the steel reinforcement.

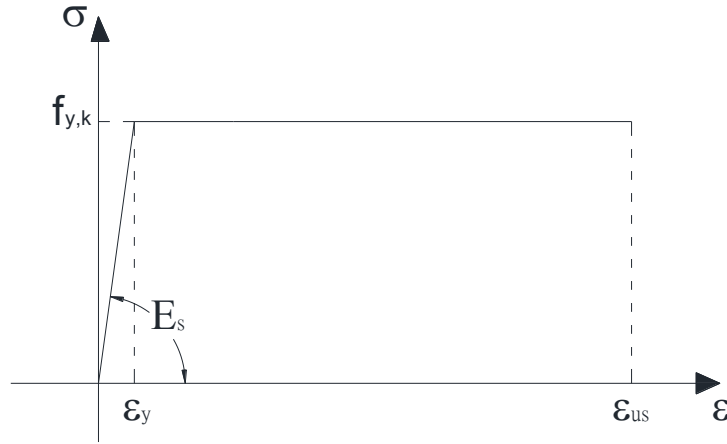


Figure 3.21: The constitutive relationship (EPP) assumed for the steel reinforcing bars and the steel joist.

f_{yk} is the value of the yield stress;

ϵ_y is the value of deformation at the yielding;

ϵ_{us} is the value of deformation at failure.

Figure 3.22 shows the constitutive law of the structural steel when the hardening is considered.

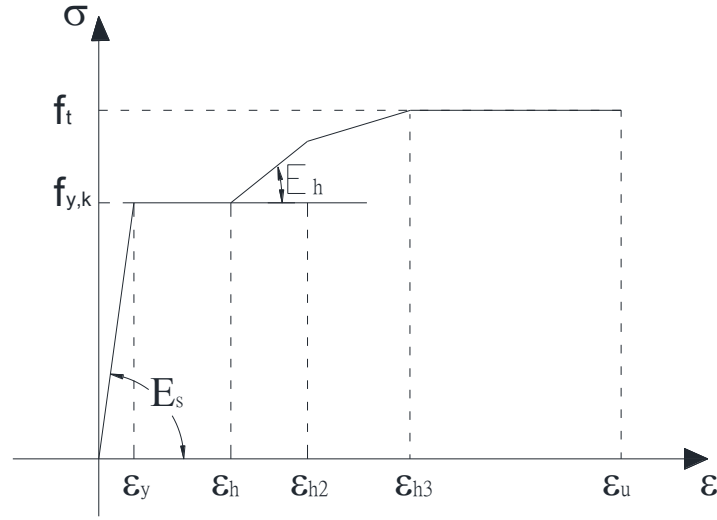


Figure 3.22: The second constitutive relationship (EPH) assumed for steel joist.

The values of the parameters for describing the constitutive law of figure 3.22 were established basing on the experimental data provided by the literature.

The concrete used has a cylindrical strength in compression f_{ck} equal to 20N/mm^2 (class C20/25); the first part of the constitutive relationship (fig. 3.23) is linear up to 40% of the compressive strength, f_{ck} , with a mean elastic modulus E_1 ; this modulus is evaluated according to the standard code formulas of NTC08 and EC2. The second part is characterised by a lower modulus, E_2 , up to the peak value of the strength that is reached at a strain of 0.002; after this peak a plastic region is assumed until the value of the ultimate strain ϵ_{cu} equal to 0.005 (Chapman et al., 1964; Scott et al., 1982, after which a linear descending branch to zero stress is adopted, until a deformation equal to 0.006.

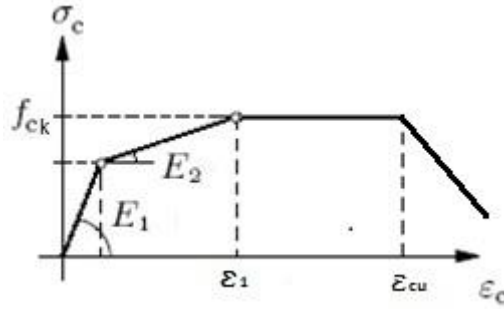


Figure 3.23: The constitutive relationship assumed for the concrete in compression.

The behavior of the concrete in tension was assumed bilinear (fig. 3.24) with the ultimate strain of concrete ε_u^{cr} fixed at 0.002.

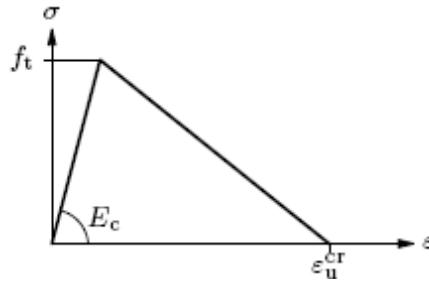


Figure 3.24: The constitutive relationship assumed for concrete in tension.

This value of the ultimate strain was assumed considering the suggestion of the software of assuming this strain equal to the yield strain of the steel reinforcing bars in order to take into account for the effect of tension stiffening

In order to evaluate the effectiveness of this assumption for the tension stiffening and cracking model used by the software, it was analyzed a reinforced concrete tie carrying and a numerical-experimental comparison with the results available in the literature and various numerical models.

The results of these comparisons are reported in summary in Section 3.3 and confirm the reliability of the model suggested by DIANA.

The constitutive law (fig. 3.25) used for the shear studs is the semi-empiric one suggested by Jorgen G. Ollgaard (Ollgaard et al., 1965) in terms of shear-slip, P-s, relation and reported in the following:

$$P = P_{max} \cdot (1 - e^{-\beta s})^\alpha$$

where:

P_{max} (P_R) is the shear strength of the connectors, that in this case was calculated according to the previsions of NTC2008, unless safety factors.

$$P_R = 0.8 \cdot f_t \cdot \left(\pi \cdot \frac{d^2}{4} \right) \quad \text{strength that depends on the stud failure}$$

$$P_R = 0.29 \cdot \alpha \cdot d^2 \sqrt{f_{ck} \cdot E_c} \quad \text{strength that depends on the concrete failure}$$

being f_t the strength of the stud steel, d the diameter of the stud.

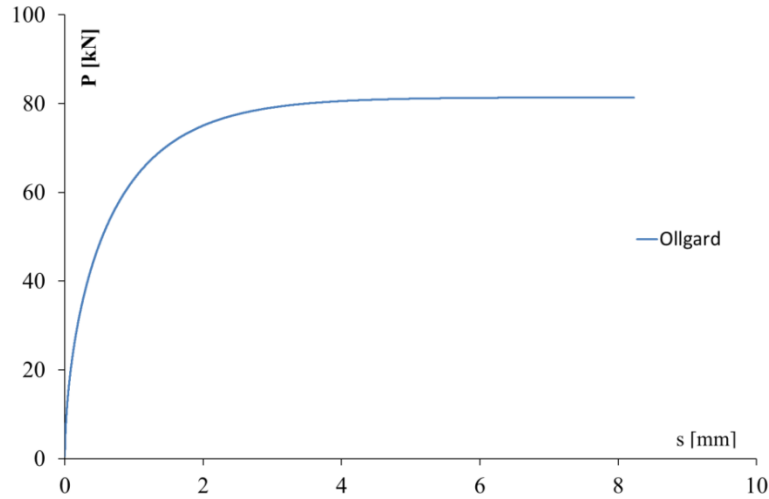


Figure 3.25: The constitutive relationship for shear studs.

This model was adopted after a numerical comparison performed for three different models of the shear connection: two based on the Ollgaard research and the third based on the research work of (Johnson et al., 1969) and used also in (Faella et al., 2003) for the characterization of the shear studs when the slab is in tension, i.e. in hogging moment region.

3.3 The tension stiffening effect in DIANA

The reinforced concrete tie used for the calibration of the model of the tension stiffening effect is that of the test reported in (Ceroni, 2002). The concrete tie has a length of 1200 mm and a square section with the side 100 mm (Fig. 3.26) while the mechanical properties of the materials are shown in Table 3.1 and 3.2, respectively for the concrete and the steel reinforcing bars.

Tie ID	Concrete Type	f_{cm} [MPa]	$f_{c,cub}$ [MPa]	f_{ctb} [MPa]	f_{cts} [MPa]	f_{ctm} [MPa]	$f_{ct,ax}$ [MPa]	E_c [MPa]	Density [kg/m ³]
Tp1	NSC	31.6	34.7	4.3	3.0	2.6	2.6	33690	2377
Tp2	NSC	34.7	37.1	4.3	3.2	2.7	2.7	32800	2386

Table 3.1: Mechanical features of the concrete.

Steel grade	Ø [mm]	f_y [Mpa]	f_u [Mpa]	E_s [Mpa]	ϵ_u
S500	10	574	670	$2 \cdot 10^5$	15,1%

Table 3.2: Mechanical features of the steel reinforcing bar.

An initial step of pre-load up to 32 kN was experienced on the tested tie, after which it was unloaded. Therefore, the test was conducted under displacement control with a speed of 1mm/min. The concrete tie failed at an ultimate load N_u equal to 48kN. The cracking framework was developed along the tie with a random sequence until the formation of seven cracks (Figure 3.27). Table 3.3 shows the experimental results in terms of crack opening $W_{np,1}$, average cracks distance $S_{m,exp,1}$, number of cracking n .

The numerical model was developed considering the approach with “concentrated cracks” arranged according to the experimental results: 7 cracks with an average distance of 149 mm. In correspondence of the cracks the interface elements (CQ48I) of thickness 10mm were placed.

Figure 3.28 shows the model with the “concentrated cracks”, placed with the interface element, and the central bar, modeled with beam elements L13BE. Between the cracks the concrete was modeled with solid elements CHX60. The numerical simulation was carried out under displacement control.

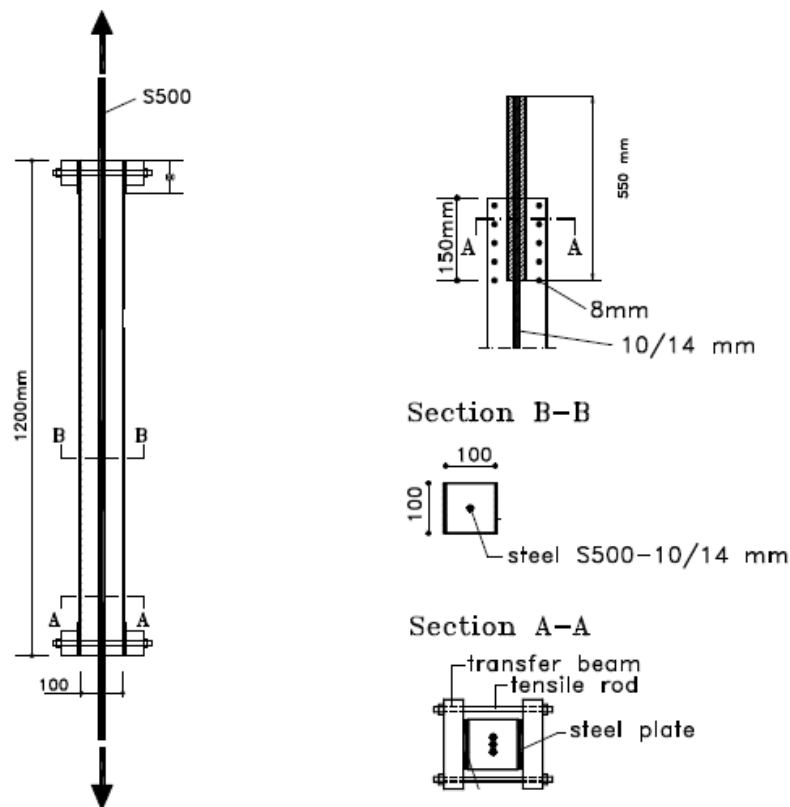


Figure 3.26: The reinforced concrete tie element tested (Ceroni, 2002).

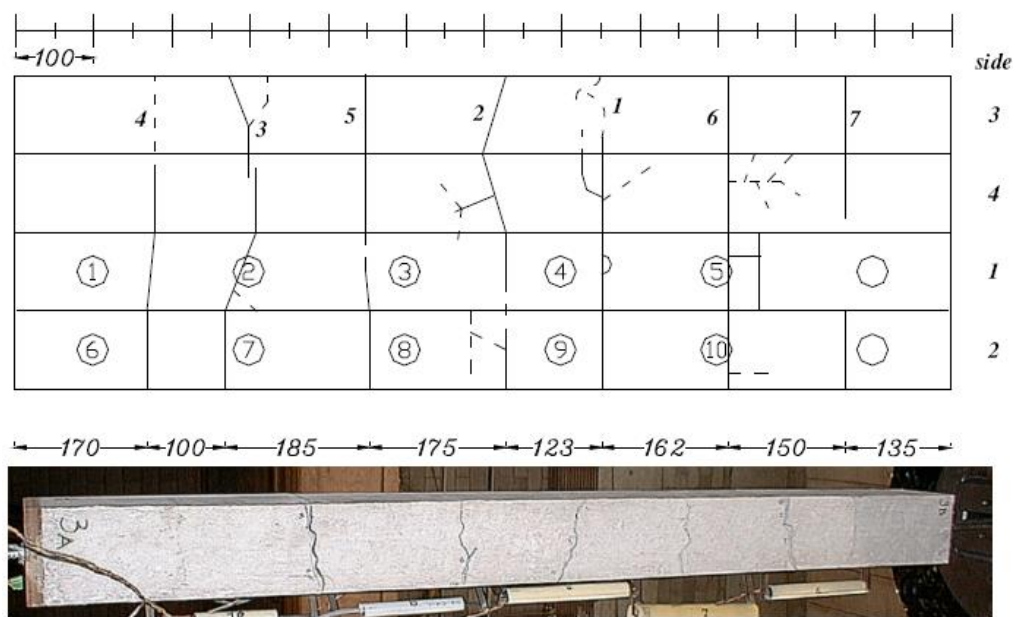


Figure 3.27: Cracking framework of the experimented tie.

Concrete Tie	N_p [kN]	$W_{np,1}$ [mm]	$S_{rm,exp,1}$ [mm]	N°_{fex}
TP1	32	0,217	149	7

Table 3.3: Experimental results.

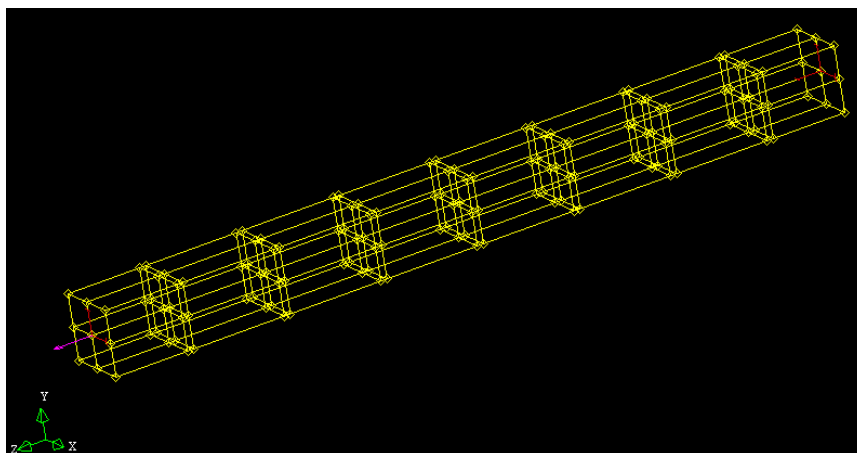


Figure 3.28: Geometry of the model.

The constitutive law of the reinforcement was described with a bilinear relationship with hardening according to actual behavior of the steel used in the tests (Fig. 3.29); the following parameters were obtained from the experimental tests on the material:

$$f_{pu} = 670 \text{ MPa};$$

$$f_y = 574 \text{ MPa};$$

$$\varepsilon_{pu} = 15\%$$

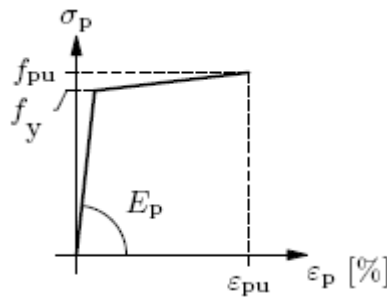


Figure 3.29: The constitutive relationship for steel reinforcing bar.

The concrete was modeled with a linear behavior up to the ultimate tensile strength after which there is a sudden softening (fig. 3.30). The tensile strength f_t is equal to 1.30MPa and the elastic modulus (E_c) equal to 33690MPa, based on the experimental values, while the ultimate strain is equal to 0.287%, based on the indications of the literature.

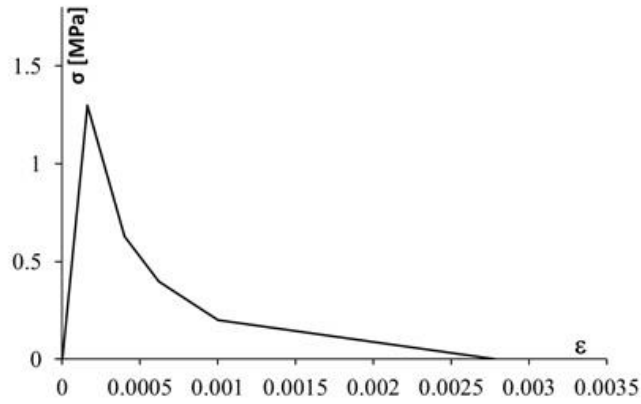


Figure 3.30: Model of the constitutive relationship for the concrete in tensile regime.

The definition of the constitutive law of the interface elements was established to take in account the tension stiffening effect. On the basis of the experimental behavior, (Fig. 3.31) the contribution of the tension stiffening was evaluated as the difference between the deformation of the bare bar and the average deformation of the tested Reinforced Concrete tie.

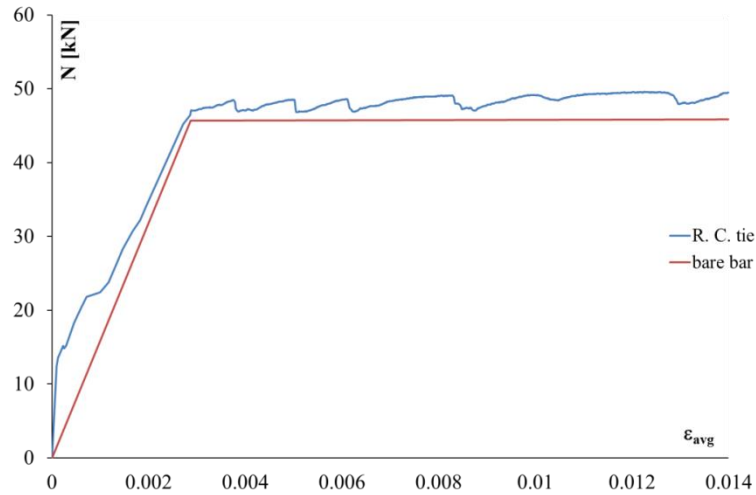


Figure 3.31: Load-average deformation curve.

The behavior of the concrete tie in the elastic range is reported in the figure 3.32 together with the one of the bare bar.

The relationship of the tension stiffening effect to be placed in the interface elements was evaluated according to the following procedure:

$$N_{tie} = N_{bar}$$

where N_{tie} is the axial force in the concrete tie and N_{bar} is the axial force in the bare steel bar.

It is possible to calculate the deformation of the bare bar (ε_{bar}) by dividing the axial force by the area of the reinforcing bar (A_s) and the elastic modulus of the steel reinforcing (E):

$$\varepsilon_{bar} = \frac{N_{tie}}{A_s \cdot E}$$

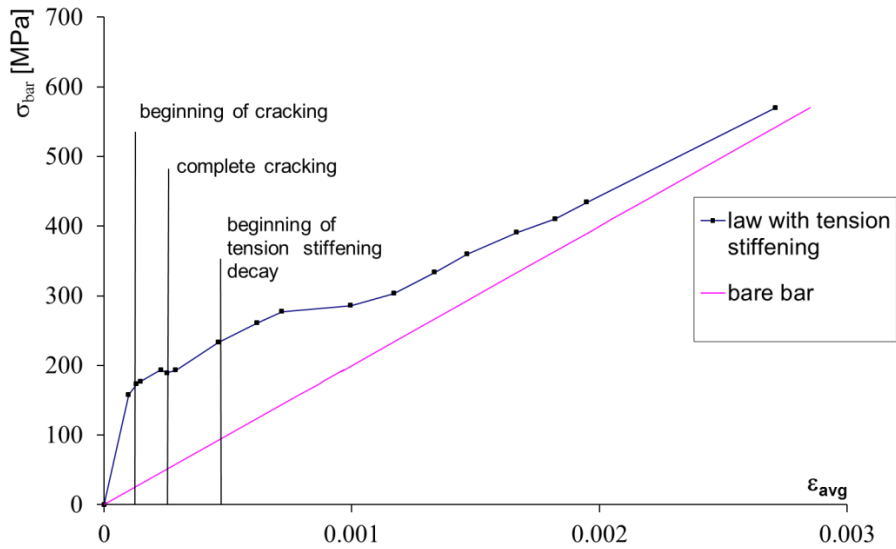


Figure 3.32: Behavior of the concrete tie.

Therefore, for each value of the average deformation of the concrete tie (ε_{avg}) it is possible to calculate the amount of the axial force to be attributed to the interface (N_{ts}) to reduce the deformation of the bare bar, simulating the effect of the tension stiffening:

$$N_{ts} = N_{tie} - \varepsilon_{avg} \cdot E \cdot A_s$$

Table 3.4 summarizes all the data obtained from the calculations.

The relationship obtained refers to the field of post-cracking while before the opening of the first crack the linear tensile behavior of the concrete was adopted.

Figure 3.33 shows the comparison between the performance of the tested concrete tie with the one of the bare bar from which it is possible to highlight the contribution of the tension stiffening.

ε_{avg}	N_{tie}/A_s	ε_{bar}	N_{tie}	N_{ts}	σ_{ts}
0	0	0	0	0	0
0.0000986	157.96	0.000790	12399.86	10851.73	1.08
0.0001311	173.24	0.000866	13599.34	11540.32	1.15
0.0001475	177.07	0.000885	13900.00	11583.60	1.16
0.0002295	193.63	0.000968	15199.96	11596.68	1.16
0.0002541	189.05	0.000945	14840.43	10850.35	1.08
0.0002897	193.25	0.000966	15170.13	10620.97	1.06
0.0004607	232.99	0.001165	18289.72	11056.57	1.10
0.0006174	260.89	0.001304	20479.87	10786.29	1.08
0.0007183	277.45	0.001387	21779.83	10502.12	1.05
0.0009964	285.86	0.001429	22440.01	6796.37	0.68
0.0011697	303.31	0.001517	23809.84	5445.94	0.54
0.0013342	333.50	0.001668	26179.99	5233.12	0.52
0.0014652	359.49	0.001797	28219.97	5216.33	0.52
0.0016663	391.08	0.001955	30699.78	4538.48	0.45
0.0018224	410.32	0.002052	32210.12	3598.91	0.36
0.0019490	434.39	0.002172	34099.62	3500.32	0.35
0.0027110	574.00	0.002870	45059.00	2496.30	0.25
0.0147300	630.00	0.150000	48000.00	0.00	0.00

Table 3.4: Data from the theoretical evaluation.

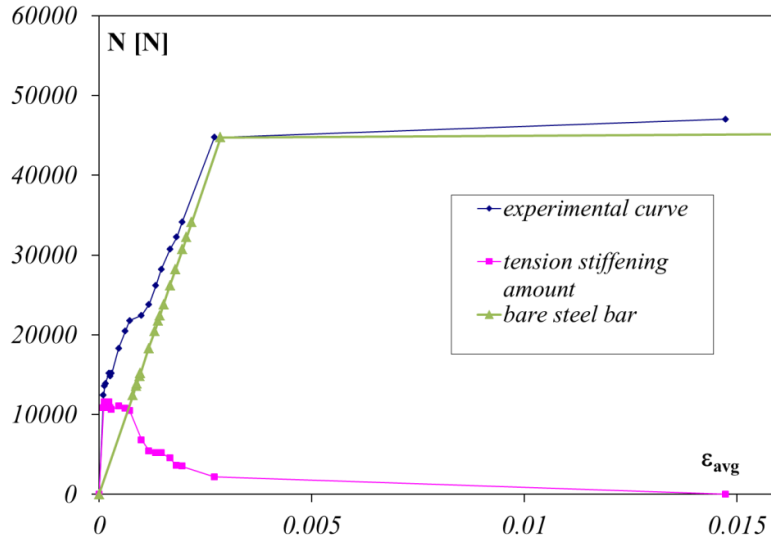


Figure 3.33: The amount of tension stiffening effect.

Dividing the axial force of the tension stiffening for the area of the tie (100×100 mm), it was obtained the stress (σ_{ts}) to be included in the constitutive law of the interface element.

The relationship due to the tension stiffening shows a first linear branch up to the tensile strength, afterward a softening branch (Fig. 3.34).

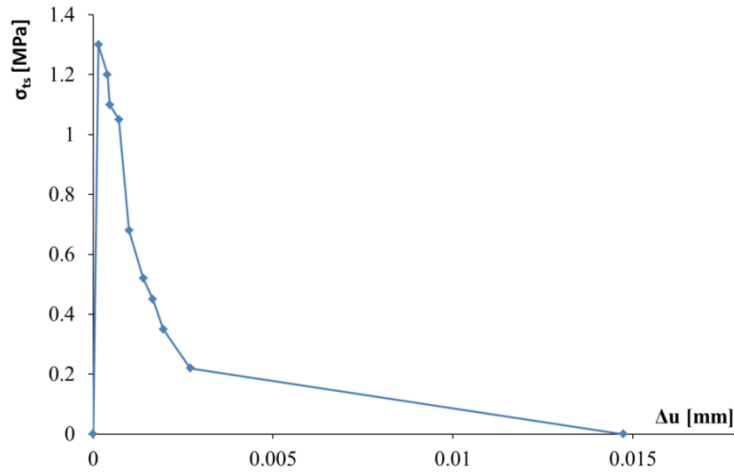


Figure 3.34: Model of the constitutive relationship for the interface elements.

After the definition of the finite elements and the mechanical features of the materials, the mesh, shown in the figure 3.35 was realized: the concrete was discretized with cubic element having dimensions $1.25\text{cm} \times 1.25\text{cm} \times 2.48\text{cm}$. The interface elements were placed at the experimental cracks distance; the reinforcing bar was divided and connected to the mother body element in which it is embedded.

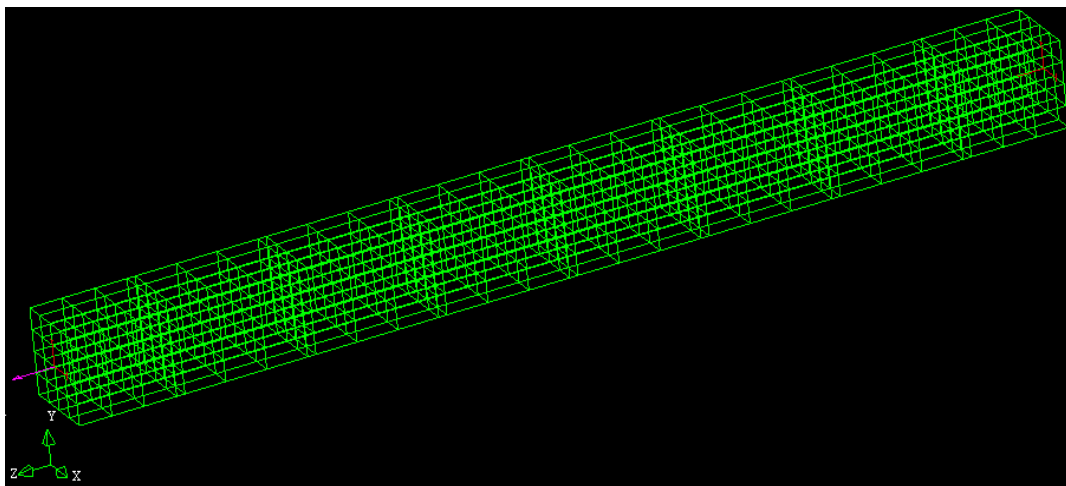


Figure 3.35: The mesh of the FE model.

In the numerical analysis with the software Diana, the first step was made with the analysis beyond the yielding of steel, with a number of 200 steps of 0.01mm amplitude.

Figure 3.36 shows the load-deformation relationship for the average experimental test and the numerical model. Up to the point where the cracking starts, therefore in the linear field, the comparison shows a good agreement between the two curves that are governed only by the values of the elastic moduli. When the cracking begins, it detects a fall of load, both in the experimental curve than in the numeric one, due to the loss of the tensile strength of the concrete at the cracks. This loss of strength is then recovered in

the phase of stabilization of the cracks in which the reinforcing bar at the cracks is able to load the entire axial force.

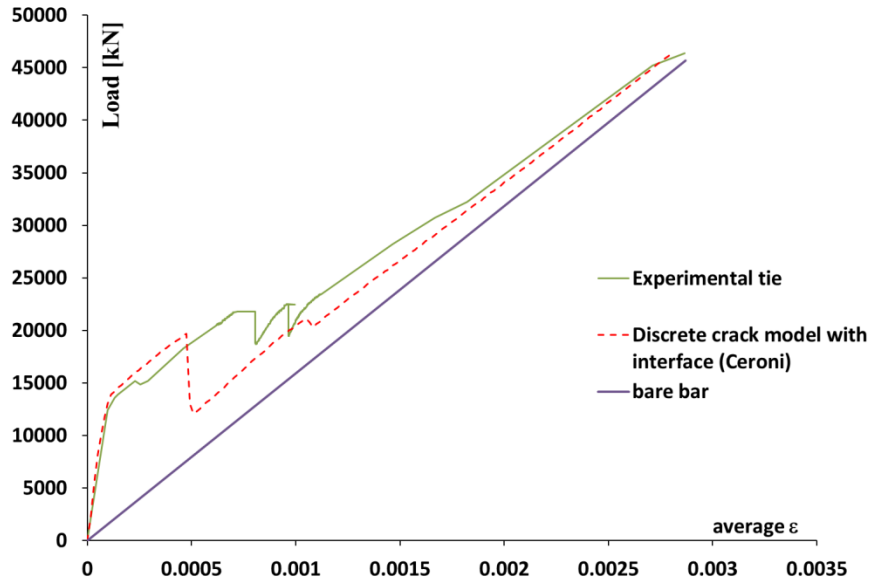


Figure 3.36: Comparison between numerical model and experimental results

This first implemented FE model was compared with two other models:

- a simple smeared cracks FE model;
- a “cracks concentrated” FE model, similar to that implemented hereafter, where the relationship used for the interface elements is reported in (Baldassino et al., 2008)

In particular, in the model with a smeared cracks approach a constitutive law of concrete was used with a linear softening behavior that takes into account for the cracking and the tension stiffening.

The constitutive law used is suggested by the software and is based on the ultimate tensile strain of concrete (or equivalently energy of fracture), as indicated in figure 3.30, where the ε_u^{cr} was set equal to the yield strain of the

steel reinforcing bar, approximately equal to 0.002, as already reported in fig. 3.24.

Figure 3.37 shows the comparison between the different FE models in terms of the relation N - average deformation.

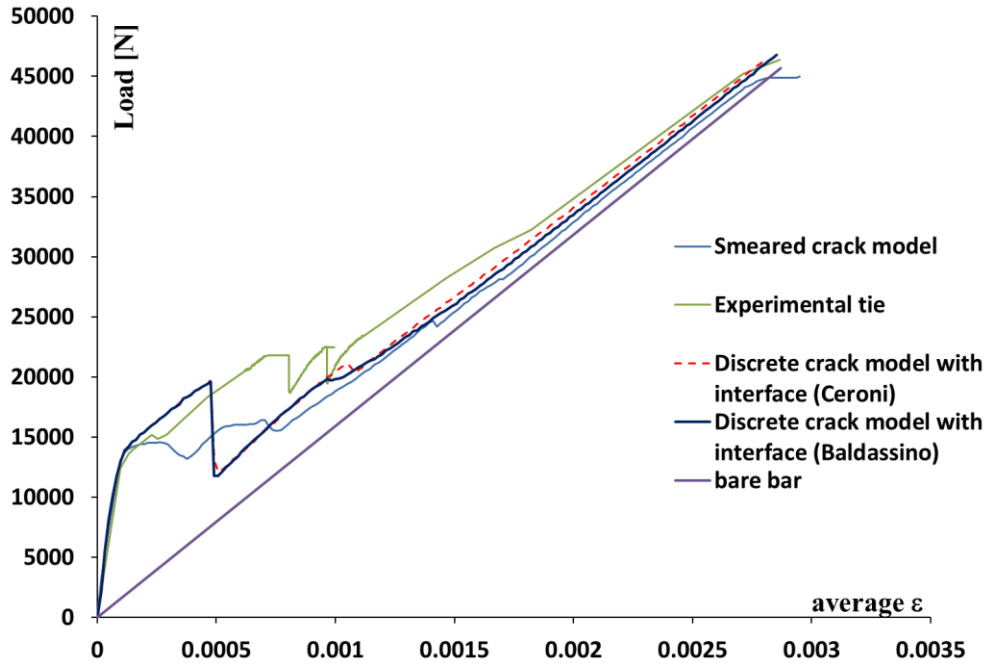


Figure 3.37: Comparison of load-average deformation curves for all the model analyzed.

The simulations obtained with the constitutive law used in (Baldassino et al., 2008), the constitutive law developed in this work and with the criteria set out in the software Diana are very similar and give results in good agreement with the experimental ones.

3.4 The residual stresses

Another important aspect that has to be introduced in the numerical analysis of composite beams regards the residual stresses along the web and the flange of the steel joist (fig. 3.38).

Noting that the values of the residual stresses could be very high, even more than half the yielding strength up to the yielding strength.

In the modeling of the composite beam, however, it was assigned a constant simplified "block scheme" as reported in the figure 3.39.

More precisely, the flanges of the steel profile are divided into 3 parts, the external ones are considered in tension while the central part is in compression; the web, in the same way, presents the central part in tension, while the upper and lower parts are in compression.

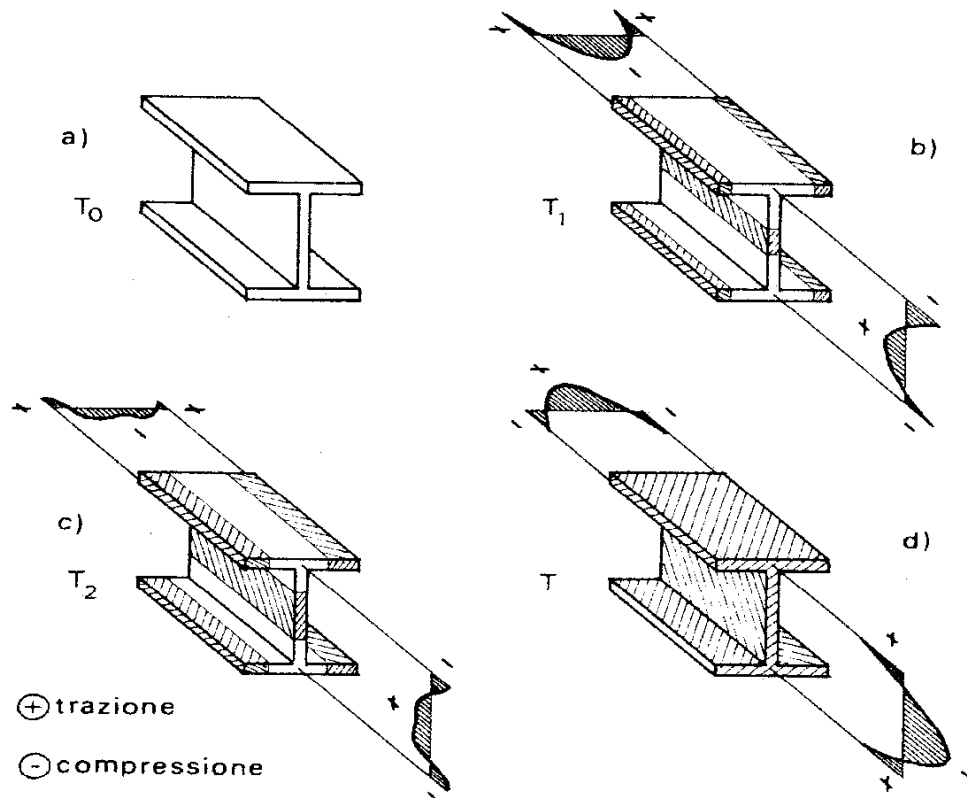


Figure 3.38: Variation of the stress field for the residual stresses.

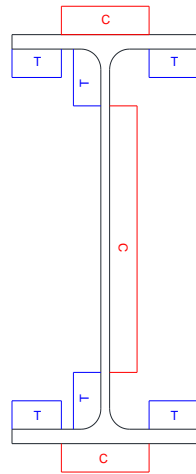


Figure 3.39: The distribution of the residual stresses adopted in the model.

3.5 Local and global buckling

Observations about the experimental results reported in (Pecce et al., 2010) were of great interest to study the problem of local and global buckling. In order to consider these issues within the model, it was decided to apply a suitable geometric imperfections in the same position where were observed in the experimental program. For this reason, several studies were analyzed from the technical literature. Each author generally simulated the problem of the local and global buckling through a parametric analysis with different geometrical arrangements of the imperfections and considered the parameters that can influence the phenomenon.

It was observed that the imperfections have a significant contribution in the non-linear numerical analysis of the structures.

In the actual practice, to introduce the geometric imperfections in the numerical models it is possible to refer to sinusoidal shapes (Dubina et al., 2002) with the wavelengths taken from the relevant buckling modes. As regard to this issue in (Schafer et al., 1998) it was proposed a numerical model to automatically

generate the geometric imperfections in the nonlinear analyses. Through a probabilistic analysis it was defined the fundamental buckling mode, necessary to define the imperfections with sinusoidal pattern, evaluating, subsequently, the frequency and magnitude of imperfections.

Furthermore, FEM analyses were developed to evaluate the influence of the shape of the geometric imperfections on the reduction of the theoretical strength due to the buckling of the steel sections, both in compression and in bending. The authors carried out numerical simulations assuming the values of the geometric imperfections equal to $L/500$ and $L/1000$. Experimental tests showed that the different pattern of the imperfections have a different effect on the buckling resistance; specifically it was observed that the value of the imperfection set to $L/1000$ leads to a higher sensitivity in terms of global buckling.

Even the problem of the local buckling was addressed by a geometrical point of view. In fact, in (Feng et al., 2004) it was illustrated the results of the numerical simulations for different values of the initial imperfections. In the paper the numerical-experimental comparisons were performed with reference to the experimental tests on beam-column elements. Observing the behavior of the structural elements through the load - displacement curves, the strength of the tested columns were not very sensitive to the values of the initial imperfections if less than $h/200$. At the same time the higher values of the initial imperfection did not involve results of particular interest that are not so far from the ones obtained with $h/200$.

3.6 Features and behaviour of the tested beams

In order to have more information on the rotational capacity of composite beams subjected to hogging moment, three points bending tests were carried out on four composite beams. The beams have a length of 4 m, that can be

significant for a frame with spans of 6-8 m. The steel profile is a double T with height=360mm, width=170mm, $t_w=8\text{mm}$ and $t_f=12,7\text{mm}$. The slab thickness is of 130mm and was constructed without and with profiled sheeting, in the latter case two widths of the slab (1000mm and 1600mm) were realized.

The meaning features of the beams are reported in Fig. 3.40, 3.41, and 3.42. The material used in the design are S275, B450C and C20/25 respectively for steel profile, steel bars and concrete according to the European codification; the nominal characteristic yielding strength f_{yk} is 275 MPa and 450 MPa, for constructional and reinforcing steel respectively, and $f_{ck}=20$ MPa is the nominal characteristic compressive strength of concrete. The classification of the sections according to Eurocode 4 was checked during the design process estimating the slenderness of the flange and web and comparing the results with code limits, as in the follow.

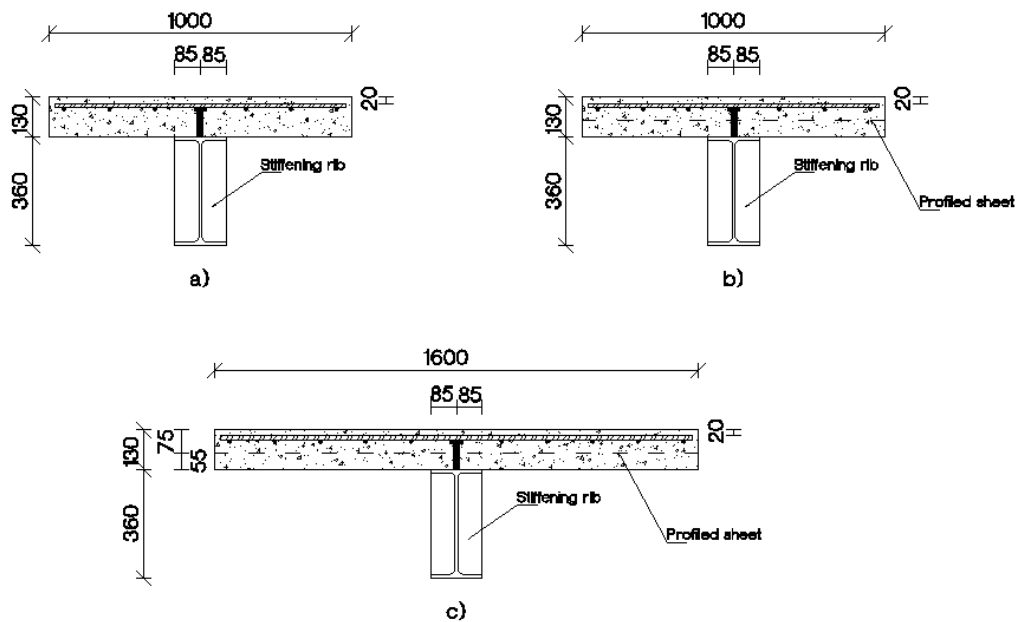


Figure 3.40: Cross-sections of the beams at mid-span [mm]: a) for Beam 1 and 2; b) for Beam 3 with profiled sheet and c) for Beam 4 with profiled sheet.

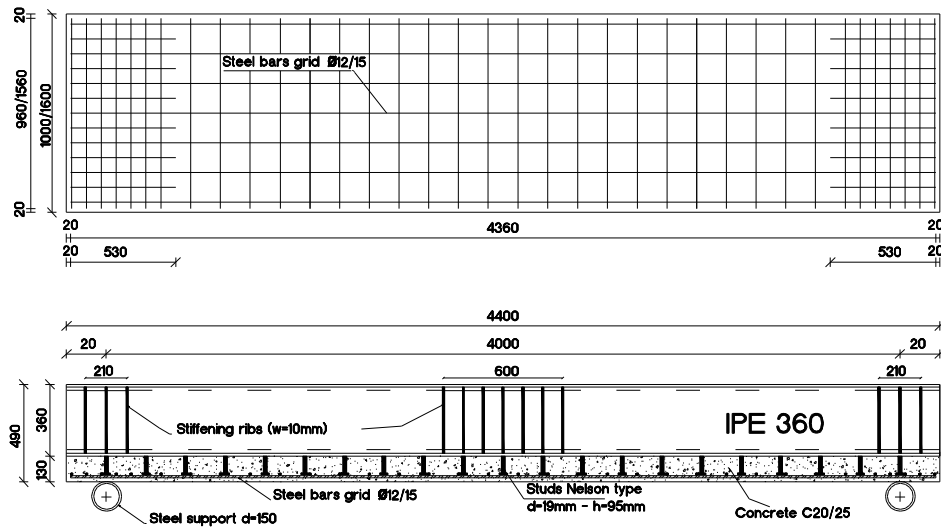


Figure 3.41a: Geometry of the beams [mm].

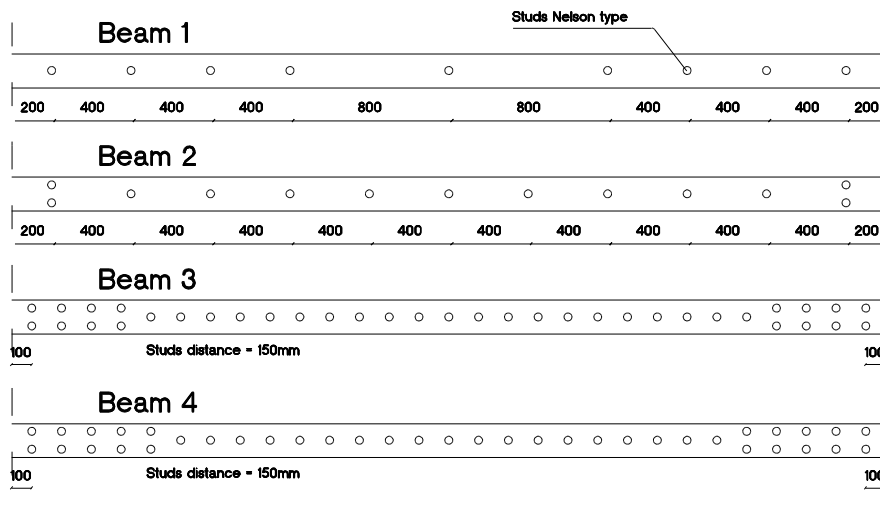


Figure 3.41b: Geometry of the connection [mm].

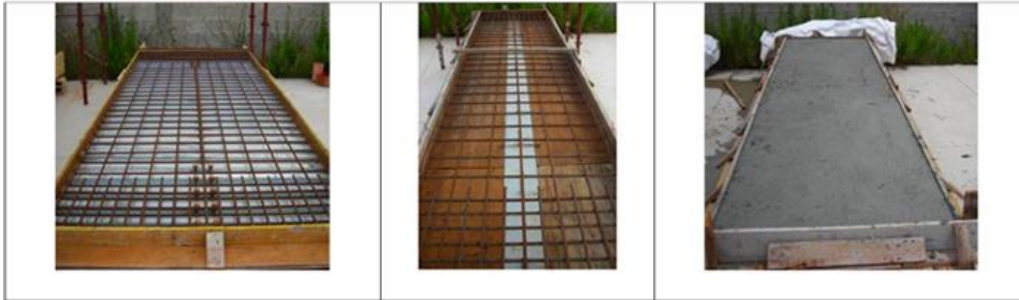


Figure 3.42: Tested beams: slab with (on the left) and without (center) profiled sheeting. Concrete cast of the slab (on the right).

3.6.1 Experimental characterization of the materials

In order to know the actual properties of the materials after the beams construction the steel and concrete used were experimentally characterized. Tensile tests were carried out on three specimens extracted from the web of the steel profile according to UNI 10002/92, obtaining the typical constitutive law depicted in figure 3.43 and the following average values:

$$f_y=401\text{MPa} \quad f_t=588\text{MPa} \quad \varepsilon_{su}=17,5 \%$$

with a standard deviation of 8,40MPa, 8,80MPa and 1,5% respectively. From the results a characteristic value $f_{yk}=369\text{MPa}$ could be estimated.

Also for the reinforcing bars three tensile tests were executed obtaining the following results and the typical constitutive relationship reported in figure 3.40, too:

$$f_y=455\text{MPa} \quad f_t=577\text{MPa} \quad \varepsilon_u=20,5\%$$

with standard deviation of 6,60MPa, 3,60MPa and 4,1% respectively, from which a characteristic value of $f_{yk}= 430\text{MPa}$ could be estimated. The compression tests on 3 concrete cubes with side of 150mm gave a mean value of 37,6MPa.

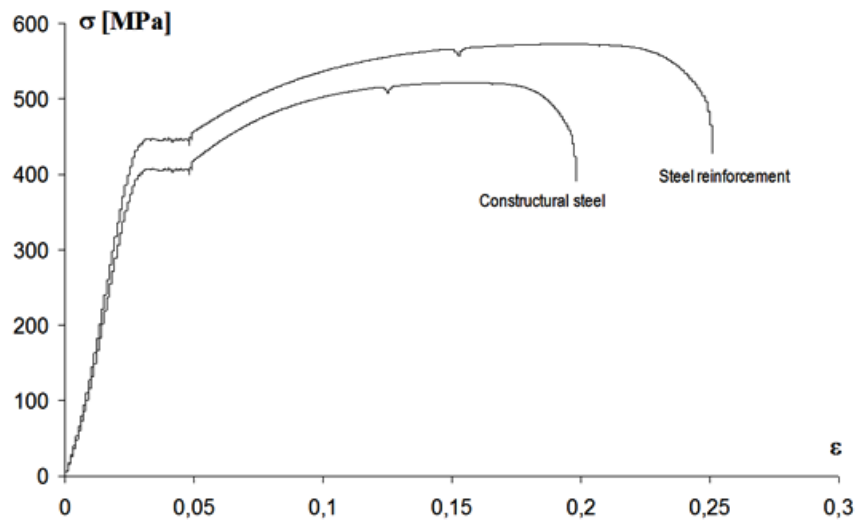


Figure 3.43: Stress-Strain relationships of the constructional and bars steel.

In conclusion the ratio of the actual characteristic value of the yield steel strength to the nominal one used in the design is about a unit for the steel reinforcement, conversely this ratio is equal to 1,34 for constructional steel, exceeding the limit of 1,20 set by Eurocodice 8 (the same in NTC 2008).

3.6.2 Evaluation of the actual characteristics of the beams

The tests on the materials suggested relevant differences between nominal and actual characteristics of constructional steel at yielding, therefore the classification of the steel cross-section was revised using the actual yield strength of steel profile also considering unitary safety factor that is significant of the experimental behaviour more than the design one. The following classification results:

- for the flanges:

$$\frac{c}{t_f} = \frac{85}{12,7} = 6,7 < 10 \cdot \varepsilon = 10 \cdot \sqrt{235 / f_y} = 10 \sqrt{235 / 369} = 10 \cdot 0,79 = 7,9 \Rightarrow \text{Class 1}$$

- for the webs

Beam 1, 2 and 3

neutral axis (web height in compression) $x = 236 \text{ mm}$

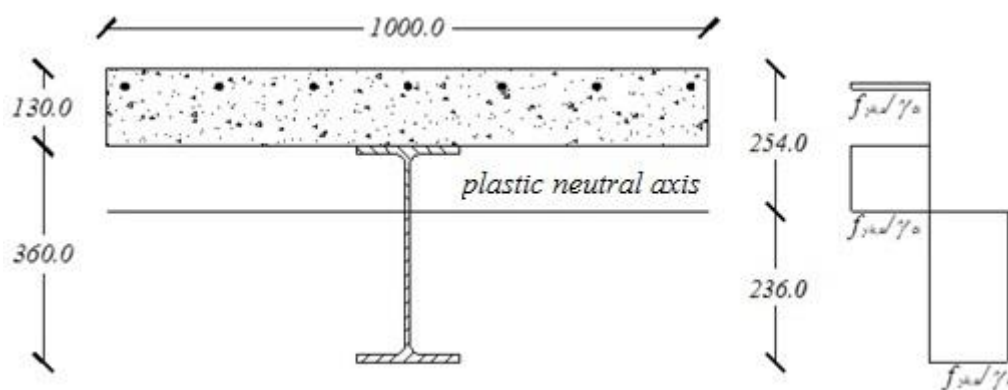


Figure 3.44a: Evaluation of the plastic neutral axis of the steel-concrete composite section with a width slab of 1000mm.

where d is the clean height of the web unless of the radius at the web joint.

$$\alpha = \frac{x - (t_f + r)}{d} = \frac{236,00 - (12,70 + 18,00)}{360,00 - 2 \cdot (12,70 + 18,00)} = \frac{205,3}{298,6} = 0,69$$

so that

$$\frac{d}{t_w} = 37,32 < \frac{393\varepsilon}{13\alpha - 1} \approx 38,18$$

therefore the profile remains in Class 1 albeit at the border line of Class 2 for the web slenderness.

Beam 4

neutral axis (web height in compression) $x = 268$ mm

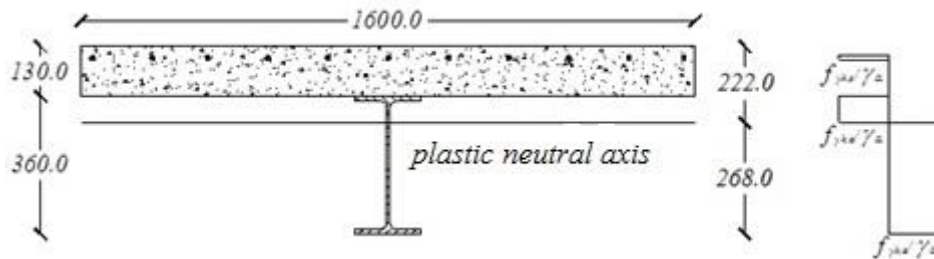


Figure 3.44b: Evaluation of the plastic neutral axis of the steel-concrete composite section with a width slab of 1600mm.

$$\alpha = \frac{x - (t_f + r)}{d} = \frac{268,00 - (12,70 + 18,00)}{360,00 - 2 \cdot (12,70 + 18,00)} = \frac{237,3}{298,6} = 0,80 \quad \text{so} \quad \text{that}$$

$$\frac{d}{t_w} = 37,32 < \frac{456\varepsilon}{13\alpha - 1} = 37,39$$

therefore the profile remains in Class 2 albeit at the border line of Class 3 for the web slenderness.

In conclusion, the actual yield strength of steel profile formally does not change the classification of the section, even if the relationship between the local slenderness and the limits of the code are significantly different from the ones used in the design.

In the design of the specimens a further variability was applied to the degree of connection and connectors distribution. The type of the connection devices was fixed using Nelson studs with diameter 19 mm, that resulted ductile for the geometry of the beams tested. The stud resistance (f_{bd}) was evaluated according to the EC4 2004 without the partial safety factors for the materials and the connectors; it resulted equal to 81,4kN for the beams with full slab and 32,7kN for the beams with profiled steel sheeting. The number of studs for the full interaction was calculated assuming the ultimate tensile force of the rebars slab (F_{cf}) as the force to be transferred between the profile and slab i.e. neglecting the concrete contribution in tension, $F_{cf} = A_s \cdot f_{y,s}$; in Table 3.5 the number of connectors for a full interaction together with the degree of connection are shown for all specimens.

	Beam 1	Beam 2
$N_f = 2 \cdot \frac{F_{cf}}{f_{bd}}$	$2 \cdot \frac{455 \cdot 791}{81,4 \cdot 10^3} = 8,84 \cong 9$	$2 \cdot \frac{455 \cdot 791}{81,4 \cdot 10^3} \cong 9$
$\frac{N}{N_f}$	$\frac{9}{9} = 1,00$	$\frac{13}{9} \cong 1,44$
	Beam 3	Beam 4
$N_f = 2 \cdot \frac{F_{cf}}{f_{bd}}$	$2 \cdot \frac{455 \cdot 791}{32,7 \cdot 10^3} \cong 22$	$2 \cdot \frac{455 \cdot 1243}{32,7 \cdot 10^3} = 34,6 \cong 35$
$\frac{N}{N_f}$	$\frac{37}{22} \cong 1,68$	$\frac{37}{35} \cong 1,11$

Table 3.5: Degree of connection of the beams.

Therefore, all Beams have a full interaction. In Table 3.6 the meaningful characteristics of the specimens are summarized.

ID BEAMS	CLASS	CONNECTION TYPE	SLAB TYPE	EFFECTIVE WIDTH
Beam 1	1	Full	Full Slab	(1.0 m)
Beam 2	1	Full	Full Slab	(1.0 m)
Beam 3	1	Full	Profiled sheeting	(1.0m)
Beam 4	2	Full	Profiled sheeting	(1.6 m)

Table 3.6: Principal features of the composite beams tested.

3.6.3 Instrumentation

On the specimens several measuring instruments were placed to identify the global and local behavior of the beams during the test. The applied load and the deflection in the middle were detected respectively by the load cell and inductive transducer integrated into the jacket used to load the beams by displacement control. Some strain gauges were glued along the height of the steel profile, in two sections respectively at 50 mm and 350 mm from the center of the specimen since it was impossible to apply the instruments in the middle where a stiffening plate was welded. Before concrete casting some strain gauges were placed on the reinforcing bars of the slab at the middle section of the beam and others were placed at a distance of 300 mm from the center.

Finally, some displacement transducers were arranged lengthwise to measure the horizontal slip between the steel beam and the concrete slab, and others in the middle of the slab to monitor the cracks opening. In Fig. 3.45 the position of the strain gauges and the longitudinal transducers are reported.

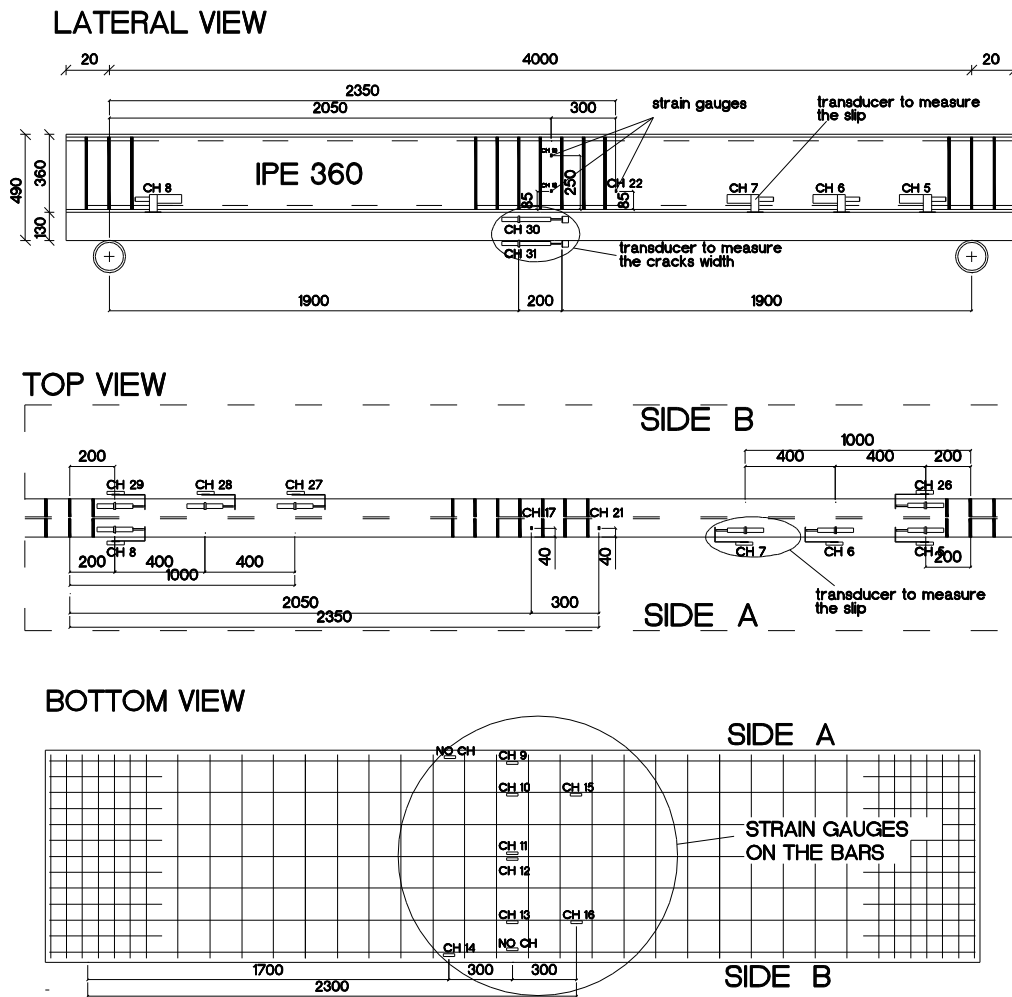


Figure 3.45: Measuring instruments position (all beams).

3.6.4 Results

The yielding of the section was evidently reached and a plastic deformation was developed. During the evolution of plasticization a phenomenon of local buckling in the compression region, the flange and part of the web, together with a global torsional buckling was observed.

In Fig. 3.46 the two phenomena can be seen in some photos. The test was stopped at a displacement of about 100 mm, when the global and local

buckling were evident and for the most of the beams a reduction of the load started.

As already introduced the global buckling phenomenon was unexpected so that the steel beam was not restrained for torsion.

The Fig. 3.47 reports the load-deflection curves of the four beams; after a similar beginning branch before concrete cracking, some differences are evident especially due to the variation of the connection or the different type of RC slab. The comparison between the Beam 1 and 2, evidences a reduction of strength and stiffness in the Beam 1 where the connection degree is lower than 1 and there are not studs in the central part of the beam; however the peak moment occurs at the same displacement for both beams and the descending branch has the same trend.

The Beam 2 can be compared to the Beam 3 that has a full connection and the slab 1000mm width, but the slab is realized with the profiled sheeting. The Beam 3 shows a lower stiffness than the Beam 2 probably due to a less efficiency of the connection when the profiled sheeting is used, however the maximum moment is lightly higher probably due to the contribution of the profiled sheeting. Furthermore the descending branch begins at a greater displacement, about when the test was stopped. Finally the Beam 3 can be compared with the Beam 4 that differs for the greater width of the slab. The maximum moment increases in the Beam 4 due to the larger amount of slab reinforcement and points out the slab width is effective. After this higher peak it follows a steeper descending branch due to the higher sensitivity of this section to the local buckling of web that has a longer part in compression, as already known from the classification (Beam 4 in Class 2, Beam 3 is in Class1).



Figure 3.46: Failure mode.

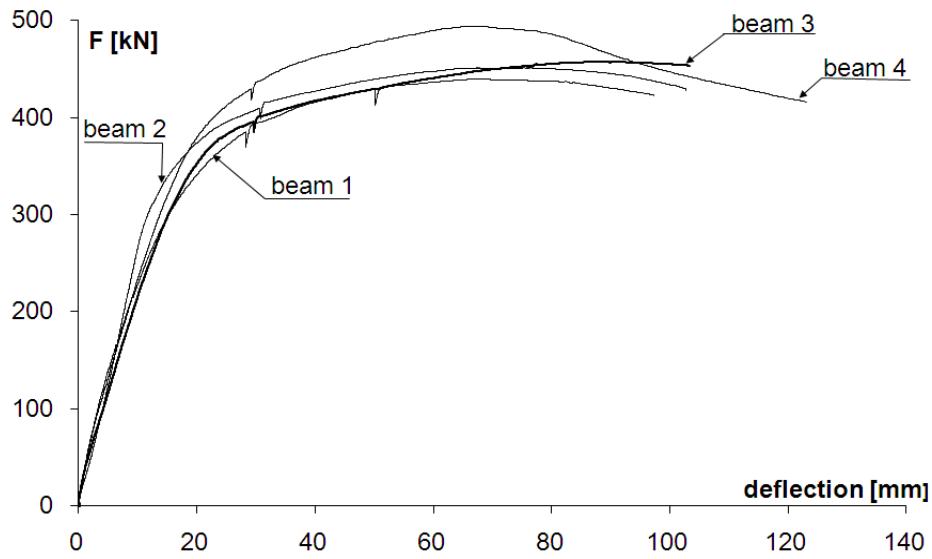


Figure 3.47: Load-deflection curves for the four beams.

In order to estimate the plastic rotational capacity the following rotations have been evaluated from the experimental results:

- θ_y , corresponding to the load when the yielding moment M_y is reached;
- θ_u , at the 85% of the maximum load ($F_{0.85}$) taken on the descending branch of the load-deflection curve, as already done for the results discussed in paragraph 2; really the tests were stopped before the development of the descending branch reached this decreasing, so this conditions coincides with the last measured load;
- θ_{max} at the maximum load.

All the rotations were estimated, dividing the deflection at the corresponding load by the half length of the beams; the results are summarized in table 3.6. The yielding moment of the composite section was computed assuming a full interaction and using the actual characteristics of the materials; it followed that the yielding of the cross-section implies the yielding of the reinforcement for

the Beams 1, 2, 3, and the yielding of the constructional steel in compression for the Beam 4. The difference between θ_y and θ_u provides the plastic rotation θ_{pl} , and the difference between θ_y and θ_{max} provides the plastic rotation $\theta_{pl,max}$; comparing the values of the plastic rotation according these two definitions (tab. 3.7), the importance of the post peak branch is clear especially in the case of the Beam 4 for which a double plastic rotation can be attained using its contribution.

Beam	M_y [kN·m]	θ_y [mrad]	θ_u [mrad]	θ_{max} [mrad]	$\theta_{pl,u}$ [mrad]	$\theta_{pl,max}$ [mrad]
1	375	13	48	34	35	21
2	375	10	51	38	41	28
3	375	12	52	38	40	36
4	434	15	60	36	45	21

Table 3.7: Significant values of the experimental rotations.

The results of the four specimens can be compared pointing out the following comments:

- the lower rotational capacity of the Beam 1 is due to the distribution of the studs since their absence in the central part of the element facilitate local and global buckling;
- the equal rotational capacity of the Beam 2 and 3 confirms the element ductility is independent from the type of slab, i.e. full slab or slab with profiled sheeting; however a better stability of the Beam 3 is observed (higher $\theta_{pl,max}$) probably due to the higher number of connectors that gives a better constraint of the steel profile to the slab retarding the global buckling phenomenon;
- the plastic rotation of the Beam 4 is about 10% higher than the one of the other specimens since the descending branch can be used that was not measured in the other cases, however the effect of an higher ratio $(A \cdot f_y)_r / (A \cdot f_y)_a$ that facilitate the local buckling is evident.

Extending the comparison to the data collected in Tab. 2.1 the parameters of the Beams 1,2 and 3 used for the tests presented herein are similar to the ones of Fabbrocino et al. (2001), the specimen CB7 of Loh et al. (2004), the ones of Amadio et al. (2004) except for a greater ratio $(\varepsilon_u / \varepsilon_y)_r$, that is not used due to the premature attaining of buckling. In all the other tests the plastic rotation is greater than the one reached in these tests but the profiles used for the specimens of other Authors are less sensible to local buckling due to the shape of the profile or the adding of longitudinal stiffeners.

In figure 3.48 an example of the load-strain curves detected by the strain-gauges is reported for the Beam 1 along the height of the cross-section at 50 mm from the mid-span; in the graph the position of each strain-gauge respect to the steel flange in compression is indicated. The graph remarks that the strain-gauges positioned at the bottom of the profile in the tensile part, show a linear trend until reaching the yielding; instead, the strain gauges placed at the top of the profile in compression, result in a nonlinear behavior at a load value just lower than the yielding one pointing out the occurrence of buckling. Even in the Beams 2, 3 and 4 similar deformation patterns were measured.

The local buckling phenomena pointed out by the strain gauges in compression, together with a global torsion observed on the entire beam, indicate that buckling occurred prematurely for the type of section used, probably due to the lack of torsional constraints of the steel cross-section in the support zone and the sensitivity to the distortional buckling of the used steel profile. However a consistent plastic rotation was arisen that can be assumed as the minimum resource of the beam since it can be surely increased by the suitable constraints in a real frame (i.e. transversal beam, continuity of the beam at the zero moment points, etc...).

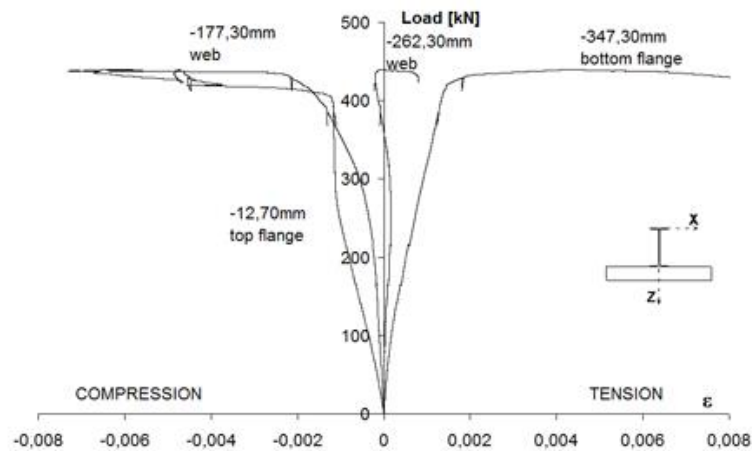


Figure 3.48: Strains along the profile of the Beam 1 in the section at 50 mm from the middle

3.7 The FE model of the composite beams tested

The following section discusses the criteria and the choices assumed for the model of the steel-concrete composite beam modeled with the aid of the finite element program TNO Diana. Regarding the choice of the finite elements and the constitutive laws of the materials, this model was developed as described above. Therefore different constraints were introduced to simulate the boundary conditions of the tested beams. Only half beam was modeled as the beam pattern is symmetrical.

According to the assumptions of par. 3.2.1 and the values obtained from the experimental tests, it were adopted the constitutive properties of the materials listed in Table 3.8.

For the shear connection it was used the interface element, that has a behavior expressed by a stress-strain law. In particular, the ultimate strength of the shear stud was evaluated in accordance with the standard code EC4 (equal to NTC08) and is equal to 380N/mm^2 with a slip equal to 8.00mm.

In the numerical simulations it was decided to assign the residual stress distribution shown in figure 3.49 and characterized by a value equal to 200N/mm^2 , which represents the average value between a null value and the yield one.

	$f_{ys} (f_{yk})$ [N/mm ²]	f_{h2} [N/mm ²]	f_t [N/mm ²]	E [N/mm ²]	ε_y [%]	ε_h [%]	ε_{h2} [%]	ε_{h2} [%]	ε_u [%]
Steel joist	401	470	588	200000	0.2	1.12	4.12	8.63	15
Steel reinforcing bars	455	532	577	200000	0.2	1.12	4.12		6.75
	f_{ck} [N/mm ²]			E [N/mm ²]	ε_l [%]	ε_{cu} [%]			
Concrete	20			25000	0.2	0.35			

Table 3.8: Mechanical features of the materials in the model

Furthermore the local and global buckling phenomena were introduced imposing a distribution of geometrical imperfections in the various sections.

With regard to the global buckling, a maximum value of the initial imperfection of magnitude equal to $L/1000$ was assigned:

$$\frac{L}{1000} = 4.00\text{mm}$$

This imperfection was not assigned section by section in a constant manner but it was given by means of a parabolic law, with the maximum value in the middle section of the composite beam and the zero value at the ends.

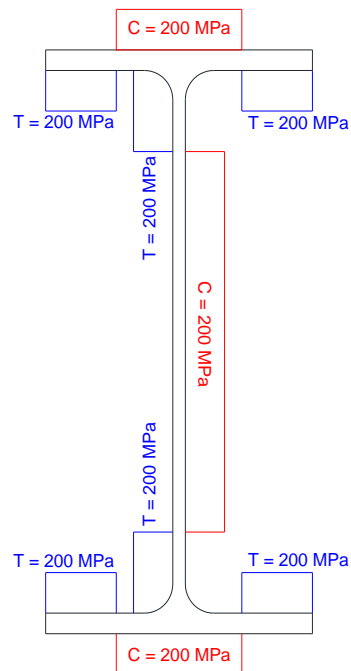


Figure 3.49: Distribution of the residual stresses.

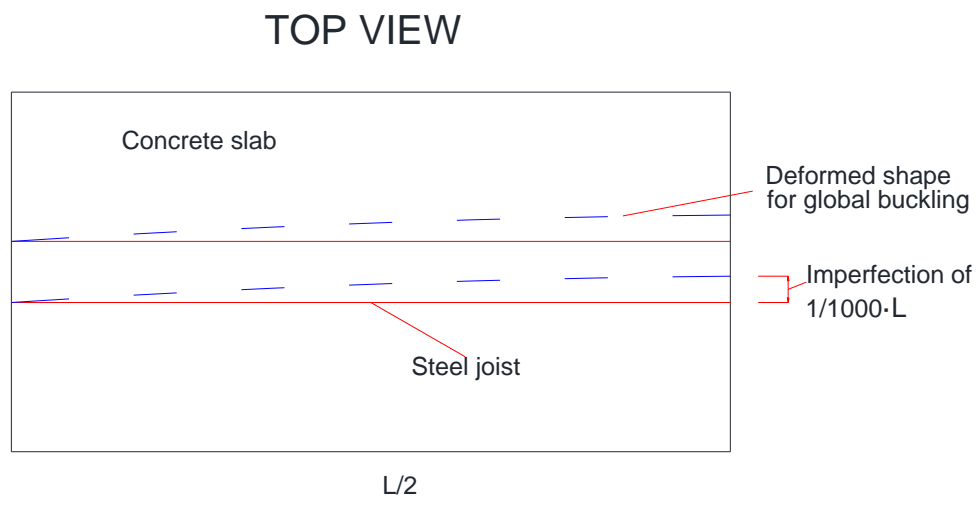


Figure 3.50: Initial shape to account for global buckling phenomena

Similarly to the global imperfection, also the local buckling was considered applying an initial geometric imperfection characterized by a maximum dimension of $h/200$ (fig. 3.51). The shape of this imperfection and the position is governed by the ones observed in the experimental tests performed on the composite beams and reported in the previous paragraph. The maximum value was computed as:

$$\frac{h}{200} = \frac{360}{200} \cong 2.00mm$$

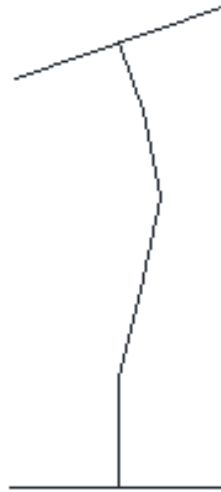


Figure 3.51: Initial shape to account for local buckling phenomena

In the actual test set-up of the composite beam it can be distinguished two different conditions of constraint: one for the concrete slab and the other one for the steel profile. The concrete slab is pinned supported at the ends with two steel plates welded to two solid steel cylinders which allow the rotation around their own axis. The steel joist, however, is constrained by the concrete slab in correspondence of the shear connectors; in fact the steel profile is supported in a continuous manner to the reinforced concrete slab and constrained in the

points where the shear studs are placed. The shear connectors also prevent the uplift of the concrete slab and avoid the horizontal translations in both directions of the same steel joist. The steel profile, however, is not provided of adequate torsional constraints at the two ends and the steel flange plate subject to compression could buckle laterally. Only in the central part of the beam, the presence of the hydraulic jack inhibited the lateral displacement of the compressed flange. In actual conditions, as for the beam in a frame, the rotational constraint would be guaranteed by the continuity of the composite beam.

As previously mentioned, the FE model implemented with Diana software refers to half length of the composite beam due to the conditions of symmetry. Then at the end of the beam it was imposed the pinned constraint: the displacement along x and z directions (transversal and vertical direction) are blocked, the displacement along the y-axis is allowed (the longitudinal axis of the beam) and all the rotations are allowed. Conversely, in the middle section of the beam all the displacements are blocked in order to simulate the lateral constraint action of the hydraulic jack and the continuity condition of the composite beam. In this section in order to ensure that all points had the same vertical displacement a rigid diaphragm was placed (MPC - BEAMS). This internal constraint is important also for the application of the load, both in term of displacement and force.

As mentioned in the previous sections, the composite beam was studied under hogging bending moment. The first analyses were dedicated to evaluate the effectiveness of the method for the control load on the beam: displacement or force control.

After several attempts the force control was adopted with load step equal to 1kN, which ensured a good convergence, while for the displacement control a step load equal to 0.01 mm was established that in the same way guaranteed a

good convergence and a result identical to that reported by the control force (Fig. 3.52).

In the further analysis it was decided to keep only the displacement control that guarantees the same result as the force control but with a computational cost, especially in terms of iterations, much less onerous .

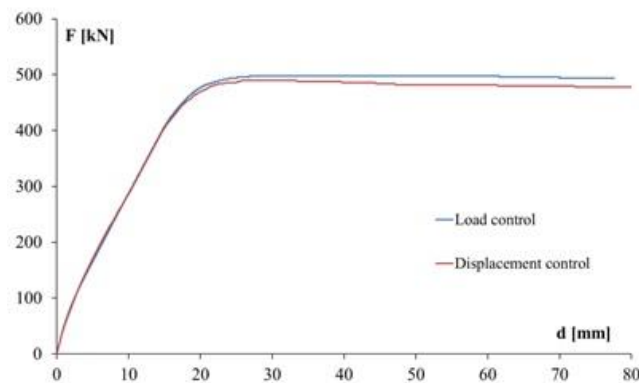


Figure 3.52: Comparison between load control method and displacement one

3.8 Calibration of the FE model by means of a numeric-experimental comparison

The value of the theoretical plastic moment of the cross-section was estimated neglecting the contribution of the tensile concrete strength and the hardening of the steel, and introducing the experimental average value of the yield strength of the profile and bars; the results are shown in Table 3.9 and compared with the maximum experimental moment:

	x_{pl} [mm]	M_{pl} [kN·m]	M_{exp} [kN·m]
Beam 1	236	484	440
Beam 2	236	484	451
Beam 3	236	484	458
Beam 4	268	529	494

Table 3.9: Comparison between the values of the theoretical plastic moment and maximum experimental ones

In the following section some comparisons between numerical and experimental results are reported, both local and global comparisons of the tested composite beams and the FE model discussed in the previous sections. The overall behavior of the composite beams can be illustrated by the Force - Displacement curves. Figure 3.53 shows the load-displacement curves for three of the four tested beams (Beam 1, 2 and 3), the theoretical curve, evaluated according to the moment-curvature relationships and the application of the virtual work, the two 3D FE models implemented in Diana, one without imperfections, neither local nor global, and without residual stresses (Base FE model) and the other one without any imperfection but with residual stress distribution in agreement with figure 3.39 with a value of 390MPa (FE Base model + Res. Stress 390).

Figure 3.54, however, reports the comparison of the three tested beams with the FE model of the only steel beam, with and without the residual stress value equal to 200MPa

The same comparisons for the tested Beam 4 are reported in 3.55 and 3.56.

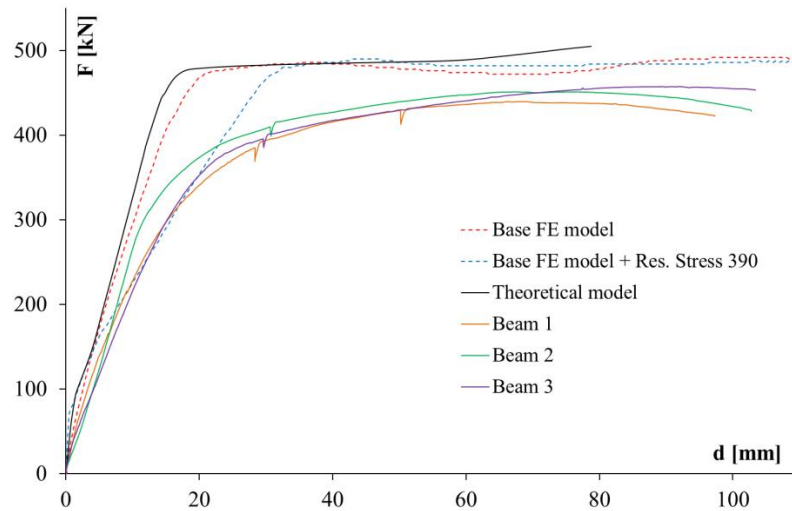


Figure 3.53: Comparison between experimental load – displacement curves for Beams 1, 2 and 3, FE model and theoretical model

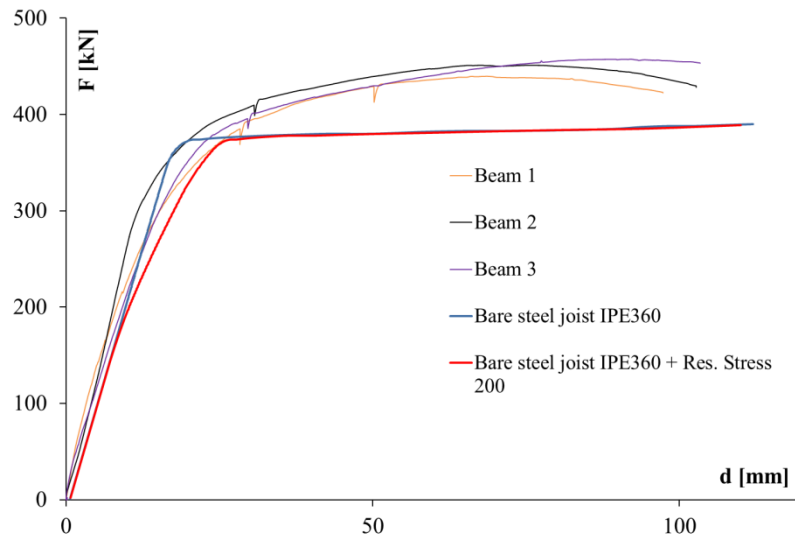


Figure 3.54: Comparison between experimental load – displacement curves for Beams 1, 2 and 3 and FE model of the steel joist IPE360, with and without residual stresses equal to 200MPa

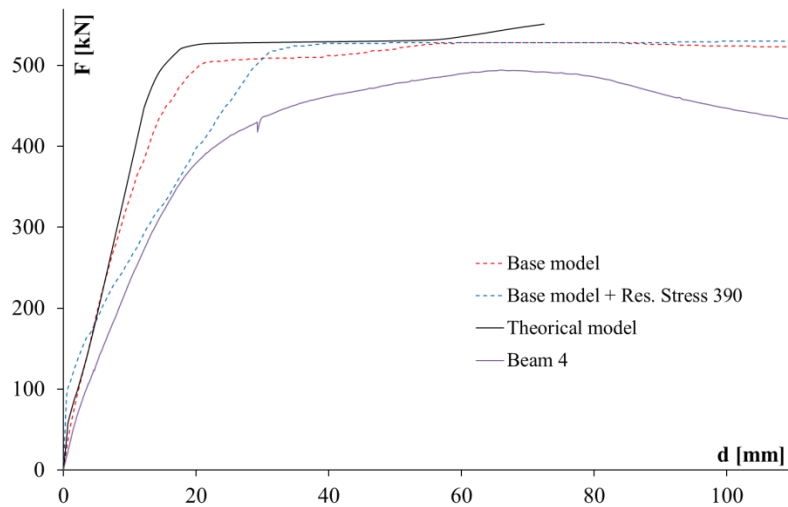


Figure 3.55: Comparison between experimental load – displacement curve for Beam 4, FE model and theoretical model

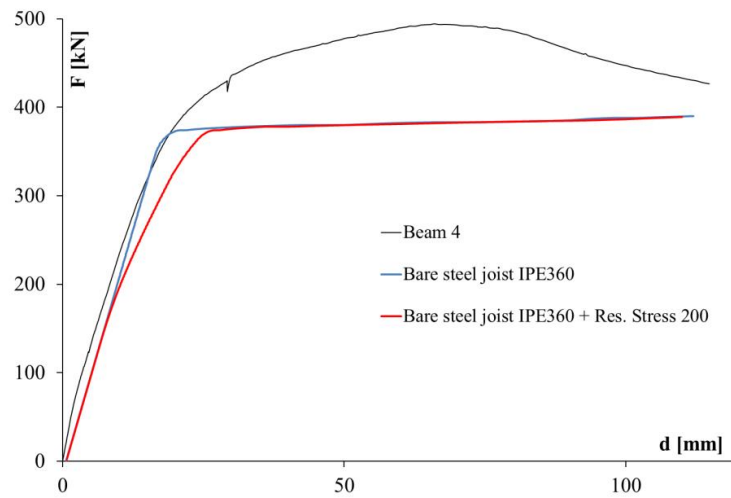


Figure 3.56: Comparison between experimental load – displacement curve for Beam 4 and FE model of the steel joist IPE360, with and without residual stresses equal to 200MPa

In this first phase, for the numerical results processed by the FE model in DIANA were considered two curves:

- Beam Model Base without the residual stresses (Base FE model)
- Model beam with the residual stresses equal to the yield strength (390 MPa)

The latter condition corresponds to a limit condition: the element has a strong reduction of the capacity due to the high value of the residual stresses and the consequent plasticization of the section already at the time of the load application.

The two trends, therefore, represent the extreme conditions of the range of variation of the load-displacement curves for different values of residual stresses.

	F_y [kNm]	δ_y [mm]	F_{max} [kNm]	δ_{max} [mm]
Beam 1	375	13.5	490	115
Beam 2	375	13.5	490	115
Beam 3	375	13.5	490	115
Beam 4	450	15.5	530	94

Table 3.10: Numerical results from FE models without residual stresses

Risultati Numerici (tensioni residue = 390MPa)				
	F_y [kNm]	δ_y [mm]	F_{max} [kNm]	δ_{max} [mm]
Trave 1	375	22	490	134
Trave 2	375	22	490	134
Trave 3	375	22	490	134
Trave 4	450	24.5	530	106

Table 3.11: Numerical results from FE models with residual stresses

In order to understand the overall behavior of the beam it is necessary to give attention to local issues that arise in the strain deformation of the materials (the steel profile and the reinforcing bars). The local behavior of the composite beams can be evaluated by the load-strains curves reported in fig. 3.57-3.60.

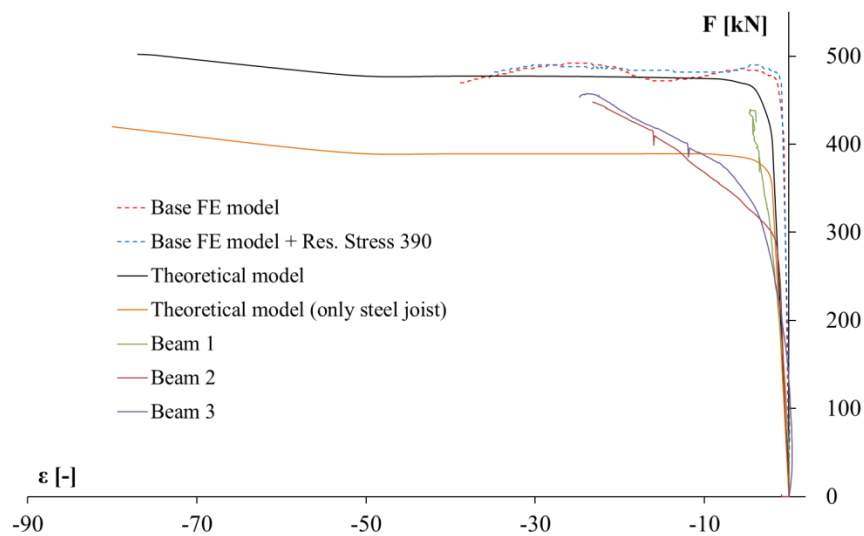


Figure 3.57: Comparison of the load-strain curves in the compressive flange for Beams 1, 2 and 3

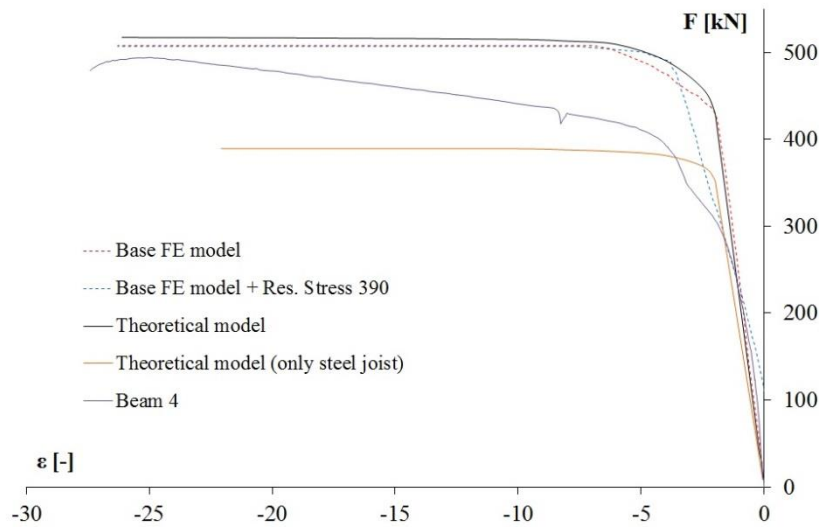


Figure 3.58: Comparison of the load-strain in the flange in compression for the Beam 4

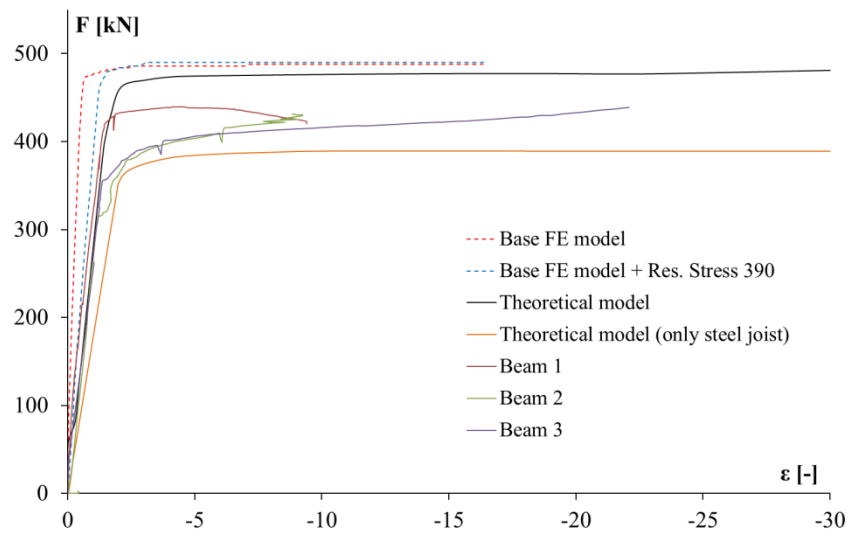


Figure 3.59: Comparison of the load-strain in the flange in tension for Beams 1, 2 and 3

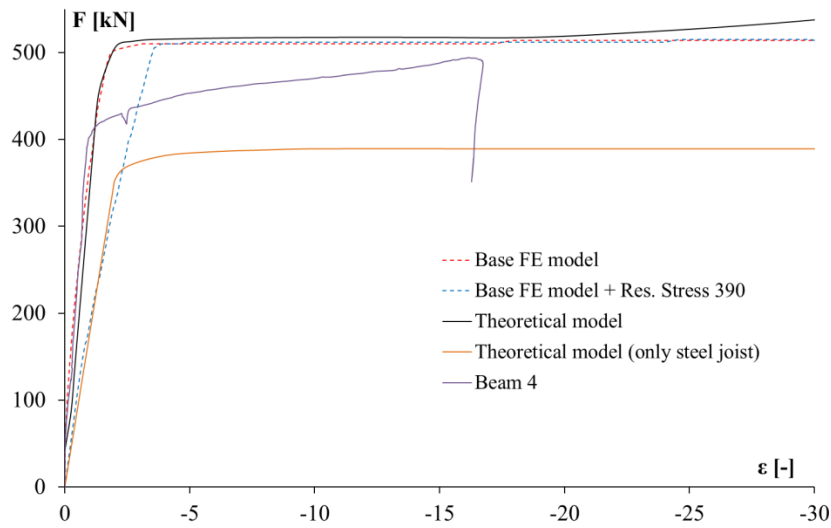


Figure 3.60: Comparison of the load-strain in the flange in tension for the Beam 4

The previous figures report the load-strain deformation curves detected by the strain gauges placed on the Beams 1, 2, 3, 4 along the steel joist section at a distance of 50mm from the centerline of the beam.

From the data it is possible to observe that the strain gauges positioned in the lower part of the steel profile, on the flange in tension, have a linear trend up to the load corresponding to the yield strength of the composite cross-section. It is possible to observe that the behavior of the flanges in tension is the same for all the four beams until the yielding point is reached.

Conversely, the strain gauges positioned in the upper part of the profile, on the flange in compression, are linear up to a load value much lower than the one corresponding to the yielding load. The early beginning of the non-linearity of the compressed part is particularly evident in the Beam 2 and 3 due to the occurrence of the phenomena of local buckling.

The theoretical results show that for low load levels the curve tends to overlap with that experimental one both for the compressed flange and for the tensile one. The difference between the curves occurs progressively as the local

buckling phenomenon in the compressed flange affected the tested beams. This phenomenon is not included in the theoretical curve.

Despite the strong nonlinearities are present only in the compressed flange, for high load levels also in the tensile flange a strong non-linear behavior far from the experimental one was observed. In fact, the yielding point on the tested composite beams was reached for stress values much lower than the theoretical ones; however, these stresses were higher than the yielding ones if only the steel joist was considered; this latter condition demonstrates the effectiveness of the steel - concrete composite section.

The same considerations could be traced for the numerical results: it describes well the initial linear branch of the experimental curves while the final trend always show a difference in terms of strength.

In the following figures (fig. 3.61 and 3.62) the trends of the strain deformation measured by the strain gauges applied on the bars of the slab are reported.

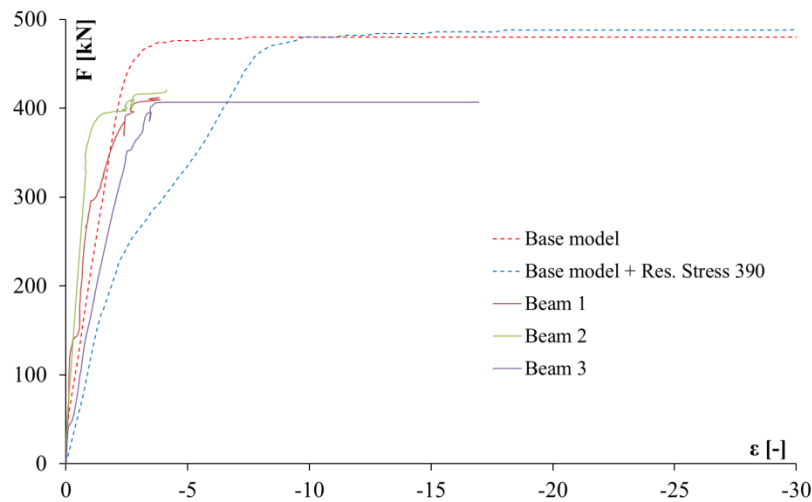


Figure 3.61: Comparison of the experimental load-strain curve of the reinforcing bar for the Beams 1, 2 and 3

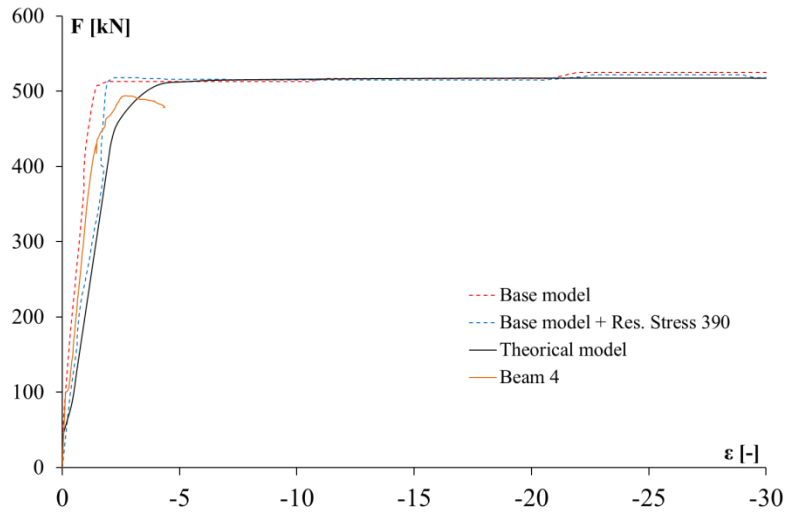


Figure 3.62: Comparison of the load-strain curve of the reinforcing bar for the Beam 4

For the Beam 4 only one strain gauge was efficient. For the 4 beams the distribution of the stresses between the reinforcing bars is almost constant as they do not have a decreasing in term of strain deformation moving from the centerline toward the edges of the slab, therefore the observed differences can be attributed to the experimental scatter. This result shows that the width of 1000mm can be considered effective while no indication could be traced on the width equal to 1600mm.

From the comparison of theoretical and numerical results with the experimental ones it could be concluded that there is a good agreement for the Beam 4 while for the Beams 1, 2 and 3 the experimental yielding strength is attained for stress values lower than the theoretical one.

Figs. 3.63 shows the comparison between the FE model and the experimental tests on the composite beams 1, 2 and 3. The FE model is defined “complete” because takes into account for the local and global imperfections and the residual stresses imposed equal to 200MPa. The same comparison is reported in the fig. 3.64 for the tested beam 4.

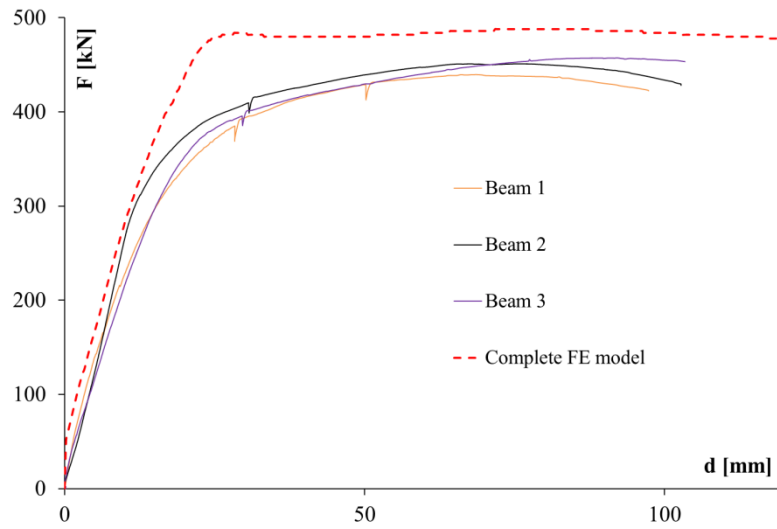


Figure 3.63: Comparison between experimental load – displacement curves for Beams 1, 2 and 3 and FE model of the steel joist IPE360, with residual stresses equal to 200MPa and global and local imperfections (complete)

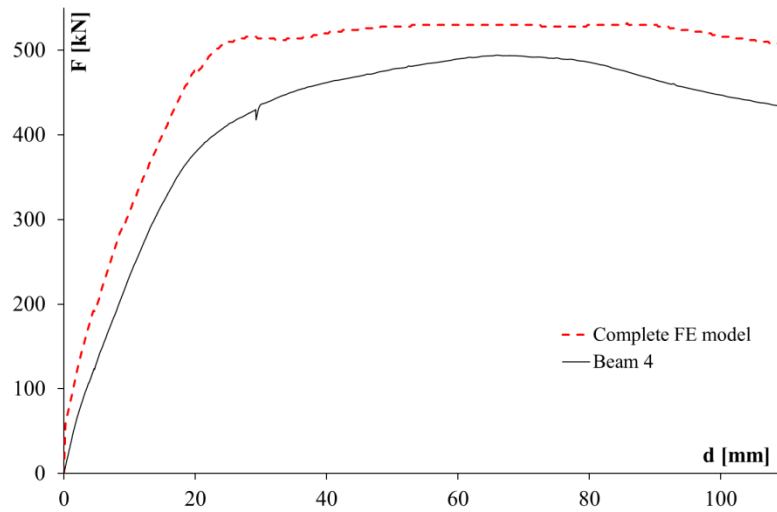


Figure 3.64: Comparison between experimental load – displacement curves for Beams 4 and FE model of the steel joist IPE360, with residual stresses equal to 200MPa and global and local imperfections (complete)

In order to better understand the influence of the shear connector model, three models were implemented in the FE model. The first two model, Ollgard01 and

Ollgard02 in the figure 3.63, are based on the theory of (Ollgard et al., 1971) and characterized as indicated in (Fabbrocino et al. 1999); while the third model (labeled as Johnson in the figure 3.63) is that one of Johnson et al., 1969, and takes into account for the tension in the concrete slab.

Fig. 3.64 reports the comparison of the FE models of the composite beams with the three different models of the shear connector and one model characterized by a rigid connection. The degree of the shear connection in all cases is equal to 100%

From the figure 3.61, it could be concluded that the influence of the model type for the shear stud connector has not a great influence on the response of the FE models of composite beams.

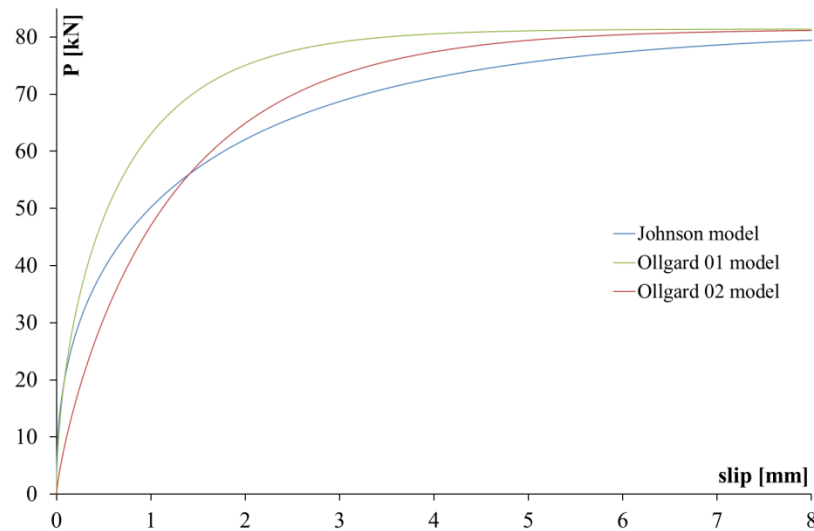


Figure 3.63: Comparison of the load-slip curve for the three models of the shear studs considered

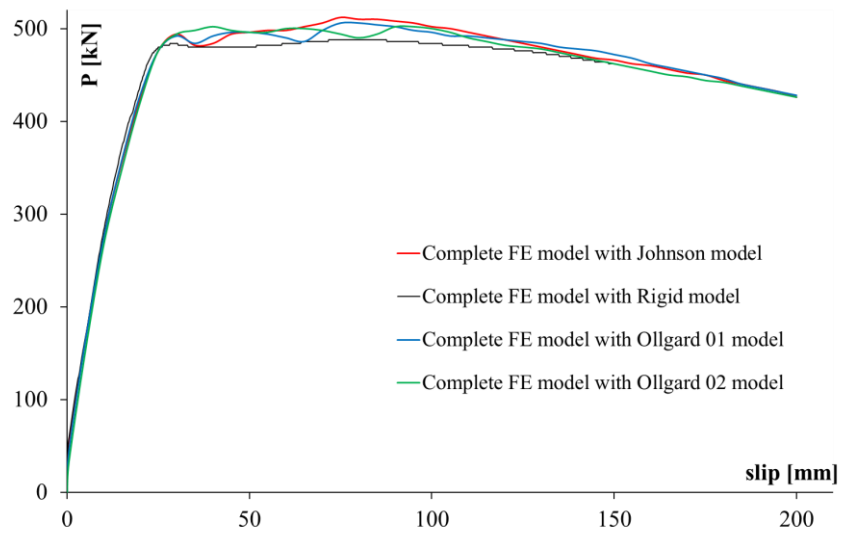


Figure 3.61: Comparison of the load-displacement for different models of the shear studs considered for the Beam 1

REFERENCES

- Amadio, C., Fragiacomio, M., "Effective width evaluation for steel–concrete composite beams", *Journal of Constructional Steel Research*, vol. 58, 2002, pp. 373–388.
- Amadio, C., Fragiacomio, M., Macorini, L., "Evaluation of the deflection of steel-concrete composite beams at serviceability limit state", *J. of Constructional Steel Research*, vol. 73, 2012, pp. 95–104.
- Baldassino, N., Seema, Zandonini, R., "La componente soletta nei giunti composti acciaio-calcestruzzo", VII Workshop italiano sulle strutture composte, Benevento, Ottobre 2008.
- Baldwin, J. W., Henry, J. R., Sweeney, G. M., "Study of composite bridges stringers. Phase 2: Development of rational analysis of composite beams which was programmed for use on computer. Experimental testing of eight composite beams to study behavior and verify analysis", University of Missouri, Engineering Experiment Station, 1965, pp. 226.
- Ballio, G., Mazzolani, F. M., "Strutture in acciaio" HOEPLI, 1979.
- Belluzzi, O., "Scienza delle costruzioni", volume quarto, Zanichelli Bologna, Giugno 1982.
- Bradford, M. A., Vrcelj, Z., "Elastic distortional buckling of continuously restrained I-section beam–columns", *Journal of Constructional Steel Research*, vol. 62, 2006, pp. 223-230.
- Bursi, O. S., Sun, F., Postal, S., "Non-linear analysis of steel-concrete composite frames with full and partial shear connection subjected to seismic loads", *Journal of Constructional Steel Research*, vol. 61, 2005, pp. 67–92.
- Ceroni, F., "Experimental tests and modeling of tension stiffening in RC Ties strengthened with FRP laminates", Tesi di dottorato in Ingegneria delle Strutture, XV Ciclo, 2002.

- Chapman, J. C., Balakrishnan, S., “Experiments on composite beams”, *The Structural Engineer*, vol. 42 (11), 1964, pp. 369-383.
- Chen, S., Jia, Y., “Required and available moment redistribution of continuous steel-concrete composite beams”, *Journal of Constructional Steel Research*, vol. 64, 2008, pp. 167-175.
- CNR 10011, “Costruzioni in acciaio – Istruzioni per il calcolo, l’esecuzione, il collaudo e la manutenzione” CNR Bollettino Ufficiale – Norme tecniche, 1985.
- CNR 10016, “Strutture composte di acciaio e calcestruzzo – Istruzioni per l’impiego nelle costruzioni”, CNR Bollettino Ufficiale – Norme tecniche, parte IV, 1999.
- Cosenza, E., Mazzolani, S., “Analisi in campo lineare di travi composte con connessioni deformabili: formule esatte e risoluzione alle differenze”, Trento, Italy. 1_ Workshop Italiano sulle Strutture Composte, 1993, pp. 1–20.
- Cosenza, E., Pecce, M., "Analisi matriciale di travi continue composte con connessione deformabile a comportamento lineare", C.T.A., Giornate italiane della costruzione in acciaio, Ancona, Ottobre 1997, pp. 208-219.
- Dai, P. K-H, "Analitical study of composite beams with inelastic shear connection", PhD thesis, University of Illinois, 1963, pp. 160.
- Dubina, D., Ungureanu, V., “Effect of imperfections on numerical simulation of instability behaviour of cold-formed steel members”, *Thin-Walled Structures*, vol. 40, 2002, pp. 239 – 262.
- Eurocode 2, “Design of concrete structures – Part 1.1: General rules and rules for buildings” ENV 1992-1-1, 1992.
- Eurocode 3, “Design of steel structures – Part 1.1: General rules and rules for buildings” ENV 1993-1-1, 1992.

- Eurocode 4, “Design of composite steel and concrete structures – Part 1.1: General rules and rules for buildings” ENV 1994-1, 2004.
- Eurocode 8, “Design of structures for earthquake resistance – Part 1: General rules, seismic actions and rules for buildings” ENV 1998-1, 1998.
- Fabbrocino, G., “Modellazione e comportamento sperimentale di travi continue composte acciaio-calcestruzzo”, Tesi di dottorato in Ingegneria delle Strutture, X ciclo, Università degli Studi di Napoli “Federico II”, 1997.
- Fabbrocino, G., Manfredi, G., Cosenza, E., “Analysis of continuous composite beams including partial interaction and bond”, *Journal of Structural Engineering*, vol. 126(11), 2000, pp. 1288-1294.
- Fabbrocino, G., Manfredi, G., Cosenza, E., “Non-linear analysis of composite beams under positive bending”, *Computers and Structures*, vol. 70, 1999, pp. 77-89.
- Faella, C., Martinelli, E., Nigro, E., "Steel and concrete composite beams with flexible shear connection: “exact” analytical expression of the stiffness matrix and applications", *Computers and Structures*, vol. 80, 2002, pp. 1001–1009.
- Fu, F., Lam, D., Ye, J., "Parametric study of semi-rigid composite connections with 3-D finite element approach", *Engineering Structures*, vol. 29, 2007, pp. 888–898.
- Gattesco, N., "Analytical modeling of nonlinear behavior of composite beams with deformable connection", *J. of Constructional Steel Research*, vol. 52, 1999, pp. 195–218.
- Johnson, R. P., Greenwood, R. D., van Dalen, K., “Stud shear-connectors in hogging moment regions of composite beams.” *Struct. Eng.*, vol. 47 (9), 1969, pp. 345–350.

- Ollgaard, J. G., Slutter, R. G., Fisher, J. W., “Shear strength of stud connectors in lightweight and normal weight concrete”, AISC, Engineering Journal, 1971.
- Oven, V. A., Burgess, I. W., Plank, R. J., Wali, A. A., "An analytical model for the analysis of composite beams with partial shear interaction", *Computers & Structures*, vol. 62(3), 1997, pp. 493-504.
- Pecce, M., Bibbò, F. A., Rossi, F., Ceroni, F., “Experimental results of steel-concrete composite beams under hogging moment”, 4th International Conference on Steel & Composite Structures, Sydney, Australia, July 2010.
- Pecce, M., Rossi, F., Bibbò, F. A., Ceroni, F., “Experimental behaviour of composite beams subjected to hogging moment”, *Steel & Composite Structures An International Journal*, Vol. 12, No. 5, 2012.
- Ranzi, G., Zona, A., "A steel–concrete composite beam model with partial interaction including the shear deformability of the steel component", *Engineering Structures*, vol. 29, 2007, pp. 3026–3041.
- Sebastian, W. M., McConnel, R. E., "Nonlinear FE analysis of steel-concrete composite structures", *Journal of Structural Engineering*, Vol. 126, No. 6, June 2000, ASCE, pp. 662–674.
- Schafer, B.W., Pekoz, T., "Computational modelling of cold-formed steel characterising geometric imperfections and residual stresses", *J. Construct. Steel Res.*, vol. 47(3), 1998, pp. 193–210.
- Wang, A. J., Chung, K. F., "Advanced finite element modelling of perforated composite beams with flexible shear connectors", *Engineering Structures*, vol. 30, 2008, pp. 2724–2738.
- Wang, A. J., Chung, K. F., "Advanced finite element modelling of perforated composite beams with flexible shear connectors", Fifth Int. Conference on Advances in Steel Structures (ICASS 2007).

Zhou, F., Mosalam, K. M., Nakashima, M., “Finite-Element Analysis of a Composite Frame under Large Lateral Cyclic Loading”, *Journal of Structural Engineering*, Vol. 133, No. 7, July 1, 2007, ASCE, pp. 1018–1026.

CHAPTER 4. THEORETICAL AND NUMERICAL ANALYSES OF COMPOSITE BEAMS UNDER HOGGING MOMENTS

In the following section a theoretical and numerical analysis on the ductility of the cross-section of composite beams under hogging moment is presented, while just a numerical analysis on the non-linear response of the entire element is reported. Afterward a numerical study is pointed out to analyze which is the value of the equivalent plastic hinge and the influence of different parameters on its estimation.

4.1 The behavior of the composite cross-section subjected to hogging moment

4.1.1 Theoretical analysis

The theoretical analysis of the cross-section behavior of the steel-concrete composite beams is conducted assuming the following hypotheses:

- the connection between the two component is full and its deformability is negligible;
- the hypothesis of plane section is valid;
- the steel profile section has a behavior of compact or semi-compact section, i.e. local buckling phenomena do not occur;
- the constitutive law of the steel, both for reinforcement and profile, is elastic-perfectly plastic (EPP);
- the tensile strength of concrete is neglected.

Under these hypotheses it can be highlighted that the section failure depends only on the characteristics and amount of construction steel and reinforcement; thus the different failure modes depend on the percentage of reinforcement in the concrete slab, ρ , but the more effective parameter is the mechanical ratio R :

the ratio between the maximum strength of the reinforcing bars and the one of the steel profile ($A_s f_{sk}/A_a f_{yk}$).

In fact, if the maximum deformation of the reinforcing bar as ε_{su} and the maximum strain in the compression part of the steel profile as ε_{au} is established, it is possible to define a limit condition when both parts arise the ultimate strain (fig. 4.1).

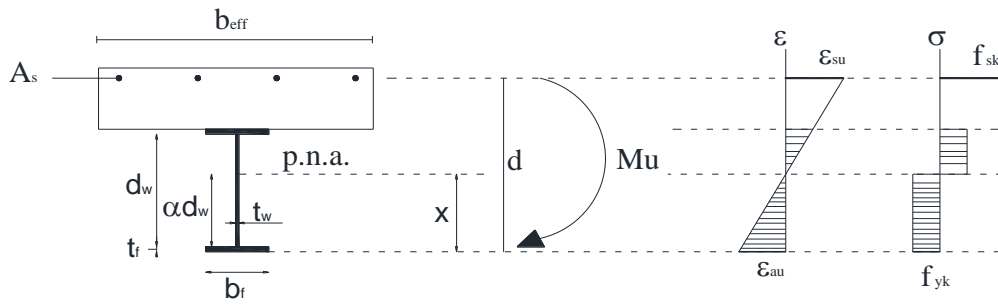


Figure 4.1: Strain and stress distribution in a composite beam at ultimate hogging moment.

In this condition it is possible define a plastic neutral axis (p.n.a.) “ x ” that corresponds to the balanced rupture for the composite cross-section, that gives the maximum ultimate curvature. This position of the neutral axis is labeled as x_{bal} , and results:

$$x_{bal} = \frac{\varepsilon_{au}}{\varepsilon_{au} + \varepsilon_{su}} d \quad (4.1)$$

This position of the plastic neutral axis depends on the amount of reinforcement and delimitates two possible modes of failure of the composite section: the failure of the reinforcement and the failure of the steel profile.

The percentage of reinforcement ($\rho = A_s/A_c$) and the mechanical ratio ($R = A_s f_{sk}/A_a f_{yk}$), that correspond to the balanced rupture can be indicated as ρ_{bal} and R_{bal} . To evaluate these two parameters the translational equilibrium of the

section, referring to the figure 4.1, is carried out considering the compression as positive:

$$b_f t_f f_{yk} + (x - t_f) t_w f_{yk} - (H - t_f - x) t_w f_{yk} - b_f t_f f_{yk} - A_s f_{sk} = 0 \quad (4.2)$$

follow:

$$x = \frac{A_s \cdot f_{sk}}{2 \cdot t_w \cdot f_{yk}} + \frac{H}{2} \quad (4.3)$$

$$x_{bal} = \frac{A_{s,bal} \cdot f_{sk}}{2 \cdot t_w \cdot f_{yk}} + \frac{H}{2} \quad (4.4)$$

$$A_{s,bal} = \frac{t_w \cdot f_{yk}}{f_{sk}} (2 \cdot x_{bal} - H) \quad (4.5)$$

given $A_{s,bal}$, it is easy to define ρ_{bal} and R_{bal} :

$$\rho_{bal} = \frac{A_{s,bal}}{b_{eff} \cdot s} \quad (4.6)$$

and

$$R_{bal} = \frac{A_{s,bal} \cdot f_{sk}}{A_a \cdot f_{yk}} \quad (4.7)$$

In the following, the two condition, $\rho < \rho_{bal}$ (or $R < R_{bal}$) and $\rho > \rho_{bal}$ ($R > R_{bal}$), are examined.

- $\rho \leq \rho_{bal}$ ($R \leq R_{bal}$)

In the condition $\rho \leq \rho_{bal}$ the position of plastic neutral axis varies in the range:

$$H/2 < x \leq x_{bal}$$

In other words, the value of x could be close to $H/2$ that corresponds to $\rho \rightarrow 0$ and the composite steel-concrete section tends to the only steel profile section or $\rho \rightarrow \rho_{bal}$ and the $x \rightarrow x_{bal}$, that corresponds to the maximum reinforcement amount still giving the failure of the reinforcement.

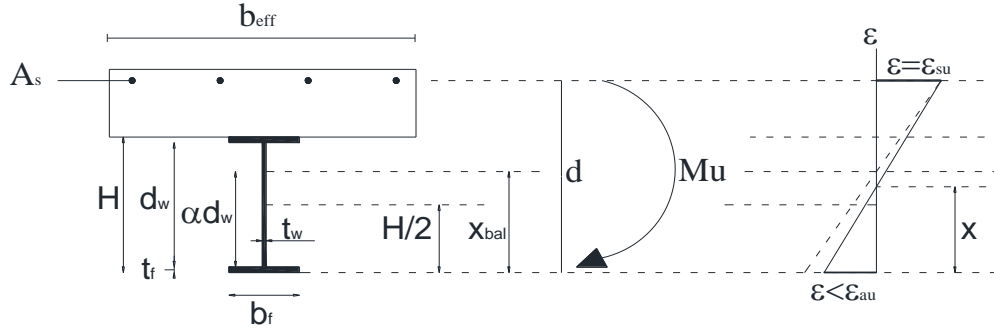


Figure 4.2: Strain distribution for a composite beam subjected to hogging moment in case of $\rho < \rho_{bal}$ ($R < R_{bal}$).

In this condition the behavior of the section is governed by the reinforcement and the values of the ultimate curvature, corresponding to the ultimate strain in the reinforcement, increases with the percentage of the reinforcement.

- $\rho > \rho_{bal}$ ($R > R_{bal}$)

In the condition $\rho > \rho_{bal}$ the position of plastic neutral axis is greater than x_{bal} as:

$$x > x_{bal}$$

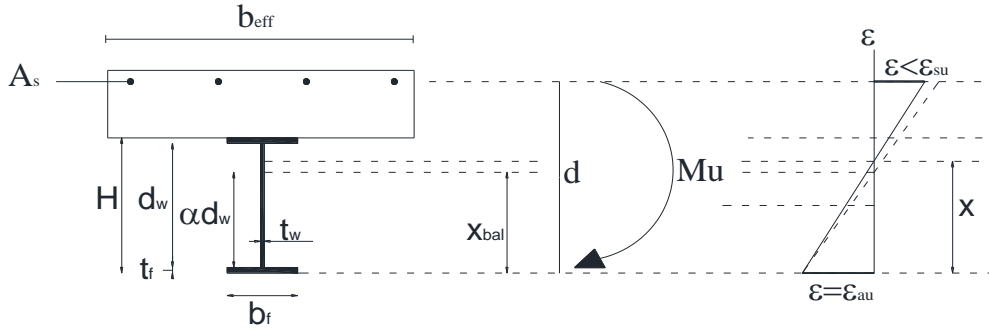


Figure 4.3: Strain distribution for a composite beam subjected to hogging moment in case of $\rho > \rho_{bal}$ ($R > R_{bal}$).

Generally in this condition the behavior of the section is governed by the steel profile and the collapse is due to the attaining of the ultimate strain of the construction steel in compression.

With this assumption, it is possible to individuate two functions for describing the failure of the composite section under hogging moment varying the

parameter R ; one is based on the failure of the reinforcement and the other on the failure of the steel profile.

In fact the equation 4.3 can be rewritten as follows introducing the parameter R :

$$x = \frac{A_s \cdot f_{sk} \cdot A_a}{2 \cdot t_w \cdot f_{yk} \cdot A_a} + \frac{H}{2} = \frac{R \cdot A_a}{2 \cdot t_w} + \frac{H}{2} \quad (4.8)$$

This expression highlights the direct influence of R on the position of the neutral axis. Fixed the steel profile (the area A_a , the height H and the web thickness of the section t_w), it is possible to evaluate the plastic neutral axis and the maximum curvature varying the parameter R for both the case of failures; it is worth to note that the relation x - R does not depends on the yielding stress of the steels.

When the failure depends on the reinforcement (Fig. 4.2) the maximum curvature could be written as:

$$\chi_{max,s} = \frac{\varepsilon_{su}}{d - x} \quad (4.9)$$

If the failure depends on the steel profile (Fig. 4.3), the maximum curvature could be written as:

$$\chi_{max,a} = \frac{\varepsilon_{au}}{x} \quad (4.10)$$

In Fig. 4.4 the curvature- R relation is graphed considering both the relations for the two failure modes, in the case of the profile IPE360, already introduced for the calibration of the model. The intersection point between the two curves provides the maximum value of curvature for the composite cross-section that corresponds to the balance rupture individuating also the R value of balanced failure (R_{bal}).

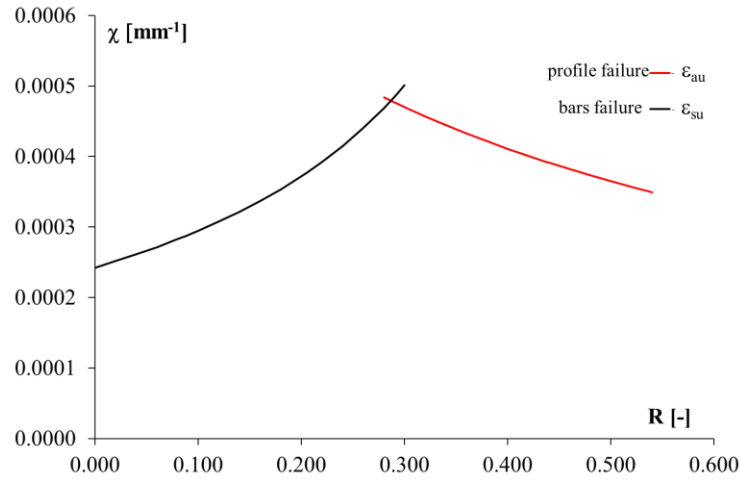


Figure 4.4: Variation of χ_{max} versus the parameter R for two mechanism.

The increasing amount of reinforcement implies a variation of the plastic neutral axis that can determine a different classification of the steel section, and then a different plastic capacity of the composite beam. In Figs. 4.5 the values of R and χ that corresponds to the limits between the class 1 and 2 are indicated for different steel grades; the same indications are reported in fig. 4.6 for the limit between class 2 and 3.

The values of the ultimate curvatures decrease when the percentage of the reinforcement increases. Increasing of the reinforcement amount implies the enhancement of the web depth in compression, i.e. the plastic neutral axis depth increases, as consequence the classification of the cross-section, according to the European code (EC3 and EC4), could change and the behavior of the overall section could be influenced by the local buckling phenomena. Therefore, the behaviour of the composite beams could be more likely characterized by local buckling if too high percentages of reinforcement are used.

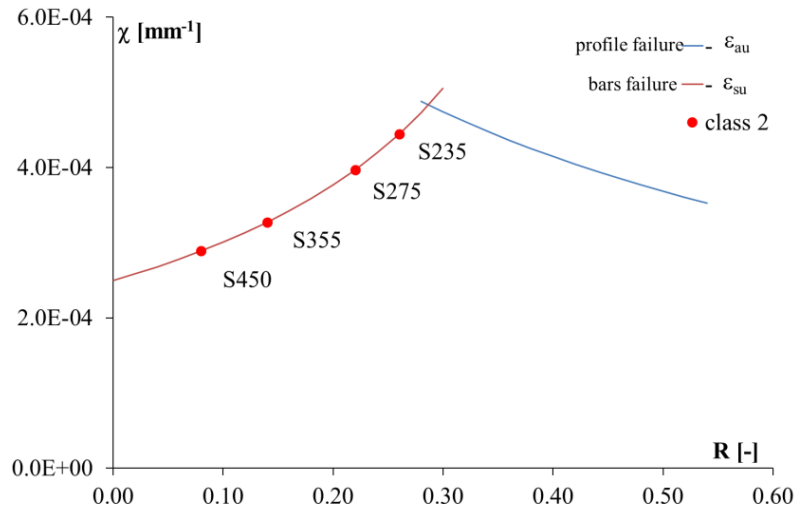


Figure 4.5: The values of R and χ at the limit between class 1 and class 2 for different steel grades.

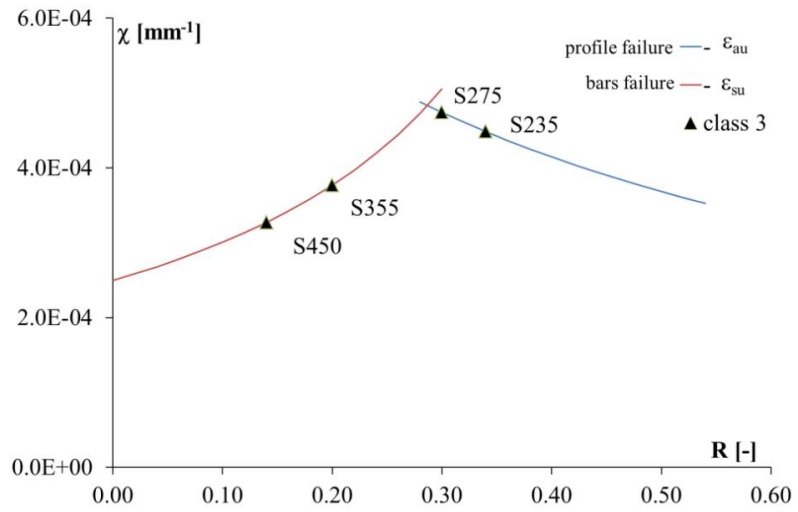


Figure 4.6: The values of R and χ at the limit between class 2 and class 3 for different steel grades.

4.1.1.1 The role of the hardening and the critical stress

In order to better understand the role of local buckling the theoretical approach is modified to take into account the phenomenon through the definition of a critical stress according the formulation of (Mazzolani et al., 1992, 1996), already introduced in chapter 2.

In order to apply the approach, the elastic-plastic (EPP) model of the structural steel and the reinforcement is substituted with an elastic-plastic with hardening law (EPH) (fig. 4.7). Table 4.1 reports the main feature of the EPH model for the S235 steel grade.

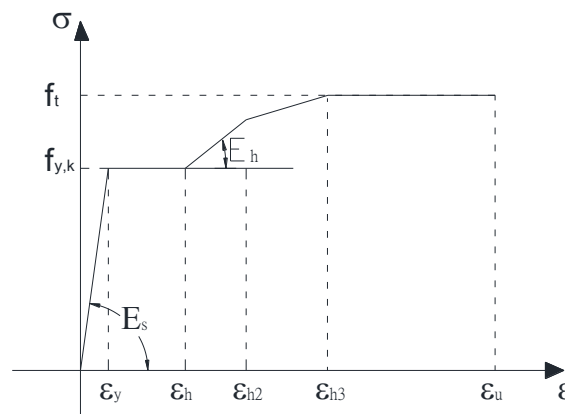


Figure 4.7: The constitutive relationship (EPH) assumed for the joist steel.

	f_{yk} [N/mm ²]	f_{h2} [N/mm ²]	f_t [N/mm ²]	E [N/mm ²]	ϵ_y [%]	ϵ_h [%]	ϵ_{h2} [%]	ϵ_{h3} [%]	ϵ_u [%]
S235	235	275	294	200000	0,12	1,56	4,63	8,63	15

Tab. 4.1: The main features of the EPH model assumed for the structural steel joist for the S235 grade.

Introducing the local buckling phenomenon a third possible mechanism of failure has to be considered that is the attaining of the critical strain in the flange in compression:

$$\chi_{max,cr} = \frac{\varepsilon_{cr}}{\chi} \quad (4.11)$$

The value of the ε_{cr} is evaluated from the EPH model adopted, as reported in the fig. 4.7, and for any branch of the EPH model is possible to define a linear function that describes the trend of the strain. For example, if the first part of the EPH model, from ε_h to ε_{h2} , is considered, it is possible to evaluate the critical strain as:

for $\varepsilon_h < \varepsilon_{cr} < \varepsilon_{h2}$

$$\varepsilon_{cr} = \varepsilon_h + \frac{\sigma_{cr} - f_y}{E_h} \quad (4.12) \quad \text{dove} \quad E_h = \frac{f_{h2} - f_y}{\varepsilon_{h2} - \varepsilon_h}$$

The critical stress σ_{cr} is assumed equal to $s \cdot f_y$, where s is evaluated from the relationship of (Mazzolani et al., 1992):

$$\frac{1}{s} = 0.546321 + 1.632533\lambda_f^2 + 0.062124\lambda_w^2 - 0.602125\frac{b_f}{L} + 0.001471\frac{E}{E_h} + 0.007766\frac{\varepsilon_h}{\varepsilon_y}$$

where:

$$\lambda_f = \frac{b_f}{2t_f} \sqrt{\varepsilon_y}$$

$$\lambda_w = \frac{d_{we}}{t_w} \sqrt{\varepsilon_y}$$

d_{we} is part of the web in compression.

Because it is not immediate to include the critical stress approach in a closed formulation as in the previous case, it is possible to evaluate the moment-curvature relationship by the strips method taking into account for the critical strain in the compressed flange. The failure of the construction steel occurs

when the critical stress is attained determining a different value of the ultimate curvature.

Thus it is possible to depict the trend of the curvature when the local buckling occurs (“critical curvature”); in figure 4.8 this curvature for various steel grades is overlapped with the one obtained assuming the failure of the materials. It is interesting to observe that the introduction of the hardening and the critical stress gives the variation of the R -curvature relation versus the steel grade; higher is the steel strength lower becomes the maximum curvature.

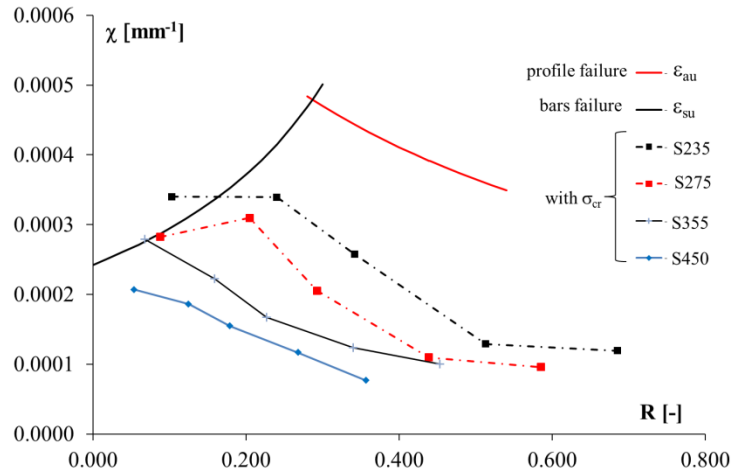


Figure 4.8: The variation of the ultimate numerical curvature at the critical stress (σ_{cr}) versus R varying the steel grade.

4.1.2 The numerical analysis

In this paragraph the results of the parametric analyses carried out by the finite element model on the composite cross-section are described referring only to the section behavior.

In these analyses the shear connection is considered infinitely stiff and the constitutive relationship of steel is elastic perfectly plastic (EPP model) in order to study the effect of the reinforcement percentage (ρ and R), steel grade

and local buckling, as it was carried out starting the theoretical approach. Then some further analyses are carried out introducing the deformability of the connection and the hardening of the steel constitutive relationship.

In figure 4.13 the moment-curvature at the mid-span of the beam is plotted varying the reinforcement both for the numerical model and the theoretical one already introduced.

The two results are in good agreement in terms of initial stiffness, and the plastic strength of the composite section (maximum moment of the theoretical curves) is achieved in all cases excluding the case whit $\rho=2$; in fact in this last instance only the yielding strength is achieved albeit a good ductility is exploited.

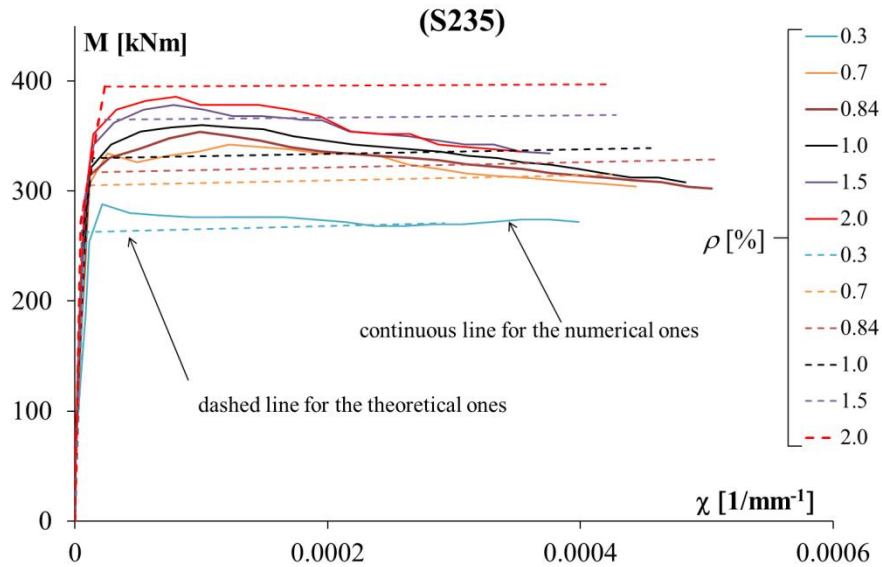


Figure 4.13: Comparison between numerical and theoretical moment-curvatures varying the percentage of reinforcement (ρ).

According to the classification of the standard EC3 (equal to Italian NTC08) the section considered for the steel joist is in class 1 for simple bending and class 2 if the axial force is considered. As widely discussed in the previously

theoretical analyses the enhancement of the reinforcement percentage gives a variation of the plastic neutral axis and could determine the change from class 1 to class 2.

The case of $\rho = 2\%$, the section results in class 2 but near the limit with class 3, in fact the yield moment is reached without exploiting the plastic strength.

The same observations could be carried out for steel grade S275, S355 and S450. The graphs and tables are reported in Appendix A, B and C.

In order to define the plastic curvature, χ_p , that is the difference between the ultimate curvature (χ_u) and the curvature at the yielding (χ_y), the ultimate curvature in the numerical analysis has been evaluated considering the failure load as the achievement of one of the following conditions:

1. the achievement of the ultimate strain of the steel reinforcement ε_{su} ;
2. the achievement of the ultimate strain in the steel profile ε_{au} ;
3. the achievement of the 85% of the maximum load on the descending branch. In some cases the curves are characterized by a sudden drop before the loss of 15% of the bearing capacity, so that the curves are stopped at this point.

Fig. 4.14 shows the variation of the plastic curvature with R for the numerical analysis and the theoretical ones already presented in the previous paragraphs. The peak of the numerical curvature varies with the steel grade and is about the same of the theoretical one for the steel grade S235; when the steel grade increases the effect of geometrical non linearity (i.e. buckling phenomena) considered in the numerical model is amplified, the value of R at the peak reduces and the slope of descending branch after the peak (i.e. the side of the profile failure) is higher.

Really in the numerical model the effect of local buckling can be considered also when an elastic-plastic behavior (EPP) of the steel is introduced due to the possibility of applying the imperfections, but in the theoretical approach, as already discussed, the effect of local buckling can be introduced only taking into account the hardening of the steel.

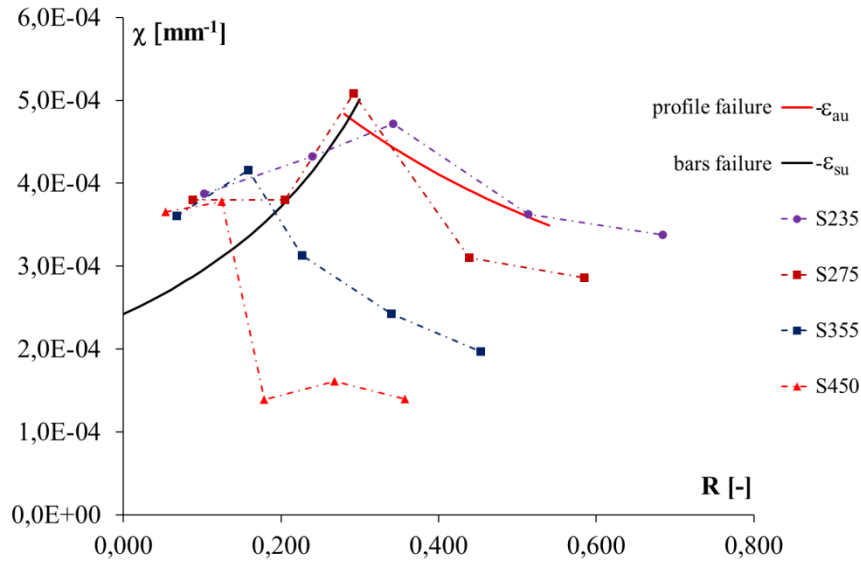


Figure 4.14: The theoretical-numerical comparison for the variation of χ_p versus R varying the steel grade of the joist.

4.1.3 The role of the steel hardening

The role of the steel hardening was examined also by the numerical model substituting the EPP model of the structural steel with the tri-linear EPH model (fig. 4.7). In figure 4.15 the Moment-Curvature relations at the mid-span of the beam are plotted varying the percentage of reinforcement and highlighting the significant points as the yielding and ultimate condition; in figure 4.16 the same curves are compared with the theoretical ones, that consider the steel hardening too, already discussed in the previous paragraphs (fig. 4.7).

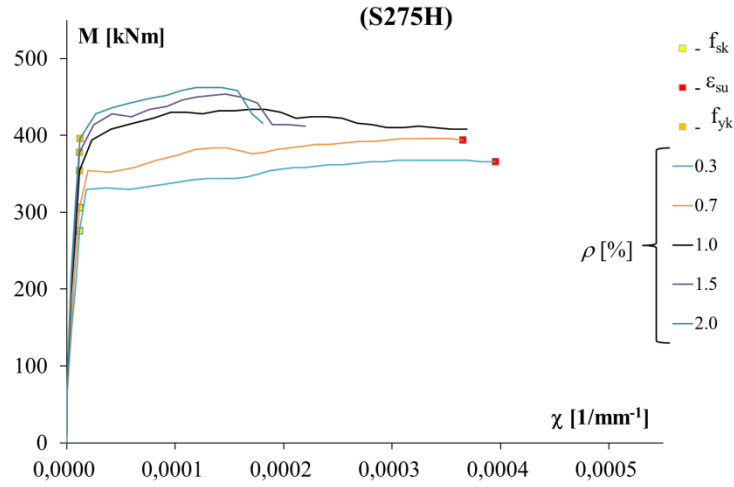


Figure 4.15: Numerical moment-curvature relationships with steel hardening varying the percentage of reinforcement (ρ).

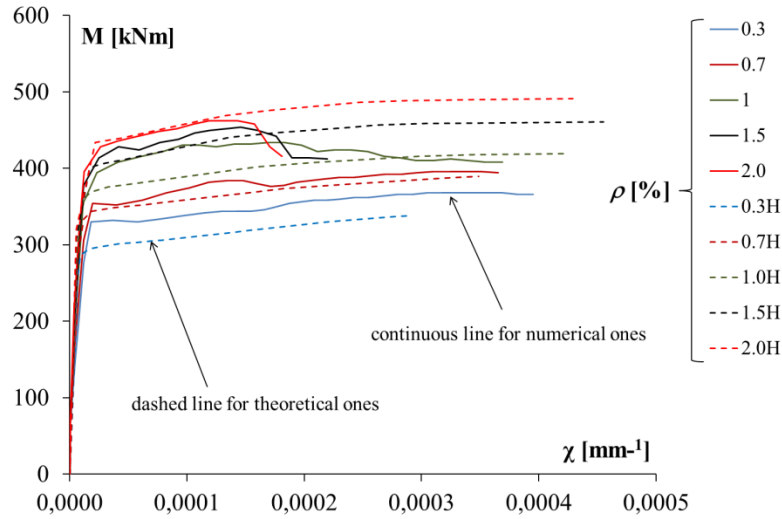


Figure 4.16: Comparison between numerical and theoretical moment-curatures relationships with steel hardening varying the percentage of reinforcement (ρ).

It is worth noticing again the role of the steel reinforcement in tension, above all when the percentage is equal to 2. In fact in this last case, the numerical model of the composite section experiences a mode of failure close to a steel section of class 3 since the section reaches the yielding strength but does not exceed the plastic one. The typical behavior of a section of class 3 is attained

when the percentage area of the reinforcing bars becomes equal to 3, as shown in Fig. 4.17; the comparison between the theoretical and the numerical model points out that the composite cross-section cannot exploit its plastic capacity.

An interesting comparison is the one between the theoretical moment-curvature curves evaluated with the critical stress approach and the numerical ones, traced until the achievement of the maximum load (F_{max}) (fig. 4.18).

The comparison shows a good agreement since the effect of local buckling through the non-linearities introduced in the numerical model is more significant in the descending branch. The mean results of the numerical analysis are reported in table 4.1 in terms of curvature at the yielding, at the maximum load and plastic curvature evaluated as the difference between the ultimate and yielding ones. The fig. 4.19 the same plastic curvatures of the numerical analysis are graphically compared with the theoretical ones obtained both with and without the hardening i.e. the buckling effect. It is very interesting to observe that the theoretical approach with hardening and critical tension effect gives a good approximation of the numerical one and it is safe for about the entire domain of R .

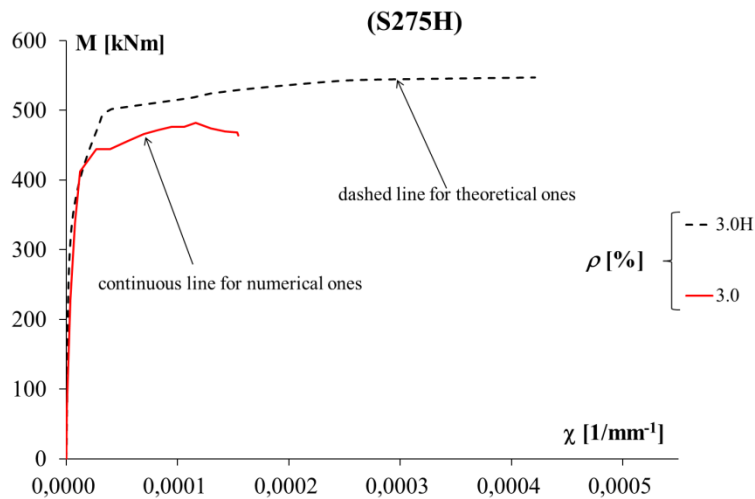


Figure 4.17: Comparison between numerical and theoretical moment-curvatures relationships for $\rho=3$.

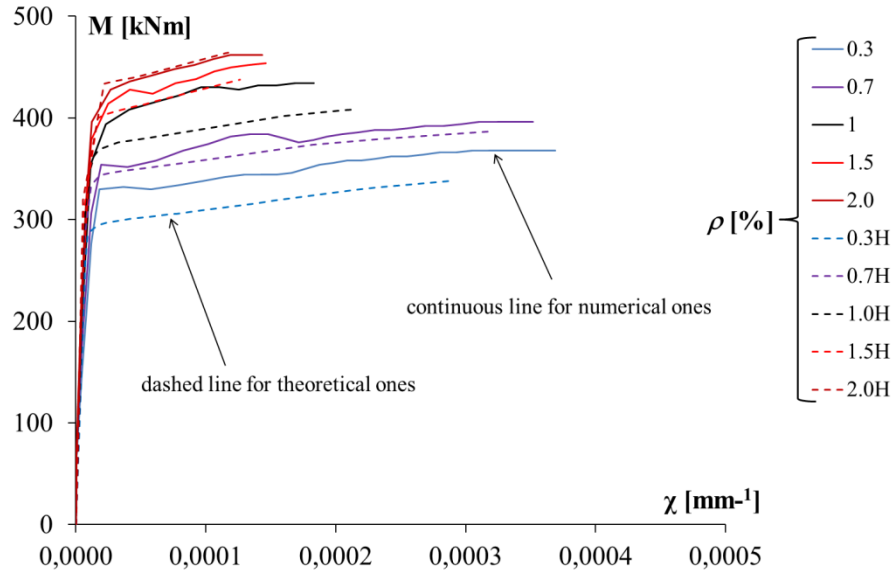


Figure 4.18: Comparison between numerical and theoretical (with σ_{cr}) M - χ relationships stopped at the maximum load (F_{max}) varying the percentage of reinforcement (ρ).

R	χ_y	χ_u	χ_p
[-]	[1/mm]	[1/mm]	[1/mm]
0.088	1.17766E-05	0.00037	0.00036
0.205	1.1719E-05	0.00035	0.00034
0.292	1.14598E-05	0.00018	0.00017
0.439	1.16902E-05	0.00015	0.00013
0.585	1.21221E-05	0.00014	0.00013

Table 4.1: Main features of the composite cross-section at the maximum load (F_{max}) varying R .

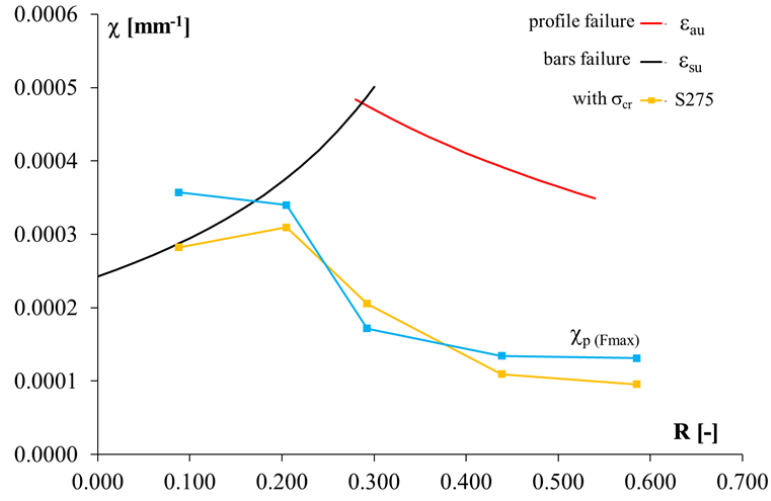


Figure 4.19: Comparison between numerical and theoretical ultimate curvatures at the maximum load ($\chi_{p(F_{max})}$) varying R .

4.2 The numerical analysis of the composite beams subjected to hogging moment

The numerical model of the entire beam allows to study also the global behavior of the element assuming as deformation parameter the rotation in the post elastic field (θ_p), i.e. the rotation of the plastic hinges in the middle of the simple supported beam.

Firstly the elastic-plastic (EPP) model for the construction steel is considered as for the section analysis of par. 4.1.2.

In Fig. 4.20 the global behavior of the beam is plotted through the relation between the applied load F and the displacement at the mid-span.

In the curves of figure 4.20 the achievement of any characteristic point is indicated: the yield strength and ultimate strain of the reinforcement, f_{sk} and ϵ_{su} , the yield strength and ultimate strain of the steel profile, f_{yk} and ϵ_{au} . The curves

are plotted until the failure load is reached that could be identified with one of the following condition:

1. the achievement of the ultimate strain of the steel reinforcement ε_{su} ;
2. the achievement of the ultimate strain in the steel profile ε_{au} ;
3. the achievement of the 85% of the maximum load on the descending branch. In some cases the curves are characterized by a sudden drop before the loss of 15% of the bearing capacity, so that the curves are stopped at this point.

The same curves are reported in non-dimensional form in Figure 4.21: the load is non-dimensional with respect to the yield strength load and also the displacements are divided by the displacement at the yield strength.

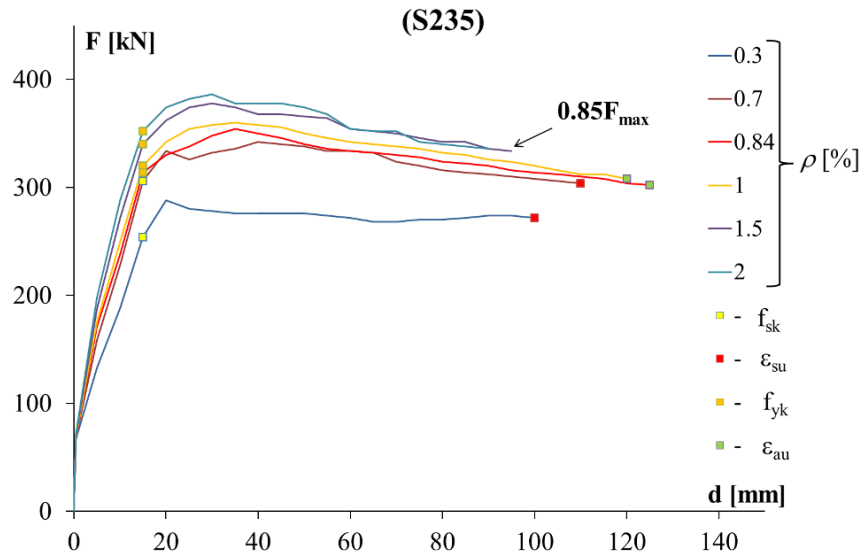


Figure 4.20: Load-Displacement curves varying the percentage of reinforcement (ρ).

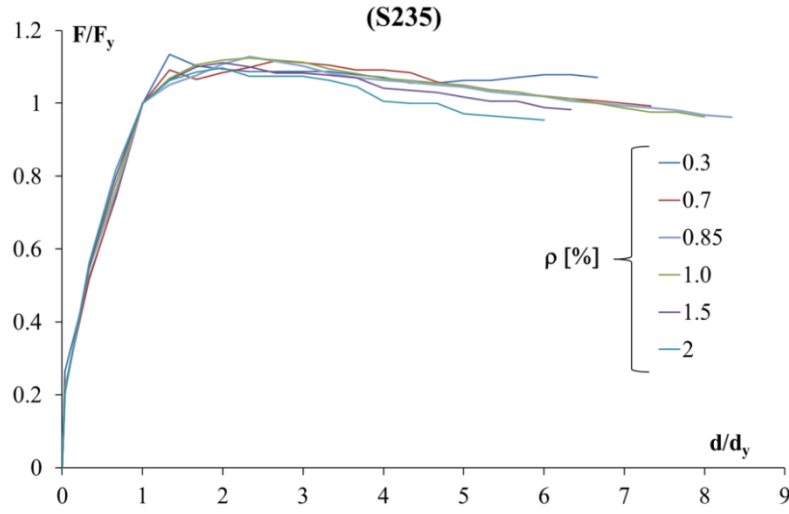


Figure 4.21: Load-Displacement non-dimension curves varying the percentage of reinforcement (ρ).

The graphs of Figure 4.20 suggests that for all values of ρ considered it could be achieved a good ductility of the composite beam. In particular defining the ductility as:

$$D_d = \frac{d_u}{d_y} - 1$$

It is worth to note that in the worst case, when $\rho=2\%$, the ductility D_d is equal to 5, while in the best situation, when $\rho=\rho_{bal}=0.84\%$, the value of D_d becomes equal to 7.3.

From the numerical results it is interesting to evaluate the plastic rotation of the composite beam and also any essential features of the plastic response of the composite system. The plastic rotation is evaluated as the ratio between the plastic displacement (d_p), obtained as the difference between the ultimate displacement (d_u) and the yielding one (d_y), and the half length of the beam ($L=2000\text{mm}$).

Table 4.2 summarizes the evaluation of the plastic rotation assuming the ultimate condition of the beams, while the values of table 4.3 are evaluated considering the performance at the maximum load. Figures 4.22 and 4.23 show the variability of the plastic rotation with ρ and R respectively, for both the cases of ultimate and maximum load conditions.

When the maximum load criterion is assumed the evaluation of the plastic rotation appears too much safe.

ρ	R	d_y	θ_y	d_u	d_p	θ_p
[%]	[-]	[mm]	[mrad]	[mm]	[mm]	[mrad]
0.3	0.103	15	7.50E-03	100	85	42.50
0.7	0.240	15	7.50E-03	110	95	47.48
0.84	0.288	15	7.50E-03	125	110	54.97
1	0.342	15	7.49E-03	120	105	52.45
1.5	0.513	15	7.49E-03	95	80	39.94
2	0.685	15	7.49E-03	90	75	37.43

Table 4.2: Numerical results at the failure varying ρ (steel grade= S235).

ρ	R	d_y	θ_y	d_{Fmax}	$d_{p,Fmax}$	$\theta_{p,Fmax}$
[%]	[-]	[mm]	[mrad]	[mm]	[mm]	[mrad]
0.3	0.103	15	7.50E-03	25	10	5.00
0.7	0.240	15	7.50E-03	40	25	12.49
0.84	0.288	15	7.50E-03	35	20	10.00
1	0.342	15	7.49E-03	35	20	9.99
1.5	0.513	15	7.49E-03	30	15	7.49
2	0.685	15	7.49E-03	30	15	7.49

Table 4.3: Numerical results at the maximum load (F_{max}) varying ρ (steel grade=S235).

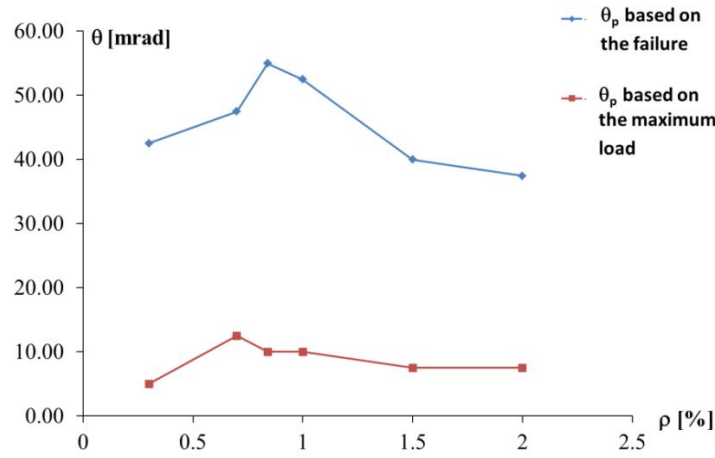


Figure 4.22: Variation of the plastic rotation versus the percentage of reinforcement

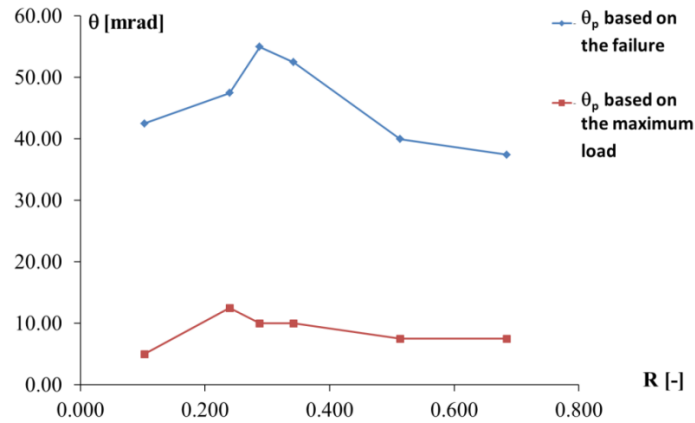


Figure 4.23: Variation of the plastic rotation versus the parameter R .

In fig. 4.24 the plastic rotation, based on the criterion of the ultimate displacement, is drawn versus the parameter R considering the variation of the steel grade; some significant points of the curves are resumed in table 4.4. The trend of the θ_p – R curves is very similar to the one of the χ_p – R curves reported in fig. 4.14 especially for the branch corresponding to the failure of the steel

profile (R greater than the peak value), in fact both the section and the beams are influenced by the non-linear phenomena due to imperfection and local buckling.

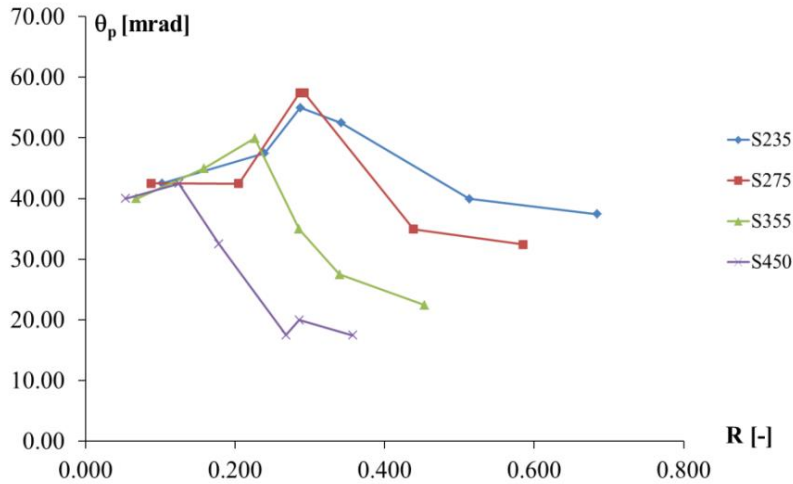


Figure 4.24: Variation of the plastic rotation at the ultimate condition versus the parameter R varying the steel grade.

S235		S275		S355		S450	
θ_p	R	θ_p	R	θ_p	R	θ_p	R
[mrad]		[mrad]		[mrad]		[mrad]	
42.50	0.103	42.50	0.088	40.00	0.068	40.00	0.054
47.48	0.240	42.48	0.205	44.98	0.159	42.48	0.125
52.45	0.342	57.44	0.292	49.95	0.227	32.47	0.179
39.94	0.513	34.95	0.439	27.46	0.340	17.47	0.268
37.43	0.685	32.44	0.585	22.46	0.453	17.47	0.357

Table 4.4: Summary of the plastic rotation of the composite beams versus R .

4.2.1 The effect of the hardening

According to the same procedure already adopted for the section, in this paragraph the numerical model was developed introducing the hardening in the construction steel behaviour (EPH constitutive relationship).

Fig. 4.25 shows the load-displacement curves of the beam varying the percentage of the reinforcing bars obtained both through the numerical model with the steel hardening and the numerical model without this effect, already presented in the previous paragraph. The curves are stopped with the same criteria assumed for the section i.e. at the failure condition of the materials or the load drop at 85% of the maximum value.

The comparison points out that the steel hardening gives an increment of the strength and ductility, but the ductility enhancement reduces at the increasing of the reinforcement percentage until that it remains constant when ρ is 1.5-2.0%.

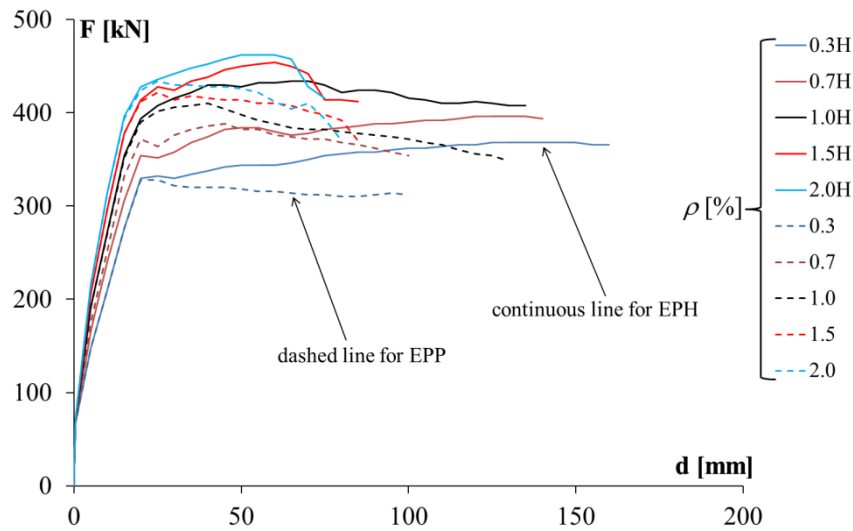


Figure 4.25: Comparison of the load-displacement curves for the EPH and EPP models.

In Fig. 4.26 the numerical results of the EPH model are drawn again but in non-dimensional form using the yielding condition as parameter for the non-dimensionalizing of the curves. The ductility ($D_d = d_u/d_y - 1$) variation is relevant and approximately from 4 at $\rho = 2\%$ up to 9 at $\rho = 0.3\%$; anyway the good performance of the composite beam is confirmed.

Table 4.5 summarizes the main features of the composite beam varying the R value at the ultimate conditions. The plastic rotation has relevant values and varies from 30 mrad at $R=0.585$ up to 72.5 mrad at $R=0.088$.

It could be more reliable to define the plastic properties of the composite beam at the achievement of the maximum load (F_{max}) (fig. 4.27), before buckling.

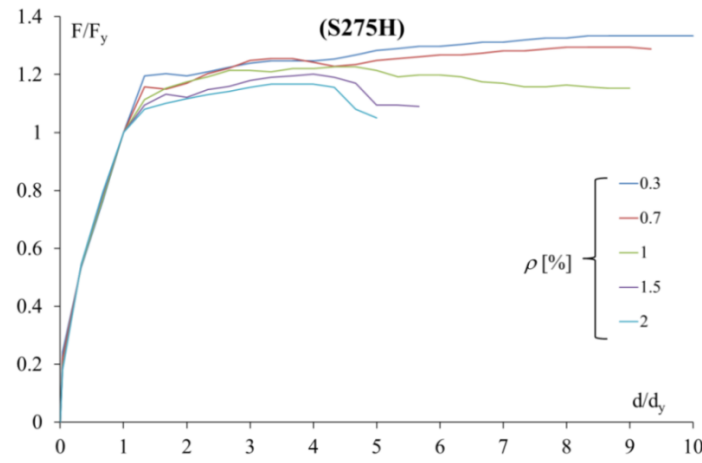


Figure 4.26: Load-displacement non-dimensional curves for the EPH model varying the percentage of reinforcement (ρ).

R	d_y	θ_y	d_u	d_p	θ_p
[-]	[mm]	[mrad]	[mm]	[mm]	[mrad]
0.088	15	7.50E-03	160	145	72.50
0.205	15	7.50E-03	140	125	62.47
0.292	15	7.49E-03	135	120	59.94
0.439	15	7.49E-03	85	70	34.97
0.585	15	7.49E-03	75	60	29.96

Table 4.5: Main features of the composite beam varying R at the ultimate condition.

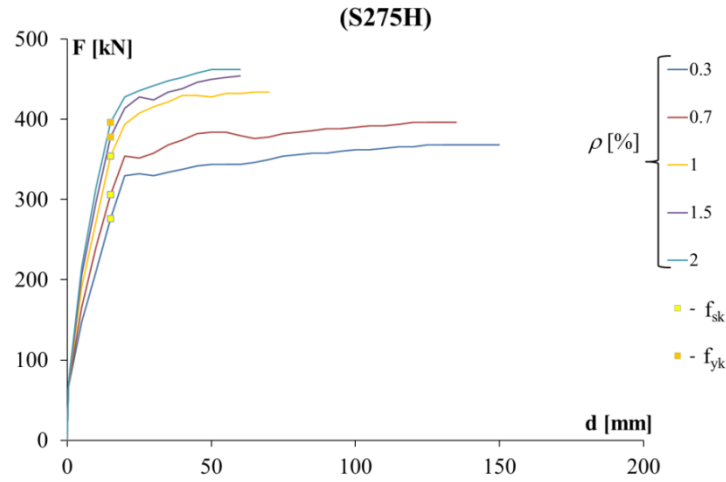


Figure 4.27: Load-displacement curves varying the percentage of reinforcement (ρ) for the EPH model stopped at the maximum load (F_{max}).

In fig. 4.28 the same results of fig. 4.27 are drawn in non-dimensional form using the yielding load and displacement to obtain the non-dimensional form; the reduction of the maximum displacement is evident especially for the highest percentage of reinforcement.

The result is synthesized in the graph of fig. 4.29 that gives the trend of the plastic rotation versus the parameter R comparing the results of the load-displacement curves at the maximum load or at the ultimate condition. The beams with R greater than about 0.2 have a large reduction of ductility as shown also by the values in table 4.6.

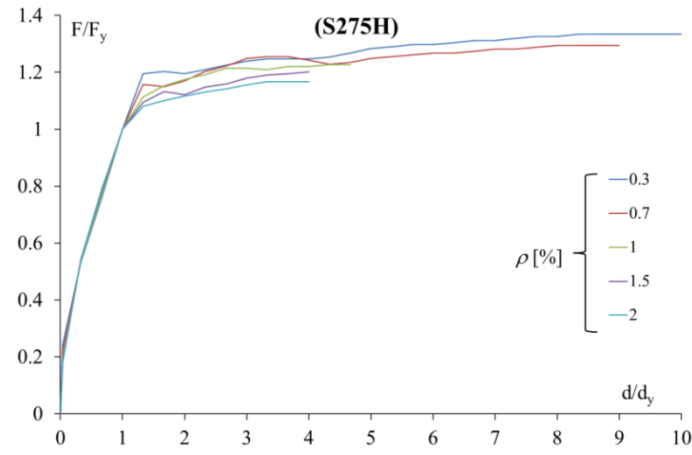


Figure 4.28: Load-displacement non-dimensional curves varying ρ for the EPH model plotted up the maximum load (F_{max}).

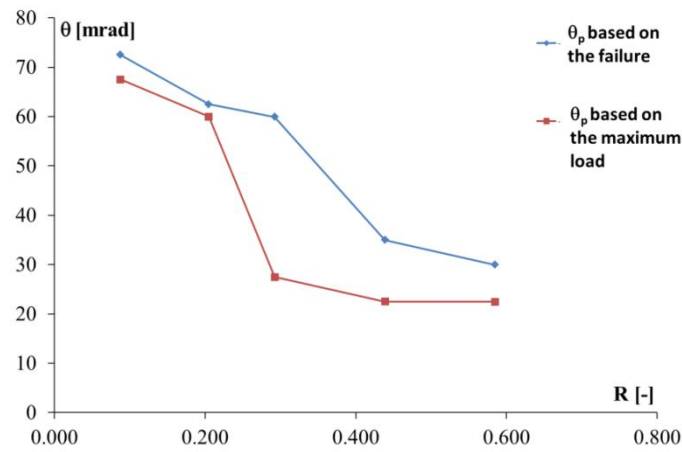


Figure 4.29: Comparison of the variation of the plastic rotation versus R .

R	d_y	θ_y	d_u	d_p	θ_p
$[-]$	$[\text{mm}]$	$[\text{mrad}]$	$[\text{mm}]$	$[\text{mm}]$	$[\text{mrad}]$
0.088	15	7.50E-03	150	135	67.50
0.205	15	7.50E-03	135	120	59.97
0.292	15	7.49E-03	70	55	27.47
0.439	15	7.49E-03	60	45	22.48
0.585	15	7.49E-03	60	45	22.47

Table 4.6: Main features of the composite beam assuming the maximum load criterion.

For low values of R of about 0.205, corresponding to percentages of the reinforcement up to 0.7% and compatible with practical application, it could be observed a good performance of the composite beams compatible also with the concept of “stable behavior”. As R increases as the plastic rotation capacity of the composite system decreases, both for any collapse criteria or maximum load rule. The rule of cutting the curves at the maximum load achievement seems to be the more reliable due to the complexity of implementing a model taking into account the post-buckling behavior in detail.

4.2.2 The effect of the connection deformability

In this paragraph the effect of the connection degree on the plastic rotational capacity is examined introducing in the model a variation of the bond-slip law of the connection.

In order to better highlight only the role of the shear connection degree, the model without steel hardening was applied again. Five degrees of connection (N/N_f): 0.4, 0.6, 0.8, 1.0 and 1.2 were considered. The number of shear studs necessary for realizing the connection degree was computed considering a reinforcement percentage of 0.7%, therefore the amount of reinforcement is given by:

$$A_s = 0.007 \cdot A_c = 0.007 \cdot 1000 \cdot 130 = 910 \text{ mm}^2$$

This amount of reinforcement, A_s , defines the maximum force that the connection has to transfer between the two components:

$$f_{yk} \cdot A_s = 910 \cdot 450 = 409500 \text{ N} = 410 \text{ kN}$$

The strength of the shear stud (P_{rk}) is assumed equal to that given in the paragraph 3.7.2 i.e 81.4kN. This resistance allows to compute the number of studs:

$$N_f = \frac{f_{yk} \cdot A_s}{P_{rk}} = \frac{910 \cdot 450}{81.4 \cdot 10^3} = 5.03$$

The continuous interface element, used in the FE model, was calibrated considering the number of shear studs; for example, the full shear strength is achieved for five connectors and the influence length of each shear stud was determined dividing the half length of the beam ($L=2200\text{mm}$) by the number of studs (5), then:

$$l_i = \frac{L_{tot}}{N_f} = \frac{2200}{5} = 440\text{mm}$$

Therefore the effective length of each shear stud provides the influence area of the distributed bond law, τ - s , of the interface element:

$$A_i = B_f \cdot l_i = 170 \cdot 440 = 74800\text{mm}^2$$

where B_f is the depth of the flange of the steel joist at the concrete slab interface.

In other word, the load-slip relation of the connector, P - s (fig. 3.25), is transformed in the bond stress-slip relation, τ - s , (fig. 4.30), dividing the load (P) by the area of influence.

The case of the full interaction is defined also in terms of stiffness and is named as full connection (FC) , therefore the partial interaction is defined as percentage of this FC case. In Fig. 4.31 the effect of the shear connection degree is shown by the force-displacement curves. The failure conditions are the ones related to the materials (reinforcing steel or construction steel) but for the curves with the lower interaction degree (0.4C and 0.6C) the collapse is due to the ultimate slip of the bond-slip law. In the comparison the beam with the rigid connection (RC), that considers the perfect bond at the concrete slab interface, was reported. It is worth noticing that already for a shear connection degree of 0.8 there is almost the full exploiting of the plastic strength of the composite beam. On the other hand, in the beams with a full shear connection, or more, (1.0C and 1.2C) and with rigid connection (RC) the failure is due to

the ultimate strain in the reinforcement, while in the case of 0.8C the failure is due to the maximum strain in the steel profile.

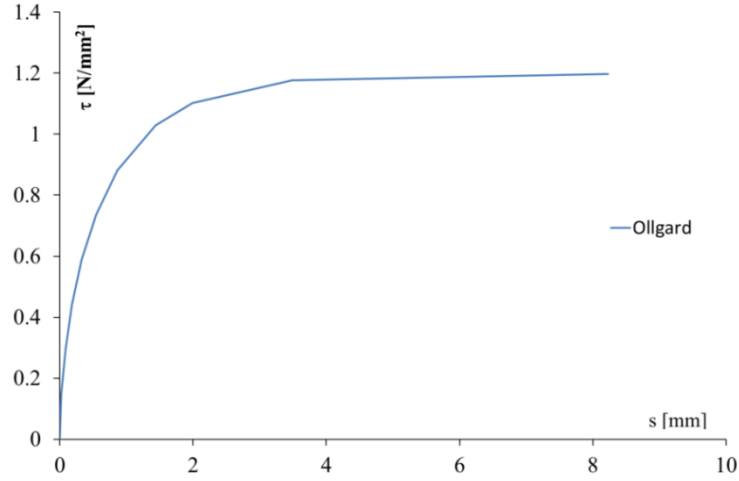


Figure 4.30: The τ - s relationship of the interface element used for the shear connection ($N/N_f=1$).

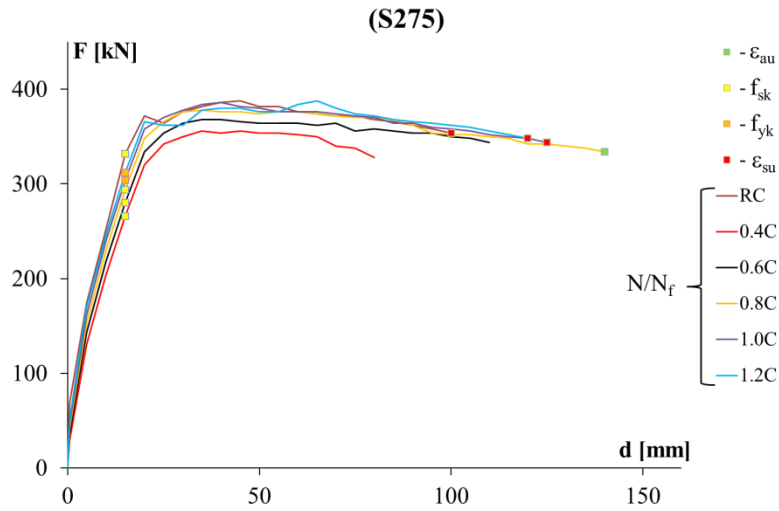


Figure 4.31: Force-displacement relation varying the shear connection degree (N/N_f).

The effect of the partial connection degree is the reduction of ductility since the failure is due to the connection devices so that the maximum curvature at the balanced failure cannot be reached; when the full connection is realized the

deformability of the beam increases, due to the presence of a deformable shear studs, in respect to the rigid one so that this last case results less ductile. In conclusion the wide parametric analysis conducted assuming the rigid connection in the numerical and theoretical model is safe in terms of available ductility.

Furthermore in the seismic design the degree of connection (N/N_f) is imposed by the standard code (EC8, 2003; NTC08, 2008) not less than 0.8, for avoiding problem of failure due to low-fatigue; the importance of the subject was highlighted also in (Bursi et al., 2005) that confirmed the necessity of avoiding the failure of the shear connectors in the central part of beams due to the effect of low-cycle fatigue phenomena on shear connections with a low interaction degree.

4.3 The equivalent plastic hinge length

In the following it is reported a summary on the analysis for determining the equivalent plastic hinge length by the results of the previous theoretical and numerical analysis of the section and beams.

In general the plastic hinge length is evaluated as the ratio between the plastic rotation and the plastic curvature (χ_p):

$$L_p = \frac{\theta_p}{\chi_p}$$

Firstly the numerical plastic rotations evaluated using the elastic-plastic relation (EPP) for the steels and the theoretical curvature (i.e. without the effect of the critical stress) are considered; in table 4.7 and 4.8 the plastic hinge length is reported respectively assuming the ultimate condition (descending branch of the force-displacement relation until 85% of the maximum load) and the maximum load condition.

Fig. 4.32 shows the trend of the plastic hinge length varying the R ratio and steel grade. The trends described by the L_p values are similar to those described by the plastic rotation in figure 4.24: in fact after the peak value of R there is a descending branch with an increasing slope as much as the strength increases. Table 4.8 and Fig. 4.33 shows as the evaluation of L_p based on the maximum load (F_{max}) is too much safe and not suitable when the EPP model is adopted.

R	θ_p	χ_p	L_p
[-]	[mrad]	[1/mm]	[mm]
0.103	42.50	0.00028	150.6
0.240	47.48	0.00041	115.1
0.288	54.97	0.00051	107.7
0.342	52.45	0.00044	118.8
0.513	39.94	0.00041	97.4
0.685	37.43	0.00040	93.5

Table 4.7: The plastic hinge length from the numerical results at failure varying R for the steel grade of the joist S235.

R	$\theta_{p,Fmax}$	χ_p	$L_{p,Fmax}$
[-]	[mrad]	[1/mm]	[mm]
0.103	5.00	0.00028	17.7
0.240	12.49	0.00041	30.3
0.288	10.00	0.00051	19.6
0.342	9.99	0.00044	22.6
0.513	7.49	0.00041	18.3
0.685	7.49	0.00040	18.7

Table 4.8: The plastic hinge length from the numerical results at the maximum load (F_{max}) of the composite beam varying R for the steel grade of joist S235.

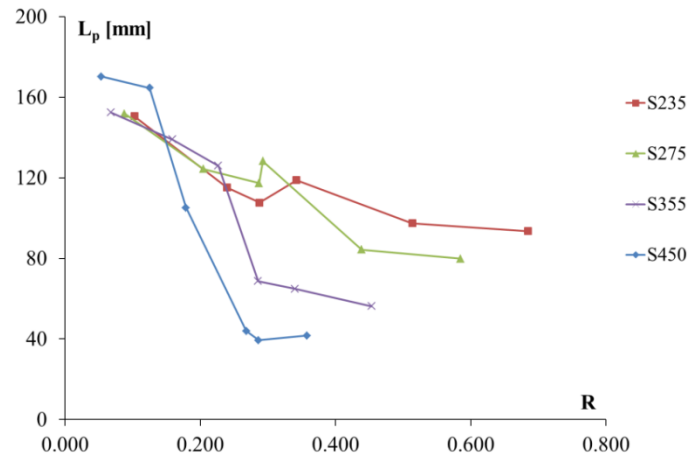


Figure 4.32: Variation of the plastic hinge length versus the parameter R varying the steel grades and considering the ultimate condition.

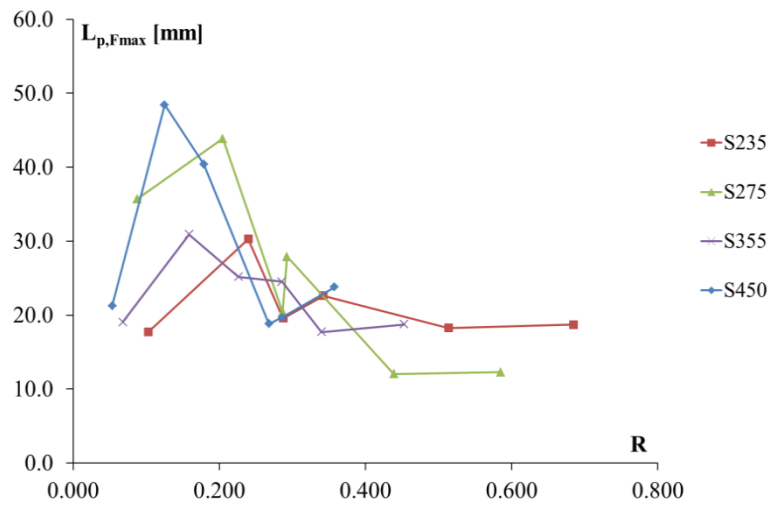


Figure 4.33: Variation of the plastic hinge length versus the parameter R varying the steel grades and considering the maximum load (F_{max}).

The plastic hinge length was evaluated also considering the hardening in the construction steel behaviour (EPH constitutive relationship) as already done for the plastic rotation in paragraph 4.1.2, and analyses were performed varying the steel grade.

The introduction of the EPH model for the steel joist makes more suitable the use of the plastic rotation at the maximum load in the evaluation of the L_p value, as already discussed, therefore only this condition is analyzed:

$$\theta_{p,Fmax} = \frac{d_{Fmax} - d_y}{L_v} \quad \rightarrow \quad L_p = \frac{\theta_{p,Fmax}}{\chi_p}$$

As regarding the plastic curvature, in this case its value is the one numerically estimated taking into account also the critical stress, as reported in the par. 4.1.2.1. This choice seems coherent with the assumption of the plastic rotational capacity at the maximum load before the softening branch governed by a post-buckling response.

Table 4.9 summarizes the plastic rotation (θ_p), the theoretical critical curvature ($\chi_{p,cr}$) and the equivalent plastic hinge length (L_p) varying the R ratio for the steel grade S275; the value appears about constant.

R	θ_p	$\chi_{p,cr}$	L_p
[-]	[mrad]	[1/mm]	[mm]
0.088	67.50	0.0002823	230.2
0.205	59.97	0.0003095	185.7
0.292	27.47	0.0001512	183.2
0.439	22.48	0.0001096	205.1
0.585	22.47	9.57471E-05	234.6

Table 4.9: The plastic hinge length computed considering the steel hardening and local buckling.

Fig. 4.35 shows the variation of L_p in non-dimensional form (ratio L_p/H with H the height of the steel profile) versus the R ratio and considering the various steel grades; the constant value obtained by the regression of the data results about 0.6.

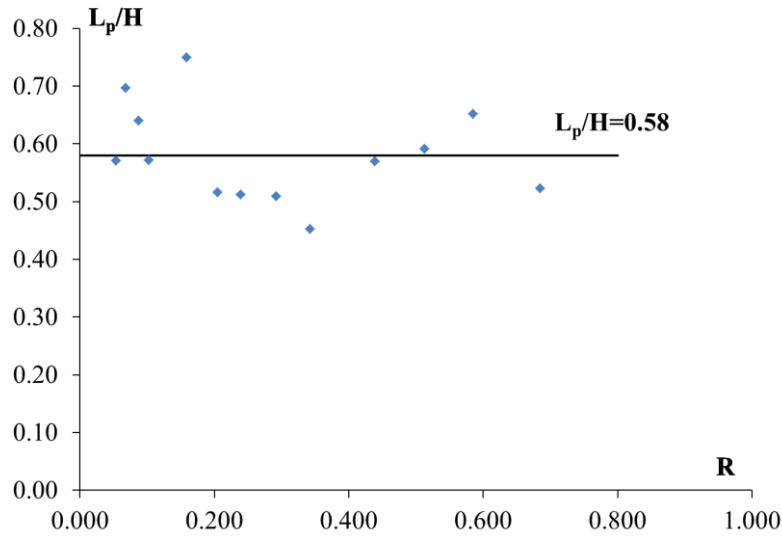


Figure 4.35: The variation of the plastic hinge length in non-dimensional form (L_p/H) versus R varying the steel grade.

4.4 Conclusions

In this chapter the results of many theoretical and numerical analyses of the cross-section of the composite beams have been presented. The theoretical approach allowed to evaluate and highlight in a closed form which are the two possible failures of the section due to the reinforcement or the steel joist, if the local buckling is neglected and a stiff connection is considered. With these assumption, it was underlined that the sectional behavior is mostly influenced by the mechanical factor R , that is the ratio between the maximum tensile strength of the reinforcing bars and the axial strength in tension of the steel joist. In order to introduce the local buckling phenomenon in the theoretical approach, the critical stress approach reported in (Mazzolani et al., 1992) was considered; a tri-linear hardening model (EPH) based on experimental data was introduced and the moment-curvature relationships was evaluated by a numerical fiber model.

The numerical model by the FE model introduced in the previous chapter was applied to carry out a parametric analysis of the entire beam behaviour varying

the mechanical ratio R and the steel grade of the joist; the model gave the plastic rotation capacity (θ_p) of the beams versus the parameters considered. The parametric analysis was extended also to evaluate the effect of the grade of connection on the global response of the composite beam highlighting that already for a shear connection grade equal to 0.8 the strength of the beam is the same of the case with the full shear connection or a rigid connection; the global ductility is greater when the connection is deformable so that the hypothesis of rigid connection assumed in the previous parametric analysis is safe.

Finally, in order to assess a simple procedure for evaluating the plastic rotation, the plastic hinge length is evaluated as the ratio between the numerical rotation and the numerical plastic curvature, both evaluated introducing the hardening and the local buckling phenomena. The plastic hinge length result quite constant and can be assumed equal to $0.6H$, being H the height of the steel joist.

This conclusion allows to evaluate the plastic rotation of a steel-concrete composite beam under hogging moment multiplying the numerical plastic curvature, obtained by a simple tool that takes into account the local buckling phenomena, by the plastic hinge length of $0.6H$.

REFERENCES

- Bursi, O. S., Sun, F., Postal, S., “Non-linear analysis of steel-concrete composite frames with full and partial shear connection subjected to seismic loads”, *Journal of Constructional Steel Research*, vol. 61, 2005, pp. 67–92
- Oehlers, D. J., Nguyen, N. T., Ahmed, M., Bradford, M. A., "Partial interaction in composite steel and concrete beams with full shear connection", *Journal of constructional steel research*, vol. 41, n. 2/3, 1997, pp. 235-248
- Faella, C., Martinelli, E., Nigro, E., "Shear Connection Nonlinearity and Deflections of Steel–Concrete Composite Beams: A Simplified Method”, *Journal of Structural Engineering*, Vol. 129, No. 1, January 1, 2003, pp. 12-20
- Mazzolani, F. M., Piluso, V., “Evaluation of the rotation capacity of the steel beams and beam-columns”, 1st Cost C1 Workshop, Strasbourg, October 1992, pp. 28-30
- Mazzolani, F. M., Piluso, V., “Theory and design of seismic resistant steel frames”, Spon Press, 1996, pp. 497

Appendix A – Numerical analyses results for S275

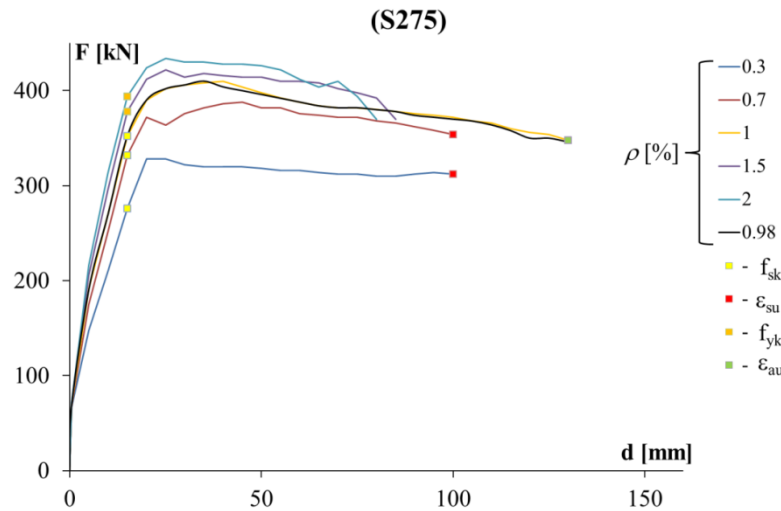


Figure A.1: Load-displacement curves varying the percentage of reinforcement (ρ)

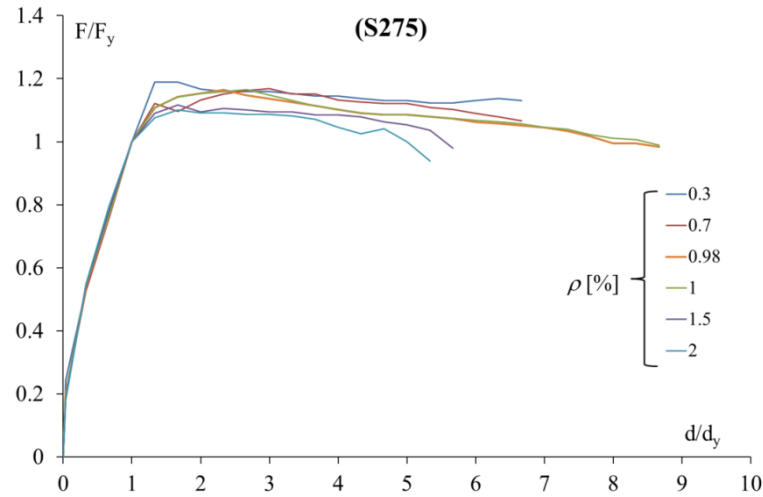


Figure A.2: Load-displacement non-dimension curves varying the percentage of reinforcement (ρ)

ρ	R	d_y	θ_y	d_u	d_p	θ_p	χ_p	L_p
[%]	[-]	[mm]	[mrad]	[mm]	[mm]	[mrad]	[1/mm]	[mm]
0.3	0.088	15	7.50E-03	100	85	42.50	0.00029	146.6
0.7	0.205	15	7.50E-03	100	85	42.48	0.00038	111.8
0.84	0.287	15	7.49E-03	130	115	57.44	0.00048	119.7
1	0.292	15	7.49E-03	130	115	57.44	0.00048	119.7
1.5	0.439	15	7.49E-03	85	70	34.95	0.00039	89.6
2	0.585	15	7.49E-03	80	65	32.44	0.00033	98.3

Table A.1: Main measurement from the numerical results at the failure varying ρ and for a steel joist grade of S275

ρ	R	d_y	θ_y	d_u	d_p	θ_p	χ_p	L_p
[%]	[-]	[mm]	[mrad]	[mm]	[mm]	[mrad]	[1/mm]	[mm]
0.3	0.088	15	7.50E-03	100	85	10.00	0.00029	34.5
0.7	0.205	15	7.50E-03	45	30	14.99	0.00038	39.5
0.84	0.287	15	7.49E-03	35	20	9.99	0.00048	20.8
1	0.292	15	7.49E-03	40	25	12.49	0.00048	26.0
1.5	0.439	15	7.49E-03	25	10	4.99	0.00039	12.8
2	0.585	15	7.49E-03	25	10	4.99	0.00033	15.1

Table A.2: Main measurement from the numerical results at the maximum load (F_{max}) varying ρ and for a steel joist grade of S275

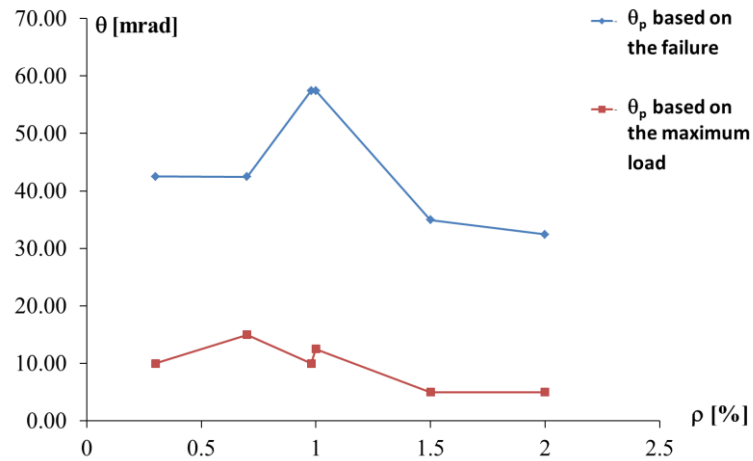


Figure A.3: Variation of the plastic rotation varying the percentage of reinforcement

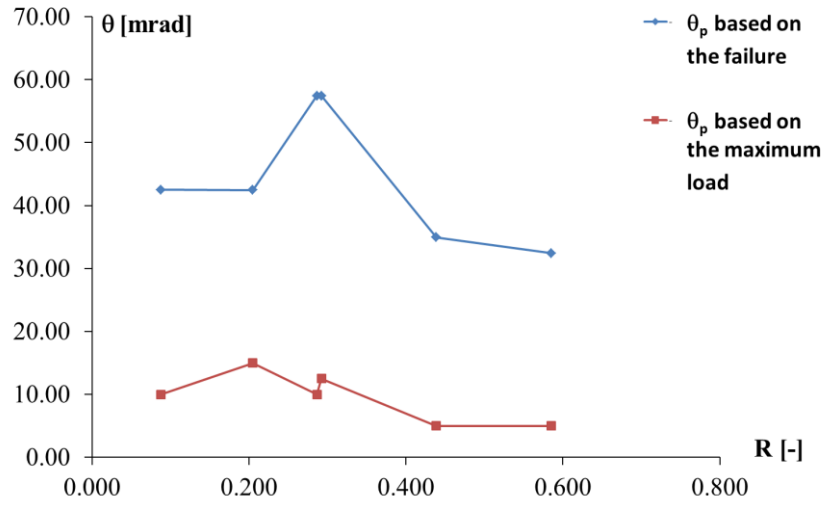


Figure A.4: Variation of the plastic rotation varying the parameter R

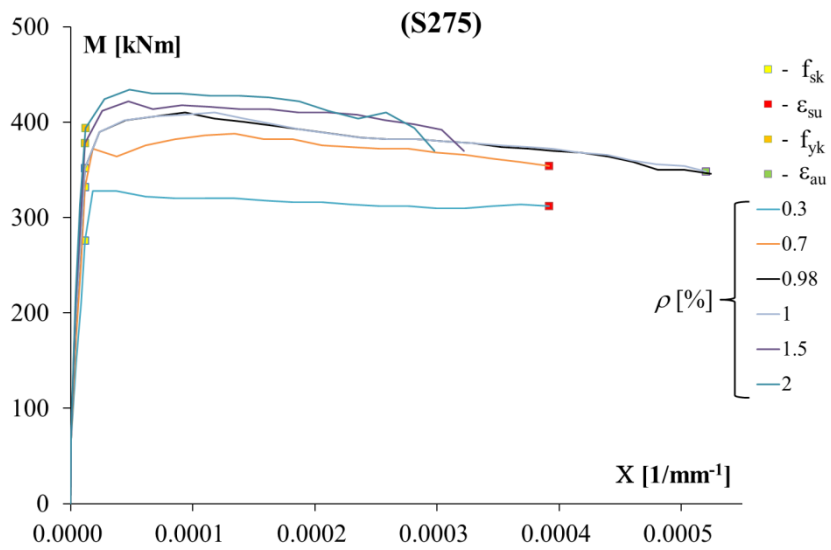


Figure A.5: Moment-curvature varying the percentage of reinforcement (ρ)

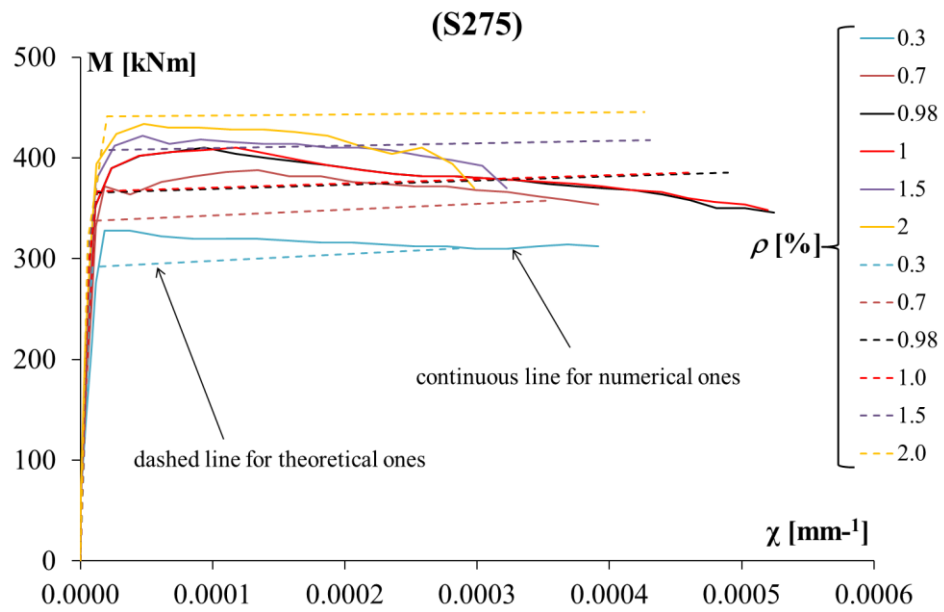


Figure A.6: Comparison between numerical and theoretical moment-curvatures varying the percentage of reinforcement (ρ)

Appendix B – Numerical analyses results for S355

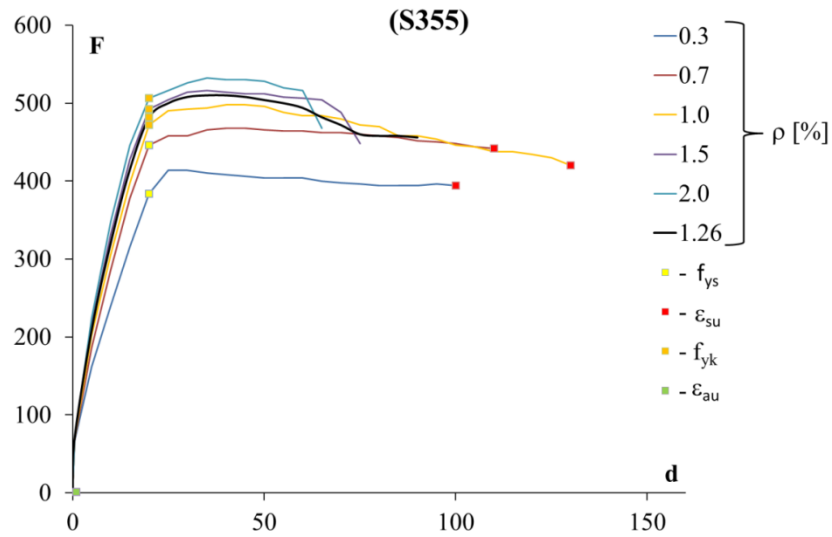


Figure B.1: Load-displacement curves varying the percentage of reinforcement (ρ)

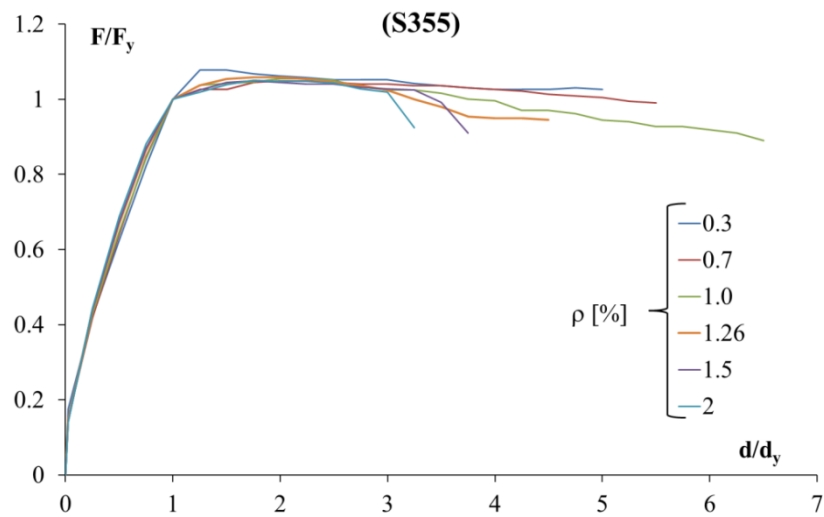


Figure B.2: Load-displacement non-dimensional curves varying the percentage of reinforcement (ρ)

ρ	R	d_y	θ_y	d_u	d_p	θ_p	χ_p	L_p
[%]	[-]	[mm]	[mrad]	[mm]	[mm]	[mrad]	[1/mm]	[mm]
0.3	0.068	20	1.00E-02	100	80	0.0400	0.00027	148.1
0.7	0.159	20	1.00E-02	110	90	0.0450	0.00033	136.3
1.0	0.227	20	9.99E-03	120	100	0.0500	0.00040	124.9
1.26	0.285	20	9.99E-03	90	70	0.0350	0.00044	79.5
1.5	0.340	20	9.99E-03	75	55	0.0275	0.00044	62.4
2	0.453	20	9.98E-03	65	45	0.0225	0.00038	59.1

Table B.1: Main measurement from the numerical results at the failure varying ρ and for a steel joist grade of S355

ρ	R	d_y	θ_y	d_u	d_p	θ_p	χ_p	L_p
[%]	[-]	[mm]	[mrad]	[mm]	[mm]	[mrad]	[1/mm]	[mm]
0.3	0.068	20	1.00E-02	30	10	0.0050	0.00027	18.5
0.7	0.159	20	1.00E-02	40	20	0.0100	0.00033	30.3
1.0	0.227	20	9.99E-03	40	20	0.0100	0.00040	25.0
1.26	0.285	20	9.99E-03	45	25	0.0125	0.00044	28.4
1.5	0.340	20	9.99E-03	35	15	0.0075	0.00044	17.0
2	0.453	20	9.98E-03	35	15	0.0075	0.00038	19.7

Table B.2: Main measurement from the numerical results at the maximum load (F_{max}) varying ρ and for a steel joist grade of S355

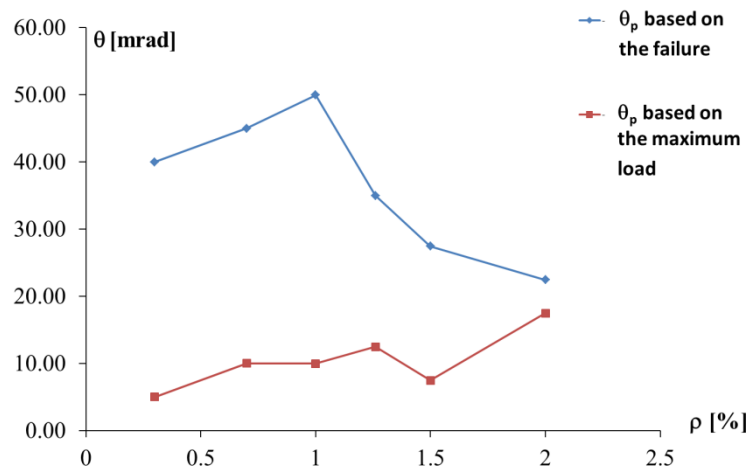


Figure B.3: Variation of the plastic rotation varying the percentage of reinforcement (ρ):

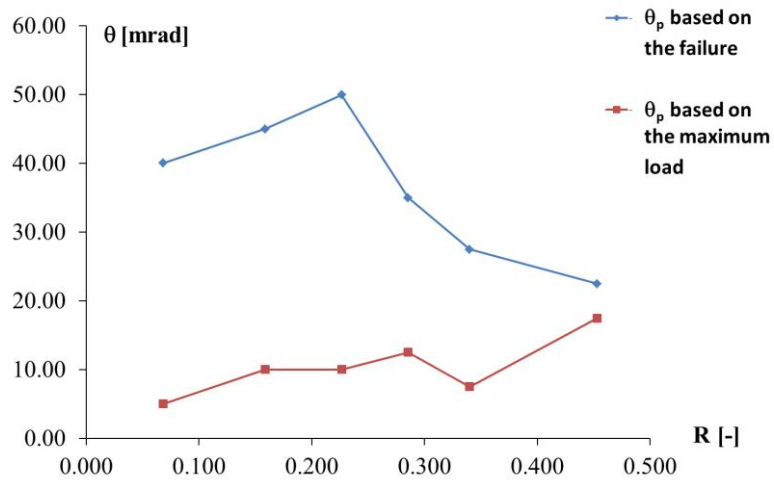


Figure B.4: Variation of the plastic rotation varying the parameter R

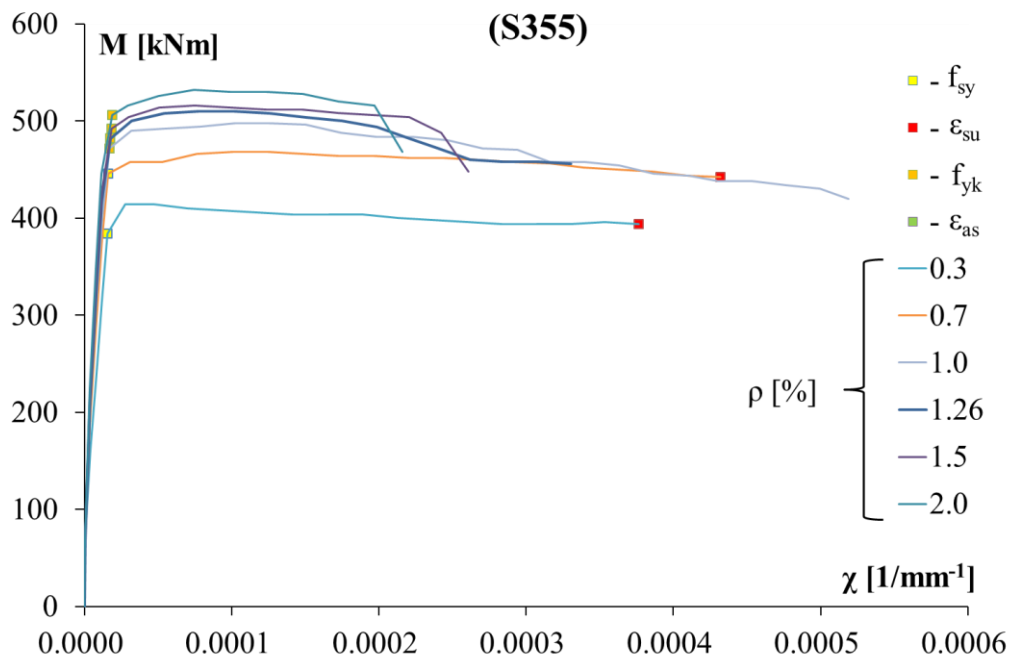


Figure B.5: Moment-curvature varying the percentage of reinforcement (ρ)

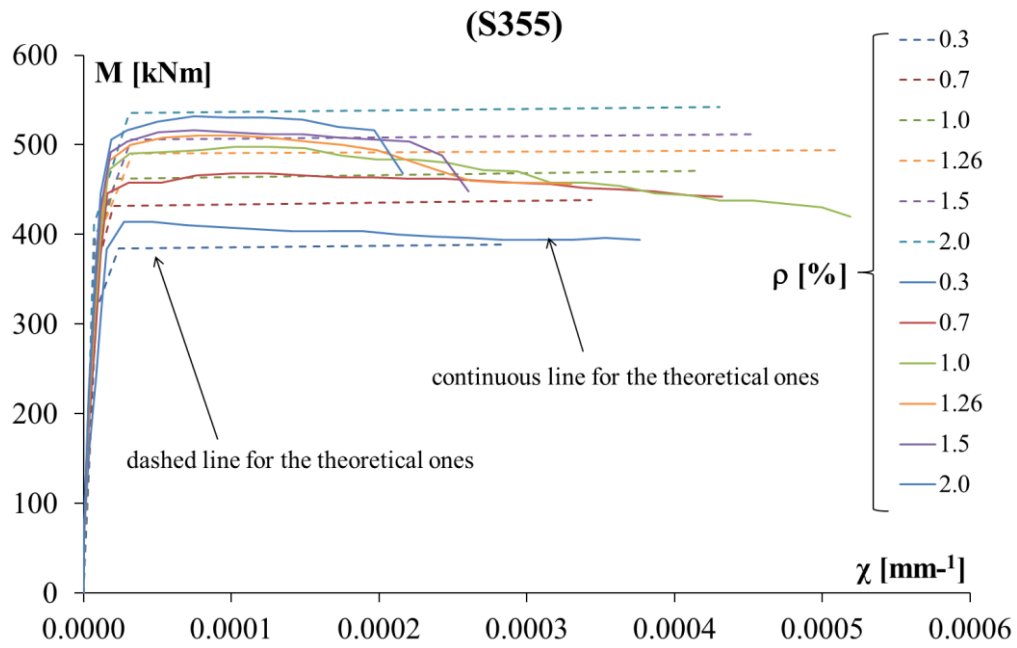


Figure B.6: Comparison between numerical and theoretical moment-curvatures varying the percentage of reinforcement (ρ)

Appendix C – Numerical analyses results for S450

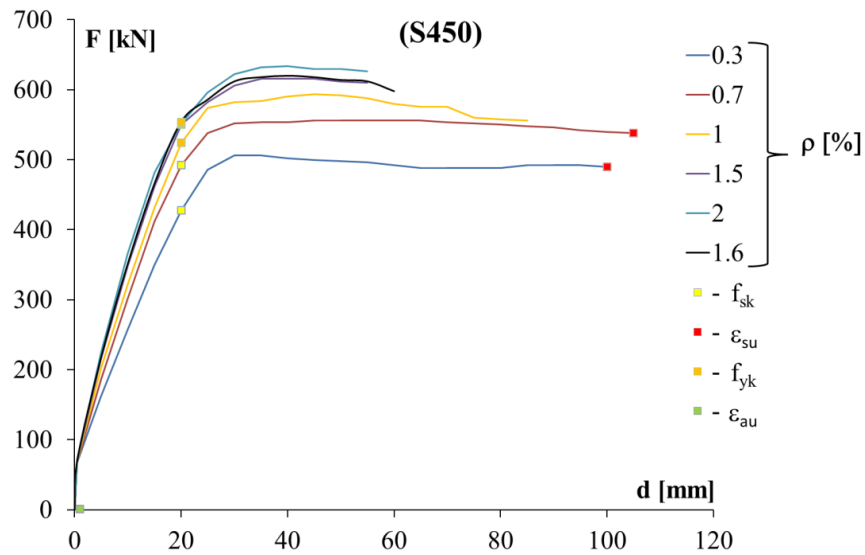


Figure C.1: Load-displacement curves varying the percentage of reinforcement (ρ)

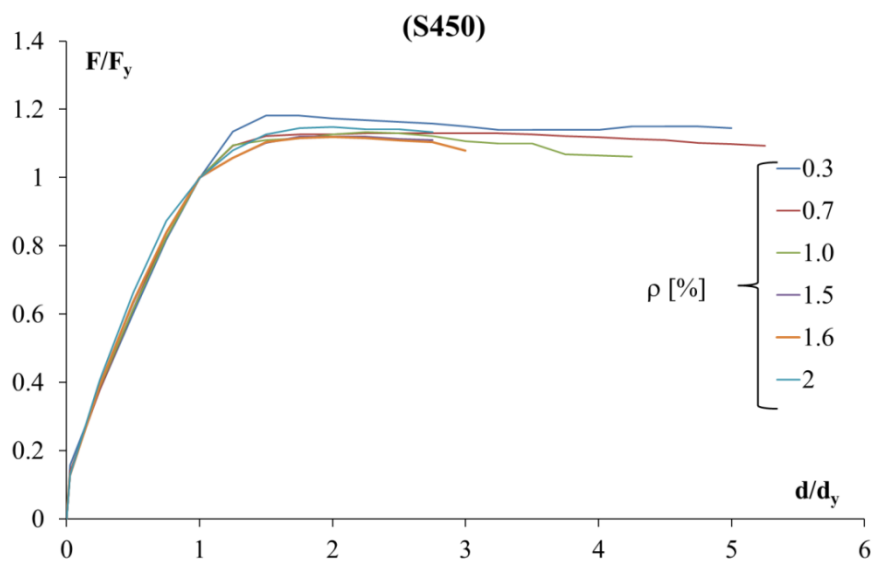


Figure C.2: Load-displacement non-dimension curves varying the percentage of reinforcement (ρ)

ρ	R	d_y	θ_y	d_u	d_p	θ_p	χ_p	L_p
[%]	[-]	[mm]	[mrad]	[mm]	[mm]	[mrad]	[1/mm]	[mm]
0.3	0.054	20	1.00E-02	100	80	40.00	0.00026	153.8
0.7	0.125	20	1.00E-02	105	85	42.48	0.00031	137.0
1.0	0.179	20	9.99E-03	85	65	32.47	0.00035	92.8
1.5	0.268	20	9.99E-03	55	35	17.47	0.00045	38.8
1.6	0.286	20	9.98E-03	60	40	19.96	0.00047	42.5
2.0	0.357	20	9.98E-03	55	35	17.47	0.00043	40.6

Table C.1: Main measurement from the numerical results at the failure of the composite beam varying ρ and for a steel joist grade of S450

ρ	R	d_y	θ_y	d_u	d_p	θ_p	χ_p	L_p
[%]	[-]	[mm]	[mrad]	[mm]	[mm]	[mrad]	[1/mm]	[mm]
0.3	0.054	20	1.00E-02	30	10	5.00	0.00026	19.2
0.7	0.125	20	1.00E-02	45	25	12.49	0.00031	40.3
1.0	0.179	20	9.99E-03	45	25	12.49	0.00035	35.7
1.5	0.268	20	9.99E-03	35	15	7.49	0.00045	16.6
1.6	0.286	20	9.99E-03	40	20	9.99	0.00047	21.2
2.0	0.357	20	9.98E-03	40	20	9.98	0.00043	23.2

Table C.2: Main measurement from the numerical results at the maximum load (F_{max}) of the composite beam varying ρ and for a steel joist grade of S450

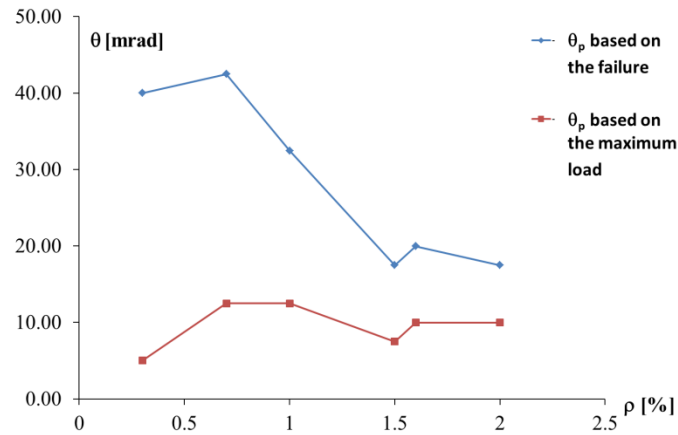


Figure C.3: Variation of the plastic rotation varying the percentage of reinforcement (ρ)

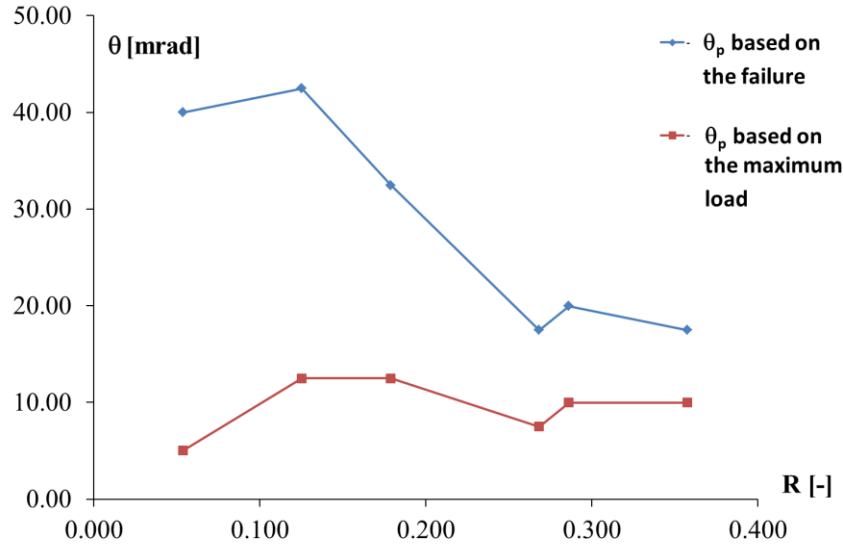


Figure C.4: Variation of the plastic rotation varying the parameter R .

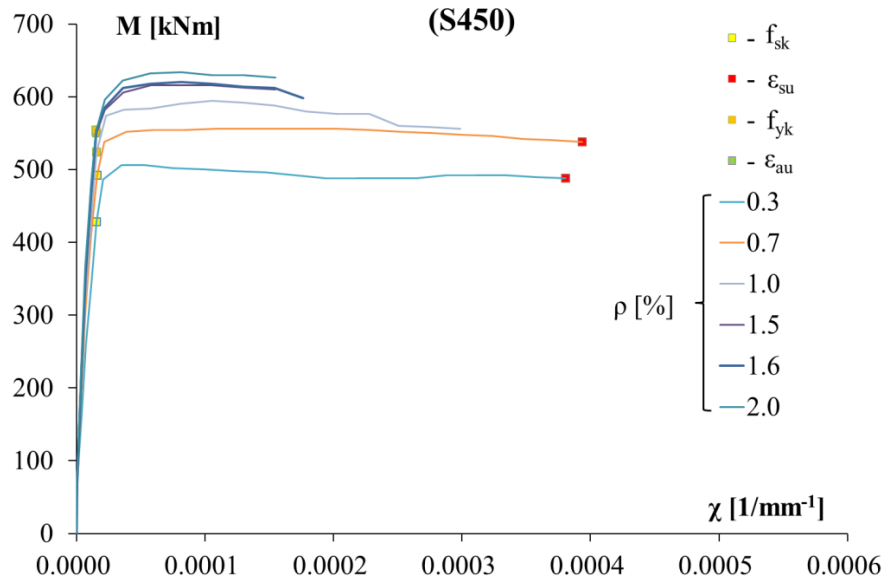


Figure C.5: Moment-curvature varying the percentage of reinforcement (ρ).

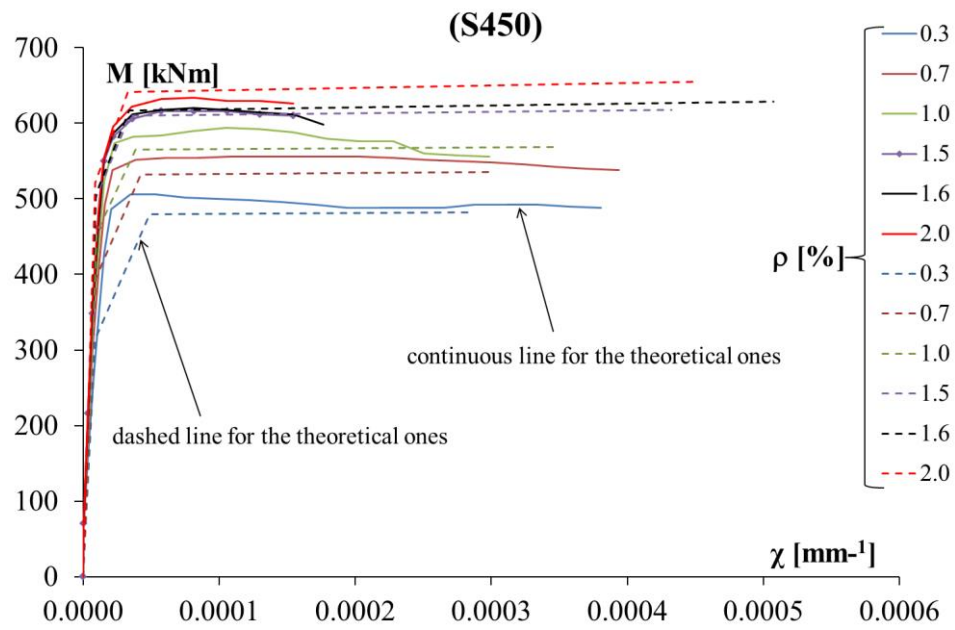


Figure C.6: Comparison between numerical and theoretical moment-curvatures varying the percentage of reinforcement (ρ)

CHAPTER 5. THE BASE CONNECTION OF COMPOSITE COLUMNS

In this chapter the problem of defining the deformability and rotational capacity of the base column connection for a composite column is treated in order to introduce this effect in the analysis of a composite frame developed in the next chapter.

A review of experimental tests and numerical model of base connections is presented considering both steel and composite columns, since currently the solutions adopted for the composite columns are the same used for the steel ones and similar performances have been observed.

In this paragraph, the experimental results from (Di Sarno et al., 2007; Ceroni et al., 2010) for a partially encased composite column connected to the block foundation with a deeply embedded joint (socket type) without end anchorage are analysed in detail to identify the rotational capacity of the connection. This typology of base connection could be useful either for steel-concrete composite building than for steel structure, In fact, the simple way of realization makes it up available also for framed steel structure.

The analysis of the experimental tests is aimed to distinguish the contributions of the fixed end rotation (due to the deformation of the embedded part of the column) and the rotational capacity of the column.

The problem of the fixed end rotation is well known and has been studied for reinforced concrete structures in the last twenty years (Priestley et al., 1987), but it has not been studied in steel and steel-concrete composite columns, which are commonly used in braced structures.

The experimental results highlight the relevant contribution of the joint deformability, both in elastic and plastic fields, for the socket type connection;

albeit this study uses an embedded length of more than 2 times the section height.

A tridimensional FE model has been developed and calibrated by the experimental results; then a parametric analysis has been carried to calibrate a non-linear spring representing the connection deformability to be introduced in a simple mono-dimensional model.

5.1 The base column connection of steel and composite columns

Composite columns could be an efficient solution to improve the performance of the structure, unfortunately, the few experimental tests and theoretical models for the complete composite systems, i.e. both composite beams and columns are employed in moment-resisting frames (Braconi et al., 2008) limit their application in seismic areas.

Composite columns can be developed with three main solutions: “fully encased,” with the steel profile completely embedded in the reinforced concrete, “partially encased,” with the RC positioned between the flanges of the steel profile, and “concrete filled,” with a steel box profile filled with concrete.

Considering the various applications of composite columns (Shanmugam et al., 2001; Hunaiti et al., 1994) and the difficulties of constructing these columns, the partially encased column appears to be a good compromise of fire resistance properties, limited local buckling behaviour (the web is totally braced and the flanges are partially braced), the efficiency of the concrete confinement and a reasonable construction procedure by pre-casting, i.e., the column arrives at the yard already filled with concrete and can be connected to the other elements using plates and bolts.

Studies of the structural behaviour of this type of composite column demonstrate the positive effect of concrete, especially in terms of hysteretic behaviour, because the cycles are stable and are not affected by the premature phenomena of local buckling that can sometimes be avoided by connecting the internal faces of the flanges with the steel bars welded to them. The combination of steel and concrete through this bond is much less efficient in partially encased columns (Ceroni et al., 2010) than in concrete-filled columns (Elnashai et al., 1994).

In the former paper (Ceroni et al., 2010) experimental results on 14 specimens for the characterization of the bond-stress law in the partially composite columns are carried out. The experimental results, obtained in different condition of load and roughness of the steel profile, highlight the low value of the shear strength, above all for the web part. A comparison with code prescriptions, European and Italian too, in any case highlight the unsafe of those ones. Furthermore, for cyclic loads the shear strength degradation is extremely rapid suggesting the inadequate behaviour of composite action in presence of seismic action and the need to introduce mechanical devices.

On this direction, the main feature of the results obtained in (Elnashai et al., 1991; Takanashi et al., 1992) is the significant improvement in the cyclic behavior of partially composite columns due to the presence of the additional bars that act not only to inhibit local buckling but also to increase the collaboration among the steel and concrete and the effect of the confinement. Fig. 5.1 shows the test set-up used in the experimental program.

In fact, the ductility of the tested members was increased by a minimum of 50%. and up to 80%. The pseudo-dynamic results demonstrate clearly the substantial increase in energy absorption capacity (fig. 5.2) of the composite columns named IC, modified as experimental program of Imperial College, in

comparison with the EM, the cross-sections designed following the European code.

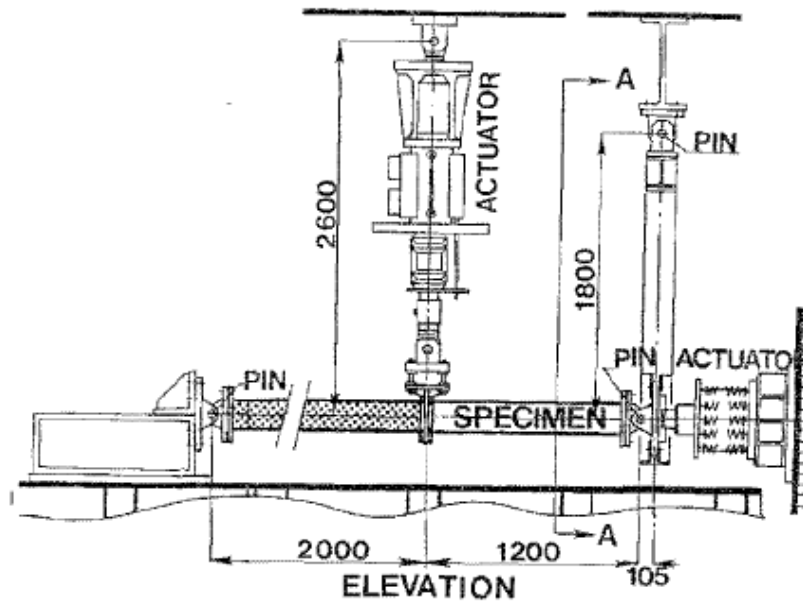


Figure 5.1: Test set-up in (Elnashai et al., 1991; Takanashi et al., 1992).

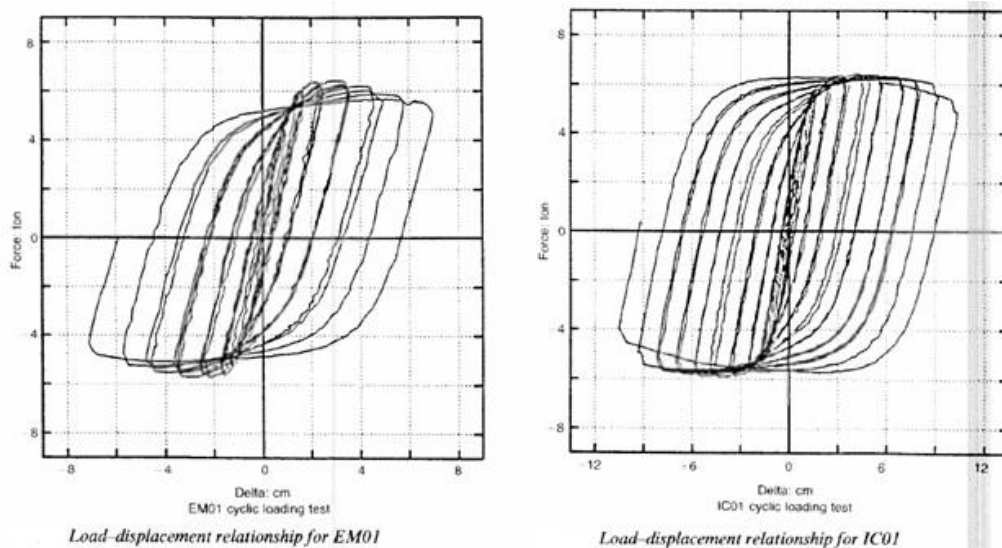


Figure 5.2: Comparison of load-displacement curves for EM and IC composite columns.

Moreover, the development of concrete cracking along the member shows a higher spread in the case of the IC section, hence absorbing more energy through crack initiation and propagation. Also, through spreading the cracked area, the potential plastic hinge zone is increased. The combined effect of increased curvature and plastic hinge length cause a substantial increase in the deflection ductility of composite members constructed with the local buckling inhibitors. Finally, the inhibition of local buckling, within the range of displacements well beyond of the acceptable drift limitations, leads to a relaxation of b/t (ratio between the flange half width and thickness) constraints, thus resulting in more economical design and efficient use of the sections. On the other hand in (Elnashai et al., 1994 and Broderick et al., 1994), through an experimental study (fig. 5.3), the same conclusion and observation are drawn for partially encased composite columns with inhibitor links and closed stirrups welded to the web (fig 5.4). Then, an analytical model (fig. 5.5) was implemented and calibrated on the experimental results that gave good results in agreement with the experimental ones. It was confirmed the fundamental role of inhibitors links that provide an optimal response also for high axial forces.

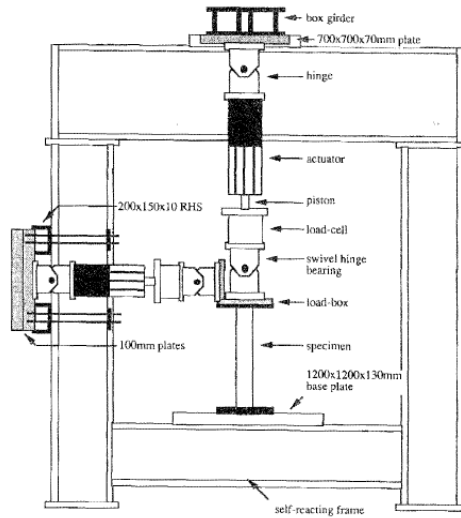


Figure 5.3: Test set-up in (Elnashai et al., 1994; Broderick et al., 1994).

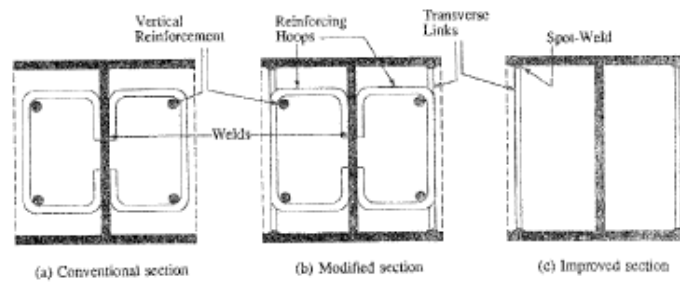


Figure 5.4: Composite columns cross-sections tested in (Elnashai et al., 1994).

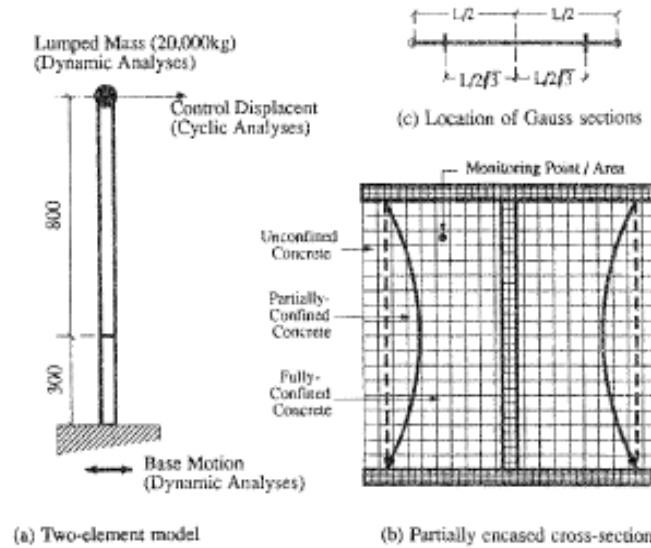


Figure 5.5: Model of the composite columns sections tested (in Broderick et al., 1994).

Another interesting experimental program (fig. 5.6) is reported in (Ballio et al., 1987). In this work the results about cyclic tests on steel column and composite ones (fig. 5.7) is provided and it was shown how the cyclic behaviour of composite column sections is increased and more stable if compared with that of simple steel columns. This improvement is due to the presence of concrete that shift beyond the local buckling phenomena and also increase the energy dissipation.

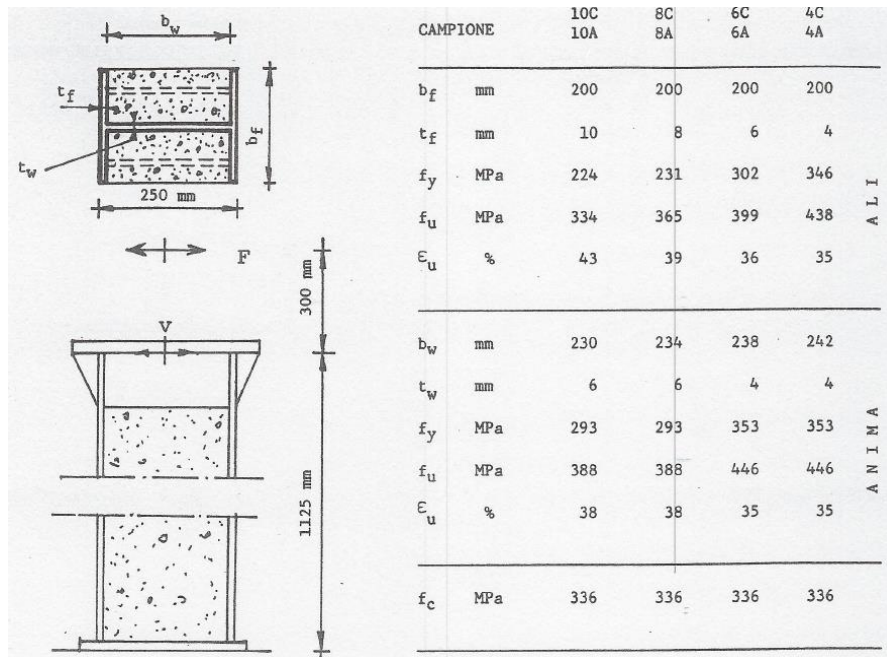


Figure 5.6: Test program in (Ballio et al., 1987).

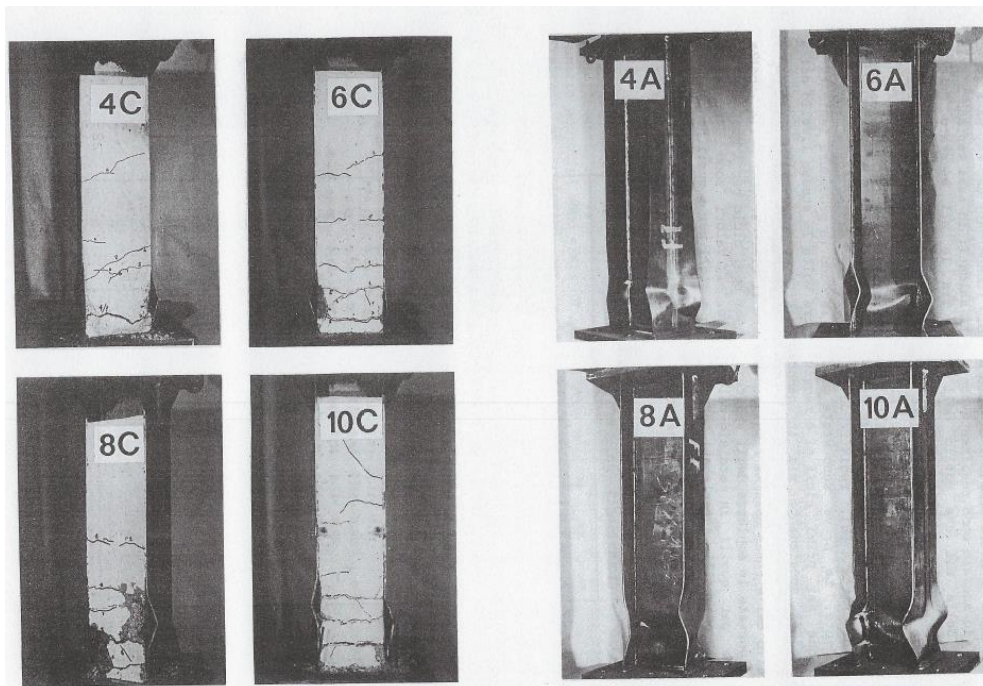


Figure 5.7: Composite and steel columns tested in (Ballio et al., 1987).

From the experimental test cited in (Elnashai et al., 1993; Elghazouli et al., 1993) an advanced non-linear model developed for the analysis of composite steel/concrete frame structures subjected to cyclic and pseudo-dynamic horizontal loads is provided. The formulation consists of beam-column cubic finite elements accounting for geometric non-linearities and material inelasticity. The non-linear cyclic concrete model considers confinement effects and the constitutive relationship for steel includes the effect of local buckling and variable amplitude cyclic degradation. The model is calibrated and compared with experimental data from cyclic and pseudo-dynamic tests conducted by the writers. The accuracy and efficiency of the developed model are demonstrated through the correlation between the experimental results and analytical simulations. The model is used to conduct parametric investigations (fig. 5.8) on the ductility of partially-encased composite beam-columns and to better understand the quantitative assessments of plastic moment capacity, rotation and displacement ductility and plastic hinge length normalized to element height, when the kinematic strain hardening factor m , that is the slope of the linear hardening branch, varies from zero to 1% of the elastic modulus. Similar results and conclusion are drawn also in (Chen et al., 2010) where the results of experimental tests on six column (cantilever scheme) subjected to axial compression and cyclic horizontal loads are reported (fig. 5.9); partially encased composite columns with thin-walled H-shaped steel plates were tested. In fact, the experimental study reveals that ductile failure mode and comparatively favourable energy dissipation ability can be expected if the width-thickness ratio does not exceed the limitation by Eurocode 4, and the axial compression load does not surpass the encased concrete capacity. It is clear that the H steel and transverse links have an important role in the resistance and ductility of composite columns. A simple numerical model is

proposed and the comparison of the numerical analysis and test results shows the validity of the model. Also a parametrical study (fig. 5.10) was performed by using the model. The research shows that the axial compression ratio (the ratio between the applied axial force and the section axial strength) on the composite column should be lower the encased steel capacity when thin plates are used for partially encased sections, and the step of the links is a key factor for preventing local buckling of steel with great width-thickness ratio.

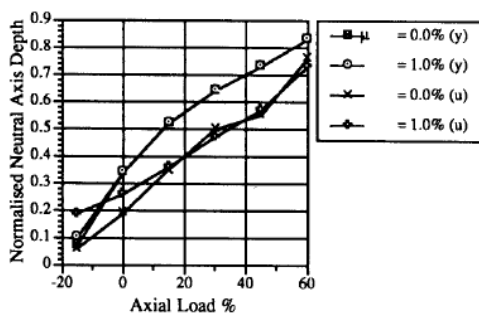


Figure 7. Normalized neutral axis depth at yield and at ultimate versus axial load for 0 and 1 per cent strain-hardening

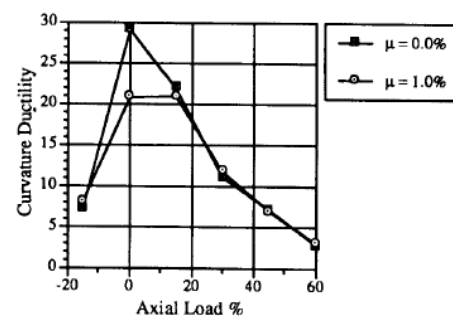


Figure 8. Curvature ductility versus axial load for 0 and 1 per cent strain-hardening

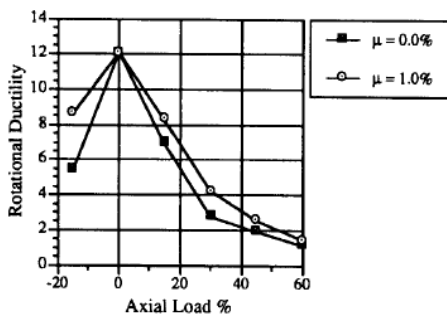


Figure 9. Rotational ductility versus axial load for 0 and 1 per cent strain-hardening

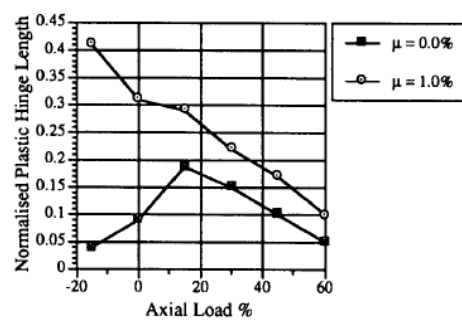


Figure 10. Normalized plastic hinge length versus axial load for 0 and 1 per cent strain-hardening

Figure 5.8: Parametric analysis on the ductility of composite columns.

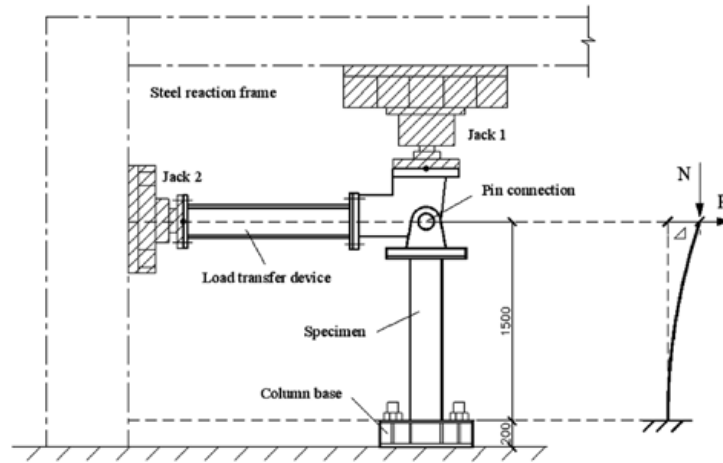


Figure 5.9: Test set-up in (Chen et al., 2010).

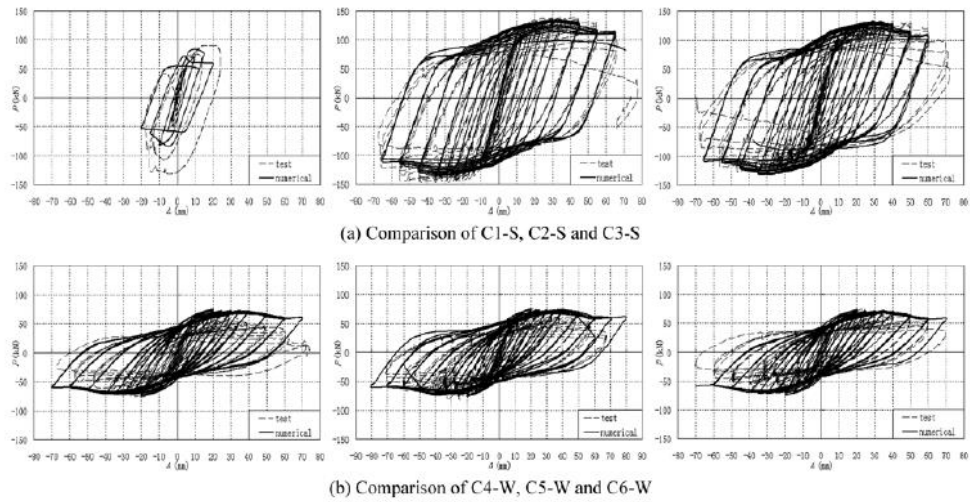


Figure 9. Simulation of hysteretic behavior of PEC columns.

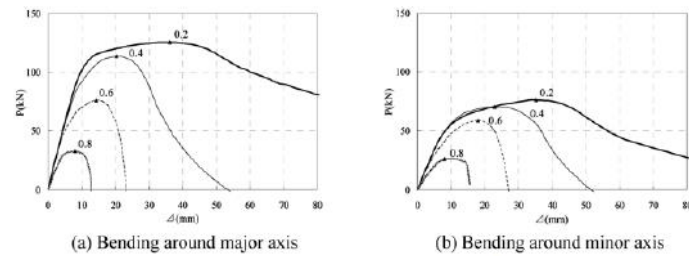


Figure 10. Comparison of effects of axial loads.

Figure 5.10: Parametric analysis on the ductility of composite columns in (Chen et al., 2010).

Thus, the ductility (Plumier et al., 1995) of the partially encased column suggests that it is an appropriate solution when framed steel structures are built in zones with high seismicity. Fig. 5.11 shows the test set-up used while fig. 5.12 reports the envelop of the hysteresis behaviour of a steel column section compared with that of a composite one for whom the buckling phenomenon was overcome.

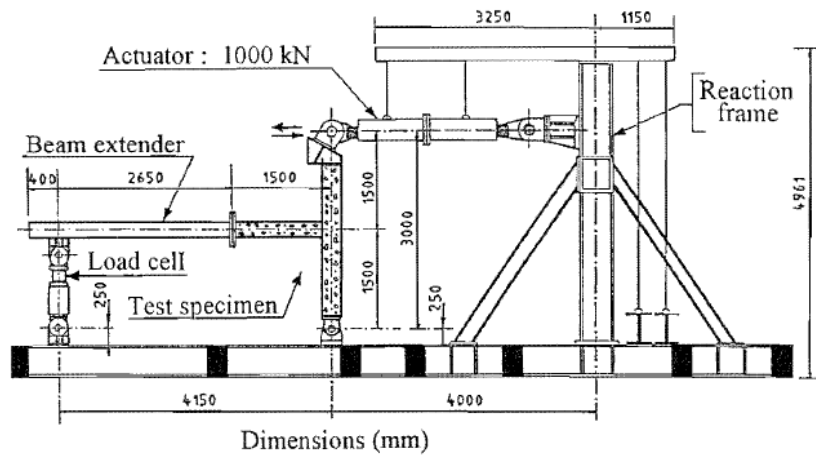


Figure 5.11: Test set-up in (Plumier et al., 1995).

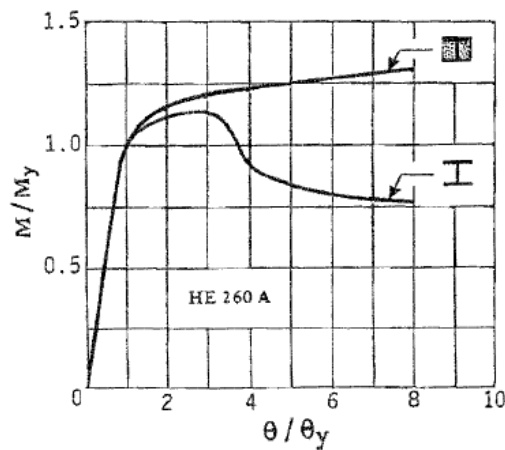


Figure 5.12: Envelope of hysteresis curves for steel and composite beams (Plumier et al., 1995).

In fact, for composite constructions, as for other structural typologies, the possible use of moment-resisting frames in areas of high seismicity depends on the available local ductility necessary to attain the global mechanisms.

However, the yielding of beams and their ductility in critical zones are necessary to avoid the structure collapse, but the global mechanism is accomplished through the yielding of the column base, where the strength and ductility depend on the base-to-foundation joint. The ductility capacity of the column base-to-foundation connection is affected by the composite column typology and its connection; in fact, the deformability of the base connection in the plastic field is composed of two contributions: the plasticisation of the critical zone of the column at the base and the fixed end rotation due to the deformability of the connection system between the column and the foundation block. As previously mentioned, the experimental results and numerical models available for composite columns do not consider the effect of the base connection; the results demonstrate that the composite solution performs well, but the plastic rotation capacity and the non-linear analysis are often derived from the field of steel structures (Eurocode 3, 2005). On the contrary in this thesis the behaviour of the base connection of composite columns is examined by the detailed analysis of an embedded solution as alternative to the traditional plate and bolts system.

A number of researchers (Akiyama et al., 1984; Nakashima et al., 1984 and 1986; Nakashima, 1992 and 1996; Kock et al., 1993) have focused their studies on determining the role of the base column joint for various types of set-ups (Grauvilardell et al., 2005) and models (Ermopoulos et al., 1996; Stamatopoulos et al., 1997; Wald et al., 2008). In (Nakashima, 1986) an

experimental study on the behaviour of traditional column base embedded in a concrete footing (fig 5.13) is reported.

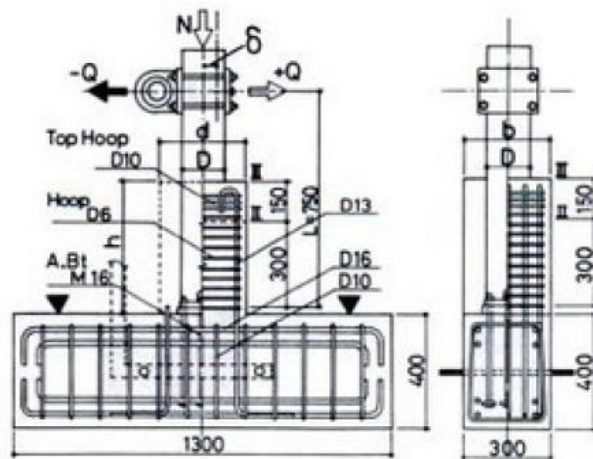


Figure 5.13: Specimen setup in (Nakashima, 1986).

The study highlights the good cyclic response of this system and the author concluded that the rigidity is influenced by the height of the embedded part and the section of the steel profile, while the strength is influenced also by the arrangement of the reinforcement in the encasement.

The same author (Nakashima, 1996) carried out the experimental study on the shallowly embedded base column connection (fig. 5.14 and 5.15) concluding that:

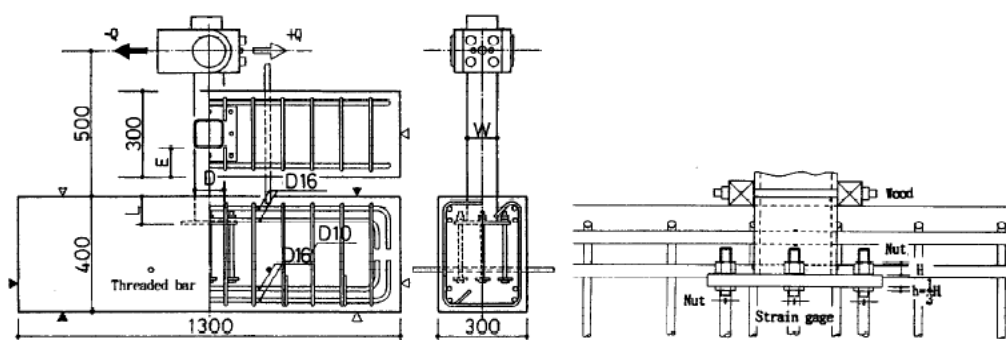


Figure 5.14: Specimen setup and installation of the steel column base in (Nakashima, 1996).

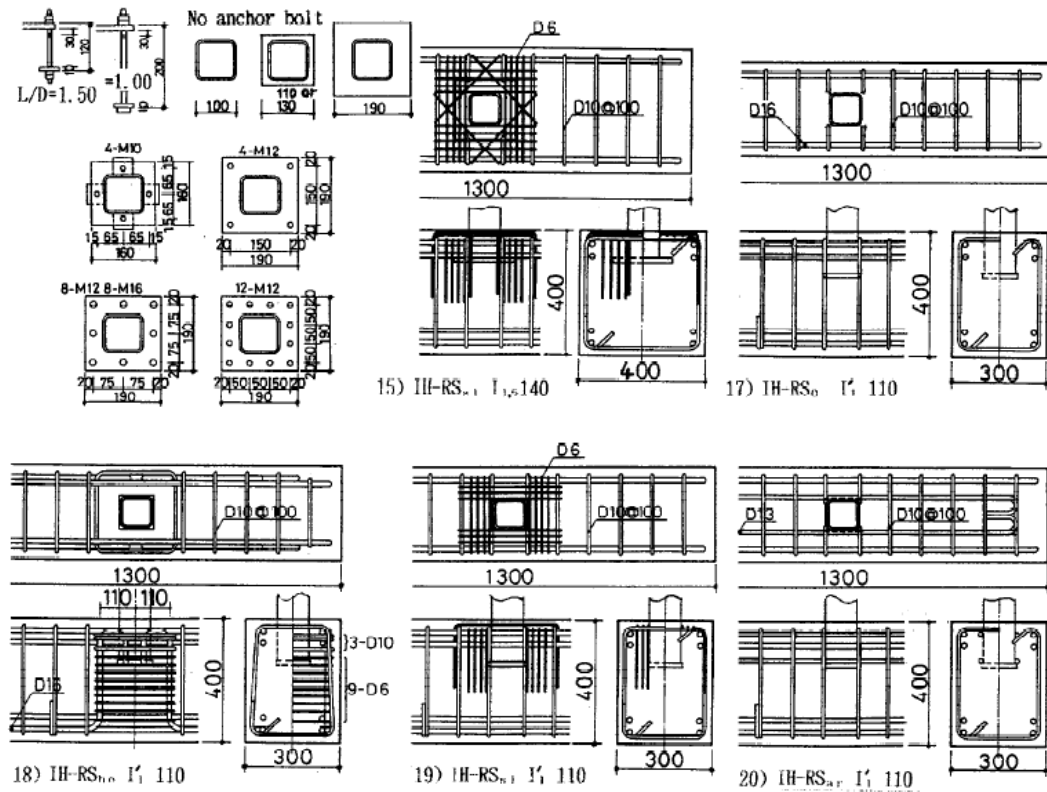


Fig. 2 Details of anchor bolts, baseplates and reinforcements for steel column bases

Figure 5.15: Details of anchor bolts, baseplates and reinforcements for steel column bases (Nakashima, 1996).

- By embedding exposed steel column bases in footing beams to a depth about equal to the depth of the tubular columns, it is possible to convert the hysteretic behavior of the column bases from a slip type to one similar to a spindle type characterized by high energy dissipation;
- the baseplate and the anchor bolts play an important role in enhancing the strength and the ductility of the column bases;
- the embedded solution reduces the sectional area and the number and thickness of baseplates if compared to the exposed solution.

The work reported in (Grauvilardell et al., 2005) is a summary of the main typologies of embedded base column connections and summarizes also the rules of the design of this system, presenting a classification of the various solutions (fig. 5.16).

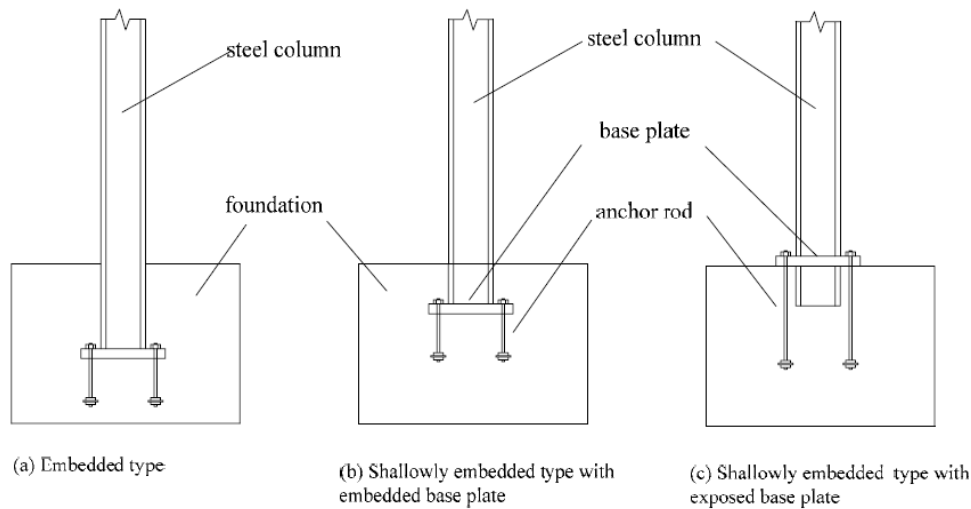


Figure 5.16: Embedded column bases configurations (Grauvilardell et al., 2005).

The various solutions are comprehensive of the exposed base plate type up to the deeply embedded type, in which the base plate has practically no role. The various solutions are for example: thick exposed base plates that act as a rigid link, transferring the external moments directly to the anchor rods that can be designed to act as a ductile component; flexible exposed base plate that dissipates significant energy in bending deformation, thus reducing the forces that load the anchor rods; shallowly embedded base plates that improve the strength and stiffness of the connection through the collaboration of the concrete filling the steel profile; deeply embedded base plates.

Additionally, further information is given in the classification in terms of degree of restraint, capacity of dissipating energy, failure mechanisms and type of structures in which the column base is used.

In (Roeder et al., 2008), the effect of varying the embedded length was analysed by observing the failure transfer from the concrete block (via the cone pull-out mode) to the steel profile of the outside part of the column. The research program was initiated to investigate a simple CFT column-to-foundation connection (fig. 5.17). Embedment depths of $0.6D$ to $0.9D$ were tested. Specimen with the short ($0.6D$) embedment depths had significant foundation damage with cone pull-out fractures (fig. 5.18). The shear reinforcement of the foundation was varied in these shallow embedded tests, but the specimen without any shear reinforcement and lighter flexural reinforcement had similar failure modes and deformation capacity, only with a slightly smaller resistance, than the specimen with significant amounts of shear reinforcement. Specimens with more significant embedment depth between $0.75D$ and $0.9D$ developed the full composite resistance of the CFT member and attained large inelastic deformations prior to attain the connection failure (fig. 5.19). Local buckling of the thin wall tubes was typically visible at drift levels of 3% to 4%.

The test results indicate that the proposed annular-ring embedded connection is effective and practical. Specimens with the longer embedment depth are capable of achieving drift capacities far in excess of the maximum seismic design drifts without degradation of the system and minimal damage of the footing.

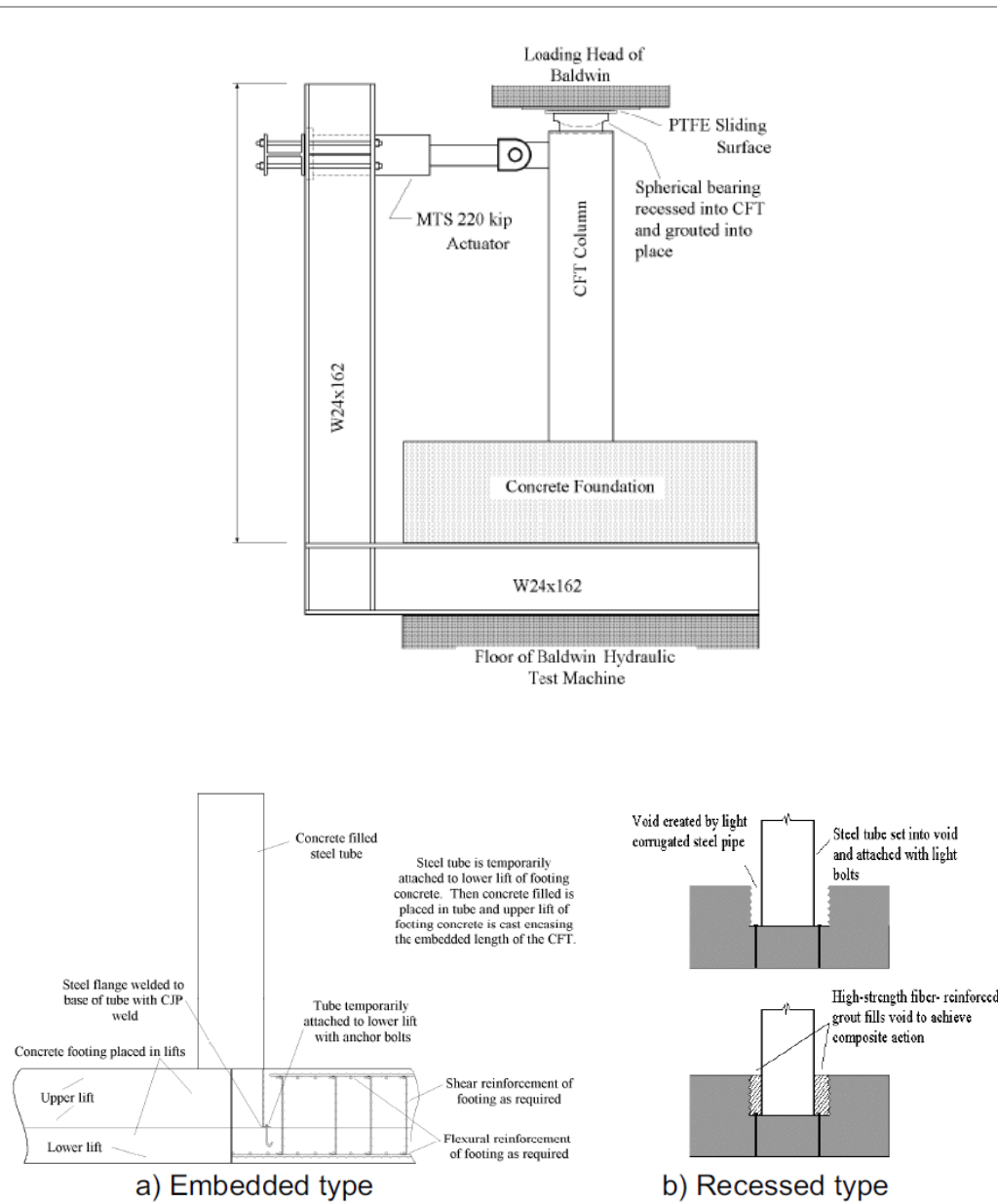


Fig. 5.17: Base connection tested and test set-up by (Roeder et al., 2008).

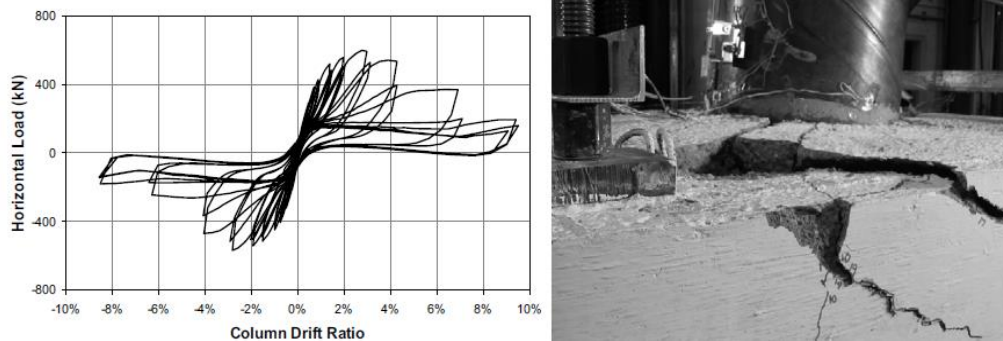


Fig. 5.18: Test of (Roeder et al., 2008) : a) hysteresis cycle; b) Cone pull-out failure mode.

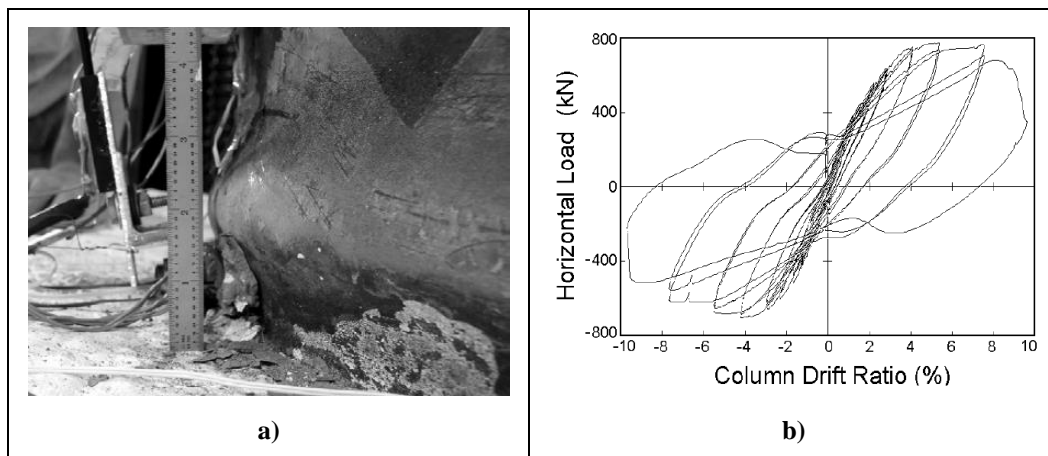


Fig. 5.19: Test of (Roeder et al., 2008). a) hysteresis cycle; b) Cone pull-out failure mode.

Similar types of embedded connections, with an end anchorage system and bonding and punching problems between the steel profile and concrete, were studied in (Pertold et al., 2000b), limiting the bonded height to less than $2h$, being h the height of the steel section. In particular, the experimental programme proved that a high level of axial load can be transferred by the bond between a steel column and its concrete base under static, medium-to-long time loading when there is low bending moment. The bond strength resulted about four times the bond between the concrete and its steel reinforcement. As the result, both punching and bond strengths contribute to the vertical load transfer. For most typical geometries of embedded column

bases, the bond resistance is higher than the resistance of the column base against punching. The bond resistance reduces of 50% if the moment is greater than the 50% of the plastic moment.

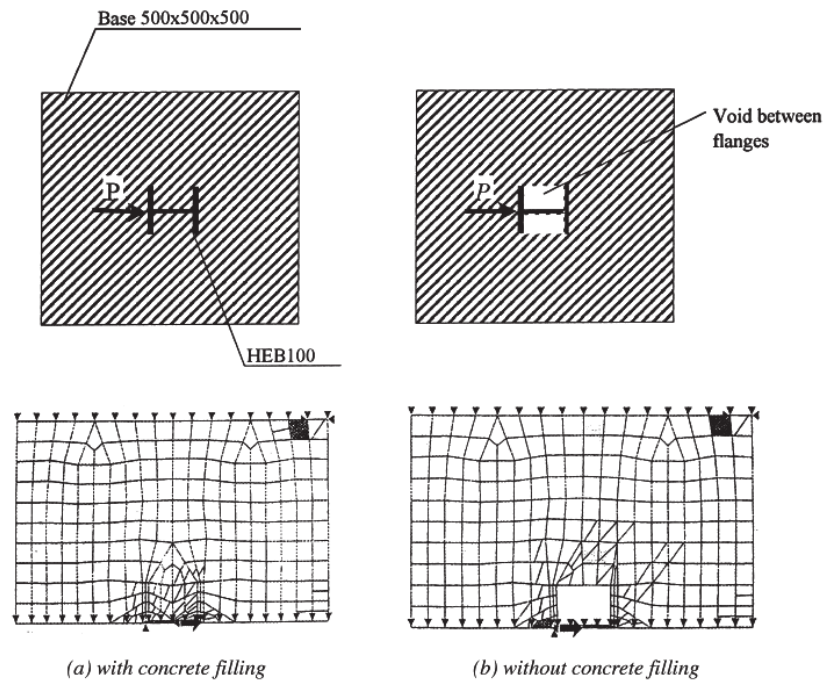


Fig. 14. FEM models of the base.

Fig. 5.20: FEM models of the base connection proposed by (Pertold et al., 2000).

A design model for an embedded steel column base is proposed in a companion paper of the same authors. They propose a model that introduces the calculation of the moment, shear and vertical resistance by the use of plastic stress distribution analysis. The design model is based on the experimental results and numerical modelling described in a companion paper of the research work (Pertold et al., 2000a). The proposed model reduces the length of the embedded column that is necessary to transfer loading forces. Compared with existing experimental results it indicates that the design model is safe and accurate.

In (Ermopoulos et al., 1996) an analytical model in a closed form for the determination of the response of exposed type column-bases under cyclic loading is proposed. In order to verify the accuracy of the results obtained using the proposed procedure, a correlation was made with some existing experimental results that gave a good agreement. The proposed model could be easily introduced into equilibrium equations for the whole structure in order to take into account, as far as possible, the influence of the deformability of the column-base connections in the superstructure subjected to cyclic loads.

In a companion paper (Stamatopoulos et al., 1997) the ultimate behaviour of column base-plate connections is studied and the corresponding interaction moment-axial force (M-P) curves are presented (fig. 5.21), taking into account the main parameters of the problem. The main parameters considered are the size and thickness of the plate, the size, length and location of the anchor bolts, the quality of materials and the value of the axial load. Finally, the typical procedure that is necessary in order to analyse a structure taking into account the influence of the semi-rigid connection is summarized in a step by step form.

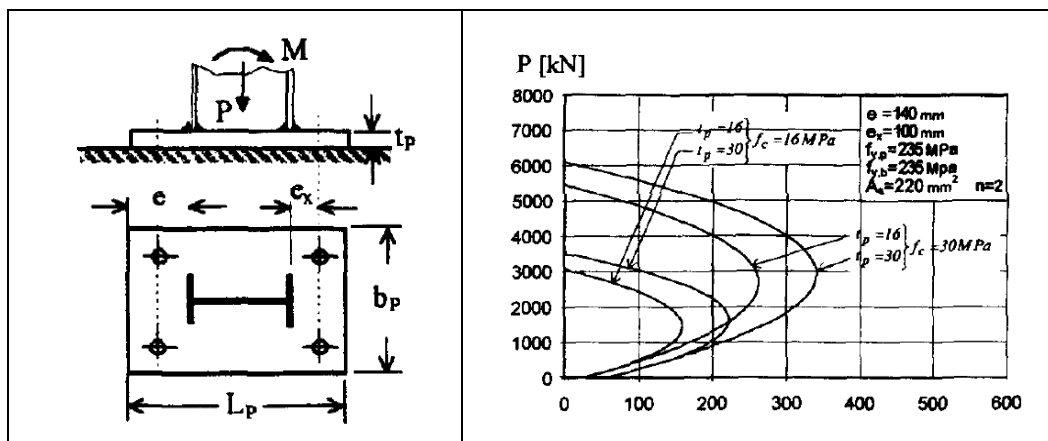


Figure 5.21: Exposed column base and its moment-axial force interaction curves (Stamatopoulos et al., 1997).

In (Wald et al., 2008) an application of the component method to steel column bases is presented. The decomposition of the connection into components is described (fig. 5.22). An analytical model is presented to determine the flexural resistance and the rotational stiffness of column bases under axial forces. The analytical model is verified by a comparison with test results. A sensitivity study of the base plate thickness and the anchor bolts length is presented.

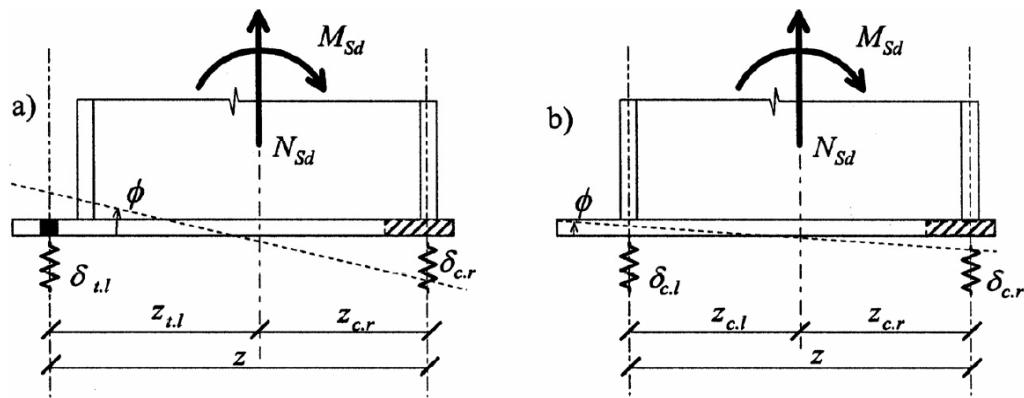


Figure 5.22: The mechanical model of the base plate (Wald et al., 2008).

For the steel column connections the solution of exposed plates with multiple anchors (fig. 5.23) have been explored (Cook et al., 1992; Stamopoulos et al., 2011) to improve the performance. In particular, in (Cook et al., 1992) a behavioral model for determining the distribution of loads to the individual anchors of a multiple-anchor connection is presented. The model is based on limit design theory. Experimental results are reported for 28 tests of multiple-anchor connections loaded monotonically by various combinations of moment and shear. Test specimens included rigid and flexible base plates connected to concrete with threaded cast-in-place or retrofit (undercut and adhesive) anchors.

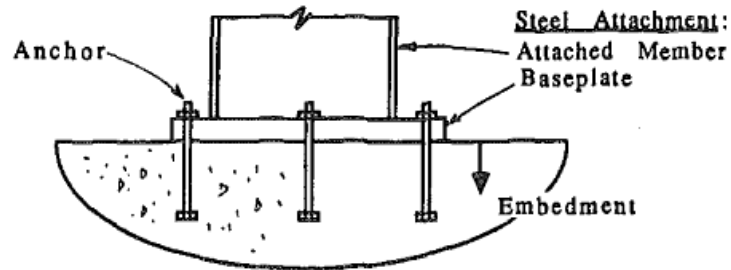


Figure 5.23: Example of multiple-anchor (Wald et al., 2008).

The (Stamatopoulos et al., 2011) reports the experimental and analytical investigation of the steel column bases; eight sets of tests, simulating the column to concrete foundation joint, were tested. Beside, three-dimensional FEM models (fig. 5.24) of the test specimens were constructed and analysed. Finally, the results of these experimental and FEM analyses were correlated with those obtained from an analytical formula proposed by the writers in a previous work, describing the relation among the bending moment and the rotation angle ($M-\varphi$) of the column base. The verification among the results seems to be satisfactory.

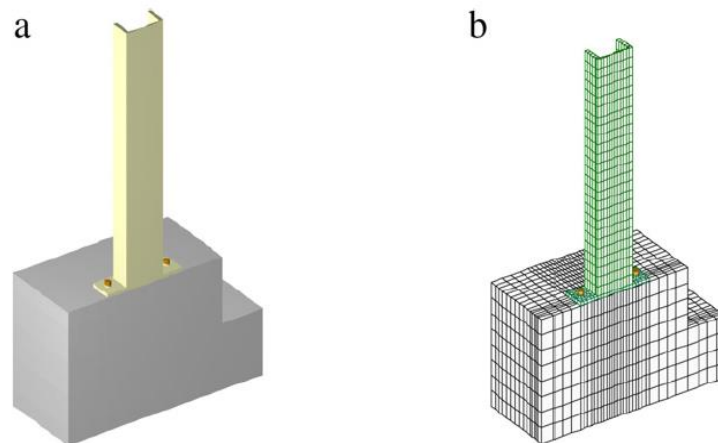


Fig. 5.24: Model of half of the experimental specimen (a) and mesh of the finite elements (b).

In the paper (Hitaka et al., 2003) the three main types of base connections used in Japan have been reviewed after the seismic events in 1978 (in Miyagi) and 1995 (in Kobe): the “base plate connection” with embedded bolts, the “encased base plate connection”, where the steel plate is covered with concrete, and the “embedded column connection”, where the steel plate is embedded in the foundation block.

The base connection described in (Marson et al., 2004) (fig. 5.25) uses steel elements, while in (Cui et al., 2011), the traditional bolted joint is covered with reinforced concrete to enhance the joint rigidity under horizontal actions.

In the former, in order to investigate their adequacy to dissipate energy during earthquakes, the paper reports on cyclic inelastic tests executed to determine the maximum strength and ductility of four concrete-filled circular steel piers joined to a foundation by a system finalized to develop the full composite strength at the base of these columns. Column diameters of 324 and 406 mm were considered, with D/t ratios (diameter/thickness of the steel tube) ranging from 34 to 64. The foundation detail had a good performance, ensuring the exploiting of the full moment resistance capacity of the concrete-filled steel column, the proposed foundation detail could be significantly optimized. The ductility of all the tested columns was good, since all columns were able to reach drifts of 7% before a significant loss of the moment capacity, due to the reduction of local buckling, suggesting that concrete-filled steel tubes can be effective as bridge piers in seismic regions of North America.

Further analyses of embedded joints are presented in (Hsu et al., 2003) using an embedded length of approximately 1.5 times the steel section height, h , of the steel profile with short bolts in the steel plate. This study is focused on the experimental investigation of the relationship between design details and column base performances (fig. 5.26), such as strength and rigidity. Results

from specimens tested under combined axial and lateral loads were used to define the effectiveness of the base connections. It was observed from test comparisons that the rigidities of base connections grows up when the embedded depths increases. It was also found that the base connections possess higher rigidity and dissipation capability when stiffeners are added to the base connections. Finally, an empirical expression for base rigidity estimation was proposed for design purposes.

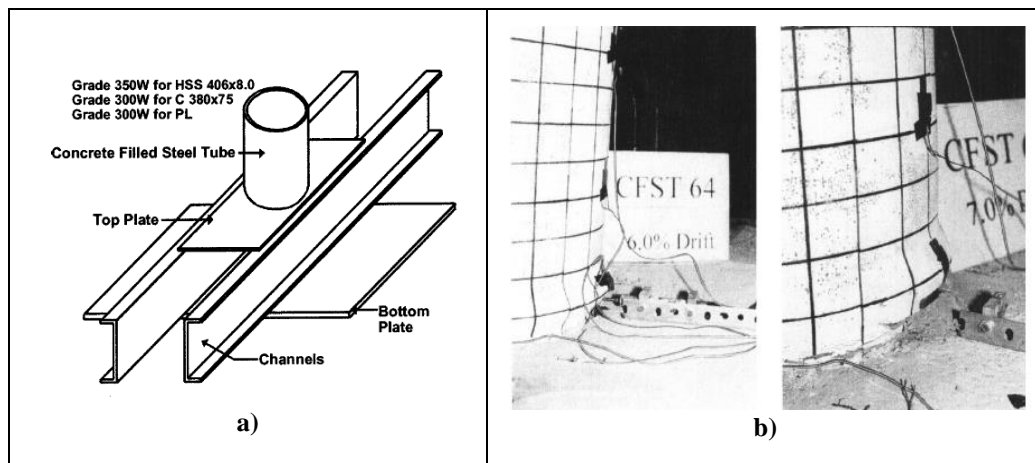


Fig. 5.25: a) Detail of the base connection; b) local buckling at 6 and 7% drift.

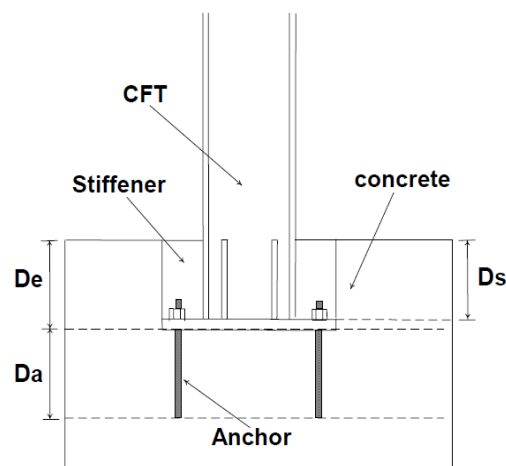


Fig. 5.26: Connection detail of the base connection (Hsu et al., 2003).

5.2. Experimental tests

5.2.1. Specimen description

The following paragraph gives a detailed analysis of the results of the experimental tests performed on base-column connections to properly assess the stiffness and ductility of the analysed systems. A general description of the tests is reported in (Di Sarno et al., 2007; Ceroni et al., 2010), but some fundamental information is summarised here.

Five partially encased columns are examined here using two types of steel with wide-flange profiles: column with a height, h , of 260 mm (referred to in Italy as HE260B) and those with a height of 280 mm (referred to in Italy as HE280B). The steel profiles used in this experimental investigation are the same as those used for another research program (Braconi et al., 2008); however, to improve the inelastic response of the composite columns, an alternative solution is proposed for the base connection. In fact, two types of base column connections are assessed: a steel extended end-plate (a traditional connection equivalent to the one used for the composite frame tested at the JRC Ispra laboratory) and a socket-type connection (innovative). The design procedure used for the traditional connection is in agreement with the provisions of Eurocode 3 (Eurocode 3, 2005) and 8 (Eurocode 8, 2008) for steel columns, furthermore the connection is the same realized for experimental tests on frames carried out at the research centre of ISPRA. About the embedded joint the connection, i.e. the steel reinforcement, the concrete thickness around the steel column, the grouting resistance and the foundation block were designed in agreement with the rules of Eurocode 2 (Eurocode 2, 2004) for the pocket foundations with smooth joint surface. In addition the overstrength suggested by Eurocode 8 for the connection of structures designed in medium class of ductility was adopted; the resistances (flexure, shear, axial

force) of the composite column amplified for a factor 1.2 were assumed as the actions on the foundation. Furthermore the embedded length of the column was realized longer than the minimum indicated for the RC columns that is 1.2 of the greater dimension of the column section, in order to assure the plasticization of the column before the collapse of the connection. Finally the concrete block dimensions were governed by the test set-up since the cantilever was connected to the laboratory floor slab by means of specific steel devices, which were adequately prestressed to prevent the slippage.

The sample specimens analysed are cantilevered with an axial load and a horizontal load at the top; for the HE260B column, the one-dimensional axial load (ratio between the applied load and the axial resistance) varies from 0.05 to 0.10, while for the HE280B column, the axial load is 0.13. In all cases, this axial load value is far from the codified limit for seismic design (Eurocode 3, 2005; Eurocode 4, 2004) of 0.3. The tests performed are summarised in Table 5.1.

Specimen	Axial Load (kN)	Loading Type	Connection
HE260B	330	Monotonic	Traditional
HE260B	170	Cyclic	Traditional
HE260B	330	Monotonic	Socket
HE260B	330	Cyclic	Socket
HE280B	520	Monotonic	Socket

Table 5.1: Tested specimens.

Property	HE260B		HE280B	
	Web	Flanges	We	Flange
f_y [MPa]	406	341	341	300
f_u [MPa]	480	449	450	430
f_u/f_y [-]	1.18	1.32	1.3	1.43
ε_u [%]	31.8	35.7	34.	37.1

Table 5.2: Mechanical properties of structural steel.

The nominal structural steel grade used in the specimens is S235 (nominal characteristic yielding strength $f_{yk}=235$ MPa); the actual mean values of the mechanical characteristics have been estimated by experimental tests and are reported in Table 5.2. The concrete strength in compressive experimental tests on cubes was 25.7 MPa for the concrete encased in the column and was 84.3 MPa for the concrete of the block foundation. Furthermore, the column was solidified into the foundation block using a no-shrink filling grout (type MAPEFILL) with 28% gravel (5-8 mm) and a nominal cubic strength of 70 MPa. The grade used for the reinforcement the steel bars is B450C (nominal characteristic yielding strength $f_{yk}=450$ MPa and $f_{uk}=540$ MPa for the ultimate strength).

The profiles used are both in class 1, in accordance with the European standards (Eurocode 3, 2005), to prevent the local buckling of flanges before the cross-section yields as the width-to-thickness ratios of the flange is $b/t_f=17.9\varepsilon$ for HE260B and $b/t_f=18.7\varepsilon$ for HE280B, both of which fulfil the limit of $b/t_f=44\varepsilon$, with $\varepsilon=\sqrt{235/f_y}=0.83$. Furthermore, the local buckling of the web profile is prevented by the constraining effect of the inner concrete. The column's cross-section is completed by a longitudinal reinforcement made of 8 steel bars with a diameter of 12 mm, which are linked by stirrups of 8 mm in diameter.

The traditional base connection consists of tapered steel plates welded to the base plates (40 mm) and anchored to the foundation block by bolted steel bars. The innovative base connection was designed in accordance with the provisions of Eurocode 2 (Eurocode 2, 2004) for pre-cast systems; the design provisions are according to a strut-and-tie model. The cross sections and the grouting system layout are reported in Figure 5.27. The thickness of the base of the socket is 300 mm; the in-plan dimensions of the base socket are 1200 mm x

1200 mm; and the total height of the foundation is 1050 mm. The composite column was embedded in the foundation socket to a depth of 750 mm.

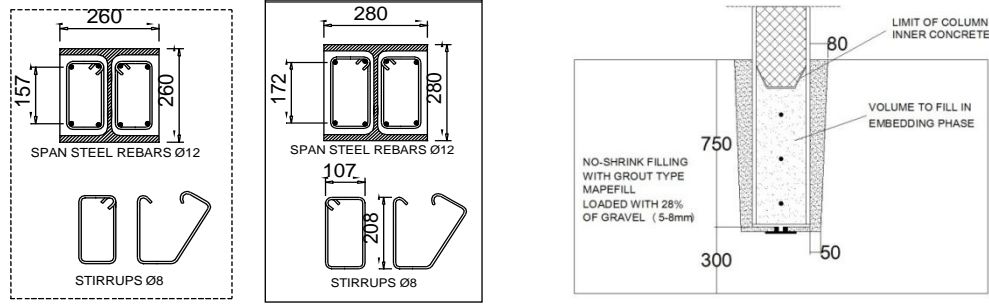


Fig. 5.27: The cross-sections and base connection of the columns.

The experimental tests were performed by applying a horizontal force under a predefined axial load ($N = 330$ kN for HE260B column and $N = 520$ kN for the HE280B column; only in one case with the traditional base joint did $N=170$ kN for HE260B) on the top of the composite columns. The horizontal force, F , which simulates seismic activity, was applied at a distance of 1700 mm above the top of the foundation for the innovative connection and at 1600 mm for the traditional connections using a hydraulic jack (maximum load: 500 kN).

The tests were conducted under displacement control. The concentration of the inelastic demand near the base was evaluated for the specimens; all specimens were equipped with displacement transducers at the top and near its base. In the two tests on the traditional connection, six LVDT displacement transducers were arranged to measure the vertical displacement and, therefore, the rotation of the base plate. Furthermore, four LVDTs were placed horizontally at the base of the column at various distances from the foundation block, as shown in Figure 5.28.

The specimens with the innovative connection were instrumented with LVDTs placed horizontally at the base of the column: four instruments were used for

monotonic tests (Figure 5.29) and six instruments were used for the cyclic test (Figure 5.30). Additionally, a series of strain gauges were glued at different distances from the top face of the block foundation on the steel flanges for the monotonic tests; Figures 5.31a and 5.31b show the positions of the strain gauges for the monotonic tests on the HE260B and HE280B specimens, respectively.

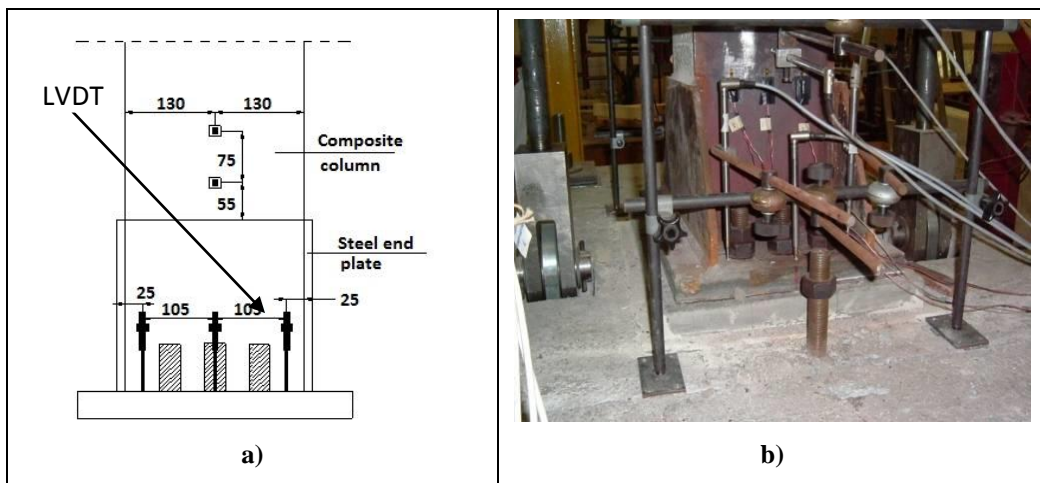


Fig. 5.28: The LVDT's position for the traditional connection: a) layout and distances in mm; b) close-up view.

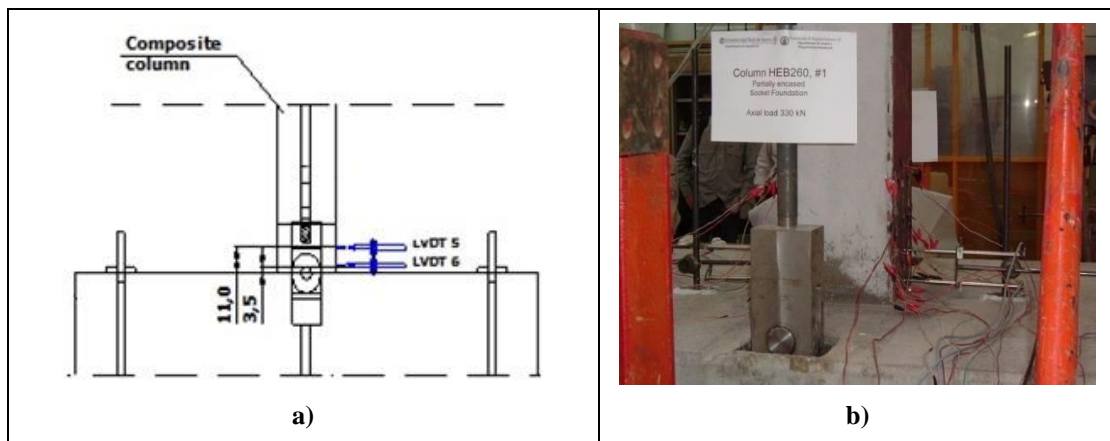


Fig. 5.29: The LVDT's position for the innovative connection in monotonic test. a) layout and distances in cm; b) close-up view.

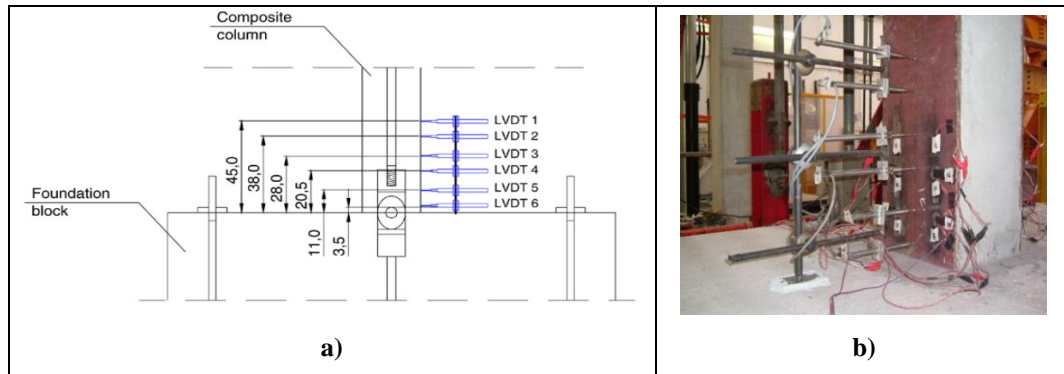


Fig. 5.30: The LVDT's position for the innovative connection in cyclic test: a) layout and distances in cm; b) close-up view.

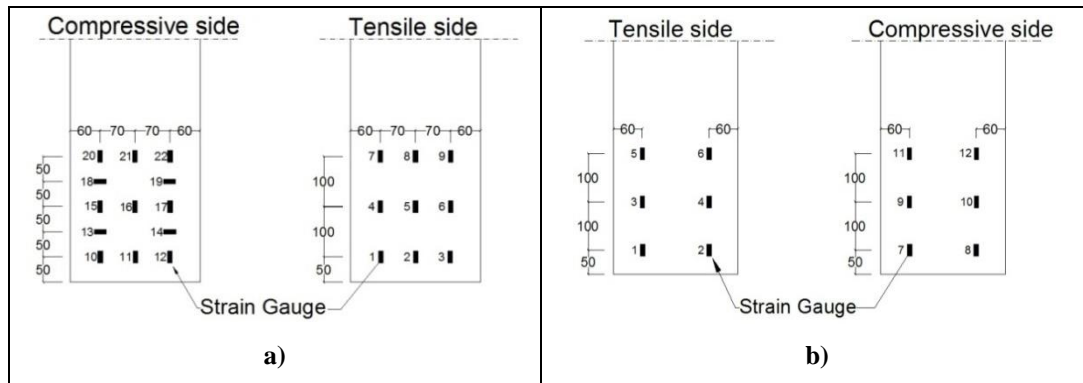


Fig. 5.31: The arrangement of strain gauges (distances in mm): a) for the specimen HE260B; b) for the specimen HE280B.

5.2.2. Test results and specimens performance

The global behaviour of the specimens is represented in terms of the horizontal load vs. drift, evaluated as the top displacement divided by the height of the column, d/H ; the curves are shown in Figure 5.32a for the five columns tested. The tests on the columns with the socket-type connection were stopped at approximately 150 mm (HE260B type) and 200 mm (HE280B type), when the buckling phenomena of the flange began to appear at the base; conversely, for the specimens with the traditional base connection, a descending region was obtained for the curves due to the slip and then failure of the steel bolts

embedded in the foundation block.

The LVDTs at the column base allowed the evaluation of the fixed end rotations (Fig. 5.32b). Fig. 5.32c shows the drift due to the columns' deformation, obtained as the difference between the global response and the response due to the fixed end rotation; Fig. 5.32d compares the global drift to the drift due to the fixed end.

For the traditional connection, the transducers attached vertically to the end plate were evaluated by dividing the difference of the measurements between the instruments at the two sides of the column by their distance. For the socket connection, the transducers placed horizontally near the base recorded the displacements at different heights close to the foundation's top face (Figs. 5.29a and 5.30a); the rotations, φ , near the base column were calculated from these measurements according to the following expression:

$$\varphi_j = \frac{v_i - v_{i+1}}{x_i - x_{i+1}} \quad (5.1)$$

where v_i and v_{i+1} are the displacements measured by two consecutive transducers and x_i and x_{i+1} are the distances of the transducers from the upper face of the foundation block; thus, the rotation can be attributed to the position $x_j = (x_i + x_{i+1})/2$ from the upper face of the foundation socket type. The fixed end rotation, ϑ^{fix} , is evaluated using the measurements of the two transducers nearest the upper face of the foundation block, i.e., the displacements at 35 mm and 110 mm from the base; the variation of the fixed end rotation at the increment of the load is depicted in Fig. 5.32b for all specimens. Finally, the rotation, ϑ^{column} , due to the column's deformation is evaluated as the difference between the drift, d/H , and the fixed end rotation; the trend for this parameter is reported in Fig. 5.32c.

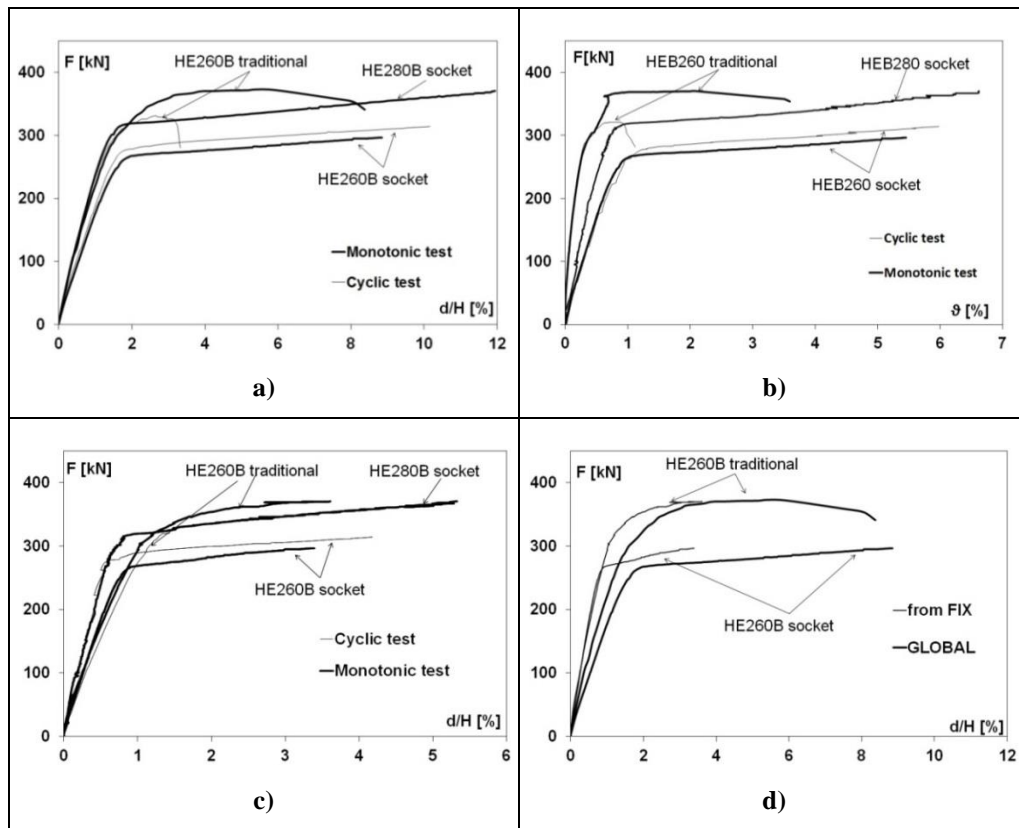


Fig. 5.32: a) Force – drift curves; b) rotation due to the fixed end rotation [%]; c) drift due to the column; d) comparison of the drift due to the fixed end rotation (labelled FIX) and that due to the global rotation of HE260B, either for the traditional or the socket type connection.

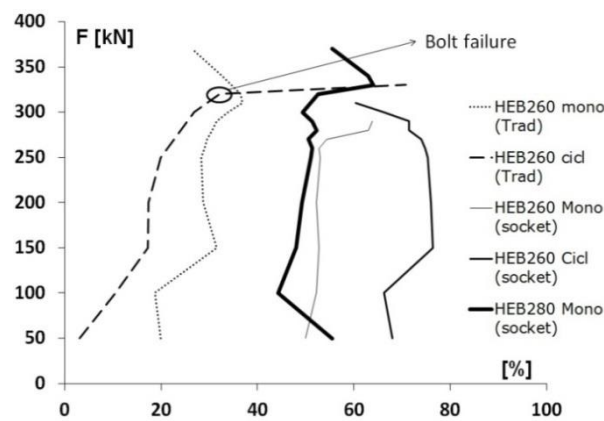


Fig. 5.33: Force vs. top displacement percentage due to the fixed end rotation.

Figure 5.33 shows the percentage of the top displacement due to the fixed end rotation to better describe the effect of the base connection's deformability on the global deformability of the element.

The experimental results produced the following conclusions:

- the fixed end rotation of the traditional connection is due to the bonding law of the bolts (Di Sarno et al., 2007); the different behaviour in the last part of the curve of the two specimens is due to the premature failure of the bolts during the cyclic test;
- the rotational capacity at the base is greater for the socket connection than the traditional connection;
- the base rotational capacities in the plastic field for monotonic and cyclic tests appear approximately equal when the socket type connection is used; conversely, for the traditional connection, the premature failure of the bolts in the cyclic test does not allow plastic rotation to develop;
- the value of the drift for the socket-type connection is considerable, and its behaviour appears stable without degradation until local buckling occurs;
- notably (Fig. 5.33), the base column's rotation contributes up to approximately 50-60% of the total displacement capacity of the columns with the socket-type connection compared to the traditional connection, which contributes only approximately 20-25%; in the case of the traditional base joint under cyclic loading, the high percentage at the ultimate load is due to the bolts' failure.

Fig. 5.34a shows the strains recorded on the profile flanges for the monotonic tests of HE260B and HE280B at 50, 150 and 250 mm from the top face of the foundation for both the side in compression and the side in tension. At the same horizontal load, the strains under compression are greater than those

under tension due to the effect of the axial load; furthermore, the strains at 250 mm overcome the yielding value under compression, but not under tension, suggesting that the yielding penetration is extended along this length and is approximately equal to the height of the section (260 mm); the same results are obtained for the specimen HE280B (Fig. 5.34b).

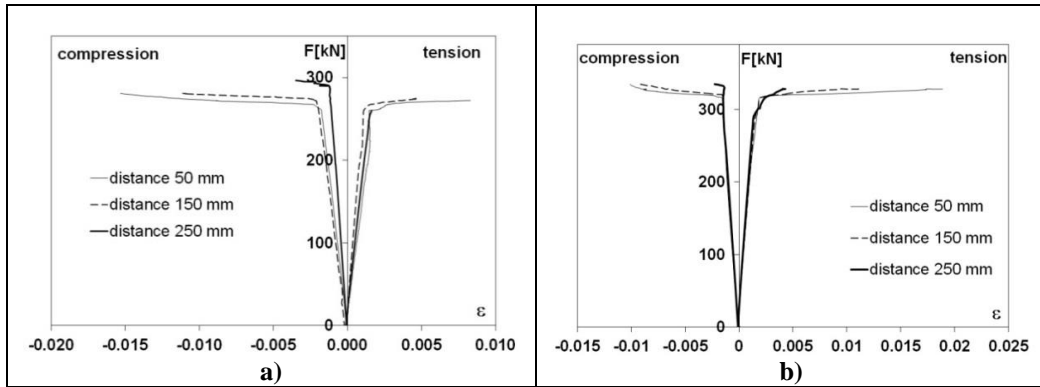


Fig. 5.34: The experimental strain-load curves under tension and compression for samples a) HE260B and b) HE280B.

5.3. The analyses by the 3D finite element model

5.3.1. The 3D numerical model

A three-dimensional finite element model of the tested system has been developed via the Finite Element Package *DIANA TNO (release 9.4.3 -2009)* to detect in detail the local and global behaviour of the base connection. The finite elements used for the discretisation are *brick*-type solids with 20 nodes (CHX60) and 6 rectangular surfaces, both for the column section inner concrete and the foundation block concrete, including the grouting. This element is based on quadratic interpolation and Gauss integration. Typically, a rectangular brick element approximates the following strain and stress distribution over the element volume. The strain ε_{xx} and stress σ_{xx} vary linearly

in x direction and quadratically in y and z direction. The strain ε_{yy} and stress σ_{yy} vary linearly in y direction and quadratically in x and z direction. The strain ε_{zz} and stress σ_{zz} vary linearly in z direction and quadratically in x and y direction. By default Diana applies a $3 \times 3 \times 3$ integration scheme.

For the steel element, a quadrilateral curved shell-type element with 8 nodes (CQ40S) was employed.

This element is based on quadratic interpolation and Gauss integration over the element area. The integration in the thickness may be Gauss or Simpson. Typically, for a rectangular element, the following strain and stress distribution along the element area. The strain ε_{xx} , the curvature κ_{xx} , the moment m_{xx} , the membrane force n_{xx} and the shear force q_{xz} vary linearly in x direction and quadratically in y direction. The strain ε_{yy} , the curvature κ_{yy} , the moment m_{yy} , the membrane force n_{yy} and the shear force q_{yz} vary linearly in y direction and quadratically in x direction.

The elements used for the discretisation of the steel profile and the adjacent concrete have been rigidly connected at the nodes, neglecting any possible interface slip.

The symmetry of the structure with respect to the plane identified by the symmetry axis of the cross-section and the vertical axis is considered to reduce the calculation time; only half of the specimen is modelled, introducing a symmetry constraint along the middle plane of the system (displacements perpendicular to the symmetry plane are hindered) and halving the horizontal force. The effect of the axial force applied at the top of the composite column is simulated by applying a uniform distribution of normal stresses. Stiffening elements are introduced in the model at the section where the horizontal force is applied, as in the actual specimen, to avoid local buckling phenomena. The socket base elements are aggregated at the base to reproduce the connection of

the foundation block underlying the stiff floor slab of the laboratory. The steel reinforcing bars are neglected; therefore, only the steel profile and the concrete are modelled.

5.3.2. Material models

Non-linear constitutive relationships for concrete and structural steel are assumed in the model under the hypothesis of isotropic and homogeneous behaviour.

Specifically, an elastic-plastic constitutive law, characterized with properties reported in Table 5.3, with a hardening branch is considered for steel, as illustrated in Fig. 9.1a, both in tension and in compression, which is described through the following relationships:

$$\varepsilon_{y,s} = \frac{f_{y,s}}{E_s}; \quad \varepsilon_s = \varepsilon_{y,s} + \frac{f_s - f_{y,s}}{f_{t,s} - f_{y,s}} (\varepsilon_{t,s} - \varepsilon_{y,s}). \quad (5.2)$$

ID	$f_{y,s}$ [MPa]	E_s [MPa]	$\varepsilon_{y,s}$ [%]	$f_{t,s}$ [MPa]	$\varepsilon_{t,s}$ [%]
HE260B (web)	460	210000	0.22	480	31.8
HE260B (flange)	341	210000	0.16	449	35.7
HE280B (web)	341	210000	0.16	450	34.5
HE280B (flange)	300	210000	0.14	430	37.1

Table 5.3: Properties used in the relationship (5.2).

The non-linear relationship trends reported in Figs. 5.35b and 5.35c for the concrete of the column and the foundation block and for the grout are introduced in the model and characterized with properties reported in the Table 5.4. Under compression (Fig. 5.35b), a tri-linear relationship is assumed, which is characterised in the first section by a stress value up to 0.4 of the compressive strength, f_c , with a mean elastic modulus E_1 . This modulus is evaluated according to the standard code formulas of Eurocode 2. In the second section, which is characterised by a lower modulus, E_2 , the peak value of the

strength is reached at a strain of 0.0024 for the foundation block, concrete and grout, and a strain of 0.002 is reached for the column concrete, after which a plastic region (Fig. 5.35b) is assumed; this plastic region can be significant due to the high confinement level of the concrete around the profile in the zone embedded in the base socket type connection and the confinement effect of the steel profile on the encased concrete.

The constitutive law of concrete under tension (Fig. 5.35c), either for the foundation or the column, is characterised by a linear ascending branch with the same elastic modulus E_I as that used under compression. Conversely, a linear softening branch after the peak strength, f_{ct} , is assumed; the ultimate strain is defined as a function of the fracture energy G_{fI} (Mode-I), as estimated by data available in the literature (Model Code, 1990).

For the grout under tension (Fig. 5.35d), a brittle law is used that better fits the real behaviour of this material.

Because three-dimensional finite elements are employed, a *total strain* model with *rotating cracking* (Selby and Vecchio, 1993) is considered; the introduced constitutive relationships are applied along the three principal directions and follow the evolution of the cracking phenomenon (rotating cracking).

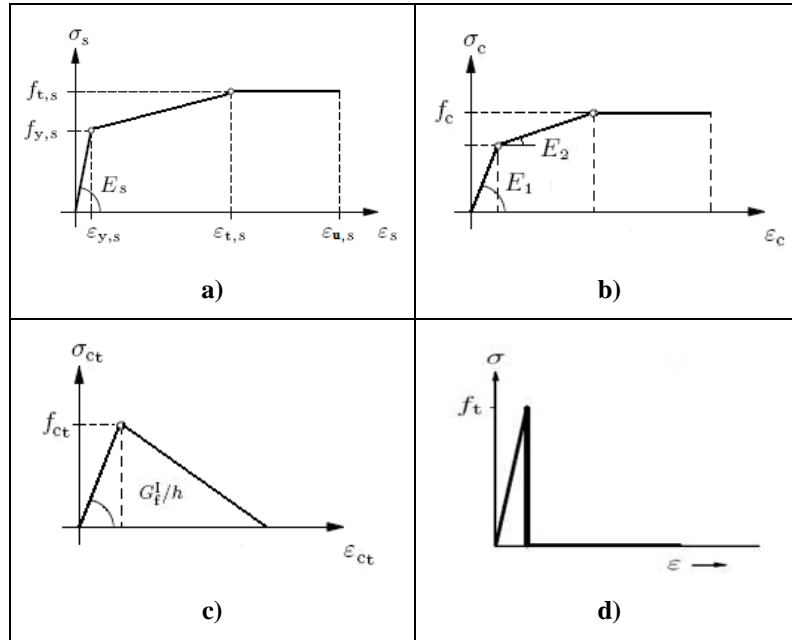


Fig. 5.35: Constitutive laws: a) steel; b) concrete and grout under compression; c) concrete under tension; d) grout under tension.

Parameter		Column concrete		Foundation concrete		Foundation grout
		HE260B	HE280B	HE260B	HE280B	HE260B/280
E_l	[MPa]	30372	30372	40743	40743	27000
f_c	[MPa]	21.3	21.3	70.0	70.0	70
f_{ct}	[MPa]	2.3	2.3	5.1	5.1	5.1
G_{fl}	[N/mm]	0.07	0.07	0.10	0.10	-

Table 5.4: The mechanical properties of materials employed in the non-linear analyses.

5.3.3. Discussion

Figs. 5.36a and 5.36b plot the comparisons between the experimental and numerical load-displacement curves for both tested columns. Globally, the numerical model estimates the experimental results well, even if the theoretical deformability in the elastic field is lower than that in the experimental field.

Numerical simulations are performed up to the maximum displacement reached during the tests; at these conditions, the maximum strains attained for the materials by the FE model are approximately equal to 0.06 in both the HE260B column and the HE280B column and are similar for the steel and concrete due to the perfect bond hypothesis

assumed for the two materials. Albeit this is a numerical result based on the rigid connection of the two materials, also the experimental behaviour of the specimen confirmed that concrete reached high strains in compression since limited damage was observed at ultimate conditions with high curvatures due to the effectiveness of the confinement effect of the steel profile on the filling concrete.

In Figs. 5.37a and 5.37b, the strain distribution is plotted along the columns for both the part above the foundation block and inside the block; a dashed line indicates the beginning of the embedded part of the column. The strain distribution shows that the yielding zone of the column, i.e., the part of column in which strains exceed the yielding limit (0.0016 for flanges), extends to approximately 450-600 mm, depending on the type of column, along the height external to the foundation block (approximately 1.5 times the height of the steel section h), while a smaller part of approximately 0.5 times the steel height is involved in the part of column inside the block.

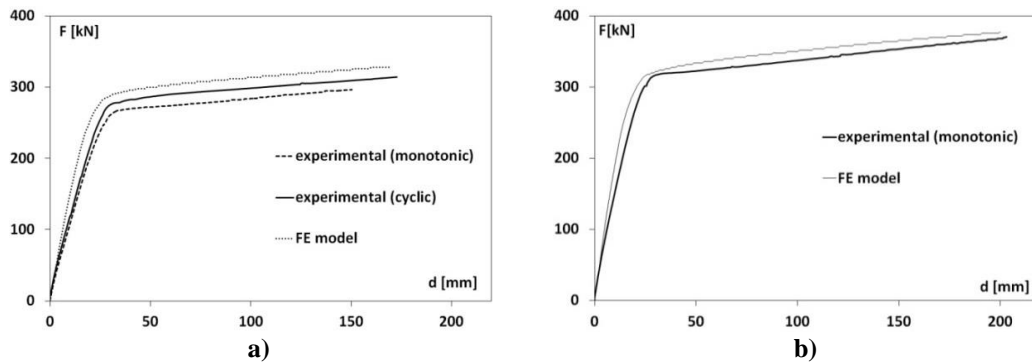


Fig. 5.36: Comparison between the experimental and FE models. a) HE260B; b) HE280B.

Fig. 5.38 plots the comparison between the moment-curvatures determined by the strain gauges attached to the two steel flanges at three different distances from the top face of the foundation block (50 mm, 150 mm and 250 mm) as well as from the numerical analysis, while Figs. 5.39 and 5.40 show the experimental force-displacement curves due to fixed end rotation (FIX) and the steel profile deformation compared with those provided by the FE model.

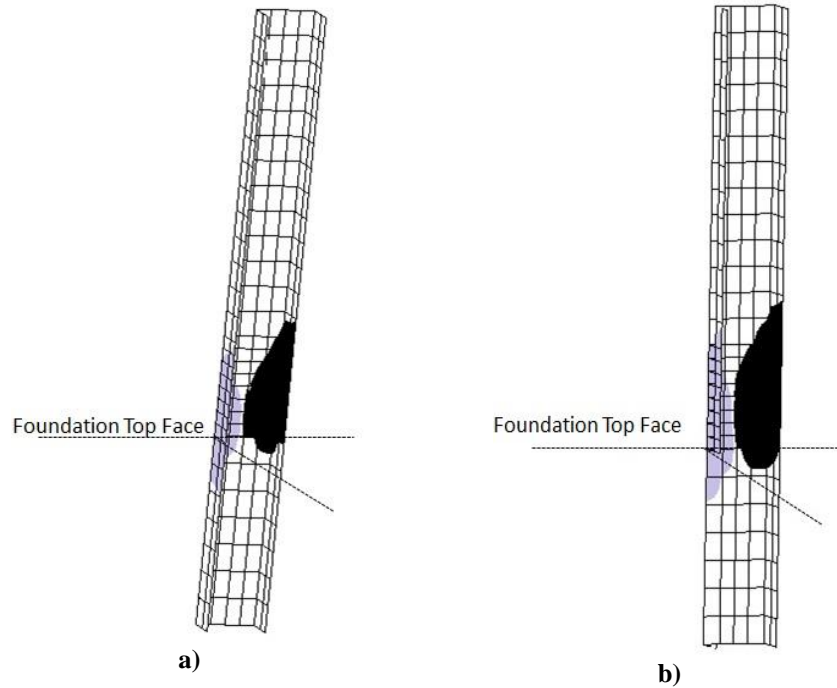


Fig. 5.37: The location of strains higher than the yielding point; black indicates compression; grey indicates tension. a) HE260B; b) HE280B.

The comparisons in Fig. 5.40 indicate that the experimental and numerical results agree well when the effect of column deformability is considered alone, while Fig. 5.39 shows that the fixed-end rotation provided in the FE model is less than the experimental rotation, possibly due to the uncertainties in the modelling of the material used for the solidification, the neglecting of the slip between the concrete block and the column, and the role of the concrete relationship under tension.

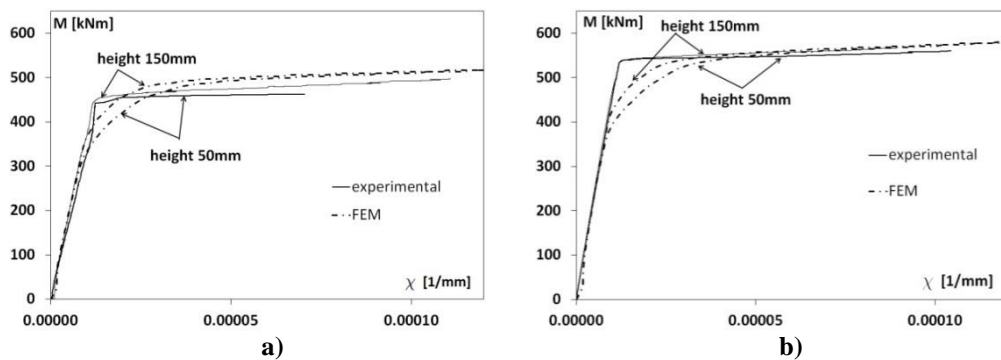


Fig. 5.38: Comparison between the experimental and numerical moment-curvature: a) HE260B; b) HE280B.

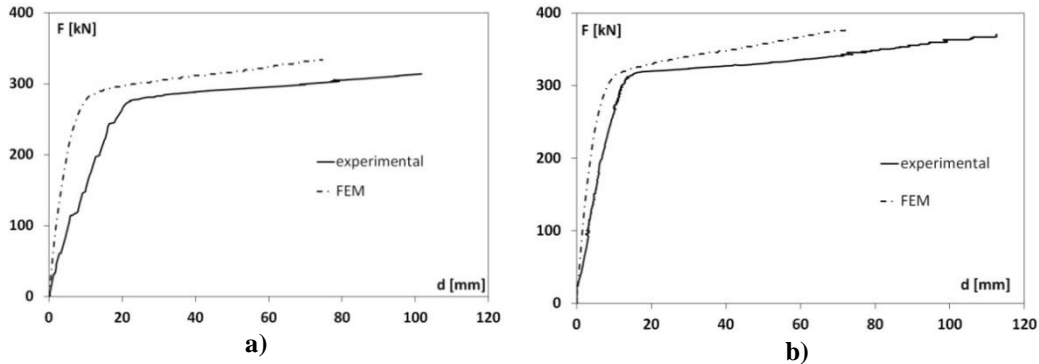


Fig. 5.39: Comparison of the force-displacement curves due to the fixed end rotation, obtained from the experimental results and the numerical results (FEM): a) HE260B; b) HE280B.

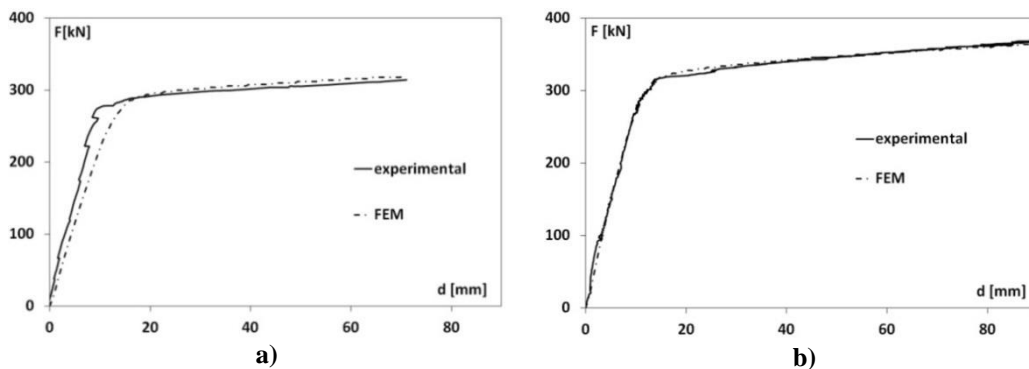


Fig. 5.40: Comparison of force-displacement curves due to the deformation of the steel profile (column) obtained from the experimental results and the numerical results (FEM): a) HE260B; b) HE280B.

5.3.4. Parametric analysis

5.3.4.1. Effect of the embedded height

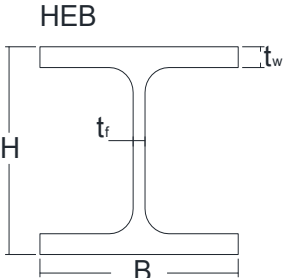
The most important parameter for a reliable design of the socket type joint is the embedded height of the column in the concrete foundation because it defines the type of failure in terms of its strength and ductility. To better understand the influence of this geometrical parameter on the connection, the 3D FE model of the column was implemented for columns with various steel

profiles (wide flange with heights of 100, 160, 260, or 280 mm (Table 5.5)), and their behaviour were analysed by varying the embedded height H_p .

The materials used in the analysis are the same as those used for the numerical and experimental comparison performed for the column HE280B and reported in the previous paragraph.

The analyses were stopped when the strain in the concrete of the column reached 0.06 under compression, which is the same value recorded in the comparison between the FE model and the experimental results, or when the strain reached a load equal to 85% of the maximum strain when a descending section occurs.

Fig. 5.41 shows the load-displacement curves for the HE280B column by varying the embedded height, H_p ; the value of H_p varies between 1000 mm (4 times the profile height h) and 300 mm, (about the profile height).

	Table 5.5: Principal geometric features of the steel profiles.				
	ID	B [mm]	h [mm]	t_f [mm]	t_w [mm]
	HE100B	100	100	10	6
	HE160B	160	160	13	8
	HE260B	260	260	17.5	10
	HE280B	280	280	18	10.5

The elemental behaviour produces the same results for H_p values greater than approximately 2 times the profile height, but when the embedded height is smaller than $2h$, both the strength and ductility are reduced, until the column yielding point is reached.

The global behaviour depends on the variation of the failure mode at the base connection. Fig. 5.42 shows the distribution of the longitudinal strains in the steel column for the various embedded heights used in the analysis (the right

side is under compression); as the embedded height increases, the steel yielding extends both along the column height (inside and outside the foundation) and along the steel section height. Fig. 5.43 shows that the local strain in the grout surrounding the column (i.e., the material damage) increases when the embedded height decreases because the failure mechanism moves from the bottom to the top of the concrete block, as shown for three cases in Fig. 5.44. This behaviour leads to the failure of the concrete at the top surface of the foundation block, which is not confined by other concrete, before the steel yielding can extend along the column. When the embedded height is at least 2 times the height of the column section, the foundation failure is avoided, allowing the extension of the steel yielding without considerable further increases in the load.

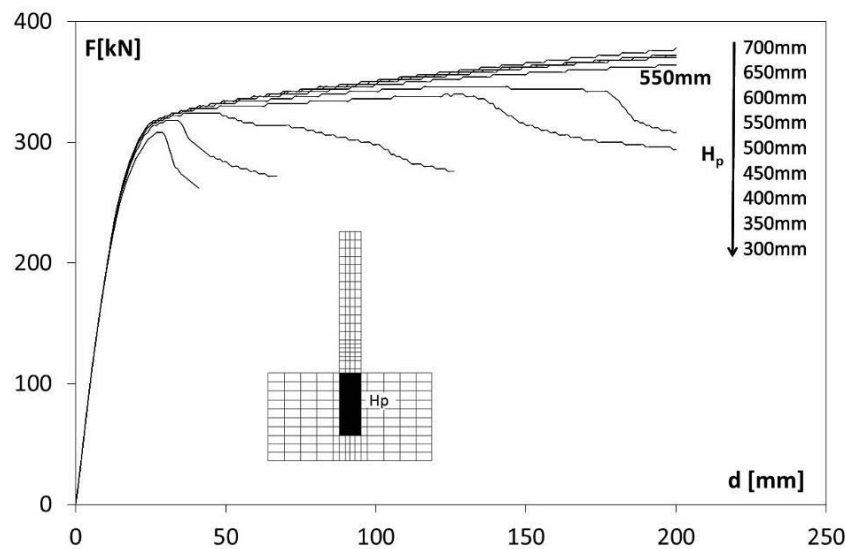


Fig. 5.41: The load-displacement curves with various embedded heights, H_p .

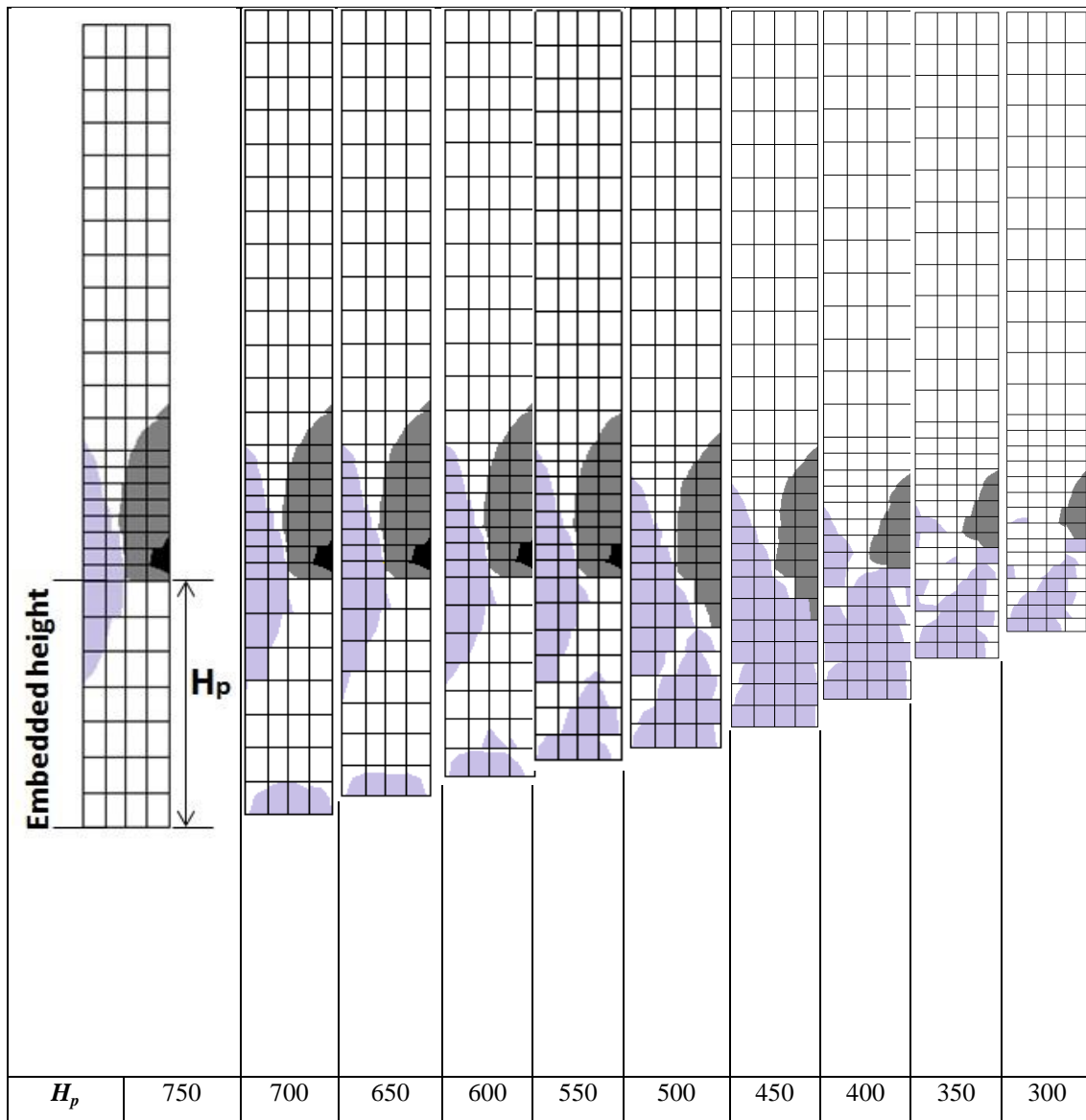


Fig. 5.42: The parts of column HE280B where the yielding strain of steel ε_y (in light grey) is overcome for various H_p (mm) (where H_p is the amount of embedded part) at the ultimate load.

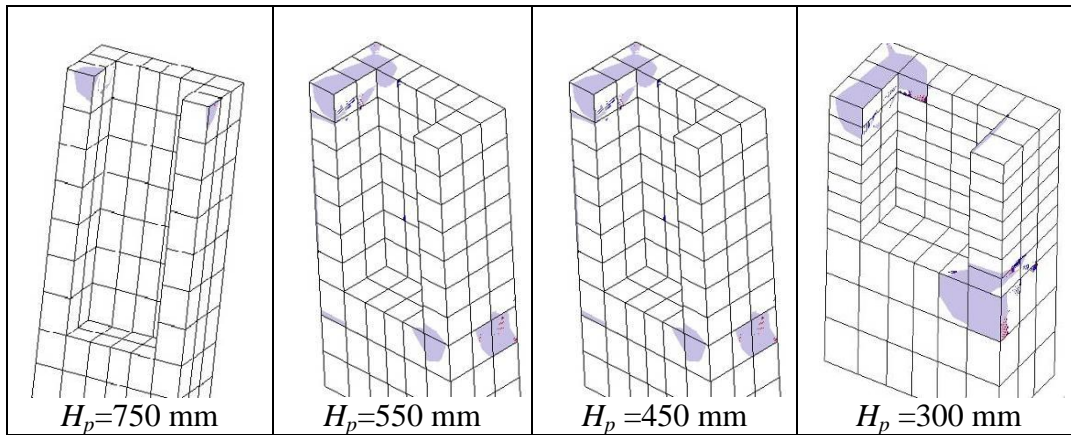


Fig. 5.43: The strains in the grout areas under compression that overcome the peak strain of concrete 0.002 at the ultimate load for the HE280B composite column.

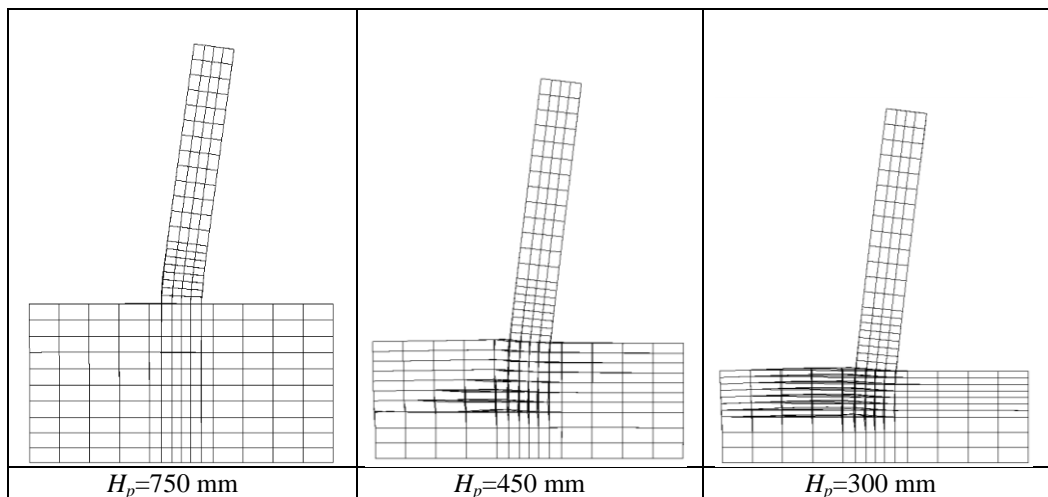


Fig. 5.44: The global deformation of the HE280B composite column at its ultimate load for three different embedded heights.

The same parametric analysis was developed for the other profiles listed in Table 5.5 to confirm the embedded height that allows the exploitation of the entire strength and ductility of the column to avoid a premature failure of the connection at the base. In Figs. 5.45, 5.46 and 5.47, the load-displacement curves are graphed by varying H_p between one and three times the section height. The results confirm the observations for the other sections, where the failure mode transitions from the column plasticisation to the mechanism of

“cone pull-out” in the block foundation, which is accompanied by a loss of ductility and resistance. However, when the column section is reduced, the embedded height necessary to avoid the “cone pull out” decreases (at approximately the section height for the wide flange profile, which is 100 mm in height) because the bearing capacity of the column, i.e., the failure load, decreases and thus decreases the stresses in the concrete block.

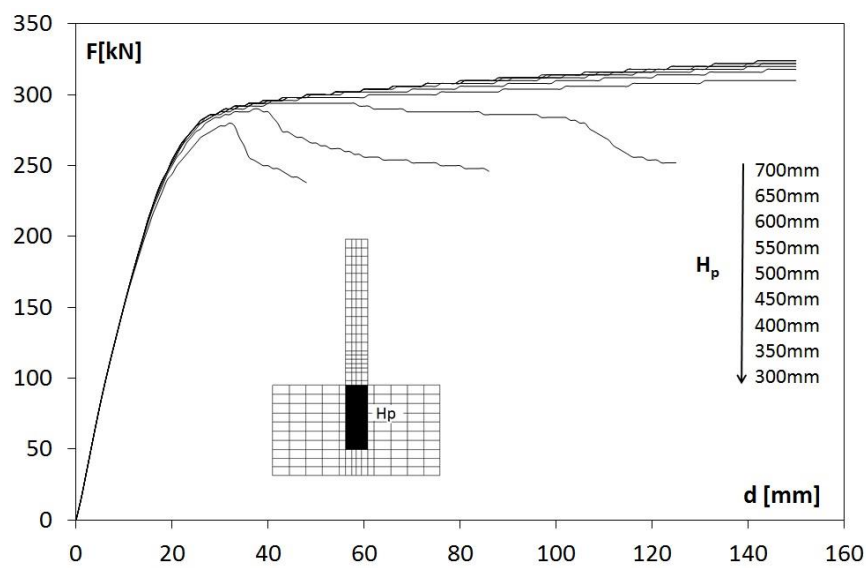


Fig. 5.45: The load-displacement curves obtained by varying the embedded height H_p for the HEB 260 column.

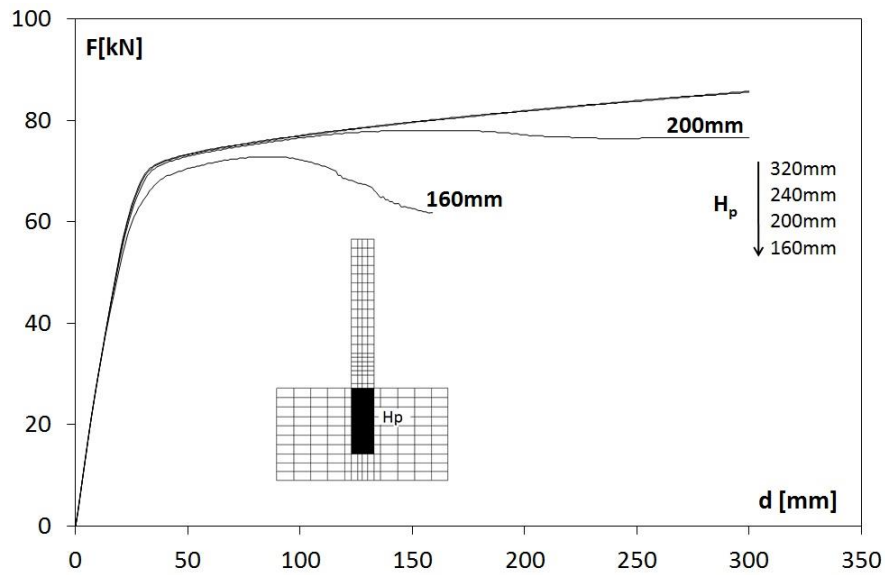


Fig. 5.46: The load-displacement curves obtained by varying the embedded height H_p for the HE160B column.

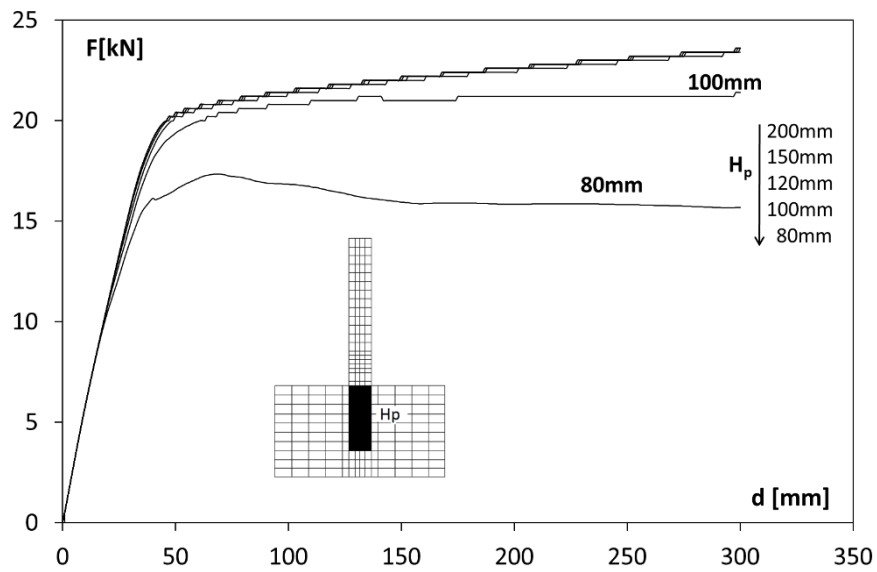


Fig. 5.47: The load-displacement curves obtained by varying the embedded height H_p for the HE100B column.

5.3.4.2 Evaluation of the elastic rigidity of the base connection

Another parametric analysis can be developed using the 3D FE model for defining the rotational rigidity of the base connection as a function of the mechanical and geometrical characteristics in the elastic field, while the post-elastic performance is approached by the simplified procedure described in the previous paragraph.

To evaluate this base joint rigidity in the elastic field, when the embedded height is sufficient to avoid the cone pull-out failure, the behaviour of the connection resembles a Winkler elastic beam, i.e., the steel profile is the beam loaded by a shear, V , and moment, M , at the base of the column, and the concrete of the foundation block is the elastic soil (Fig. 5.48).

The theoretical solution of the Winkler beam (Fig. 5.48), using the hypothesis of an infinite length of the beam, in terms of the rotation, θ , at the loaded end and assuming $F=1$ and $M=1$, can be written as follows:

$$\theta_{x=0} = \frac{2 \cdot \alpha^2}{k_s B} + \frac{4\alpha^3 \cdot H}{k_s B} \quad (5.3)$$

where B is the width of the beam, H is the height of the column, k_s is the constant of the elastic soil, and α is the reverse of the characteristic length of

the beam (or wave length) whose value is computed as: $\alpha = \sqrt[4]{\frac{k_s B}{4EI}}$

Thus, the rotational rigidity of the connection can be evaluated using the following expression:

$$K_\theta = \frac{1}{\theta_{x=0}} = \frac{k_s \cdot B}{2 \cdot \alpha^2 + 4 \cdot \alpha^3 \cdot H} \quad (5.4)$$

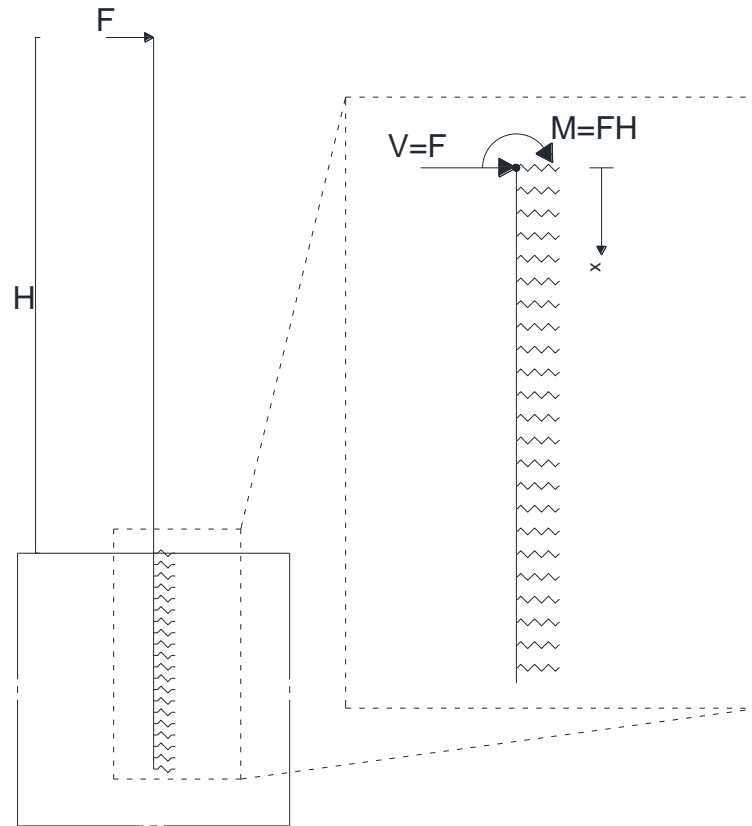


Fig. 5.48: The Winkler model of the embedded height in the block foundation.

The most difficult feature of this approach is the evaluation of the soil constant k_s ; this problem was studied using a simple bi-dimensional model of a stiff beam (representing the profile flange of width B) embedded in the concrete (Fig. 5.49a) to represent the stress distribution (Fig. 5.49b) in concrete loaded by the profile flange. For the concrete, a Young's modulus of 27,000 MPa was assumed, but it is clear that the results are proportional to this parameter due to the linear elastic field considered.

The value of k_s is the ratio between the load applied to the beam and the corresponding displacement (Fig. 5.49a).

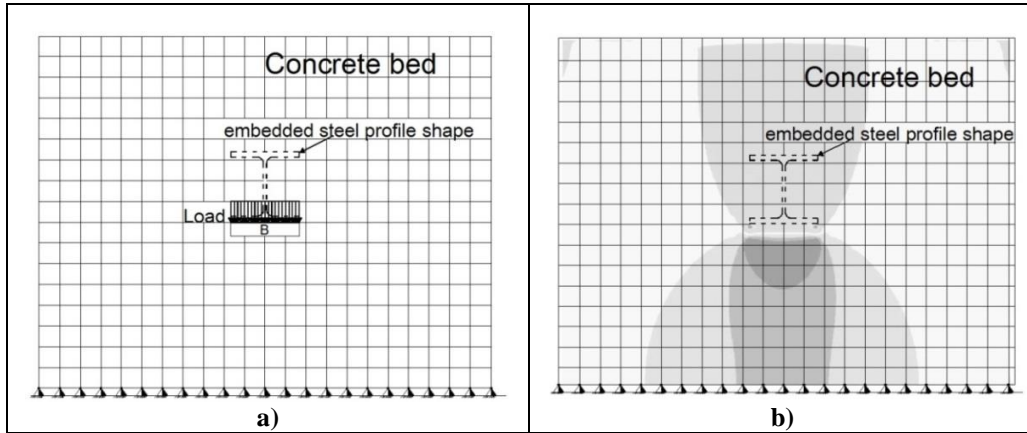


Fig. 5.49: a) Bi-dimensional model of the stiff beam with length B embedded in a concrete bed; b) distribution of the vertical stress in the concrete.

The analysis was conducted by varying B between 60 and 300 mm depending on the width of the profiles considered. In Fig. 5.50, the variation of k_s versus B is reported with the corresponding regression line. Assuming that the regression line depends only on the value of the concrete elastic modulus, the expression for the constant k_s becomes:

$$k_s = 0.146 \cdot E_c \cdot B^{-0.58} \quad (5.5)$$

The reliability of the simple model of the restraint at the base column in the elastic field was validated by evaluating the rotation of the column at the base using the 3D FE model and by varying the wide flange profiles (profiles with a flange width from 100 mm to 300 mm with a step of 20 mm), the load level in the elastic range, and the elastic modulus of concrete. Additionally, these numerical results were compared with the theoretical results obtained from eq. 5.5. Specifically, this model considered a load that applied an average compressive stress value of 0.10 MPa at the top interface of the concrete foundation with the column and the loads corresponding to the 50%, 70% and 90% of the yielding load (F_y) of the steel profile, i.e., when the yielding strain is reached in the flange. All of the analyses were performed assuming a

Young's modulus of the grout surrounding the column of 27,000 MPa (as in the experimental case), but for the load level at 50% of the yielding load, a Young's modulus of 35,000 MPa (indicated with E_{35} in the Figure 5.51) was also used in the model.

Fig. 5.51 shows the ratio between the numerical results of the 3D FE model and the simplified Winkler model, which confirms that these models agree well.

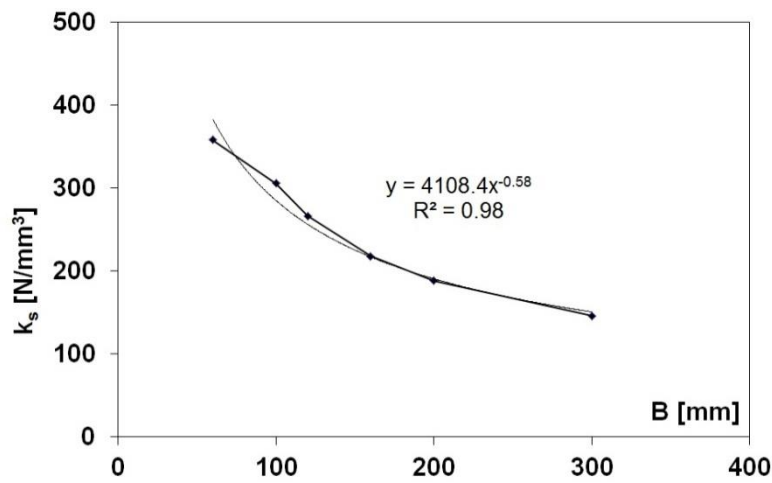


Fig. 5.50: The plot of the 2D model in terms of k_s versus B .

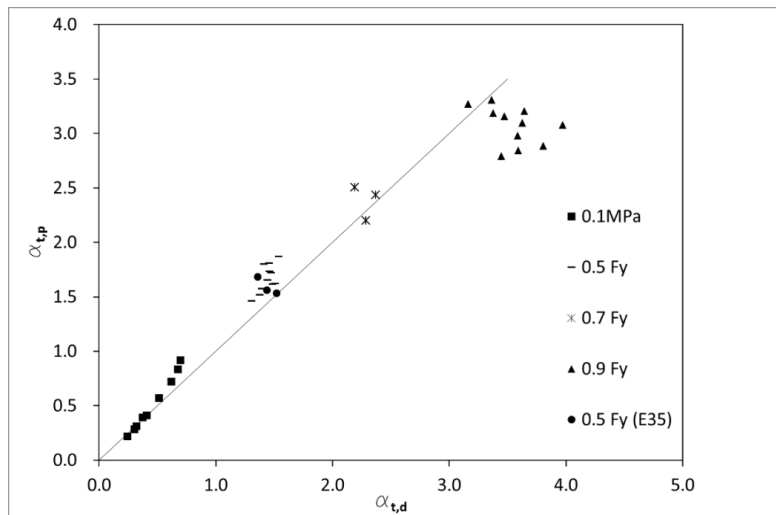


Fig. 5.51: The comparison between the rotation at the base of the column obtained with the FEM model and that obtained with theoretical equation (5.3).

5. 4 Mono-dimensional modelling of the column with a socket type connection

5.4.1 The moment curvature relationship

The behaviour of the composite section was modelled in terms of the moment-curvature relationship, which established the following data:

- the constitutive relationship of the concrete under compression σ - ε is elasto-plastic with a maximum strength of 21.3 MPa and an ultimate deformation ε_{cu} equal to 0.06 to account for the confinement effect of the steel profile (Scott et al., 1982), as confirmed by the previous numerical analysis; the constitutive relationship of concrete under tension is linearly elastic with a maximum strength of 2.31 MPa;
- an elastic-hardening law with a yield strength of 450 MPa, a maximum strength of 540 MPa and a conventional ultimate strain equal to 0.075 was used for the steel reinforcement;
- the σ - ε law for the construction steel is elastic-hardening and the experimental values obtained for the yielding and ultimate strengths are the mean values between the flange and web strength; the ultimate strain is assumed 0.0428 in order to consider local buckling phenomena.

This last hypothesis considers that the rotational capacity of partially encased composite columns is influenced by local buckling, as in the case of steel columns, but the phenomenon is mitigated by the concrete boundary. Typically, to account for the local buckling effect in a numerical analysis, the stress-strain relationship can be modified by reducing the ultimate strain (Chen et al., 2008; Kemp, 1985) or by considering a critical stress (Kato, 1989; Mazzolani et al., 1992 and 1996) beyond which strength degradation is observed. Here, the following expression of the steel strain at the critical load,

ε_{cr} , for partially encased composite columns is proposed (Elghazouli et al., 1993) based on previous studies:

$$\frac{\varepsilon_{cr}}{\varepsilon_y} = \frac{k\pi^2 E}{12\sigma_y(1-\nu^2)(b/t)^2} \quad (5.6)$$

where k is a coefficient that depends on the boundary conditions of the flanges or web, σ_y is the yielding strength, b/t is the slenderness ratio for the flanges or the web, ε_y is the yielding strain, E is the Young's modulus and ν is the Poisson ratio.

Fig. 5.52 shows the moment-curvature relationship for the two types of columns with the socket-type connection using the experimental results and the theoretical results obtained by a numerical analysis. The experimental curves were created from the readings of the strain gauges at the three levels from the foundation (50, 150 and 200 mm), which have already been introduced; the experimental results terminate at different values of the ultimate curvature due to their position along the column.

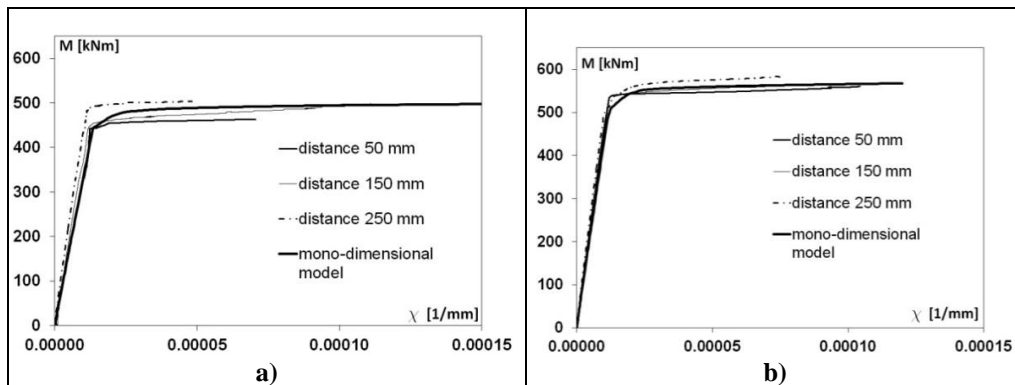


Fig. 5.52: The experimental-numerical comparison of the moment-curvature relationship: a) HE260B; b) HE280B.

The comparisons shown in Fig. 5.52a) and 5.52b) show that the experimental and numerical results agree well and further demonstrate that the ultimate

curvature available is actually greater than the recorded curvature because the tests were stopped before a descending region occurred.

5.4.2 Definition of the plastic hinge length

To estimate the length of the plastic hinge in the column both outside and inside the foundation block, the experimental plastic rotation due to the column and the fixed end rotation were evaluated as the difference between the ultimate and yielding values:

$$\vartheta_p = \vartheta_u - \vartheta_y \quad (5.7)$$

The experimental rotation of the column (Fig. 5.32c) outside of the foundation block was calculated as the difference between the drift (Fig. 5.32a) and the fixed-end rotation (Fig. 5.32b).

At the same time, the theoretical plastic curvature was evaluated as the difference between the ultimate and yielding curvatures:

$$\chi_p = \chi_u - \chi_y \quad (5.8)$$

The plastic hinge length is defined as the ratio of the plastic rotation to that of the plastic curvature (ϑ_p / χ_p); therefore, its value can be calculated for the column outside and inside the foundation block:

$$\begin{array}{ll} \text{Outside the} & L_p^{column} = \vartheta_p^{column} / \chi_p \quad (5.9) \\ \text{block} & \end{array} \quad \begin{array}{ll} \text{Inside the} & L_p^{fix} = \vartheta_p^{fix} / \chi_p \quad (5.10) \\ \text{block} & \end{array}$$

The numerical results are reported in Table 5.6 and Table 5.7 for the 3 tests on the columns with the socket-type connection.

	Load	χ_y	χ_u	χ_p	\mathcal{G}_y^{fix}	\mathcal{G}_u^{fix}	\mathcal{G}_p^{fix}	L_p^{fix}	L_p^{fix}/h
[id]	[id]	[1/mm]	[1/mm]	[1/mm]	[1/mm]	[1/mm]	[1/mm]	[mm]	[-]
HE260B	Mono	0.000036	0.000371	0.000335	0.0100	0.0543	0.044	132	0.51
HE260B	Cicl	0.000036	0.000371	0.000335	0.0125	0.0585	0.046	137	0.53
HE280B	Mono	0.000030	0.000428	0.000398	0.0086	0.0657	0.0571	143	0.51

Table 5.6: The plastic hinge length due to the fixed-end rotation.

	Load	H	d_y	d_u	d_p	χ_p	\mathcal{G}_p^{column}	L_p^{column}	L_p^{column}/h
[id]	[id]	[mm]	[mm]	[mm]	[mm]	[1/mm]	[1/mm]	[mm]	[-]
HE260B	Mono	1700	18	92	74	0.000132	0.043529	129	0.50
HE260B	Cicl	1700	12.6	71	58	0.000132	0.034329	102	0.39
HE280B	Mono	1700	13.4	90	76	0.000398	0.045059	113	0.40

Table 5.7: The plastic hinge length due to the column.

The plastic hinge length of the column is approximately 0.5 times the section profile height (Tab. 5.3); using this value, a simple mono-dimensional model of the cantilever fixed at the base with lumped plasticity was implemented; the moment-rotation relationship is rigid-hardening. In Fig. 5.53, the experimental and numerical force displacement curves ($F - d$), both without the contribution of the fixed end rotation, are compared and show good agreement. In the same graphs, another numerical curve is reported that uses a plastic hinge length equal to the section profile height, which is less effective (Bruneau et al., 1998).

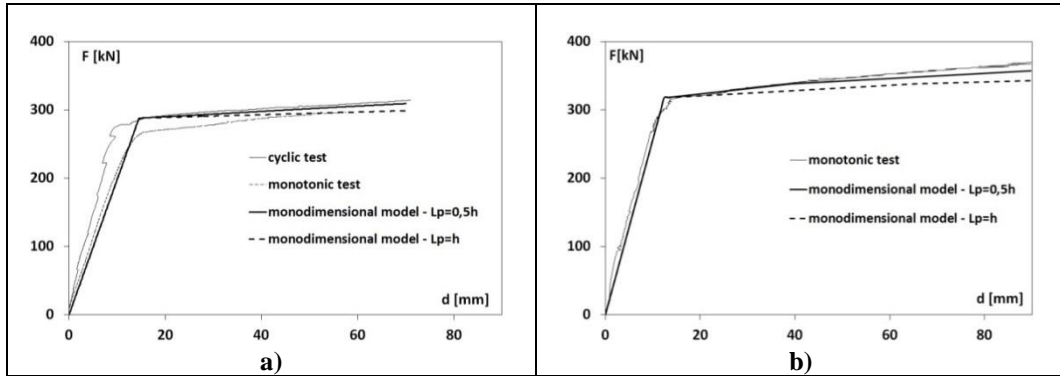


Fig. 5.53: Comparison of the experimental load-displacement curve with that from a mono-dimensional model, without fixed end rotatio: a) HE260B; b) HE280B.

5.4.3 The non-linear mono-dimensional model with a semi-rigid connection at the base

The simple modelling of the base rigidity developed previously using the Winkler beam can be implemented in the mono-dimensional model of the column with the plastic hinge. In fact, the column can be restrained at the base with an elastic-hardening non-linear rotational spring, that has elastic rigidity, according to the expression K_ϑ (eq. 5.4), and a post-elastic section beginning at the yielding moment-rotation point and ending at the ultimate moment-ultimate rotation (Fig. 5.54). The ultimate rotation is evaluated by multiplying the ultimate curvature of the section by the total plastic length $L_p = L_p^{fix} + L_p^{column}$, which is assumed to be $L_p = h$, which is the sum of the contribution of the column outside and inside the foundation, equal to $0,5h$.

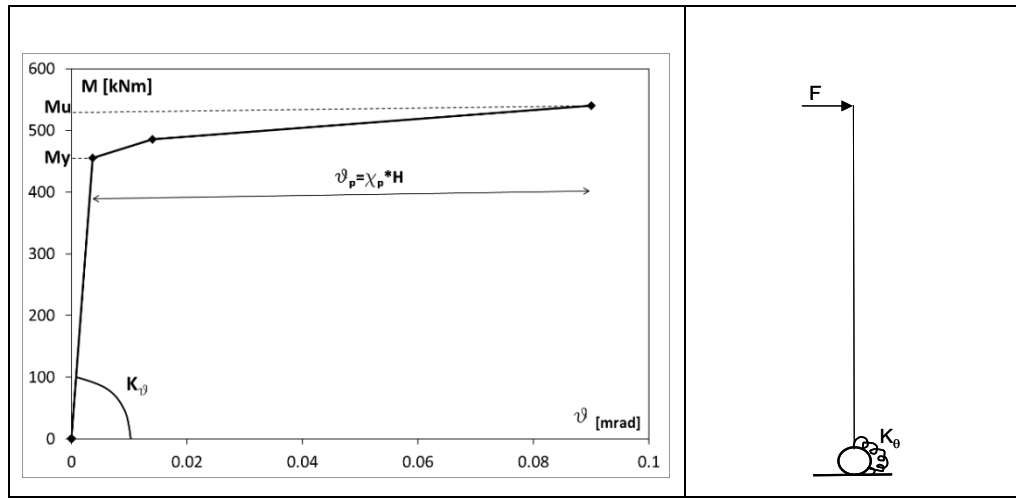


Fig. 5.54: The moment-rotation relationship for the HE260B mono-dimensional model.

In Figs. 5.55a and 5.55b, the numerical results of the 3D FE model are compared with the experimental and the numerical results of the mono-dimensional model in terms of the force-displacement relationship, taking the global behaviour into consideration, i.e., accounting for the fixed-end rotation for profiles HE260B and HE280B. The mono-dimensional model agrees well with the 3D-model and fits the experimental curves well.

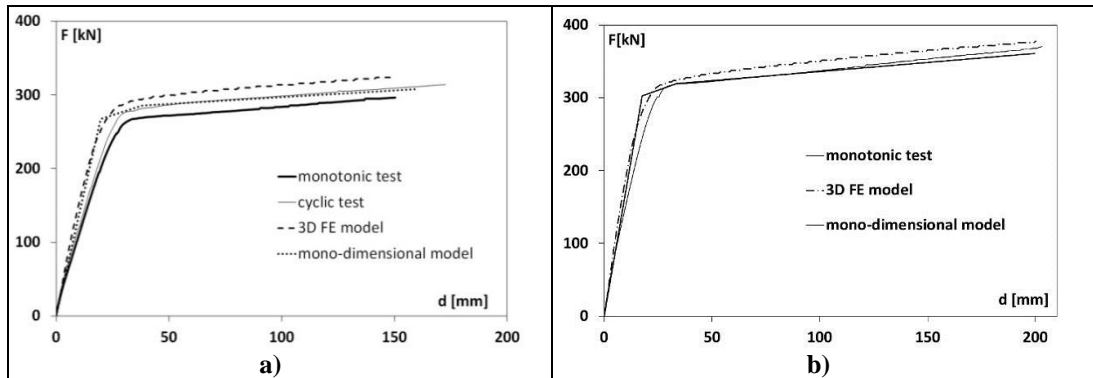


Fig. 5.55: Comparison of the experimental load-displacement curve with the SAP mono-dimensional model and the FE models: a) HE260B; b) HE280B.

5.5 Conclusions

The experimental results, which have been presented in previous studies (Di Sarno et al., 2007; Ceroni et al., 2010), performed well at the base connection with the composite column embedded in the concrete foundation block in terms of the ductility capacity, undoubtedly indicating its suitability for use in seismic areas, especially compared with the traditional connection made with plates and bolts.

The detailed analysis of the experimental strain distributions developed herein suggests that the critical zone of the column outside of the block is long and is approximately equal to the height of the steel section. Furthermore, the contributions of the fixed-end rotation due to the plasticization of the materials inside the block appears paramount with respect to the traditional connection with plates and bolts; this fixed end rotation represents approximately 50-60% of the total deformation of the column in the plastic field, confirming its importance in the definition of the structure ductility.

The three-dimensional model, which neglects the contribution of the steel bars and assumes a perfect bond between the column and the foundation, appears effective for evaluating the global (force-displacement) and local (steel strains and curvatures) behaviour of the system.

Therefore, this model was used to identify the embedded height necessary to guarantee the failure of the column before the failure of the block.

A simple mono-dimensional model was implemented to calibrate the plastic hinge length to evaluate its contribution to the plastic rotation capacity at the base due to the column inside and outside of the foundation block. The plastic hinge length is approximately half the height of the steel profile for the parts both inside and outside of the foundation. This definition allows to evaluate the rotational capacity of the column basing on the dimension and the moment-

curvature relation-ship of the section, however the result refers to the examined case and needs to be confirmed for other types of columns.

A simple model of the base joint in the elastic field was assessed based on the behaviour of a Winkler beam for the embedded part of the column. The model allowed the calibration of a formula for defining the elastic rigidity of the joint by a formula dependent on the dimension of steel cross-section and the Young's modulus of the concrete surrounding the column in the block.

Implementing the results of the elastic rigidity together with the definition of the plastic rotational capacity a non-linear spring was assessed to represent the behaviour of the base joint; this non-linear restraint can be introduced in the mono-dimensional model, resulting in a very simple model that takes into account the complex behaviour of the base connection.

The simple model obtained through the numerical analysis appears very useful for introducing the base joint rigidity in the linear analysis and the plastic behaviour in the non-linear analysis of composite frames under seismic actions.

REFERENCES

- Akiyama, H., Kurosawa, M., Wakuni, N., Nishimura, I., “Strength and deformation of column bases embedded in base concrete”, Annual meeting of A.I.J. 335, 1984, pp. 45-53.
- Ballio, G., Calado, L., Iori, I., Mirabella Roberti, G., “Sul comportamento delle sezioni miste acciaio e calcestruzzo sottoposte a carichi ciclici: indagine sperimentale e modellazione numerica”, Giornate AICAP: I problemi delle grandi costruzioni in zona sismica, 1987
- Braconi, A., Bursi, O. S., Fabbrocino, G., Salvatore W., Tremblay, R., “Seismic performance of a 3D full-scale high-ductility steel–concrete composite moment-resisting structure—Part I: Design and testing procedure”, *Earthquake Engng Struct. Dyn.*; vol. 37, 2008, pp. 1609–1634.
- Braconi, A., Bursi, O. S., Fabbrocino, G., Salvatore W., Taucer, F., Tremblay, R., “Seismic performance of a 3D full-scale high-ductility steel–concrete composite moment-resisting structure— Part II: Test results and analytical validation”, *Earthquake Engng Struct. Dyn.*, vol. 37, 2008, pp. 1635–1655.
- Broderick., B. M., Elnashai, A. S., “Seismic resistance of composite beam-columns in multi-storey structures. Part 2: Analytical model and discussion of results”, *J. Constr. Steel Research*, vol. 30, 1994, pp. 231 – 258
- Bruneau, Whittaker and Uang ,”Ductile design of steel structures”, McGraw Hill Edition, 1998
- CEN, European Committee for Standardization. “Eurocode 3: Design of steel structures - Part 1.1: General rules and rules for buildings. Brussels, Belgium, 2005

- CEN, European Committee for Standardization. Eurocode 4. Design of composite steel and concrete structures - Part 1.1: General rules and rules for buildings. Brussels, Belgium, 2004.
- CEN, European Committee for Standardization, Eurocode 2. Design of concrete structures. Part 1-1: General rules and rules for buildings. PrEN 1992-1-1:2004. Brussels, Belgium, 2004.
- CEN (2008-b) Eurocode 8. Design provisions for earthquake resistance of structures. Part 1.1: General rules. Specific rules for various materials and elements. Eur. Comm. for Stand., Brussels, Belgium.
- Ceroni, F., Garofano, A., Pecce, M., “Numerical model of a base connection for partially encased columns”, The 14th European Conference on Earthquake Engineering, 2010.
- Ceroni F., Pecce M.; “Bond tests of partially encased composite columns”, International Journal of Advanced Steel Construction (IJASC), Vol. 6, No. 4, December 2010.
- Chen, S., Jia, Y., “Required and available moment redistribution of continuous steel–concrete composite beams”, Journal of Constructional Steel Research, vol. 64, 2008, pp. 167–175.
- Chen, Y., Wang, T., Yang, J., Zhao, X., “Test and Numerical Simulation of Partially Encased Composite Columns Subject to Axial and Cyclic Horizontal Loads”, International Journal of Steel Structures, Vol. 10, No 4, December 2010, pp. 385-393.
- Comité Euro-International du Béton, “CEB-FIP Model code 1990”, Thomas Telford, 1991.
- Cook, R. A., Klingner, R. E., "Ductile multiple-anchor steel-to-concrete connections", J. of Struct. Eng., vol. 118, No. 6, ASCE, June 1992.

- Cui, Y., Nakashima, M., “Hysteretic behavior and strength capacity of shallowly embedded steel column bases with SFRCC slab”, *Earthquake Engng Struct. Dyn.*, vol. 40, 2011, pp. 1495–1513.
- Di Sarno, L., Pecce, M.R., Fabbrocino, G., “Inelastic response of composite steel and concrete base column connections”, *Journal of Constructional Steel Research*, vol. 63:6, 2007, pp. 819-832.
- Elghazouli, A. Y., Elnashai, A. S., “Performance of composite steel/concrete members under earthquake loading. Part II: Parametric studies and design considerations”, *Earthquake eng. struct. dyn.*, vol. 22, 1993, pp. 347-368.
- Elnashai, A. S., Elghazouli, A. Y., “Performance of composite steel/concrete members under earthquake loading. Part I: Analytical model”, *Earthquake eng. struct. dyn.*, vol. 22, 3, 1993, pp. 15-345.
- Elnashai, A. S., Broderick, B. M., “Seismic resistance of composite beam-columns in multi-storey structures. Part 1: Experimental studies”, *J. Constr. Steel Research*, vol. 30, 1994, pp. 201 – 229
- Elnashai, A. S., Takanashi, K., Elghazouli, A. Y., Dowling, P. J., “Experimental behaviour of partially-encased composite beam-columns under cyclic and dynamic loads”, *Proc. inst. civil eng., Part 2*, vol. 91, 1991, pp. 259-272.
- Ermopoulos, J. C., Stamatopoulos, G. N., “Analytical Modelling of Column-base Plates Under Cyclic Loading”, *J. Construct. Steel Res.* Vol. 40, No. 3, 1996, pp. 225-238.
- Grauvilardell, J. E., Lee, D., Hajjar, J. F., Dexter, R. J., “Synthesis of design, testing and analysis research on steel column base plate connections in high-seismic zones”, *Structural Engineering Report No. ST-04-02*; Department of Civil Engineering; University of Minnesota; October 1, 2005.

- Hajjar, J.F., “Composite Steel and Concrete Structural Systems for Seismic Engineering”, *Journal of Constructional Steel Research*, vol. 58:5-8, 2002, pp. 702-723.
- Hitaka, T., Suita, K., and Kato, M., “CFT Column Base Design and Practice in Japan” *Proceedings of the International Workshop on Steel and Concrete Composite Construction (IWSCCC-2003)*, Report No. NCREE-0.-0.26, National Center for Research in Earthquake Engineering, Taipei, Taiwan, October 8-8, 2003, National Center for Research in Earthquake Engineering, Taipei, Taiwan, 2003, pp. 291-290.
- Hunaiti, Y. M., Abdel Fattah, B., “Design considerations of partially encased composite columns”, *Proc. Instn Civ. Engrs structs & Bldgs*, vol. 106, 1994, pp. 75-82.
- Hsu, H., Lin, H., “Performance of Concrete-Filled Tube Base Connections Under Repeated Loading,” *Proceedings of the International Workshop on Steel and Concrete Composite Construction (IWSCCC-2003)*, Report No. NCREE-0.-0.26, National Center for Research in Earthquake Engineering, Taipei, Taiwan, October 8-8, 2003, pp. 291-299.
- Kato, B., “Rotation capacity of H-section members as determined by local buckling”, *J. construct. steel res.*, 13, 95-109, 1989.
- Kemp, A. R., “Interaction of Plastic local and Lateral Buckling”, *Journal of Structural Engineering, ASCE*, vol. 111 n. 10, October 1985, pp. 2181-2196.
- Kock, E., Mang, F., Schleich, J.B., Seiler, J., Stiglat, K., “Steel columns embedded in concrete foundation”, *Fourth international conference on structural failure, durability and retrofitting*. Singapore, July 1993.

- Marson, J., Bruneau, M., “Cyclic Testing of Concrete-Filled Circular Steel Bridge Piers Having Encased Fixed-Base Detail”, ASCE Journal of Bridge Engineering, Vol.9, No.1, pp.14-23, 2004.
- Mazzolani, F. M., Piluso, V., “Evaluation of the rotation capacity of the steel beams and beam-columns”, 1st Cost C1 Workshop, Strasbourg, October 1992, pp. 28-30.
- Mazzolani, F. M., Piluso, V., “Theory and design of seismic resistant steel frames”, Spon Press, 1996, pp. 497.
- Nakashima, S., "Response of steel column bases embedded shallowly into foundation beams", Eleventh World Conference on Earthquake Eng., Paper N. 1225, 1996.
- Nakashima, S. “Experimental behaviour of encased steel square tubular column-base connections”, Proceedings of the First World Conference on Constructional Steel Design, World Developments. Acapulco. Dowling, P., Harding, J.E., Bjorhovde, R., Martinez-Romeo, E., editors. Elsevier Applied Science, 1992, pp. 240-249.
- Nakashima, S., Igarashi, S., “Behaviour of steel square tubular column bases embedded in concrete footings”, Proceedings of International Conference Recent Research Advances and their Application to Design. Part I. Budva, 1986, pp. 119-128.
- Nakashima, S., Igarashi, S., Suzuki, T., Kadoya, H. “Experimental behaviour of encased steel column-base connections”, IABSE Symposium Mixed Structures Including New Materials. Part A. Brussels, 1990, pp. 289-295.
- Nakashima, S., Nakagawa, N., “Experimental study on square steel tubular column – bases embedded in foundation beams”, Part 1, 2 and Part 3, 4, Abstracts. Annual Meeting of A.I.J. (September), 1389-1392 and (October), 1984, pp. 1251-1254.

- Pertold, J., Xiao, R.Y., Wald, F., “Embedded steel column bases – I. Experiments and numerical simulation”, *Journal of Constructional Steel Research*, vol. 56:3, 2000a, pp. 253-270.
- Pertold, J., Xiao, R.Y., Wald F., “Embedded steel column bases – II. Design model proposal”, *Journal of Constructional Steel Research*, vol. 56:3, 2000b, pp. 271-286.
- Plumier, A., Abed, A., Tilioune, B., “Increase of buckling resistance and ductility of H-sections by encased concrete”, *Behaviour of Steel Structures in Seismic areas: Stessa '94*, ed. by F. M. Mazzolani and V. Gioncu, E&FN Spon, London, 1995, pp. 211-220.
- Priestley, M. J. N. & Park, R., “Strength and Ductility of Concrete Bridge Columns Under Seismic Loading”, *ACI Structural Journal*, vol. 79(1), 1987, pp. 61-76.
- Roeder, C.W., Lehman, D.E., "An Economical and Efficient Foundation Connection for Concrete Filled Steel Tube Piers and Columns", *International Conference on Composite Construction in Steel and Concrete*, 2008.
- Scott, B. D., Park, R., Priestley, M. J. N., “Stress-Strain behavior of concrete confined by overlapping hoops at low and high strain rates”, *ACI journal*, 1982, pp. 13-27.
- Shanmugam, N.E., Lakshmi, B., “State of the art report on steel–concrete composite columns”, *Journal of Constructional Steel Research*, vol. 57, 2001, pp. 1041–1080.
- Stamatopoulos, G. N., Ermopoulos, J. C., "Interaction Curves for Column Base-Plate Connections", *J. Construct. Steel Res.* Vol. 44, Nos. 1-2, 1997, pp. 69-89.

- Stamatopoulos, G. N., Ermopoulos, J. C., "Experimental and analytical investigation of steel column bases", J. Construct. Steel Res. Vol. 67, 2011, pp. 1341-1357.
- Takanashi, K., Elnashai, A. S., "Experiments on partially encased composite columns", In Stability and Ductility of Steel Structures under Cyclic Loading, Fukumoto Y, Lee GC (eds), CRC Press: Boca Raton, FL, 1992, pp. 175–186.
- Wald, F., Sokol, Z., Steenhuis, M., Jaspart, J. P., "Component method for steel column base", HERON, vol. 53, No. 1/2, 2008.

CHAPTER 6. THE STEEL-CONCRETE COMPOSITE FRAMES

6.1 Introduction

In the steel-concrete composite buildings in which the dissipative behavior is addressed to the moment resisting frames, generally the plastic hinges are located at the beams ends, close to the column connection, where the beam is predominantly subject to negative moment. In this working condition the coupling of the two materials puts them in unfavorable conditions and involve problems of local buckling, as widely discussed in this thesis. Moreover, the concrete slab of the beam in direct contact with the column could be subjected to pick of stresses which lead it to premature failure, invalidating the transfer mechanisms (Braconi et al., 2008; Bursi et al. 2005), especially at the external joints and also in presence of U-shaped reinforcing bars around the column. This problem, under severe cyclic actions and in presence of semi-rigid joint connection, makes difficult the transfer mechanism from the beam to the components of the nodal zone mining the effectiveness of the plasticization of the beam.

Therefore, the current state of the art concerning the characterization of the behavior of steel-concrete composite structural systems subjected to seismic actions is not exhaustive and requires further numerous theoretical and experimental study in order to develop reliable design procedures of the framed structures. To this regard, it has been noted that there are many aspects of the Italian Standard (NTC, 2008) and its guide (Circolare 617/2009), which are not of immediate implementation or require any precise quantitative references for their effective application. It could be underlined a similar situation in standards or international guidelines (AISC, 2010; Eurocode 4, 2008; Eurocode 8, 2008) because there are several aspects that needs further theoretical and

experimental developments. Among the more complex aspects there is surely the characterization of the column-to-beam and the column-foundation connections; in the case of composite structures the possible solutions are more numerous than the ones of the steel structures, and the transfer mechanisms between the steel components and the ones of the reinforced concrete parts in the nodal zone can provide different performance. Currently the Italian standard (NTC2008) provides rules for addressing a hierarchy characterized by the beam-column-joint pattern which ensures the plasticization at the beam ends, making negligible the role of the joint in the determination of the performance of the structure in terms of strength and ductility.

On the base of the high number of parameters that characterize the steel-concrete structures, this chapter presents the results of a nonlinear static analysis of composite frames designed according to Eurocode 8 (2004), that is about the same procedure of the Italian Code, carrying out a detailed evaluation of the influence of the beams rotational capacity and beam-column joints deformability. The results are principally synthesized in terms of behaviour factor (q -factor) in order to evaluate the variability of this parameter and compare the values obtained with those suggested by the codes.

The last comparisons are dedicated to the non-linear behaviour of the composite frames where the rotational capacity of the beams is evaluated by the simple formulation provided in chapter 4.

6.2 The response of steel-concrete composite frames under seismic action

The experimental tests performed on the full-scale composite MRFs (Braconi et al. 2008) or parts of them (Bursi et al. 2000; Nakashima et al. 2007), even if limited, indicate how the performance under seismic actions of such systems could be compared with the steel or concrete ones.

To this regard (Zhou et al., 2007) has reported a numerical-experimental comparison where the FE model has been referred to experimental program reported in (Nakashima et al., 2007). This latter research work was centered on the comparison of the different experimental response between a steel-concrete composite frame and an only steel one: two half-frames (Fig. 6.1) (the columns, completely made of steel, have been cut and hinged at half-height), one with composite beams and the other one entirely of steel have been subjected to horizontal cyclic loading. The strength capacity and the effects of the reinforced concrete slab on steel beams, with respect to the deformation capacity of the same without concrete, has been examined. For each amplitude of the displacement until a drift of 0.06 three cycles have been performed, while for other ones only one cycle, until reaching a drift equal to about 0.13, has been experienced.

The experimental test has highlighted that the composite frame shows a higher resistance to shear in respect to the steel one; furthermore, it was observed a recurrent type of damage, namely, the failure of the connection in the welding of the lower flange of the steel beam that has failed in a fragile way without yielding penetration or plasticity close to the damaged area, similarly to what happened during the Northridge earthquake of 1994. This type of fracture, according to the authors opinion, was due to the position of the neutral axis significantly shifted upwards when the composite beam is subjected to positive moment, causing a considerable demand of deformations to the bottom flange welded.

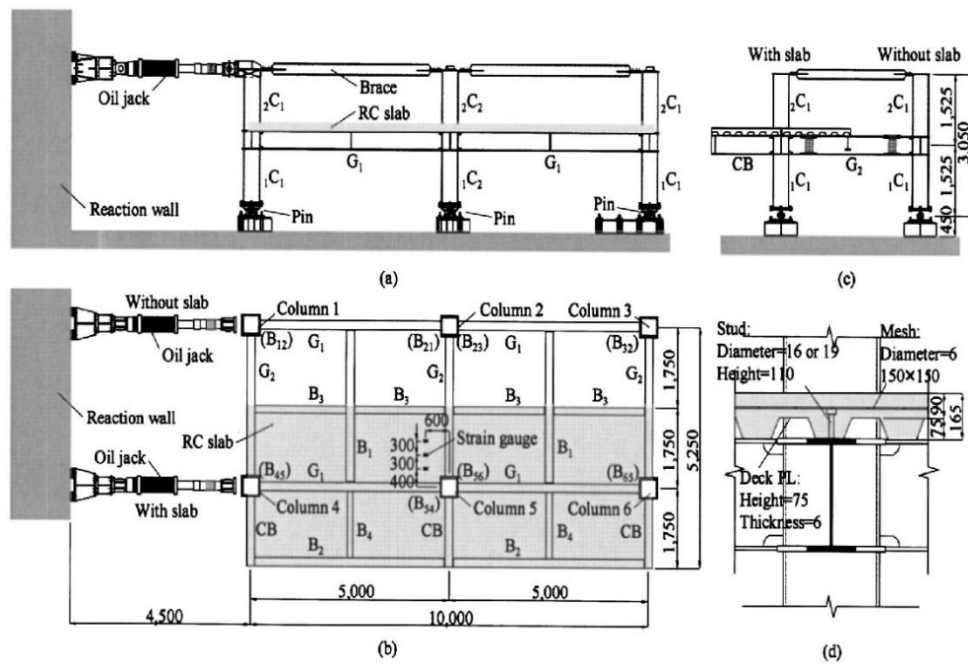


Fig. 6.1: Views of the experienced frame.

The experimental tests gave also data relating to the effective width of the RC slab, even if the external joints of the frame had not any structural detail that could mobilize a greater width.

On the basis of the above-mentioned experiments, (Zhou et al., 2007) have developed a FE model (Fig. 6.2) of a semi-dimensional frame implemented with the software TNO Diana: one part is a composite structure and the other one is steel only.

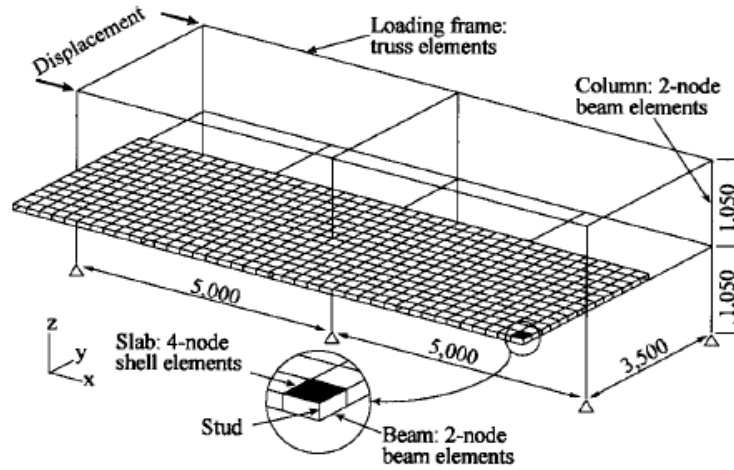
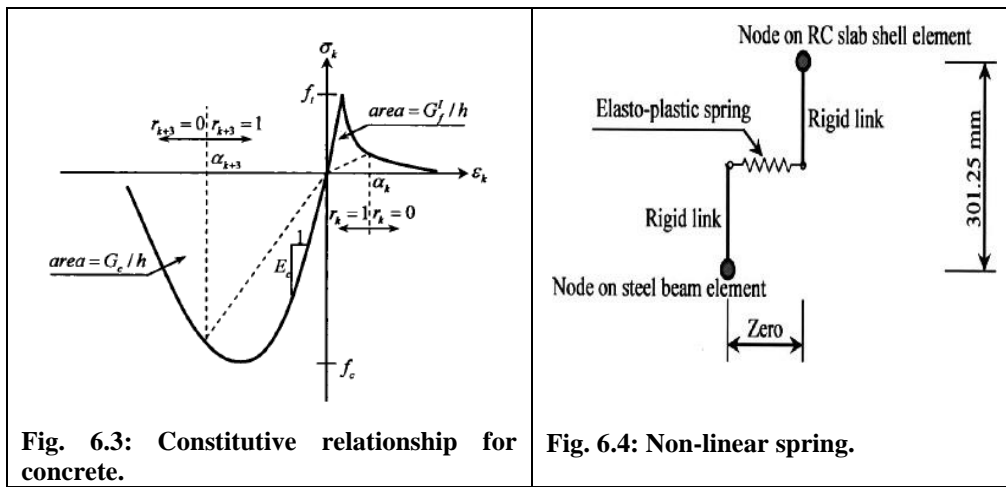
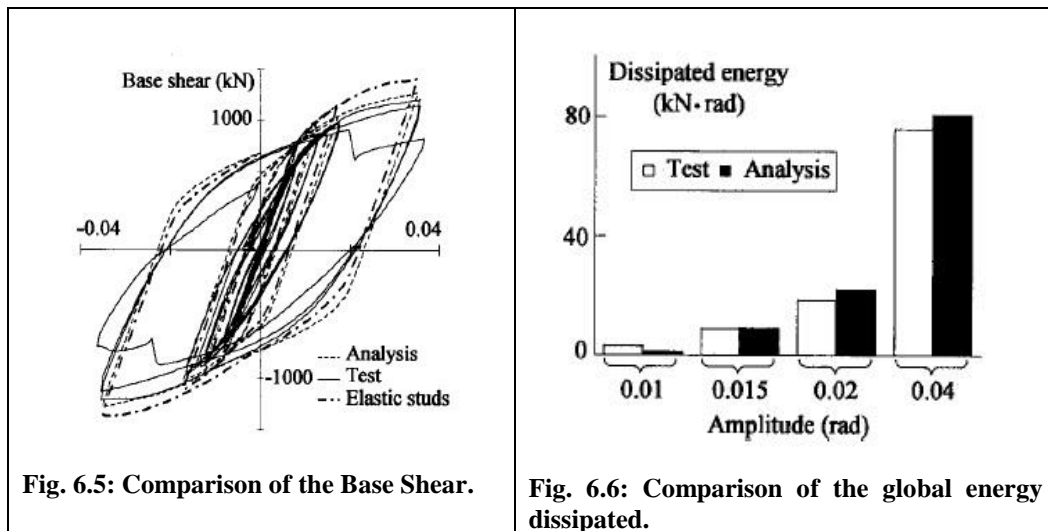


Fig. 6.2: FE model.

The beam and columns elements were modeled with one-dimensional FE elements. For the composite beams the concrete slab was modeled with 2D elements, reinforced with an equivalent grid element. The connection between the steel beam and the concrete slab was provided by rigid elements which have a spring element in the middle of their height simulating the behavior of the shear studs (fig. 6.4). Fig. 6.3 reports the constitutive law adopted for the concrete in the FE model.



In the analyses the geometrical non-linearities and a geometric model of the fracture of the welded steel beam, which exploits the interface elements with an asymmetrical relationship, were considered.



The validation of the model was done through a comparison with the experimental results (fig. 6.5), both global and local. The comparison is also in

terms of dissipated global energy (fig. 6.6) showing a good agreement at different levels of deformation.

In the experimental work (Bursi et al., 2000) three composite substructures tested under cyclic loading and pseudo-dynamic actions have been considered (fig. 6.7) in order to investigate their response varying the degree of connection: $\eta=1.6$, 0.74 and 0.56. In (Bursi et al., 2005) this experimental work was compared with a tri-dimensional numerical model of ABAQUS (fig. 6.8). By the model a parametric analysis on the effective width and the behavior of the panel zone of the joint, that has likely contributed with its deformability to avoid any fracture problems in the steel beam. In this model, the smeared cracking model was managed by the Druker-Prager criterion and the constitutive laws of the materials take into account both the softening and the tension stiffening effect. The results of the 3D FE model were used to implement a mono-dimensional model of the same sub-structures with a fiber approach. Finally, the modeling of two composite frames with DRAIN-3DX tool were implemented varying: the connector type, the connection degree, the shear-slip law, the effective width from code or from the results carried out with ABAQUS software. For the shear studs two cyclical behaviors have been considered: one with bilinear hardening and the other one with pinching effect.

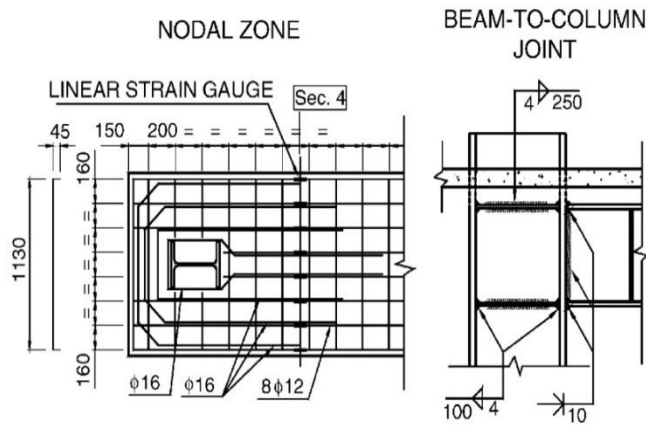
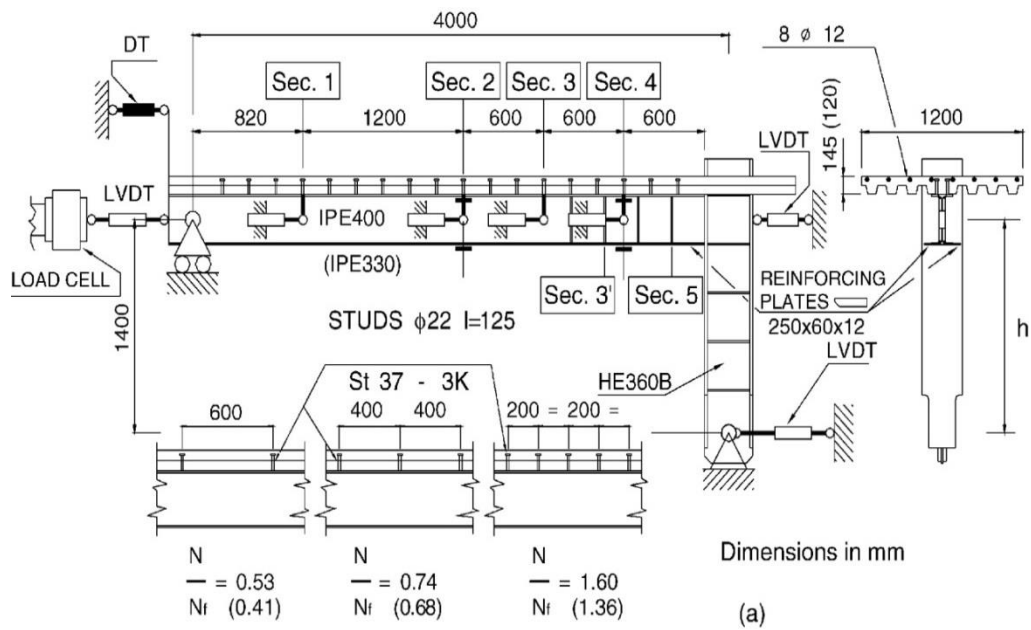


Fig. 6.7: Experienced sub-structure.

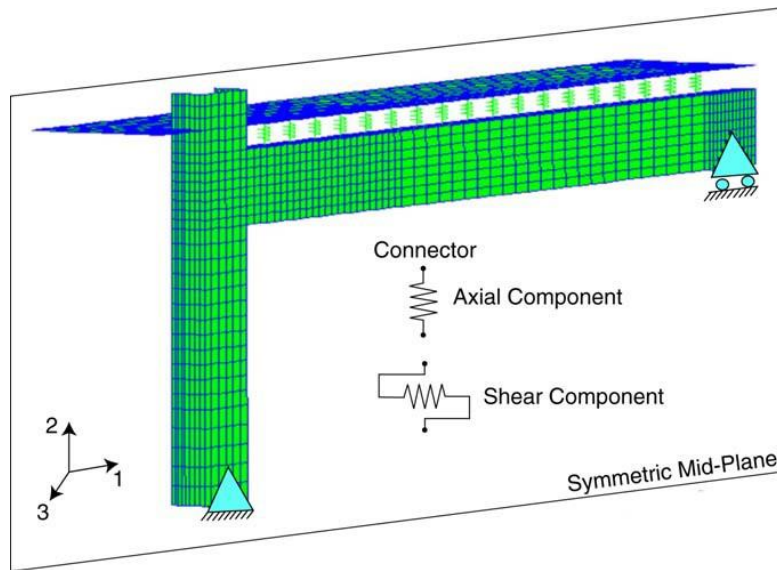


Fig. 6.8: Sub-structure FE model.

Both the 3D and 1D FE model have been validated by comparison with experimental data available. Furthermore, for the panel zone it was also performed a comparison with a theoretical model.

The parametric analysis, limited to the two frames of four floors, have shown that a composite frame characterized by a low degree of shear connection, about 0.4, subjected to strong seismic loads, has a performance similar to that one with a full shear connection. In general, it was observed that in the case of full connection the energy dissipation was given only by the shear studs at the ends of the beams, while for the beams that have a low degree of connection all the shear devices have contributed to energy dissipation. However, the degree of shear connection must be high enough so as to protect the devices from the collapse in the central part of the beams and so as to protect them from failure due to cyclic low fatigue.

The analyses on the mono-dimensional FE model, performed with DRAIN-3DX tool, however, didn't consider the degradation of stiffness and strength of the material, as well as the local buckling of the steel beam. Therefore, the comparisons for validation of the models have been carried out only by global parameters but not local ones.

Anyway, in the capacity design procedure of the composite frames, it is possible to identify different strategies for dealing with the problem of energy dissipation, which in some cases are typical of reinforced concrete structures and in other cases of steel ones. Aligned with the international standards guidelines, a strategy to exploit the dissipative capacity of the frames is to develop the plasticity at the ends of all beams instead of in the columns (strong columns / weak beams), and finally at the base of the columns. To achieve this result, the use of full-strength beam-column joints ensures that the plasticization is realized only in the beams and not in the joints. Numerical studies (Broderick et al., 1996; Elnashai et al., 1996) focused on this approach, have shown that the ductility and dissipation capacity of the composite frames are greater than those expressed by the behaviour factors of the standard rules, proving that it could get a significant plastic rotation in beams and at the base column connection.

In fact, in the two cited research works the FE models for 20 frames have been developed (Fig. 6.9), 10 with partially encased composite columns and 10 with steel columns. The FE models, to which they have referred, were based on beam elements characterized by a cubic polynomial formulation that identifies four Gauss sections that potentially can develop a plastic hinge. The sections are based on a fiber model and the cyclic constitutive laws of the materials are introduced. Among these, the concrete constitutive relationship took into

account the variable degree of confinement provided by the partially encased columns.

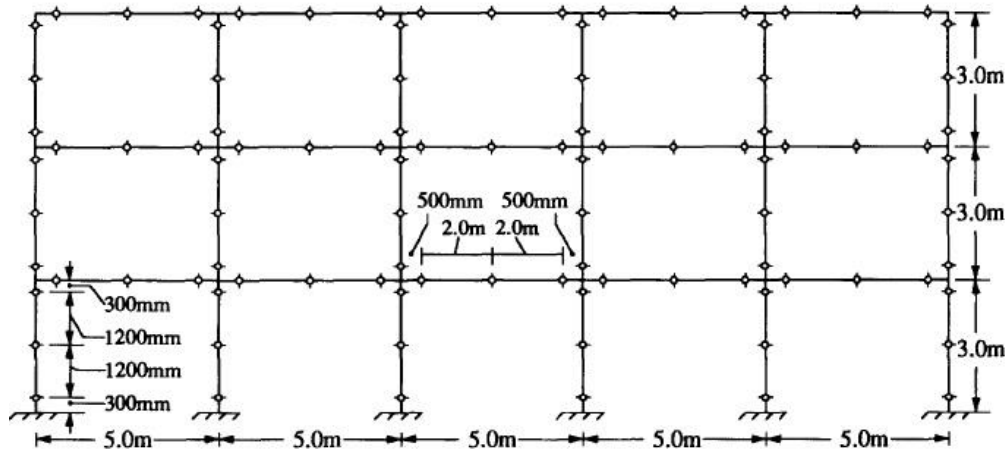


Fig. 6.9: The FE model of composite MRFs.

Therefore, it has been reported also the evaluation of the behavior factors, both for steel structures and composite ones, highlighting that they are too safe.

Since the criteria used (seven criteria) to identify the collapse seem too conservative and some problems of the beams are treated approximately it cannot be concluded that the behavior factors are so safe.

However, on the basis of experimental studies (Braconi et al. 2008), it has also been verified the effectiveness of concentrating the plasticization in the elements of the connection, for example in the beam-column joint connection (end-plate), in the web panel of the column, and at the base column relying on the plasticity of the connection to the foundation. In this case, the use of semi-rigid and partial strength beam-column connections could be realized with the use of T-stub elements or angle, at least in the lower part of the beams (Green et al. 2004). Therefore, the design approaches could be varied according to appropriate capacity design criteria.

Therefore (Braconi et al., 2008) have discussed the design criteria used for the realization of a spatial frame in real scale, 5 MRF (Moment Resisting Frames) in the X direction and 3 frames CBF (Concentric Braced frames) in Y direction (Fig. 6.10a). In particular, the research paper was focused on one of the MRFs characterized by two bays (5 and 7 m), the partially encased columns and two floors, both of height equal to 3.5 m. The capacity design was cleverly calibrated to address the plasticization in the panel node, into the end plates of the beams and at the base connection of the columns characterized by a traditional plate bolted connection. In the work it is also reported the Pseudo-Dynamic test procedure with 4 levels of acceleration, as well as the description of the test setup. The design has been taken into account also of another experimental work carried out on sub-structures for the nodal zone and for the partially encased columns.

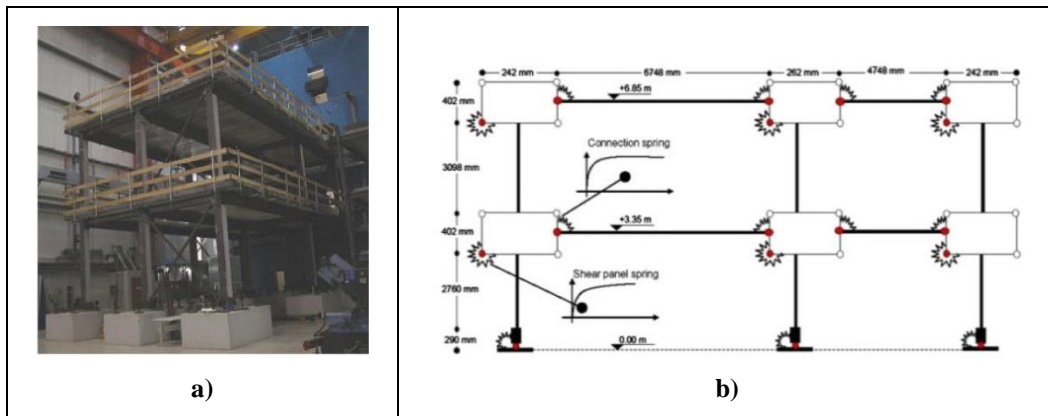


Fig. 6.10: a) The real MRF tested; b) the FE model of one MRF.

In order to better calibrate the steps of the pseudo-dynamic test and therefore the target of the experimental program, a FE model of the frame (Fig. 6.10b) has been implemented. This model was characterized by beam elements with a

widespread plasticity approach for beams and columns and by the rotational spring elements with a hysteretic model for the ends of the beams and for the base column connections. The panel is modeled with four rigid bar elements with rotational springs characterized by a hysteretic relation. The effective width of the beams (B_{eff}) were calculated in accordance with EC8. The moment-curvature relationships of the columns were evaluated by a fiber model of the sections and the degree of confinement of the concrete has been taken into account by the model of (Mander et al., 1988). The hysteresis parameters of the joint were calibrated on previous experiments (Braconi et al., 2007). The validation of the FE model of the nodal sub-structure has referred to (Salvatore et al. 2005); as well as for the validation of the rotational capacity of the traditional base column connection it has been referred to the experimental results reported in (Di Sarno et al., 2006), in which the N-slip law of the bolts was calibrated on experimental data. The work also shows an interesting comparison between standard codes, EC8 and AISC. In the design procedure the capacity concept was applied to take into account a balanced behavior between the components of the joint to have the exploitation of the energy dissipations between end-plates of the steel beams and the panel zone; the components were well designed to avoid fracture phenomena in the beam or plasticization at the top of the columns due to the excessive participation of the panel component.

The results of the experimental tests are reported for four pseudo-dynamic acceleration levels: 0.1 g, 0.25 g, 1.4 g, and 1.8 g. For each step of acceleration it has been shown the participation that each element has provided on the overall deformation capacity of the frame (Fig. 6.11). It has been also noted that a certain participation was given not only by the flash end plate connection of the beams and the panel zone, but also by the concrete slab and the yielding of the steel rods of the foundation. The authors themselves have emphasized

how these mechanisms may affect the response of the structure in the plastic field because the overall increasing deformability may lead to the onset of second order effects.

In the second part of the research paper, the FE model, that has been previously exploited to calibrate the pseudo-dynamic procedure, was compared with the cyclical history of displacements recorded in the experimental test. The comparison was in good agreement up to the value of 1.4 g, while afterward the model was not able to capture properly the displacements history of 1.8 g, perhaps because of the additional deformation caused by slab and foundation bolts.

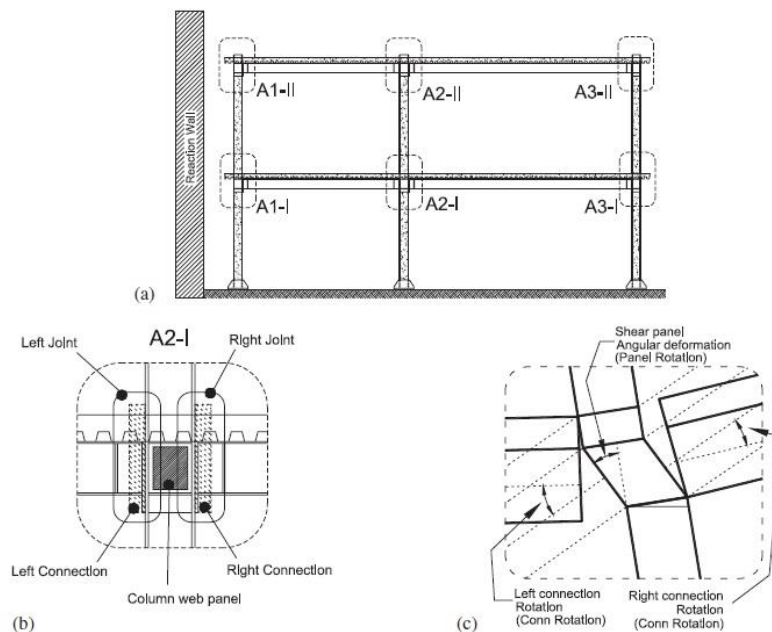


Fig. 6.11: a) the different joints; b) the parts that characterize the A2-I joint; c) the rotations involved in the global deformation.

The performance of the tested frames was more than satisfactory. The rotations in the nodal zones were equally distributed between the two floors doing to exclude any local mechanism. Most of rotation for the internal nodes was given

by the deformation of the panel component that became the main plastic component for important acceleration levels. On the other hand for the external joints the concrete slab did not allow that the nodal panels had this preponderance, then the rotations were almost equally distributed between the connection end plates and the panel zones, while the rotations at the base column connections were governed by the anchoring rods. The experimental data have underlined that the required rotation of 35 mrad, imposed by EC8, was ensured, but the limit of 30% as the maximum deformation to be assigned to the panel component was inadequate. The behavior factor, evaluated both from the results of non-linear static analysis and IDA (Identification Dynamic Analysis), was well above than the one indicated in the standards.

The evaluation of the behavior factor has highlighted a considerable over-strength of the structure, a common feature of the composite MRFs such as the steel structures that are affected by some features in the design phase: the safety factors of materials, the limits on the drifts for SLD, the design for vertical loads, the difference between the nominal values and the real ones of the strength, the standard cross-sections for steel profiles, the estimation of the period of vibration in the evaluation of the horizontal seismic loads, etc. ...

Also (Aribert et al., 2006) has taken into account the influence of the joint on the response of composite frames reporting the results of a study on numerical models of steel-concrete composite frames with and without the behavior of the joints. In particular, the response of two typologies of frames (Fig. 6.12) were discussed, one characterized by two floors and the other one by four floors. The frames have been designed and tested in accordance with the rules of the EC4 and EC8. For the frame with two floors the dimensions of the structural elements have been mainly governed by the load combinations of vertical loads, while in the frame with four floors the dimensions of the

composite beams have been still governed by gravitational loads and the design of the columns have been addressed by the seismic load combinations. In the latter case the limits imposed to the drift to respect the damage limit state influenced the design.

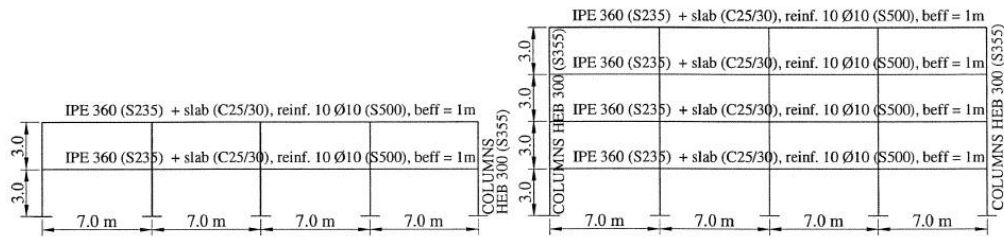


Fig. 6.12: The layout of the two composite MRFs.

After the design, a series of non-linear analyses, both static and dynamic, were carried out. The models of the frames were implemented with a distributed plasticity approach. For the time-history analyses two artificial accelerograms, that provided a good compatibility with the spectrum of the standard code, were generated. Since a comparison between composite frames with and without deformable joint was carried out, it was also introduced a cyclic model for the joint behavior that was previously calibrated by experimental tests.

For the frame without deformable connections subjected to non-linear dynamic analysis the comparison of the ductility demands in the beams imposed by the standard code was carried out noting that these rotation requirement was always lower than the standard limits: 25mrad for medium ductility class (DCM) class and 35mrad for high ductility class (DCH).

The same comparison was also done for the frames with deformable joints that clearly have shown a greater capacity in terms of displacement.

The evaluation of the required behavior factor was carried out and it has assumed always values greater than that used in the design. In the case of frames with semi-rigid joints the available ductility was considerably higher.

The research work did not focus on the capacity but on the demand assuming that the steel-concrete composite frame could always satisfy the standard requirements. Since this attention to the demand was given, the authors did not give the same attention to the choice of the input.

Some authors (Thermou et al., 2004), however, have focused on the influence of the design procedure and the standard rules on the nonlinear response of the composite frames. The design of six frames using Sap2000 was reported. The modeling of the beams and columns have been performed with the equivalent inertia approach and three types of frames characterized by three different configurations have been implemented. For subsequent non-linear analyses, static and dynamic, the INDYAS software have been used in which the beams have been designed as two beams rigidly connected: one for the concrete slab and the other one for the steel profile (Fig. 6.13).

The two currents have been discretized using beam elements (beams and columns) characterized by a cubic polynomial formulation and in each beam two Gauss sections that could develop a plastic hinge have been identified. Concrete has been characterized by a constitutive law according to Mander model while the steel had an elasto-plastic model.

The study is based on the requirements of EC4 and EC8, and the authors have critically highlighted some limitations in the design using these standard codes. In particular, it was shown that very often, in the design based on the achievement of a given seismic performance, actually the design of the composite frames is governed by the gravitational loads and not by the capacity design.

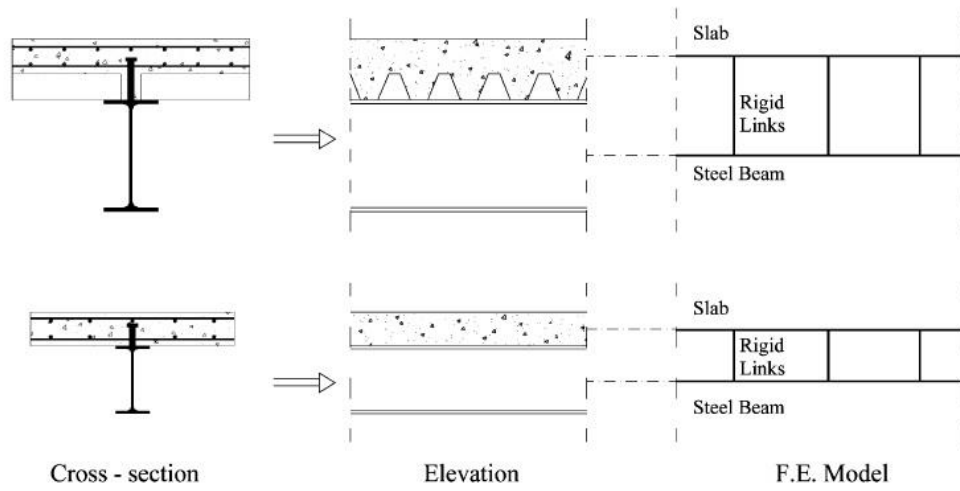


Fig. 6.13: Modeling of two types of composite beams.

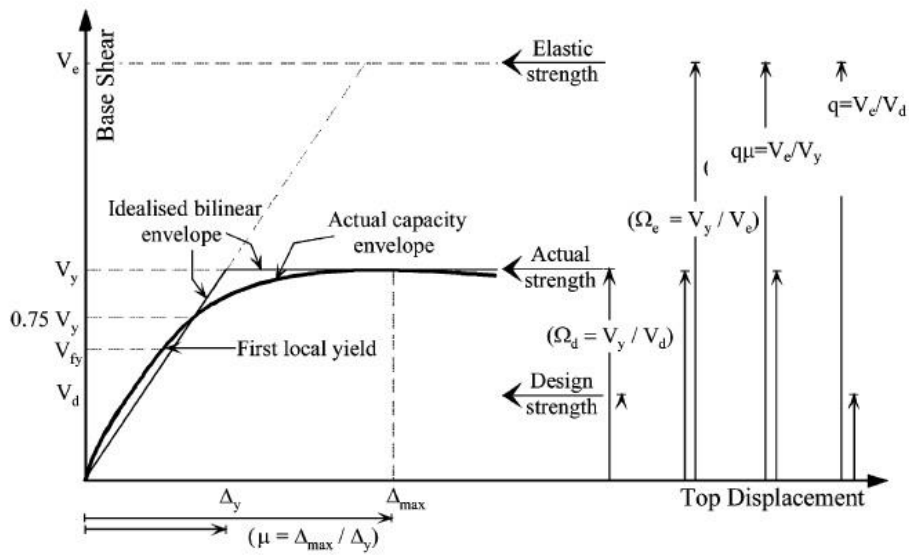


Fig. 6.14: The relationships between the force reduction factor, structural over-strength and the ductility reduction factor.

Therefore, it was shown that there is a large discrepancy between the behavior factors (fig. 6.14) assumed in the design and then evaluated on the basis of the nonlinear analysis results; it is important the role of the over-strength due to the collapse criterion assumed to avoid the P-delta effects that have led to assume very stiff, but also strong, columns.

6.3 The design of a composite frame

The analyzed frame is extracted from the design of a multi-storey building used as offices. The building is regular both in elevation and plan. The plan dimensions of the building are: 31m in longitudinal direction and 24m in transverse direction, with a total covered area of 744 m². The height from the ground plan is 14.50 m for a total of 4 stories. The height of the first floor is 4 m, while all others are characterized by an interstory height of 3.5 m (Fig. 6.15).

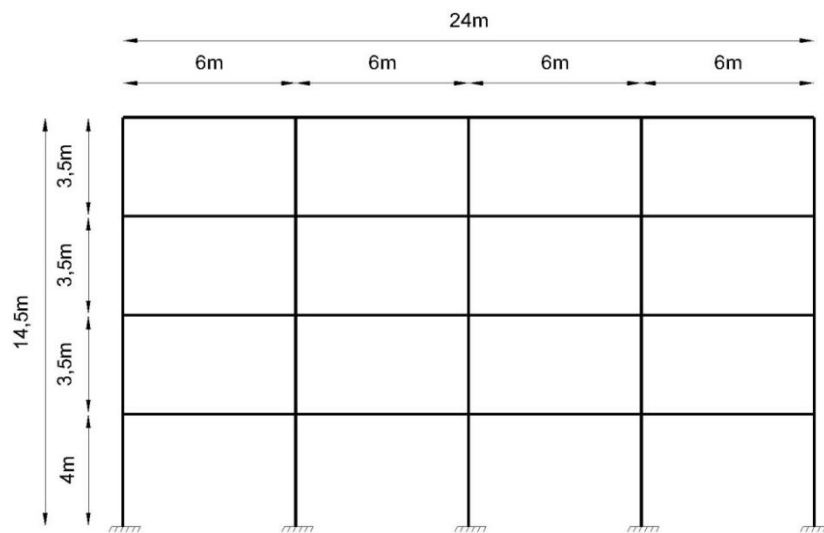


Figure 6.15: The frame analyzed.

Partially encased columns were used; the beams were composed with IPE profiles and reinforced concrete solid slabs with a height of 120mm connected by shear studs. The materials used in the design of the structure, and their mechanical features are given in Table 6.1.

The design was developed according to the Eurocode 8 rules, applying the concept of capacity design by the column-beam strength hierarchy in bending and shear criteria for beams and columns. For the seismic actions characterization, reference was made to a site characterized by a medium-high level of seismicity with a PGA value of 0.08g for service limit state (in particular SLD) and 0.25g the ultimate limit state (ULS) (in particular SLV). The calculation of the stresses in the elements was arisen with the aid of the software SAP2000 (2011); both the performances at the ultimate limit state (ULS) and service limit state (SLS) were checked. For ULS, verifications of the flexural and shear strength were considered for the static (vertical loads) and seismic (vertical and seismic loads) combination loads. For the SLS the stress and deflections were checked.

Material	Class	Mechanical features				
		f_{ck}	f_{yk}	f_u	γ_m	E
		MPa	MPa	MPa	(-)	MPa
Concrete	C20/25	20			1.50	29962
Steel bar	B450C		450	540	1.15	210000
Steel	S275		275	430	1.1	210000

Table 6.1: Mechanical characteristics of the materials.

The definition of the effective widths of the beams was carried out according Annex C of the Eurocode 8 in all linear and nonlinear seismic analyses and the

par. 5.4.1.2 of Eurocode 4 for vertical loading effects. The characterization of the response spectra for SLS and ULS (tab. 6.2), was referred to the seismic hazard Italian classification. Particularly it was assumed a reference life of 50 years, a class of use II (Importance class II), a ground type C and a normal topographical condition.

SLS					
a_g	F_0	T_c^*	S_s	C_c	S_T
0.819	2.35	0.29	1.58	1.58	1
ULS					
a_g	F_0	T_c^*	S_s	C_c	S_T
2.519	2.31	0.37	1.34	1.46	1

Tab. 6.2: Parameters of seismic hazard for the referred site (NTC08).

Assuming in the design a high ductility class (DCH) and the regularity of the structure, the behavior factor results:

$$q_0 = 5 \frac{\alpha_u}{\alpha_1}$$

$$q = q_0 \cdot k_R = 5 \cdot 1.3 \cdot 1 = 6.5$$

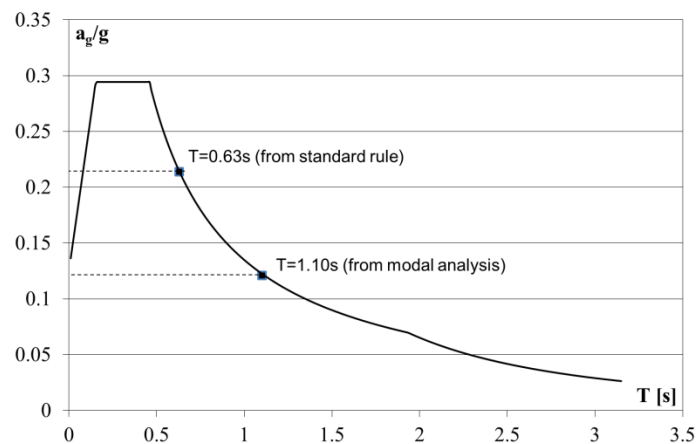


Figure 6.16: Elastic Spectrum SLS.

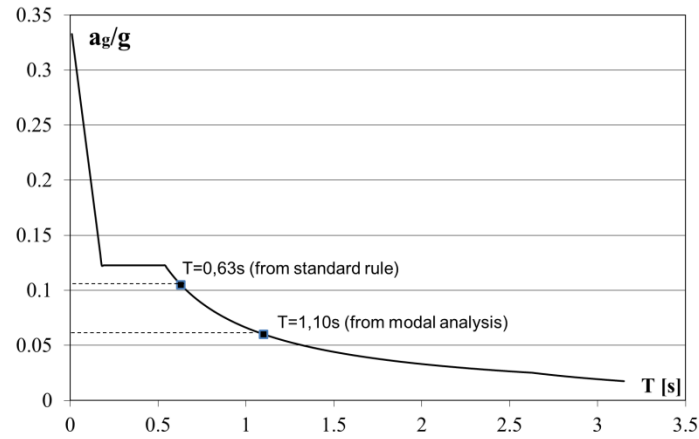


Figura 6.17: Inelastic Spectrum ULS.

By means of a first pre-dimensioning step and an iterative design process, using a static linear analysis, the final solution was identified.

In figures 6.16 and 6.17, the pseudo-acceleration spectra, based on the parameters reported in Tab. 6.2, were traced for SLS state (Low Damage state) and ULS state (Life Safety state). In the same figures the approximate value of the structural fundamental vibration period, evaluated with the rule provided by Italian standard code (NTC08), and the effective modal period are signed. It could be observed a difference in the acceleration value of about 40%.

The rule of NTC08 is as follows:

$$T_I = C_I \cdot H^{3/4}$$

Where:

T_I is the fundamental vibration period;

C_I depends on the structural system typology;

H is the height of the structure.

On the base of seismic forces (Tab. 6.3) a satisfactory solution for the structural elements has been identified adopting beams IPE270 and columns

HE320B for the first two stories and beams IPE240 and columns HE280B for the other ones.

Horizontal seismic forces		
Floors	Forces [kN]	
	SLS	ULS
1	35	18
2	66	33
3	97	49
4	99	50

Table 6.3: Seismic forces for the single frame.

The effective width of the beams evaluated according to the standard code, varies along the length and with the loading condition (vertical or horizontal loads). In the seismic condition, for section under sagging moment an effective width of 900mm has been assumed that increase to 1200mm for those subject to hogging moment, both for internal and external joints.

The slab reinforcement was characterized by bars of 12mm diameter, spaced at 150mm. The partially encased columns are reinforced with 4 bars of 12mm diameter.

The shear connection of the beams was calculated according to the plastic theory with ductile shear studs (19mm diameter - class S275), with a spacing of 140mm along the entire length of the beams.

The modal elastic period of the 3D structure is 1.1s and the design spectral acceleration is 0.065g at ULS and 0.125 at SLS.

For the ULS it has been verified that the bending moments were smaller than those resistant (Table 6.4) calculated considering the b_{eff} as indicated by NTC2008 and assuming for the external joints that the reinforcing bars are

anchored to the transverse beam and the effective width is the same as internal joints (0.10 L).

Check of the beams					
Floors	Beam	M_{sd}^- [kNm]	M_{sd}^+ [kNm]	M_{Rd}^- [kNm]	M_{Rd}^+ [kNm]
1 ; 2	IPE270	121.4	46.6	265	191.2
3 ; 4	IPE240	96.6	37.5	223	153.8

Table 6.4: Maximum stress and resistant moments of the beams for all the floors.

The check of the shear strength of the beam was performed according to the hierarchy of moment-shear mechanisms at the ends of the beams assuming the development of the upper bound plastic flexural strength ($M_{U,Rd} = 1.1 \cdot \gamma_{Rd} \cdot M_{Rd}$), according to the diagram shown in Fig. 6.18, and considering the different combinations of the vertical load in analogy to reinforced concrete structures.

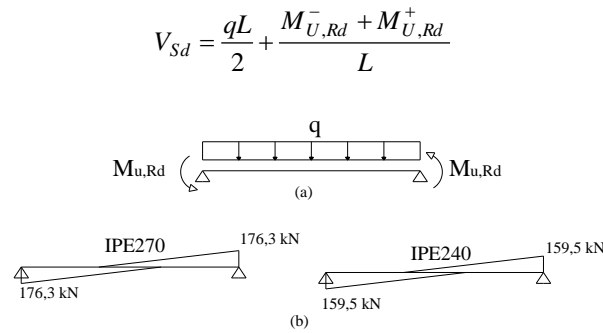


Figure 6.18: Loading patterns for the evaluation of the shear forces in the beams.

These values were compared with the plastic shear strength of the steel profile web. For the connection between the concrete slab and the steel joist the standard code does not explicitly state which is the distribution of the bending

moments along the beam to refer in the evaluation of the shear stress in the case of ductile connectors. Therefore, it was established to evaluate the maximum shear stress corresponding to the transferred force between the sections where positive and negative resistant plastic moments are achieved (Fig. 7).

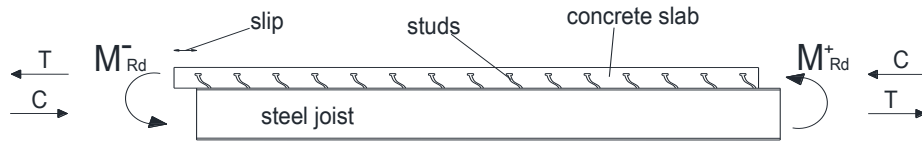


Figure 6.19: Scheme for the evaluation of the maximum shear force on the studs

The sum of these two components provides the maximum shear force that the connection have to transfer:

$$V_{ld} = \left(F_{cf, \min} + \frac{A_s f_{sk}}{\gamma_s} \right)$$

where:

$F_{cf, \min}$ is the minimum value between the maximum resistance of the concrete slab and that of the steel profile when the cross-section is subject to sagging moment, i.e. the minimum between the following values:

$$F_{cf} = \frac{A_a f_y}{\gamma_a}$$

$$F_{cf} = \frac{0,85 A_c f_{ck}}{\gamma_c} + \frac{A_s f_{sk}}{\gamma_s}$$

while the second term represents the maximum strength of the reinforcement, i.e. the maximum action that the connection has to transfer to the point where the hogging moment acts.

By this calculation the number of shear connectors was determined in a similar manner for both vertical loads and in presence of seismic load combinations

dividing the shear force by the connector strength (P_{Rd}), but in the case of seismic conditions the following correction factors were applied:

- the shear forces were amplified for taking into account the over-strength factor (γ_{Rd}) and hierarchy of the mechanisms (1.1):

$$V_{ld, seismic} = 1,1 \cdot \gamma_{Rd} \left(F_{cf, min} + \frac{A_s f_{sk}}{\gamma_s} \right)$$

- the strength of the connectors was reduced by a factor equal to 0.75:

$$N = \frac{V_{ld, seismic}}{0.75 \cdot P_{Rd}}$$

Considering the amplification of the shear forces and the reduction of the strength of the connectors, the number required by the seismic actions is greater than about 69% respect to the case of the vertical loads. Dividing the number of the shear studs by the length of the beam it was obtained the spacing. However under the seismic actions the length of the beam to be considered for introducing the studs (fig. 6.20) is the entire span length, since the upper bound plastic moments are developed at the beam ends, while in the case of the vertical load combination the maximum moment is not far from the middle of the beam. Therefore in seismic condition the spacing of the connectors required for a full shear connection is 17cm, that is greater than that calculated for the gravity loads (14cm).

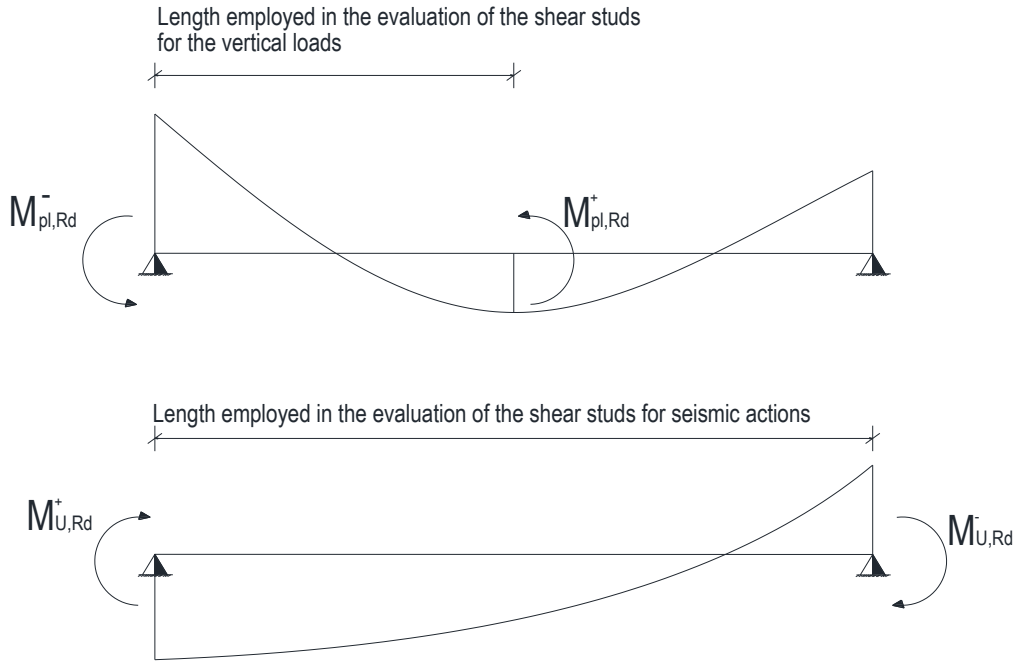


Figure 6.20: Beam length considered in the evaluation of the shear studs

$$N_{Sd} = N_{sd,G} + 1.1 \gamma_{Rd} \cdot \Omega \cdot N_{Sd,E}$$

$$M_{Sd} = M_{sd,G} + 1.1 \gamma_{Rd} \cdot \Omega \cdot M_{Sd,E}$$

$$\sum M_{C,pl,Rd} > \gamma_{Rd} \cdot \sum M_{b,pl,Rd}$$

Figure 6.21. Capacity design scheme adopted for the beam-column.

$$M_{U,Rd} = 1.1 \cdot \gamma_{Rd} \cdot M_{pl,Rd}$$



Figure 6.22. Scheme for the hierarchy of the mechanisms in the columns

Also the axial-bending strength, considering the global buckling of the columns were checked. For these last verification the rules of the capacity design between the beam and column, as shown in Figure 6.21, were considered.

For the shear strength of the columns the upper bound plastic moments at both ends (Fig. 6.22) were applied, as already done for the beams; the shear plastic resistance is the one of the steel profile web.

6.4 The non-linear analysis of the steel-concrete composite MRF

After the frame design, a nonlinear static analysis was performed to assess the actual resources of ductility of the structural system. This analysis was carried out assembling a lumped plasticity model. Elastic frame elements were adopted for columns and beams with plastic hinges at the ends. The advantage of this modeling is that it allows working primarily with elastic elements which are less onerous from the computational point of view, leaving into few points the concentration of the material non-linearity. The limit of this modeling approach is that it requires some experience of the operator to determine where the

plastic hinges have to be allocated and choose for them adequate moment-rotation relationships. In this case study a non-linear moment rotation curve was adopted, multiplying the moment-curvature relation of the section by a plastic hinge length (L_p).

It is clear that the global response accuracy may be compromised if a wrong calibration of the moment-curvature relationship or plastic hinge length is done. Therefore, particular attention must be reserved for the estimation of the moment-curvature diagrams, even in presence of axial load, in the prediction of an equivalent plastic hinge length in order to define a rotational ductility close to the real one. For composite structures the formulations for direct evaluation of the rotational capacity are not available, due to a lack of experimental tests and influence of many parameters, in contrast to the reinforced concrete structures for which different formulas were defined by the researchers (Paulay et al., 1992, Panagiotakos et al., 2001). On the other hand also the determination of the equivalent plastic hinge length for such structural systems is not immediate, since even in this case the scientific resources are lack (Chen et al., 2008). In the paragraph 6.3.2, an analysis of the various L_p expressions and their impact on the overall response of the designed MRF is conducted; the expressions considered for the determination of the plastic hinge length are the ones available for reinforced concrete structures, steel and steel-concrete composite structures in the technical literature.

6.4.1 The moment-curvature relationships of beams and columns

The moment-curvature relationships of composite sections were tailored for the various sections of beams and columns assuming the Bernoulli hypothesis (the plane section remains plane) between the various components (concrete, structural steel, reinforced steel) and nonlinear constitutive relationships for the materials. The slip between the concrete component and the steel ones was

assumed as negligible. The mechanical characteristics of the materials are the same used for the design and already summarized in Table 6.1.

For the concrete a non-linear model, that describes well the inelastic behavior of the material and is simple in terms of implementation, was chosen. In particular, the constitutive nonlinear model of (Mander et al., 1988) (fig. 6.23) was used because it is able to simulate also the confinement degree of concrete. In fact, in the case of the partially encased composite columns considered in this study, the concrete located between web and flanges of the steel profile cross-section (HEB), could be considered with a behavior that varies from confined to unconfined, with a transition zone (partially confined).

The instantaneous elastic modulus, tangent at the origin of the constitutive relationship, in the absence of direct experimentation may be assumed equal to the standard code value (NTC, par. 11.2.10.3):

$$E_{cm} = 22000 \cdot [f_{cm} / 10]^{0.3} \quad (\text{in N/mm}^2)$$

$$f_{cm} = f_{ck} + 8$$

$$f_{ck} = 0.83 \cdot R_{ck}$$

Then for the examined case (C20/25) it follows:

$$f_{ck} = 0.83 \cdot 25 = 20 \text{ N/mm}^2$$

$$f_{cm} = 20 + 8$$

$$E_{cm} = 22000 \cdot [28 / 10]^{-0.3} = 29962 \text{ N/mm}^2$$

The ultimate tensile strength and the corresponding strain of the concrete, according to the Italian standard (NTC, par. 11.2.10.2) are defined by the following rules:

$$f_{ctm} = 0.30 \cdot f_{ck}^{2/3} = 0.30 \cdot 20^{2/3} = 2.21 \text{ N/mm}^2$$

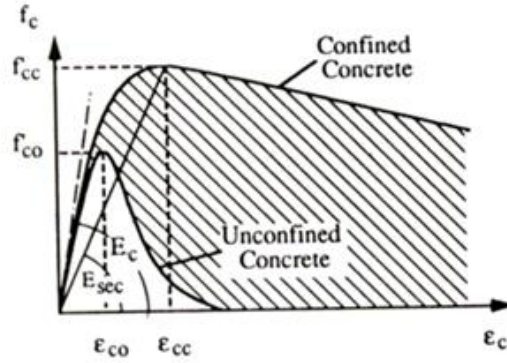


Figure 6.23 – Constitutive relationship of concrete in compression of (Mander et al., 1988).

The relationships that define the constitutive law of Mander are the following ones:

$$f_c = \frac{f'_{cc} \cdot x \cdot r}{r - 1 + x}$$

where:

$$f'_{cc} = f'_c \cdot \left(+ 2.254 \cdot \sqrt{1 + \frac{7.94 \cdot f'_l}{f'_c}} - \frac{2 \cdot f'_l}{f'_c} - 1.254 \right) \quad x = \frac{\epsilon_c}{\epsilon_{cc}}$$

$$\epsilon_{cc} = 0.002 \times \left[1 + 5 \times \frac{f'_{cc}}{f'_c} - 1 \right]$$

$$r = \frac{E_c}{E_c - E_{sec}} ; \quad E_c = 5000 \cdot \sqrt{f'_c} \text{ (in MPa)} ; \quad E_{sec} = \frac{f'_{cc}}{\epsilon_{cc}}$$

In the previous relations, f'_{cc} and ϵ_{cc} are the stress and deformation of concrete at the peak. To obtain the appropriate equation for the unconfined concrete it should be put $f'_l = 0$ in the previous expressions.

For rectangular sections, the value of the effective stress can be determined as follows:

$$f'_{lx} = K_e \cdot \rho_x \cdot f_{yh}$$

$$f'_{ly} = K_e \cdot \rho_y \cdot f_{yh}$$

and in the case of the same areas of stirrups along the two main directions x and y of the cross-section ($\rho_x = \rho_y$) it results:

$$f'_{lx} = f'_{ly} = f'_{ly} = K_e \cdot \rho \cdot f_{yh}$$

The coefficient K_e , which represents the ratio between the area actually confined and that enclosed by the perimeter of the stirrups, it can be assumed for the rectangular sections approximately equal to 0.75. A conservative estimation of the ultimate strain was given by the following expression (Scott et al., 1982):

$$\varepsilon_{cu} = 0.004 + 0.9 \cdot \rho_s \left[\frac{f_{yh}}{300} \right]$$

where the constant term 0.004 takes into account the longitudinal strain for which the concrete cover is detached, ρ_s is the volume ratio of transverse stirrups and the confined concrete core, f_{yh} is the yield stress of the stirrups.

Therefore, the ultimate strain of the confined concrete, determined by the previous expression reported in (Scott et al., 1982), assumes a value of 6%. Instead, for unconfined concrete the ultimate strain of 0.5% was established (Scott et al., 1982), and justified also by the experimental values reported in (Chapman et al., 1964). The stress-strain of concrete in tension was assumed linear-brittle.

For the constitutive law of the structural steel the prescriptions given in the Italian standard for steel S235 can be summarized as follows:

Characteristic yield strength: $f_{yk} = 235 \text{ N/mm}^2$

Characteristic rupture strength: $f_{tk} = 360 \text{ N/mm}^2$;

For the structural steel of the columns, according to the method exposed in the chapter 5, it was chosen the stress - deformation curve with an elastic perfectly plastic model (EPP) considering the asymmetric response; in fact, the constitutive law was stopped at a strain of 15% for the branch that describes the tensile strength while for the part that describes the compression behavior a value of strain was estimated to take account of the local buckling in the plastic range for the partially encased columns, as already explained in chapter 5; the value of ε_{su} assumed for the columns is based on the formulation of (Elnashai et al. 1998) and gave about 3.5%.

For the composite beams subject to hogging moment, the procedure used to trace the moment-curvature relationship was carried out according the procedure explained in chapter 4; the structural steel was characterized by an elasto-plastic with hardening constitutive law (EPH), the local buckling for the compression part was taken into account by the critical stress approach, the ultimate tensile strain was set to 15% and that one of the reinforcement was established equal to 6.75%.

The moment-curvature for the composite beams under sagging moment was implemented adopting the model above discussed for the concrete in compression and the EPH model with ε_{su} equal to 15% for the structural steel in tension. The effect of the reinforcement in compression was neglected. The moment-curvature diagrams for beams (Fig. 6.24a) show how the behavior is highly asymmetric comparing sagging and hogging bending moments. As regards the columns, taking into accounts the confinement effects, the diagrams of Figure 6.24b were obtained. They show as the ductility and the strength decreases when the axial force ratio ν (ratio between the axial load and the axial strength of the section) increases.

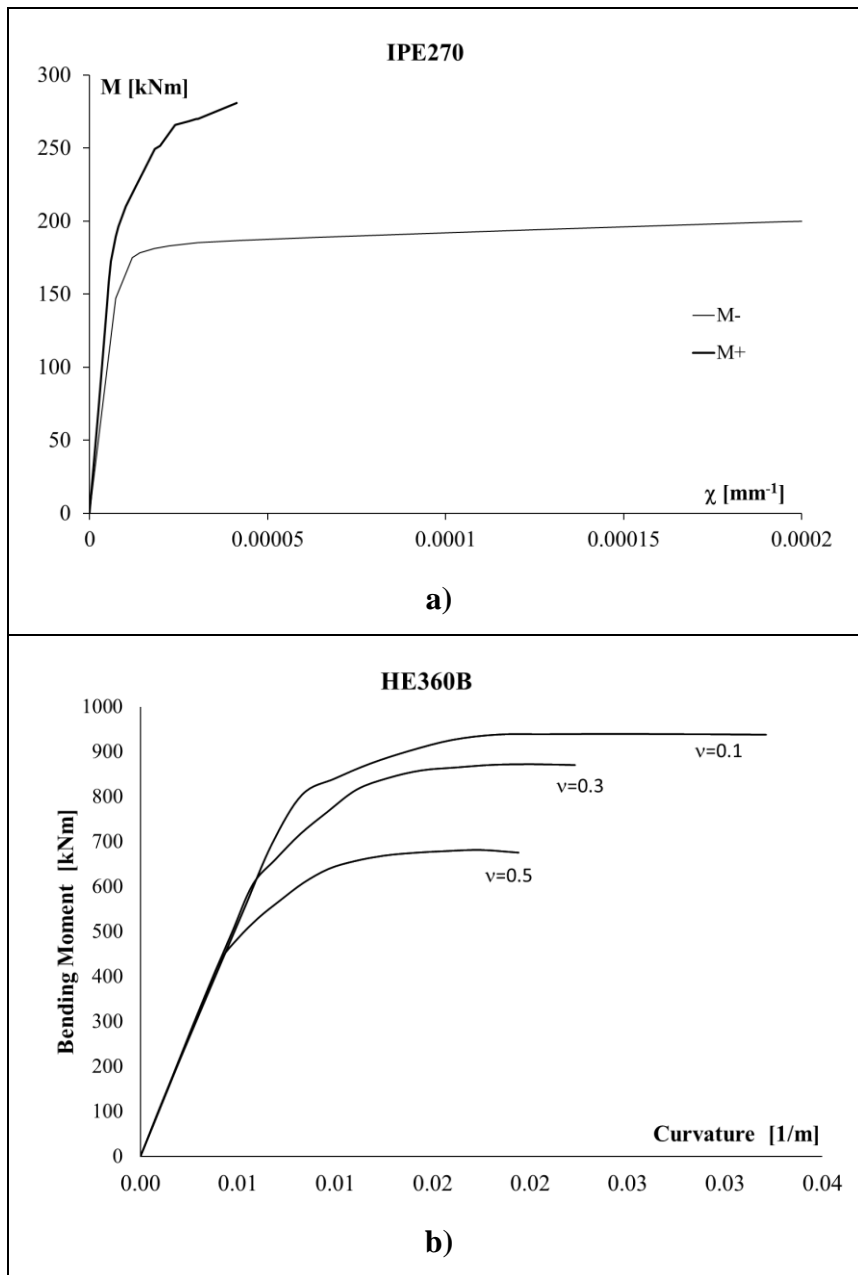


Figure 6.24: The moment-curvature diagrams: a) for a beam b) for a column

6.4.2 The plastic hinge length

The plastic hinge lengths used in the non-linear analyses reported in par. 6.3.3 were based on the results of chapters 4, for the beams under the hogging moment, and 5, for the columns, but for the composite beams under sagging moment, some formulations, indicated in the technical literature for the reinforced concrete, steel and steel-concrete composite elements were considered. In fact, for the R.C. structures over the years different expressions have been formulated (Table 6.5) based on experimental results (Paulay et al., 1992; Panagiotakos et al., 2001) while for steel elements a plastic hinge length approximately equal to the profile height itself is usually assumed (Bruneau et al., 1998) For the steel-concrete beams, the expressions of the plastic hinge length for steel-concrete composite beams (Table 6.6) are simply equal to 1.75 times the total height of the composite beam (Chen et al. 2008) or 1.7 times the height of only steel profile (Kemp et al., 2001). Figures 6.25a and 6.25b show the variation of the plastic hinge length, respectively for a beam and a column of the designed frame. It is clear that, the 10 formulations give very different results, except for some ones that overlap: number 6 and 8 for the beam and column, number 3 and 5 for the column.

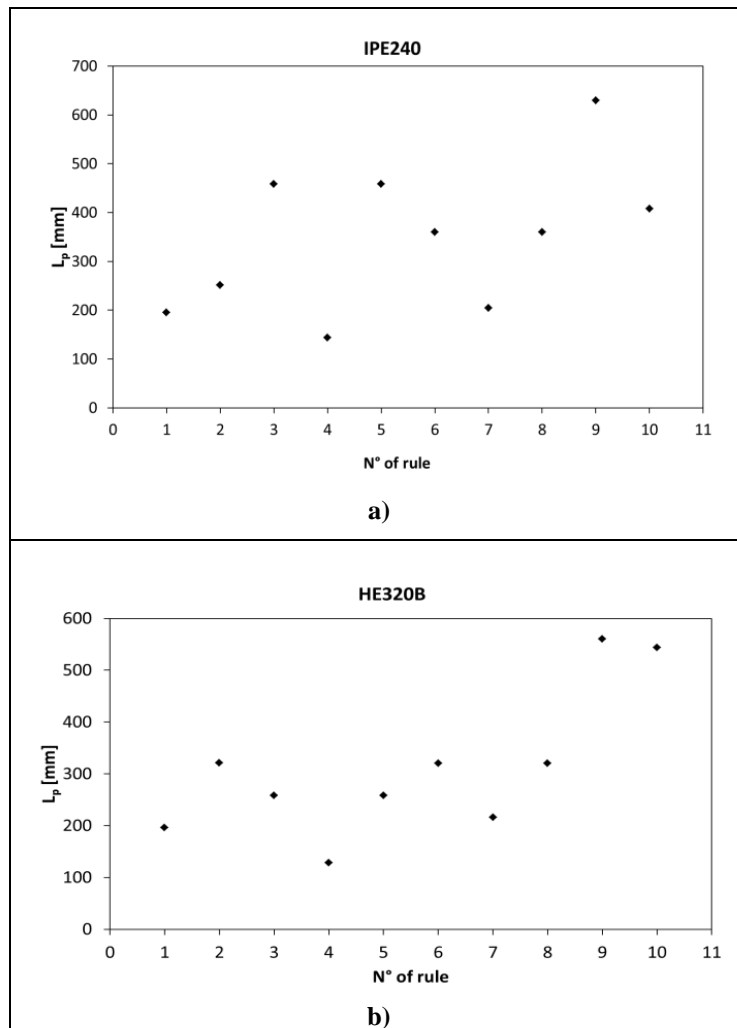


Figure 6.25: Plastic hinge length with the formulations of tables 6.5 and 6.6 for composite beam IPE240 (a) and for composite column HE320B (b).

The scattering of the results shows how it could be not suitable to adapt the formulations of reinforced or steel concrete structures to the case of a composite MRF. Therefore in the analyses reported in the next paragraph for the beams under sagging moment a plastic hinge length equal to 1.75 times the composite section height was adopted, that was developed for composite beams (Chen et al., 2007).

Expressions	Parameters	Bibliography
1 $l_p = \frac{d}{2} + 0.2 \frac{z}{\sqrt{d}}$	d: height of cross-section z: shear span length	Corley, W. G, 1966
2 $l_p = \frac{d}{2} + 0.05z$	d: height of cross-section z: shear span length	Mattock, A. H., 1967
3 $l_p = 0.08L + 6d_b$	L : element length d _b : long. steel bar diameter	Priestley, M. J. N., and Park, R., 1987
4 $l_p = 0.4h$	h : height of cross-section	Park, R.; Priestley, M. J. N.; Gill, W.D., 1982
5 $l_p = 0.08L + 0.022d_b f_y$	L: element length d _b : long. steel bar diameter f _y : yielding strenght of bars	Paulay, T., and Priestley, M. J. N., 1992
6 $l_p = 1.0h$	h: height of cross-section	Sheikh, S. A., and Khoury, S. S., 1993
7 $L_p = 0,1L_v + 0,17h + 0,24 \frac{d_{bL} f_y}{\sqrt{f_c}}$	L _v : shear span length h : height of cross-section d _{bL} : long. steel bar diameter f _y : yielding strength of bars f _c : concrete cylindrical strength	Circolare NTC #C8A.6

Table 6.5: Expressions of the plastic hinge length for r.c. elements

Expressions	Parameters	Bibliography
8 $L_p = h$	h: height of steel cross-section	Bruneau et al., 1998
9 $L_p = 1.75h_{tot}$	h: height of composite cross-section	Chen, S. and Jia, Y., 2007
10 $L_p = 1.7h$	h: height of steel cross-section	Kemp, A. R., Nethercot, D.A., 2000

Table 6.6: Expressions of the plastic hinge length for steel elements (expression 8) and steel-concrete composite beams (expressions 9 and 10)

6.4.3 *The non-linear response*

In this paragraph the results of non-linear static analyses are reported concerning the designed steel-concrete composite frame; the effect of the base column deformability of a socket type connection, widely examined in chapter 5 is also considered. In particular, in the first analysis a rigid base connection was assumed for the partially encased composite columns while in the second case the deformability of the base connection was introduced according the non-linear spring model defined in chapter 5. Thus, the equivalent plastic hinge length of the column was established equal to $0.5h$ (h is the height of the steel profile) in the case of rigid base connection, to introduce the plasticization of the column. When the deformability of the base connection was added the effect of the elastic deformability and the fixed end rotation in the plastic field was considered enhancing the plastic hinge length up to $1.0h$ at the base of the columns. This difference of L_p , as extensively discussed in the previous chapter, is due to the global plastic mechanism of the base column connection that can be divided in two plastic components, one properly due to the upper part of the composite column and the other one due to the embedded part of the column.

As discussed in the previous paragraph, for the composite beam under sagging moment the L_p value was established equal to $1.75h$ while in the case of hogging moment this length was equal to $0.6h$ as concluded in chapter 4.

Table 6.7 reports the main information about the modal analyses performed on the two composite frames. From the table 6.7 it could be noticed a little elongation in the period values for the composite frame characterized by a deformable base column connection. Therefore, a little variation in the participating mass was also registered.

	Rigid base column		Deformable base column	
Mode	Period	Partec. Mass	Period	Partec. Mass
Unitless	Sec	Unitless	Sec	Unitless
1	1.282	0.829	1.304	0.838
2	0.408	0.120	0.414	0.117
3	0.208	0.036	0.211	0.033
4	0.134	0.014	0.135	0.012

Table 6.7: Main modal information for the two analyzed frames

Fig. 6.26 shows the Pushover curves for the composite frame with rigid base column connection compared with the deformable one for a modal distribution of the seismic forces. It could be noticed that the global response is almost the same: a little difference could be highlighted before the yielding point.

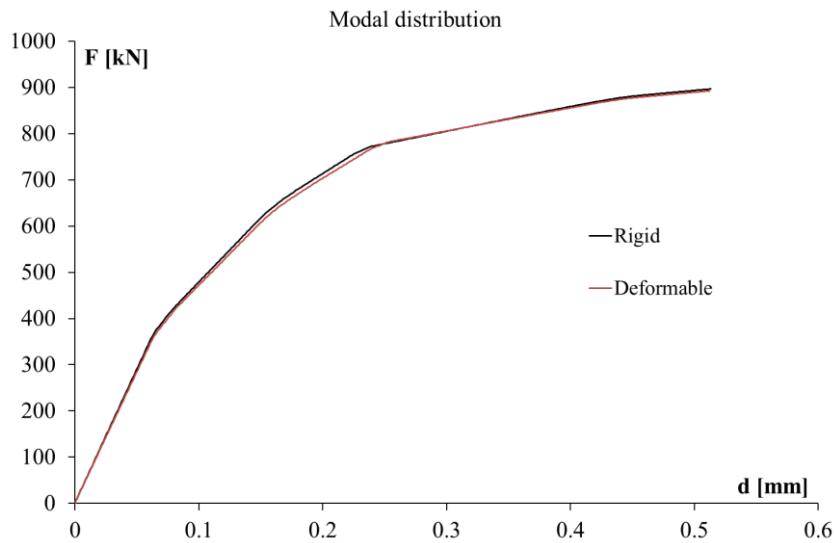


Figure 6.26: Comparison of the Pushover curves for the composite frame with rigid base column connection and that one with deformable connection (modal distribution of the seismic forces)

Fig. 6.27 reports the screenshots for the two frames at collapse condition: the orange color of the plastic hinge indicate the achievement of the collapse

condition, the yellow indicates the overcome of the 75% of the plastic capacity and the magenta color is valid from zero plastic rotation to the 75% of that.

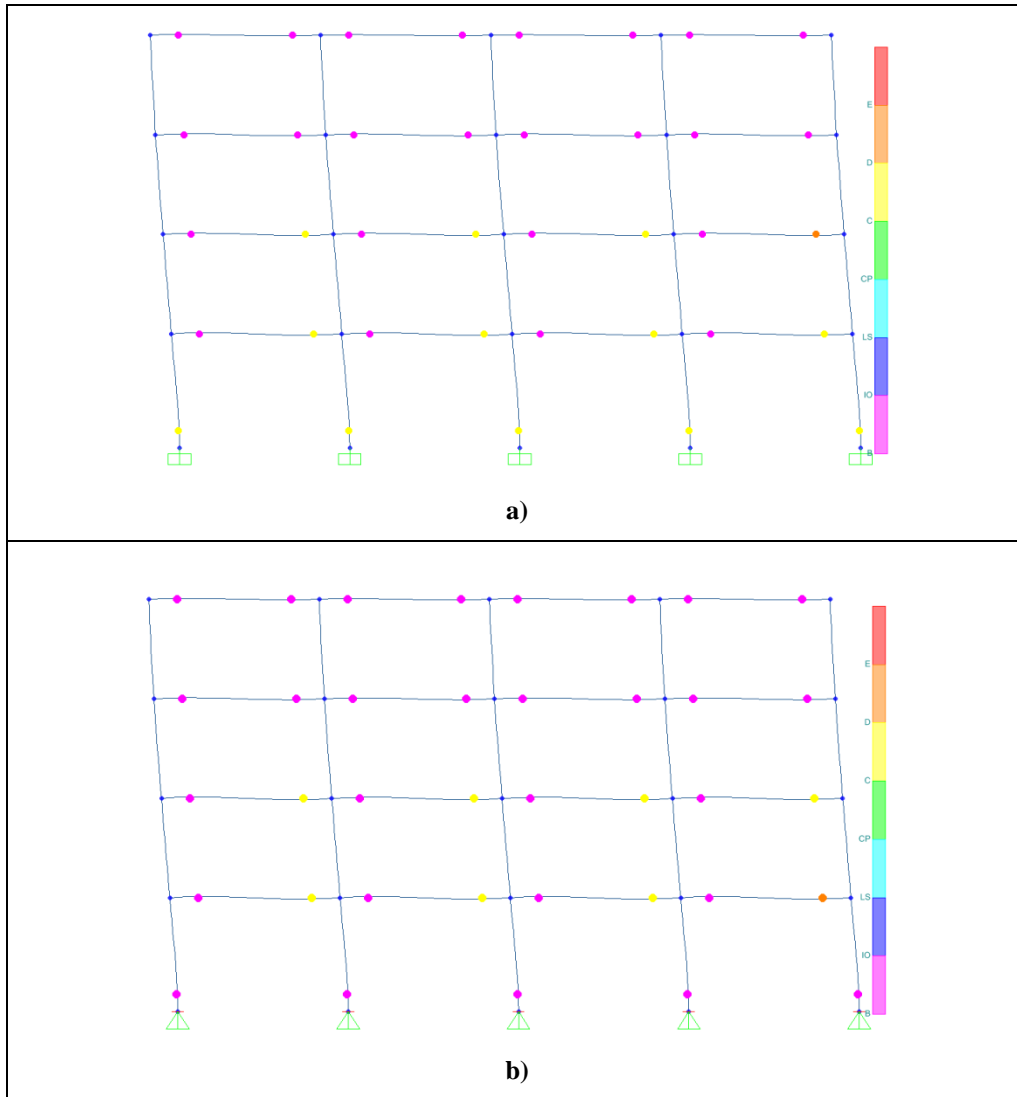


Figure 6.27: Status of the plastic hinges at the collapse condition for a modal distribution of the seismic forces; a)rigid base connection; b)deformable base connection.

In the case of rigid base column connection, fig. 6.27a, the collapse was due to the beam of the second floor subject to sagging moment while in the second case it was the beam at the first floor to govern the collapse.

It seems interesting to highlight the condition of the base column connection that in the first case was near to the collapse condition while in the second case, due to the greater plastic capacity considered through the adoption of a greater equivalent plastic hinge, the base columns were in a safer condition.

Fig. 6.28 reports the comparison in terms of Pushover curves when a constant distribution of the seismic forces was adopted. Also in this case it could be highlighted a little difference before the yielding point presumably due to the deformability of the base column connection; while a certain difference could be observed in the ultimate displacement capacity. In fact, in the case of the deformable base connection the global displacement capacity was greater than in the case of the rigid one.

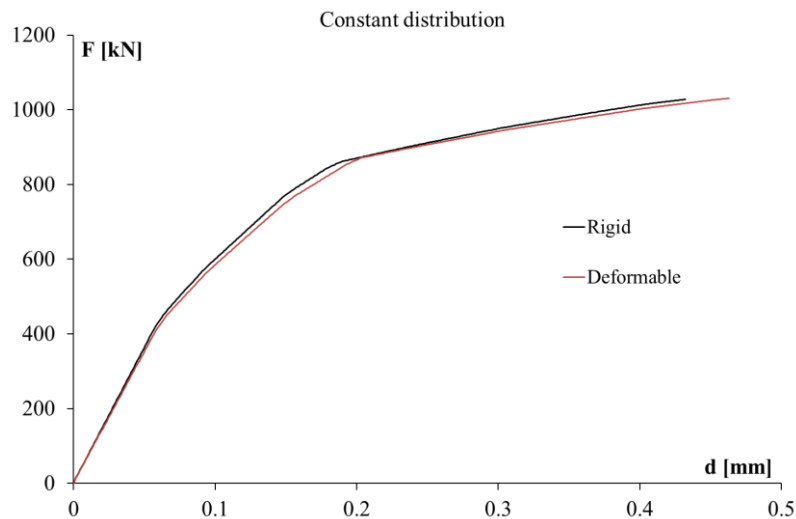


Figure 6.28: Comparison of the Pushover curves for the composite frame with rigid and deformable base connection (constant distribution of the seismic forces)

Fig. 6.29 shows the screenshots of the frames at the collapse condition when a constant distribution of the seismic forces was adopted. Fig 6.29a shows that the collapse was governed by the achievement of the maximum possible rotation in the rigid base column connection (orange color) while fig. 6.29b shows how the collapse condition in the case of deformable base column connection moves to the beam of the first floor. This is due to the greater plastic capacity attributed to the deformable connection in respect to the rigid one.

The period of the inelastic equivalent SDOF system (T^*) is evaluated according to EC8, together with the following parameters of the nonlinear analyses were evaluated and reported in Tables 6.8 and 6.9 the displacement (δ_1) and the base shear (V_1) at the formation of the first plastic hinge, the design base shear (V_d), the base shear at the formation of the mechanism (V_y), the base shear corresponding to an elastic system (V_e), the ductility factor $R_\mu = V_e/V_1$, the over-strength ratio $R_s = V_1/V_y$ and the design over-strength $R_\omega = V_y / V_d$, the global behaviour factor q .

All results show that the deformability of the base column connection did not influence too much the variability of q -factor and in all cases its value is greater than provided the standard code EC8 (about $5 \div 6$).

Furthermore it is worth noticing that the over-strength factor assumes always a value widely over the standard code indication ($\alpha_u/\alpha_1=1.3$). Finally, it is evident that the values R_ω of the design over-strength have a significant role in the overall response of structure, thanks to the over-dimensioning of the members in order to satisfy the deformability limitations at the serviceability limit state in seismic conditions.

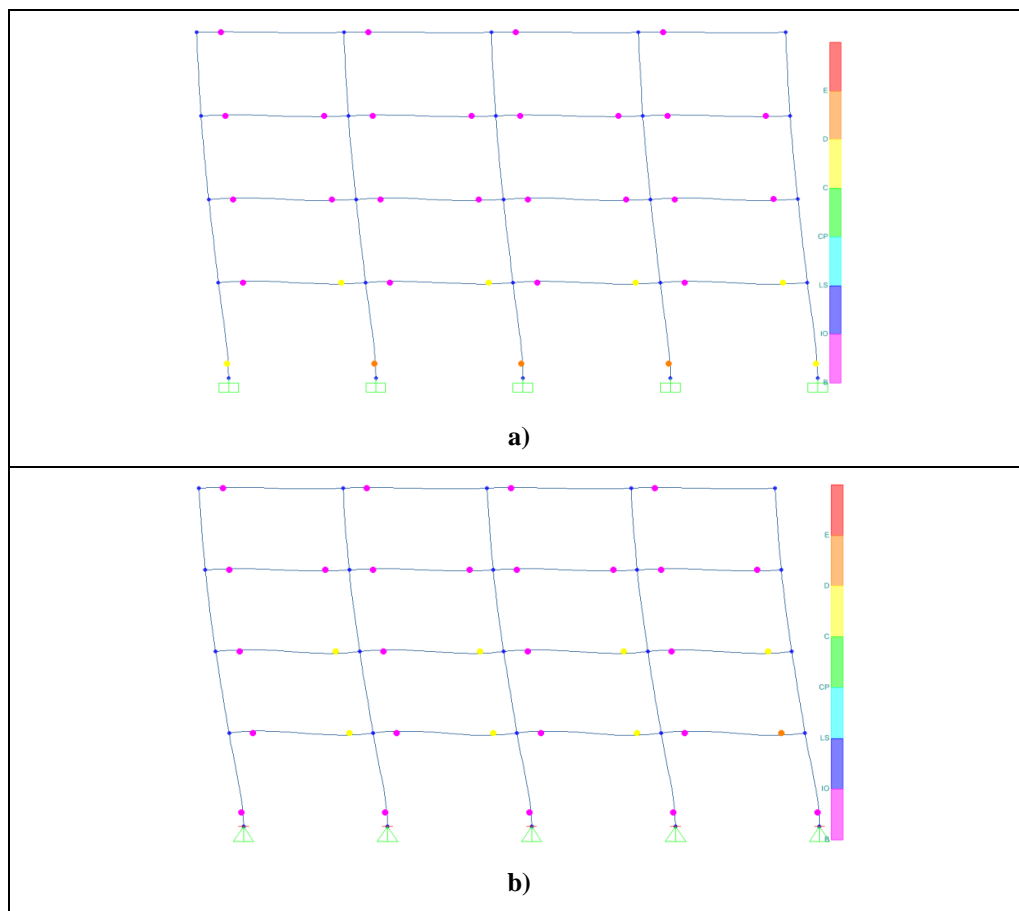


Figure 6.29: Status of the plastic hinges at the collapse condition for a constant distribution of the seismic forces; a)rigid base connection; b)deformable base connection.

Base column type	Pushover with modal distribution										
	T^*	δ_1	δ_u	V_d	V_l	V_y	V_e	R_ϕ	R_s	R_μ	Q
	[s]	[m]	[m]	[kN]	[kN]	[kN]	[kN]	[-]	[-]	[-]	[-]
Rigid	1.06	0.067	0.513	150	363	831	2269	2.42	2.29	2.73	15.13
Deformable	1.07	0.061	0.512	150	352	828	2224	2.35	2.35	2.69	14.83

Tab. 6.8: Parameters of the nonlinear static analysis with a triangular distribution of seismic forces.

Base column type	Pushover with constant distribution										
	T^*	δ_1	δ_u	V_d	V_l	V_y	V_e	R_ϕ	R_s	R_μ	q
	[s]	[m]	[m]	[kN]	[kN]	[kN]	[kN]	[-]	[-]	[-]	[-]
Rigid	0.92	0.056	0.432	150	408	944	2530	2.72	2.32	2.68	16.87
Deformable	0.94	0.056	0.463	150	395	948	2597	2.64	2.40	2.74	17.32

Tab. 6.9: Parameters of the nonlinear static analysis with a constant distribution of seismic forces.

6.5 Conclusions

In conclusion the resistance hierarchy was respected according the capacity design approach and the deformability of the base connection introduced a little modification in the overall stiffness and global nonlinear response of the frames; however it influenced the distribution of the damage because in the case of deformable base column connection the plastic capacity of the beams were completely used before the ultimate rotation of the base column was reached. The base column deformability did not affect the behavior factor (q) and the over-strength of the structure, although the obtained overall values were very high if compared with the standard code values. Since the global mechanism was often governed by the plastic capacity of the composite beams under sagging moment, it seems interesting as future development to investigate the reliability of the plastic hinge length adopted in these non-linear analyses.

REFERENCES

- Amadio, C., Bella, M., Bertoni, V., Macorini, L., 2011. Numerical modeling and seismic assessment of steel and steel-concrete composite frames. The line 5 of the ReLUIS-DPC 2005-2008 Project, 409-448, 2011, Doppiavoce, Napoli, Italy.
- Braconi, A., Bursi, O. S., Fabbrocino, G., Salvatore W., Tremblay, R., 2008. Seismic performance of a 3D full-scale high-ductility steel–concrete composite moment-resisting structure—Part I: Design and testing procedure. *Earthquake Engng Struct. Dyn.*; **37**:1609–1634.
- Braconi, A., Bursi, O. S., Fabbrocino, G., Salvatore W., Taucer, F., Tremblay, R., 2008. Seismic performance of a 3D full-scale high-ductility steel–concrete composite moment-resisting structure— Part II: Test results and analytical validation. *Earthquake Engng Struct. Dyn.*; **37**, 1635–1655.
- Berry, M. P., Lehman, D. E., Lowes, L. N., 2008. Lumped-Plasticity Models for Performance Simulation of Bridge Columns. *ACI Structural Journal*, V. 105, No. 3, May-June.
- Broderick, B.,M., Elnashai, A.,S., 1996. Seismic response of composite frames. Response criteria and input motion. *Engineering Structures*, vol.18, N.9, pp. 696-706.
- Broderick, B.,M., Elnashai, A.,S., 1996. Seismic response of composite frames. Calculation of behavior factors. *Engineering Structures*, vol.18, N.9, pp. 707-723.
- Bruneau, Whittaker and Uang ,”Ductile design of steel structures”, McGraw Hill Edition, 1998.
- Bursi, O. S., Gramola, G., 2000. Behaviour of composite substructures with full and partial shear connection under quasi-static cyclic and pseudo-

-
- dynamic displacements. *Materials and Structures/Materiaux et Constructions*, Vol. 33, April, pp 154-163.
- Bursi O.S., Sun F., Postal S., 2005. Non-linear analysis of steel-concrete composite frames with full and partial shear connection subjected to seismic loads. *Journal of Constructional Steel Research* **61**, 67–92.
- CEN, European Committee for Standardization, Eurocode 2. Design of concrete structures. Part 1-1: General rules and rules for buildings. PrEN 1992-1-1:2004. Brussels, Belgium, 2004.
- CEN, European Committee for Standardization, Eurocode 3. Design of steel structures. Part 1-1: General rules and rules for buildings. PrEN 1993-1-1:2005. Brussels, Belgium, 2005.
- CEN (2008-a). Eurocode 4. Design of composite steel and composite structures. Part 1.1: General rules and rules for buildings. Eur. Comm. for Stand., Brussels, Belgium.
- Chen, S., Jia, Y., “Required and available moment redistribution of continuous steel–concrete composite beams”, *Journal of Constructional Steel Research* 64 (2008), 167–175
- Di Sarno, L., Pecce, M.R., Fabbrocino, G., 2007. Inelastic response of composite steel and concrete base column connections, *Journal of Constructional Steel Research*, **63**, 819-832
- Elnashai, A. S., Elghazouli, A. Y., “Performance of composite steel/concrete members under earthquake loading. Part I: analytical model”. *Earthquake Engng Struct. Dyn.* 1993; 22, 315-345
- Eurocode 8, 2004. “Design provisions for earthquake resistance of structures. Part 1.3: General rules. Specific rules for various materials and elements”, European Committee for Standardisation, Brussels, Belgium.

- Green, T.P., Leon, R.T., Rassati, G.A., 2004. Bidirectional Tests on Partially Restrained, Composite Beam-to-Column Connections, *Journal of Structural Engineering*, Vol. 130, No. 2,
- Kato, B., 1989. Rotation capacity of H-section members as determined by local buckling, *Journal of Constructional Steel Research*, **13**, 95-109
- Kemp, A. R., 1985. Interaction of Plastic local and Lateral Buckling, *Journal of Structural Engineering*, ASCE, vol. 111 n. 10
- Kemp, A.R., e Nethercot, D.A. (2001). Required and available rotations in composite beams with semi-rigid connections. *Journal of Constructional Steel Research*, 57 (4), 375-400.
- Mander, J. B., Priestley, M. J. N., Park, R., “Theoretical stress-strain model for confined concrete”, *Journal of Structural Engineering*, Vol. 114, No. 8, August, 1988,ASCE
- Nakashima, M., Matsumiya, T., Suita, K., Zhou, F., 2007. Full-Scale Test of Composite Frame under Large Cyclic Loading. *Journal of Structural Engineering*, Vol. 133, No. 2.
- Oehlers, J.,D., Bradford, M.,A., 1999. Elementary behaviour of composite steel & concrete structural members. Butterworth Heinemann.
- Panagiotakos, T. B., Fardis, M. N., 2001. "Deformations of RC Members at Yielding and Ultimate", *ACI Structural Journal*, Vol. 98, No. 2, pp. 135-148.
- Paulay, T., Priestley, M. J. N., “Seismic Design of Reinforced Concrete and Masonry Buildings”, John Wiley and Sons, New York, 1992, pp. 767.
- Pertold, J., Xiao, R.Y., Wald, F., 2000. Embedded steel column bases I. Experiments and numerical simulation, *Journal of Constructional Steel Research*, **56**, 253-270

-
- Pertold, J., Xiao, R.Y., Wald, F., 2000. Embedded steel column bases II. Design model proposal, *Journal of Constructional Steel Research*, **56**, 271–286
- Sap2000 User's Manual, Computer and Structures, inc., Berkeley, 2011.
- Scott, B. D., Park, R., Priestley, M. J. N., “Stress-Strain behavior of concrete confined by overlapping hoops at low and high strain rates”, *ACI journal*, 1982
- Shanmugam, N.E., Lakshmi, B., 2001. State of the art report on steel–concrete composite columns, *Journal of Constructional Steel Research*, **57**, 1041–1080
- Zhou, F., Mosalam, K. M., Nakashima, M., “Finite-Element Analysis of a Composite Frame under Large Lateral Cyclic Loading”, *Journal of Structural Engineering*, Vol. 133, No. 7, July 1, 2007, ASCE, pp. 1018–1026
- Amadio, C., Bella, M., Bertoni, V., Macorini, L., 2011. Numerical modeling and seismic assessment of steel and steel-concrete composite frames. The line 5 of the ReLUIS-DPC 2005-2008 Project, 409-448, 2011, Doppiavoce, Napoli, Italy.
- Braconi, A., Bursi, O. S., Fabbrocino, G., Salvatore W., Tremblay, R., 2008. Seismic performance of a 3D full-scale high-ductility steel–concrete composite moment-resisting structure—Part I: Design and testing procedure. *Earthquake Engng Struct. Dyn.*; **37**:1609–1634.
- Braconi, A., Bursi, O. S., Fabbrocino, G., Salvatore W., Taucer, F., Tremblay, R., 2008. Seismic performance of a 3D full-scale high-ductility steel–concrete composite moment-resisting structure— Part II: Test results and analytical validation. *Earthquake Engng Struct. Dyn.*; **37**, 1635–1655.

-
- Berry, M. P., Lehman, D. E., Lowes, L. N., 2008. Lumped-Plasticity Models for Performance Simulation of Bridge Columns. *ACI Structural Journal*, V. 105, No. 3, May-June.
- Broderick, B.,M., Elnashai, A.,S., 1996. Seismic response of composite frames. Response criteria and input motion. *Engineering Structures*, vol.18, N.9, pp. 696-706.
- Broderick, B.,M., Elnashai, A.,S., 1996. Seismic response of composite frames. Calculation of behavior factors. *Engineering Structures*, vol.18, N.9, pp. 707-723.
- Bruneau, Whittaker and Uang ,”Ductile design of steel structures”, McGraw Hill Edition, 1998.
- Bursi, O. S., Gramola, G., 2000. Behaviour of composite substructures with full and partial shear connection under quasi-static cyclic and pseudo-dynamic displacements. *Materials and Structures/Materiaux et Constructions*, Vol. 33, April, pp 154-163.
- Bursi O.S., Sun F., Postal S., 2005. Non-linear analysis of steel-concrete composite frames with full and partial shear connection subjected to seismic loads. *Journal of Constructional Steel Research* **61**, 67–92.
- CEN, European Committee for Standardization, Eurocode 2. Design of concrete structures. Part 1-1: General rules and rules for buildings. PrEN 1992-1-1:2004. Brussels, Belgium, 2004.
- CEN, European Committee for Standardization, Eurocode 3. Design of steel structures. Part 1-1: General rules and rules for buildings. PrEN 1993-1-1:2005. Brussels, Belgium, 2005.
- CEN (2008-a). Eurocode 4. Design of composite steel and composite structures. Part 1.1: General rules and rules for buildings. Eur. Comm. for Stand., Brussels, Belgium.
- Chen, S., Jia, Y., “Required and available moment redistribution of continuous

-
- steel–concrete composite beams”, *Journal of Constructional Steel Research* 64 (2008), 167–175
- Di Sarno, L., Pecce, M.R., Fabbrocino, G., 2007. Inelastic response of composite steel and concrete base column connections, *Journal of Constructional Steel Research*, **63**, 819-832
- Elnashai, A. S., Elghazouli, A. Y., “Performance of composite steel/concrete members under earthquake loading. Part I: analytical model”. *Earthquake Engng Struct. Dyn.* 1993; 22, 315-345
- Eurocode 8, 2004. “Design provisions for earthquake resistance of structures. Part 1.3: General rules. Specific rules for various materials and elements”, European Committee for Standardisation, Brussels, Belgium.
- Green, T.P., Leon, R.T., Rassati, G.A., 2004. Bidirectional Tests on Partially Restrained, Composite Beam-to-Column Connections, *Journal of Structural Engineering*, Vol. 130, No. 2,
- Kato, B., 1989. Rotation capacity of H-section members as determined by local buckling, *Journal of Constructional Steel Research*, **13**, 95-109
- Kemp, A. R., 1985. Interaction of Plastic local and Lateral Buckling, *Journal of Structural Engineering*, ASCE, vol. 111 n. 10
- Kemp, A.R., e Nethercot, D.A. (2001). Required and available rotations in composite beams with semi-rigid connections. *Journal of Constructional Steel Research*, 57 (4), 375-400.
- Mander, J. B., Priestley, M. J. N., Park, R., “Theoretical stress-strain model for confined concrete”, *Journal of Structural Engineering*, Vol. 114, No. 8, August, 1988, ASCE
- Nakashima, M., Matsumiya, T., Suita, K., Zhou, F., 2007. Full-Scale Test of Composite Frame under Large Cyclic Loading. *Journal of Structural Engineering*, Vol. 133, No. 2.

- Oehlers, J.,D., Bradford, M.,A., 1999. Elementary behaviour of composite steel & concrete structural members. Butterworth Heinemann.
- Panagiotakos, T. B., Fardis, M. N., 2001. "Deformations of RC Members at Yielding and Ultimate", ACI Structural Journal, Vol. 98, No. 2, pp. 135-148.
- Paulay, T., Priestley, M. J. N., “Seismic Design of Reinforced Concrete and Masonry Buildings”, John Wiley and Sons, New York, 1992, pp. 767.
- Pertold, J., Xiao, R.Y., Wald, F., 2000. Embedded steel column bases I. Experiments and numerical simulation, Journal of Constructional Steel Research, **56**, 253-270
- Pertold, J., Xiao, R.Y., Wald, F., 2000. Embedded steel column bases II. Design model proposal, Journal of Constructional Steel Research, **56**, 271-286
- Sap2000 User’s Manual, Computer and Structures, inc., Berkeley, 2011.
- Scott, B. D., Park, R., Priestley, M. J. N., “Stress-Strain behavior of concrete confined by overlapping hoops at low and high strain rates”, ACI journal, 1982
- Shanmugam, N.E., Lakshmi, B., 2001. State of the art report on steel–concrete composite columns, Journal of Constructional Steel Research, **57**, 1041–1080
- Zhou, F., Mosalam, K. M., Nakashima, M., “Finite-Element Analysis of a Composite Frame under Large Lateral Cyclic Loading”, Journal of Structural Engineering, Vol. 133, No. 7, July 1, 2007, ASCE, pp. 1018–1026